Développement de détecteur gazeux à micropistes pour le trajectographe de l'expérience CMS et mesures de rapports d'embranchement de désintégrations hadroniques du méson B dans l'expérience BaBar

A. Zghiche

LAPP-H-2007/01

Laboratoire D'Annecy-le-Vieux de Physique des Particules

Synthèse des travaux scientifiques

Pour obtenir le diplôme

Habilitation à Diriger des Recherches

DE L'UNIVERSITE DE SAVOIE

Spécialité: Physique des particules

par

Amina Zghiche

SUJET:

Développement de détecteur gazeux à micropistes pour le trajectographe de l'expérience CMS et mesures de rapports d'embranchement de désintégrations hadroniques du méson B dans l'expérience BaBar

Soutenue le 22 janvier 2007 devant la commission d'examen

D. Boutigny	Rapporteur
L. Di Ciaccio	
Y. Karyotakis	
O. Pène	
G. Rolandi	Rapporteur
M.-H. Schune	Rapporteure

Table des Matières

Activités de recherche

I. Introduction

Dans ce document je résumerai mes activités de recherche depuis ma thèse. Celle-ci portait sur l'étude de la diffusion quasi-élastique d'électrons sur un noyau lourd, le ^{208}Pb avec séparation transverse-longitudinale de la section efficace inclusive (e,e'). J'ai effectué mes travaux de thèse au DPhN/HE du CEA-Saclay et je l'ai soutenue le 12 octobre 1989 à l'université Paris-XI.

Après un séjour post-doctoral au Laboratoire National d'Argonne (Chicago, USA), où j'ai principalement travaillé sur la mise au point d'une cible polarisée de deutérium pour la mesure de son pouvoir d'analyse tensoriel T_{20}, j'ai poursuivi mes travaux au Laboratoire National Saturne (CEA-Saclay, France) sur la production au seuil des mésons **K** et η; en particulier, j'ai étudié l'effet ABC et l'état quasi-lié **η-^{4}He**, dans la production du η au seuil dans la réaction ^{2}H(^{2}H,α) X. J'ai ensuite rejoint le groupe CMS de l'IReS- Strasbourg, pour travailler sur le trajectographe gazeux du détecteur CMS au LHC-CERN. Actuellement, je suis investie dans des analyses de physique dans la collaboration BaBar à SLAC. Je couvre ainsi plusieurs facettes du domaine: étude et construction de détecteurs, développement de logiciels et analyse.

II. Thèse d'université

J'ai effectué ma thèse[1] d'université au Département de Physique Nucléaire de Haute Energie (DPhN/HE) à l'Orme des Merisiers au CEA-Saclay. Celle-ci portait sur l'étude de la diffusion quasi-élastique d'électrons sur un noyau lourd, le ^{208}Pb avec séparation transverse-longitudinale de la section efficace inclusive(e,e'). La problématique abordée a permis la mise en évidence des deux aspects suivants:

- Les effets de la distorsion coulombienne sur la section efficace différentielle inclusive de diffusion quasi-élastique d'électrons sur le ^{208}Pb[2].

- Les effets de la densité nucléaire et de la charge atomique sur la règle de somme coulombienne[3].

[1] **Etude de la diffusion quasi-élastique d'électrons sur un noyau lourd, le ^{208}Pb. Séparation transverse-longitudinalede la section efficace inclusive(e,e')**, A. Zghiche –Thèse de l'université Paris-XI, Orsay , soutenue le 12 octobre 1989

[2] **Deep Inelastic Electron Scattering In The Distorted Wave Born Approximation: An Analytic Approach**, M. Traini (Trento U.) , S. Turck-Chieze, A. Zghiche (Saclay), Phys.Rev.C38:2799-2812,1988

[3] **Longitudinal and Transverse Responses in Quasi-Elastic Electron Scattering from Pb-208 and He-4**, A. Zghiche *et al.*, Nucl.Phys.A572:513-559,1994, Erratum-ibid.A584:757,1995

III. Le pouvoir d'analyse tensoriel T_{20} du Deutéron

Au cours de mon séjour post-doctoral au Laboratoire National d'Argonne à Chicago-USA, j'ai travaillé sur la conception et la mise au point d'une cible polarisée de deutérium dans le but de mesurer le pouvoir d'analyse tensoriel T_{20} du Deutéron. Le but était de construire une cible épaisse à placer à l'intérieur de l'anneau de stockage d'électrons VEPP-3 au Budker Institute of Nuclear Physics, à Novosibirsk, Russie. Les jets de Deutérium polarisé obtenus par les techniques de polarisation classique permettaient une intensité de 1.5×10^{16} atomes/s et une épaisseur de cible à l'intérieur de l'anneau de 10^{12} atomes/cm^2. Le but était d'augmenter cette épaisseur en jouant sur deux paramètres:

- construire une cible polarisée de plus grande intensité. Elle a été réalisée en utilisant une technique de polarisation par échange de spin entre un atome alcalin, le potassium ^{39}K et l'atome de deutérium. Le ^{39}K étant polarisé au départ à l'aide d'un laser. L'intensité a atteint 2.1×10^{17} atomes/s avec cette technique[4], avec une amélioration de la figure de mérite (le carré de la polarisation x l'intensité de la source) d'un facteur 3.4. Ce facteur pouvant s'améliorer avec l'utilisation d'une source laser plus intense.
- construire une cellule de stockage placée à l'intérieur de l'anneau de stockage VEPP-3. Celle-ci a permis l'augmentation d'un facteur 30 de la figure de mérite de la cible[5].

IV. L'état quasi-lié η-^{4}He et l'effet ABC dans la réaction $\vec{d}\, d \rightarrow \alpha X$

Le faisceau de deutérium polarisé tensoriellement, délivré par le synchrotron du Laboratoire National SATURNE a permis la mesure de la section efficace de la réaction $\vec{d}\, d \rightarrow \alpha X$ ainsi que le pouvoir d'analyse tensoriel du deutéron avec le détecteur à très grande acceptance, SPES III.

La mesure de la section efficace[6] à six différentes valeurs de l'impulsion du η dans le centre de masse a montré que la variation de l'amplitude de réaction est plus lente que celle de la réaction $pd \rightarrow {}^3He\, X$, suggérant l'existence d'un état quasi-lié **η-^{4}He.**

Une structure dite "effet ABC" a aussi été observée dans cette réaction. La distribution d'impulsion manquante après détection de la particule α. montre un double pic correspondant à une masse manquante aux environs de 310 MeV/c^2, avec une largeur de 40 MeV/c^2. Le modèle qui décrit le mieux la section efficace mesurée ainsi que les pouvoirs d'analyse tensoriel et vectoriel mesurés suppose deux excitations Δ, celle d'un nucléon de la cible et celle d'un nucléon du faisceau, lesquelles en se désexcitant forment un α et une "structure **ABC**"[7].

---

[4] **Spin-Exchange Optical Pumping as a Source of Spin-Polarized Atomic Deuterium**, K.P. Coulter *et al.* Phys. Rev. Lett. 68:174-177,1992 **.**

[5] **An Active storage cell for a polarized gas internal target,** K.P. Coulter *et al.*, Nucl.Instrum.Meth.A350:423-429,1994

[6] **η - 4He quasi-bound states.** N. Willis *et al.* **Phys.Lett.B406:14-19,1997**

[7] **Study of the ABC Enhancement in the $\vec{d}\, d \rightarrow \alpha X$** , R. Wurzinger *et al.* **Phys.Lett. B445 (1999) 423-427**

V. Etude et développement de détecteurs gazeux à micropistes pour le trajectographe de l'expérience CMS au LHC

Lorsqu'en 1995 j'ai rejoint le groupe "LHC" de l'IReS- Strasbourg, il était impliqué dans la partie "bouchon" avant-arrière du projet du trajectographe "MicroStrip Gas Chambers" (MSGC) du détecteur Compact Muon Solenoid (CMS) au LHC. Sur ce projet, nous étions en collaboration avec cinq groupes universitaires belges et l'institut russe BINP-Novosibirsk. En 1996 plusieurs groupes ont rejoint le projet MSGC "bouchon": le RWTH-Aachen, le IEKP-Karlsruhe et l'IPN-Lyon. En accord avec le LHCC, un premier "milestone", "MF1", a été défini dans le but d'évaluer les aspects "système" du projet MSGC en construisant plusieurs prototypes à dimension réelle. Après la validation du TDR par le LHCC en avril 1998, des "milestones" supplémentaires ont été définis. Il était alors question de prouver qu'une production de masse auprès de compagnies industrielles, des MSGCs "baseline" décrits dans le TDR était réaliste. Début 1999, les premiers prototypes "MF2", MSGC-baseline et MSGC+GEM ont été construits dans le cadre d'une collaboration de l'IReS avec IEKP-Karlsruhe et IIHE-Bruxelles. Un autre milestone défini après l'acceptation du TDR par le LHCC, est celui qui concerne l'électronique de lecture du trajectographe: le chip APV et les deux chaînes, analogique et de contrôle qui lui sont associées. Je me suis impliquée dans la réalisation de ce milestone dès le début de mon séjour au CERN dans le cadre d'un contrat d'associée scientifique (septembre 1999- août 2000).

V.1. Les détecteurs micropistes gazeux MSGC: principe et paramètres critiques pour le détecteur CMS

Les détecteurs gazeux à micropistes MSGC sont construits selon le principe des compteurs proportionnels multifils MWPC[8]. Ces derniers ont un temps de réponse de quelques centaines de ns et une résolution spatiale au mieux de l'ordre de 300 μm. Les détecteurs gazeux à micropistes[9] sont affranchis de ces limitations grâce au fait que anodes et cathodes sont gravées par lithographie sur un substrat de verre. Avec des anodes de 10 μm de large gravées avec un pas de 200 μm et intercalées de cathodes de 100 μm, la résolution est au plus de 60 μm et peut être améliorée par des méthodes d'analyse comme celle du barycentre. Le volume gazeux est défini par le substrat et un plan de dérive situé à 3 mm au dessus, associés à une électronique frontale rapide, le temps de réponse des MSGC peut alors être réduit à moins de 100 ns[10].

En 1995, la collaboration "Forward-MSGC" visait à équiper les parties externes du trajectographe "bouchon" avec des MSGC dont la technologie était alors très récente, complétant ainsi les couches internes de pixel et le détecteur MicroStrip Silicium. Au total, une surface de 225 m^2 de MSGC devait être produite pour construire le trajectographe gazeux à micropistes de CMS et cela en collaboration avec l'institut italien INFN-Pisa, responsable de la partie "tonneau". Pour la phase haute luminosité du LHC, onze

[8] G. Charpak *et al.*, NIM62(1968) 262
[9] A. Oed, NIM A263 (1988) 351
[10] J. Croix et al., NIM A484(2002)503

disques en fibre de carbone portant 2000 modules multi-substrats MSGC étaient prévus de chaque côté des six couches concentriques MSGC de la partie "tonneau".
Plusieurs paramètres des détecteurs MSGC devaient être maîtrisés dans le but de les qualifier pour l'environnement LHC dont la fréquence de croisement est de 40 MHz, et l'irradiation estimée pour dix ans de fonctionnement, à 10 MRad pour le trajectographe externe de CMS. D'abord, le choix de la géométrie devait permettre une résolution spatiale meilleure que 40 μm, déterminante pour la capacité de reconstruction des particules par le trajectographe de CMS. Ensuite, le choix du gaz devait influer sur le gain du détecteur, sur son temps de réponse et sur son taux de claquages. Dans l'environnement du LHC où les particules hautement ionisantes sont abondantes, deux autres paramètres du détecteur MSGC étaient importants pour la réduction du taux de claquages :
- la résistivité du substrat était un facteur déterminant pour l'écoulement rapide des charges.
- la passivation des bords de pistes cathodes avec un polyimide (choix de 4 μm).

Ces paramètres ont été optimisés pour obtenir un fort gain permettant un échantillonnage rapide de la réponse du détecteur, un temps mort réduit (les décharges étant moins fréquentes) et un minimum de pistes anodes endommagées par les claquages.

V.2. Le gain du détecteur en fonction du choix du "coating" avec des couches minces semi-conductrices

Tout en participant à l'élaboration du projet MSGC "bouchon", j'ai rejoint le programme de recherche et développement sur cette nouvelle technologie en collaborant étroitement avec les groupes belges et russes. J'ai commencé par tester de petits échantillons de 3x3 cm^2 produits par le laboratoire local de recherche en physique du solide, PHASE[11]. J'ai concentré mes efforts sur l'investigation des couches minces semi-conductrices[12] et leur comportement lorsqu'elles sont soumises à des champs électriques intenses. Un test sous faisceau de haute intensité de pions de 3 GeV/c de 5 MSGC de 10x10 cm^2, sur lesquels ont été déposées des couches minces semi-conductrices de différentes résistivités (entre 10^{15} et 10^{16} Ω/cm^2) a été réalisé au PS-CERN dans l'aire expérimentale T10. Le faisceau était composé de 1% de particules hautement ionisantes engendrées par des réactions nucléaires. Le test a montré une meilleure robustesse des détecteurs MSGC avec "coating" comparés aux MSGC sans coating. Ils étaient soumis à 7 heures d'équivalent faisceau LHC[13]. Avec les dépôts de couches minces conductrices sur le substrat de verre, l'écoulement des charges est plus rapide, les champs électriques appliqués peuvent être plus intenses améliorant le gain et le temps de réponse du

[11] Laboratoire PHASE ,UPR 292 du CNRS, Strasbourg, France}
[12] **A study of various coatings for MSGCs.**
V. Mack, J.C. Fontaine, D. Huss (Haute Alsace U., GRPHE) , J.M. Brom, A. Zghiche (Strasbourg, CRN) , J. Schunck . 1999.
Nucl.Instrum.Meth.A423:369-375,1999
[13] **Test of a CMS MSGC tracker prototype in a high intensity hadron beam.**
D. Abbaneo *et al.* 1998. Prepared for 7th Pisa Meeting on Advanced Detectors: Frontier Detectors for Frontier Physics, La Biodola, Isola d'Elba, Italy, 25-31 May 1997. **Nucl.Instrum.Meth.A409:37-42,1998**

détecteur. La procédure de métallisation et de démétallisation "etching" ainsi que le comportement sous faisceaux intenses de neutrons ont aussi fait l'objet d'études approfondies et ont donné lieu à des thèses de Doctorat d'université (A. Pallares[14], V. Mack[15] pour l'IReS.).

V.3. La résolution spatiale et le gain en fonction du choix de la géométrie du détecteur

En 1995, les premiers prototypes de grande dimension ont été dessinés et produits par l'IReS et en Belgique pour être exposés à un faisceau de pions dans l'aire expérimentale X7 du SPS au CERN. Nous avons évalué à cette occasion deux points importants: la géométrie trapézoïdale des compteurs dans le but d'équiper les disques "bouchon" avec des anneaux concentriques à pistes radiales et l'assemblage de modules multi-substrats sans séparation entre deux compteurs adjacents.

Le prototype de l'IReS, dont j'étais responsable, était composé de deux détecteurs MSGC trapézoïdaux de 512 pistes anodes et 513 cathodes chacun. Le pas entre anodes variait de 180 à 200 μm sur une longueur de piste de 120mm. Avec cette géométrie, la résolution spatiale attendue est de l'ordre de 40 μm avec une variation de 6% due à la variation du pas sur la longueur de la piste. Les compteurs étaient assemblés dans une enceinte commune et légère (en composite de fibre de carbone en "nid d'abeille"). L'endroit de la jointure entre deux substrats correspond à un "φ-crack" de deux fois la distance nominale entre deux anodes consécutives. La lecture des signaux était réalisée avec le "chip" H1 APC64. Le test sous faisceau de pions de 50 GeV/c a validé deux points essentiels pour la géométrie "bouchon": il n'y a pas de perte d'efficacité dans la région du "φ-crack" et il y a un gain uniforme sur toute la surface du substrat malgré la variation de l'intervalle entre anodes et ceci grâce à la règle homothétique appliquée à la largeur de la piste cathode ainsi qu'au pas entre anode et cathode.

Le ''milestone MF1''

En 1996 plusieurs groupes ont rejoint le projet MSGC "bouchon": le RWTH-Aachen, le IEKP-Karlsruhe et l'IPN-Lyon. En accord avec le LHCC, un premier "milestone", "MF1", a été défini dans le but d'évaluer les aspects "système" du projet MSGC en construisant plusieurs prototypes à dimension réelle. Un total de 40 MSGCs de grandes dimensions correspondant à l'anneau le plus externe (180mm de longueur de piste) ont été construits et assemblés dans 6 modules multi-substrats qui contenaient soit 4 soit 8 substrats de 512 canaux chacun. Le groupe de Novosibirsk a quant à lui, construit un module à 9 substrats correspondant à l'anneau le plus interne (50 mm de longueur de piste).

Les signaux délivrés par les détecteurs étaient lus avec une électronique frontale basée sur le "chip" PREMUX128 intégrant la chaîne préamplificateurs et multiplexeurs développée dans le cadre de CMS pour un prototype du chip final du trajectographe de CMS (APV).

[14] "Etude de substrats pour chambres gazeuses à micropistes dans le cadre de l'expérience CMS au LHC ", Thèse de l'université Louis Pasteur de Strasbourg, soutenue le 14 juin 1996.

[15] "Etude des Chambres Gazeuses à micropistes " Thèse de l'université Louis Pasteur de Strasbourg, soutenue le 27 octobre 1997.

Grâce aux connaissances acquises lors des développements des premiers prototypes, le groupe de l'IReS était une force motrice dans le projet "MF1". Parmi les responsabilités que j'ai assumées je peux souligner les suivantes:

- Transfert de technologie du travail de recherche du laboratoire PHASE vers l'industriel OPTIMASK[16], qui était responsable de la production des substrats MSGC de "MF1" pour l'IReS et l'IPN-Lyon.
- Mise en place des procédures et des bancs de tests pour le contrôle et la validation de la qualité des substrats et de l'électronique de lecture.
- Dessin et production pour toute la collaboration, des hybrides en céramique pour l'alimentation en tension des MSGCs.
- Construction de l'hodoscope et de l'acquisition de données pour la lecture des "chips" PREMUX128 à 1 MHZ. Construction du banc de test avec rayons cosmiques et avec source radioactive.

J'ai pris part à plusieurs autres responsabilités qui incombaient à l'IReS telles que:

- Dessin et production du banc à déplacement vertical et horizontal utilisé sous faisceau et qui devait contenir les 7 modules détecteurs.
- Dessin et production des cadres de collages et des pièces de positionnement de précision nécessaires à l'alignement des substrats à l'intérieur du module.

Le succès du test de ce système sous faisceau de muons de 100 GeV/c dans l'aire expérimentale X5 du CERN-SPS en fin 1997, a donné lieu d'abord à une note CMS[17] puis à une publication dans NIM[18]. En plus de l'évaluation de l'efficacité du détecteur, une bonne performance de l'assemblage au "φ-crack" et l'uniformité du gain du détecteur MSGC trapézoïdal ont été confirmées. Enfin, la résolution spatiale mesurée variait de 40 à 44 μm en fonction du pas entre les anodes, une variation très voisine de celle attendue. Ces résultats ont été inclus dans le "Tracker Technical Design Report TDR " à la rédaction duquel j'ai contribué.

V.4. Tenue aux radiations: tests sous faisceaux intenses et multiples étages d'amplification

Après la validation du TDR par le LHCC en avril 1998, des "milestones" supplémentaires ont été définis. Il était alors question de prouver qu'une production de masse auprès de compagnies industrielles, des MSGCs "baseline" décrits dans le TDR était réaliste. Il fallait exposer les prototypes produits à des conditions de faisceau semblables à celles du LHC pour démontrer leur robustesse. Ce "milestone" pour la partie "bouchon" a été baptisé "MF2". Plusieurs périodes de test sous faisceau de pions de 300 MeV/c délivrés par le cyclotron du Paul Scherrer Institute (PSI) près de Zurich, ont été prévues à cette fin. Avec un cycle utile de 100% et une intensité de 10^4 particules par mm^2 et par seconde sur une surface allant au delà de la surface d'un substrat, les conditions expérimentales correspondent à celles attendues au LHC pour les anneaux internes du trajectographe MSGC. De plus, un taux important de particules très ionisantes est présent dans ce genre de faisceau, ce qui a pour effet de réduire les marges de fonctionnement

[16] OPTIMASK, 12 av. Ferdinand-de-Lesseps, 91420 Morangis, France.

[17] O. Bouhali et al., The CMS FORWARD-BACKWARD MSGC MILESTONE , CMS NOTE-1998/095

[18] **Large Scale Test of Wedge Shaped Micro Strip Gas Counters**, M.Ackermann et al., **Nucl.Instrum.Meth.A436(1999)313**

stable des MSGCs. Il fallait néanmoins démontrer qu'elles restaient suffisantes pour ce genre d'opération.

J'ai lancé une collaboration avec OPTIMASK pour la production de prototypes "baseline". Le premier pas était de construire des compteurs à pistes en or (Au), puis de passiver électriquement les bords des pistes cathodes sur 4 μm de large. Malgré une très grande volonté de la part de l'industriel, le manque d'équipement n'a pas permis de réussir la partie " passivation" qui promettait en outre d'augmenter le prix du substrat de manière substantielle. J'ai alors décidé de concentrer nos efforts sur les prototypes de base sans passivation et de nous orienter vers une deuxième solution prometteuse permettant aussi de larges marges de fonctionnement. Elle consistait à coupler deux étages d'amplification de charge (Figure 1). En conservant un compteur MSGC simple au dessus duquel était assemblée une grille de multiplication d'électrons (GEM[19]: Gas Electron Multiplier), il était alors possible de faire fonctionner le compteur MSGC à des tensions plus faibles, éloignées des régimes "streamer", qui favorisent les décharges, affaiblissant les pistes qui finissent par rompre. Le détecteur MSGC+GEM était en cours d'études[20] à l'IReS en parallèle des milestones pour CMS.

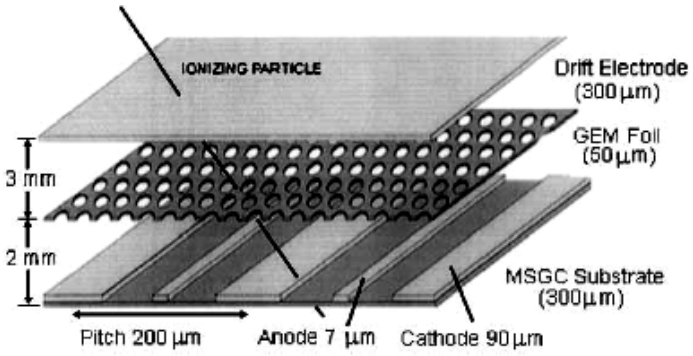

Figure 1: Schéma de principe d'un détecteur MSGC + GEM

Début 1999, les premiers prototypes "MF2", MSGC-baseline et MSGC+GEM ont été construits dans le cadre d'une collaboration de l'IReS avec IEKP-Karlsruhe et IIHE-Bruxelles. Quatre modules contenant 4 substrats MSGC de 512 canaux chacun et de longueur de piste de 10 cm, ont été soumis à un faisceau de pions de 350 MeV/c d'intensité atteignant 10kHz/mm^2 sur une surface de 10x10 cm^2. Au-delà de cette surface, l'intensité du faisceau était réduite d'un facteur 2. Tous les substrats MSGC étaient produits par l'IMEC[21]. Deux des modules testés étaient composés de substrats MSGC passivés "baseline", les deux autres équipés de substrats MSGC sans passivation et d'une grille GEM montée 2mm au dessus des compteurs MSGC. Les modules "baseline" n'ont pas donné les résultats escomptés perdant de plus en plus de pistes avec le temps. En revanche, un fonctionnement stable des modules MSGC+GEM a encouragé la collaboration "bouchon" à proposer la construction d'un milestone "MF2", MSGC+GEM,

[19] F.Sauli, NIM A386 (1997)531

[20] **Beam test results of a wedge-shaped MSGC + GEM detector at CERN,** Y. Benhammou *et al.*, **Nucl.Instrum.Meth.A441:452-458,2000**

[21] IMEC,KAPELDREEF 75,3001 Leuven, Belgique

aux rapporteurs du projet pour le LHCC. Basés sur les résultats et problèmes rencontrés par la collaboration Hera-B à DESY, nous avons décidé de construire deux modules MSGC+GEM supplémentaires et les soumettre au faisceau PSI en juin 1999. Deux mélanges de gaz ont été testés et ont confirmé que les régimes de fonctionnement des MSGCs au LHC seraient bien moins contraignants que ceux de Hera-B (un gain de $2.5x10^3$ est suffisant au LHC alors que Hera-B requérait un gain de $8\text{-}12x10^3$ pour utiliser le signal dans le déclenchement). A l'issue de ce test, la collaboration "bouchon" a imposé la combinaison MSGC+GEM comme milestone "MF2" pour la partie avant-arrière du trajectographe MSGC de CMS. La collaboration "tonneau" a maintenu le milestone tel que défini dans le TDR après le même test sous faisceau au PSI. J'ai présenté les résultats de ce test pour les deux collaborations à la conférence EPS[22] en juillet 1999.

Le ''milestone MF2''

Pour le milestone MF2 à PSI (au cours des mois d'octobre et de novembre 1999), des modules correspondant au deuxième anneau le plus interne ont été produits (10 cm de longueur de piste, 300μm d'épaisseur de verre, 7 μm de largeur de piste anode et 200 μm d'intervalle entre deux anodes). Trois compagnies différentes (IMEC, IMT[23] et OPTIMASK) ont produit au total 91 substrats. 72 substrats ont été sélectionnés pour construire 18 modules détecteurs MSGC+GEM, contenant chacun 4 substrats MSGC. Parmi ces modules, 17 ont été équipés de GEM produites au CERN et un seul d'une GEM produite par une firme allemande. La surface produite représente plus de $1m^2$ et près de 1% de la surface totale nécessaire pour le détecteur "bouchon" MSGC. Durant cinq semaines d'exposition au faisceau de pions de 350 MeV/c, aucun des problèmes observés par les détecteurs de Hera-B n'a été détecté. Le taux de décharges induites par les particules très ionisantes a été très modeste et le nombre de pistes perdues en résultant est resté très en dessous du plafond fixé pour un fonctionnement normal dans les conditions du LHC. L'extrapolation à dix ans de fonctionnement LHC indique que la perte anticipée de pistes peut engendrer une détérioration de la résolution spatiale inférieure à 4%. Il a aussi été démontré que le gain nominal pouvait être augmenté d'un facteur trois tout en restant dans un régime de fonctionnement stable. Au vu de ces résultats, les rapporteurs pour le LHCC ont donné un avis favorable à la technologie des MSGC+GEM pour le trajectographe de CMS.

La technologie Silicium ayant par ailleurs montré qu'elle devenait de moins en moins coûteuse, les instances de l'expérience CMS ont pris la décision de ne choisir qu'une seule technologie pour le trajectographe, celle du Silicium.

Le milestone MF2 a donné lieu à deux publications[24].

---

[22] **Status Report on Micro Strip Gas Chamber**, A. Zghiche, **Proceedings of the International Europhysics Conference on HEP'99, 15-21 July 1999, Tempere, Finland.**

[23] basée à Zurich

[24] **Robustness test of a system of MSGC+GEM detectors at the cyclotron facility of the Paul Scherrer institute.**
M. Ageron *et al.*, **Nucl.Instrum.Meth.A471:380-391,2001**
Experimental and simulation study of the behaviour and operation modes of MSGC + GEM detectors.
M. Ageron *et al.* 2002. **Nucl.Instrum.Meth.A489:121-139,2002**

VI. L'électronique de lecture et le système de contrôle du trajectographe de CMS

Un autre milestone défini après l'acceptation du TDR par le LHCC, est celui qui concerne l'électronique de lecture du trajectographe: le chip APV et les deux chaînes, analogique et de contrôle qui lui sont associées. Une horloge de 25 ns sera distribuée par le LHC afin de séquencer le déclenchement de la lecture des événements intéressants. Dans le cas de l'APV, l'horloge est transmise par l'intermédiaire d'une chaîne digitale de contrôle qui permet la synchronisation de tous les éléments du trajectographe de façon interne mais aussi avec les autres détecteurs de CMS. Les éléments du contrôle sont structurés en anneau, "ring", autour d'une interface de communication avec l'utilisateur. Chaque unité de l'anneau peut transmettre des messages à plusieurs composants de contrôle de l'APV. Les paramètres de fonctionnement de l'APV sont alors réglables à distance afin d'en permettre l'ajustement au cours des 10 années de prise de données au LHC. Le milestone consistait à rendre disponible tous les éléments des deux chaînes dans la version la plus proche de la version finale et d'en réaliser une intégration avec des détecteurs en Silicium. La période de test sous faisceau de muons ou de pions pulsé à 25ns et délivré par le CERN-SPS a été fixée au 12-24 mai 2000.

Je me suis intéressée à ce milestone dès le début de mon séjour au CERN dans le cadre d'un contrat d'associée scientifique (septembre 1999- août 2000). Plusieurs instituts ont collaboré à ce milestone: l'équipe de Micro-Electronique du CERN, l'INFN-Pise, le RAL-Londres, l'IC-Londres et l'IReS- Strasbourg. Le RAL et l'IC étaient impliqués dans la conception de l'APV et de son Chip de synchronisation, le PLL. L'APV25 conçu en technologie sub-micronique n'étant pas encore disponible pour les tests, nous avons utilisé l'APV6 non durci aux radiations pour le milestone. La version durcie aux radiations pour tous les autres composants de la chaîne électronique était prévue pour mi-2001. L'INFN- Pise a fourni les détecteurs Micro Strip Si. L'IReS était responsable de l'interface de communication avec l'APV6, le PLL, et les convertisseurs des signaux optiques en signaux électriques et vice-versa, utilisés dans le but de minimiser le bruit affectant les signaux qui traverseront une centaine de mètres de câble dans CMS avant d'atteindre la salle de comptage. Nous étions aussi responsables de l'interface de la base de données contenant les paramètres à transmettre à l'appareillage avec la librairie qui permet d'envoyer les messages jusqu'aux composants.
J'ai présenté les résultats du test sous faisceau du milestone à la conférence "Frontier Detectors for Frontier Physics[25] " qui a eu lieu à Elbe (du 21 au 27 mai 2000).

Le trajectographe de CMS est maintenant dans sa phase d'installation. Plusieurs groupes de travail ont été constitués pour mettre en place la procédure de qualification et d'assemblage des composants du trajectographe. L'IReS était entre autre, responsable de la conception et la réalisation de l'hybride de lecture frontal qui est connecté au détecteur Si et sur lequel APV, PLL et DCU sont intégrés. Pour la collaboration

[25] **Test of the CMS Microstrip Silicon tracker readout and control system.**
A. Zghiche *for the CMS TRACKER collaboration.* **Nucl.Instrum.Meth.A461:470-473,2001**Prepared for 8th Pisa Meeting on Advanced Detector: Frontier Detectors for Frontier Physics, La Biodola, Isola d'Elba, Italy, 21-25May 2000.

"bouchon", l'IReS s'était impliqué aussi dans la définition des tests "burn-in" qui réalisaient le cyclage en température des microstrip Si entre -20 et +40 degrés centigrades.

VII. Evolution des détecteurs micropattern gazeux

La multiplication des charges dans le gaz dite avalanche de Townsend est la caractéristique principale exploitée dans les détecteurs gazeux. Un des développements les plus réussis du siècle dernier est le compteur proportionnel multifils MWPC qui a réalisé la multiplication dans le gaz avec une résolution spatiale de l'ordre de 300 μm. G. Charpak[8] a été récompensé par le Prix Nobel en 1992 pour cette invention. Cependant, les expériences de physique des particules nécessitaient la conception de détecteurs de granularité élevée pour parvenir à de meilleures résolutions spatiales. Plusieurs développements ont été suggérés mais les techniques de fabrication n'étaient pas faciles à mettre en oeuvre à grande échelle. Lorsque A. Oed[9] a suggéré l'utilisation des techniques de microélectronique pour la fabrication des détecteurs gazeux MSGC, une multitude d'autres détecteurs a vu le jour. Une grande granularité de ces détecteurs est ainsi devenue possible, permettant des résolutions spatiales de l'ordre de quelques dizaines de μm et offrant une excellente résolution temporelle (de 100ns et jusqu'à 50ps pour certains développements) et une capacité de taux de comptage importante (jusqu`à des flux de 10^6 Hz/mm^2). Parmi les détecteurs les plus performants, on compte les microgap MGC[26], MICROMEGAS[27] et GEM[28]. Ces nouveaux détecteurs sont regroupés sous la dénomination de détecteurs micropattern gazeux et sont schématiquement représentés sur la *Figure 2*.

Structure	Name	Abbreviation
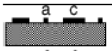	Micro Strip Gas Chamber	MSGC
	Small Gap (micro strip) Gas Chamber	
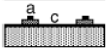	Micro Gap Chamber	MGC
	Compteur à Trous = Micro Well counter	CAT
	Micro Trench Gas Counter = Micro Groove	MGD
	Micro Dot Gas Avalanche Detector	
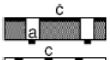	Micro Slit Gas Detector	
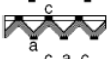	Micro Wire Detector	
	Micro Pin Array Detector	MIPA
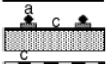	Micro Gap Wire Chamber	
	Capillary Plate Proportional Counter	
	Gas Electron Multiplier	GEM
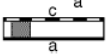	Micromesh Gaseous Structure	MICROMEGAS

Figure 2: Représentation schématique des détecteurs micropattern gazeux recensés par A.Oed[29]. Le plan de dérive (le plus souvent posé à 3-5mm au dessus) n'est pas représenté.

[26] F. Angelini et al., *Nucl .Instr. and Meth.,* **A335,** 69 (1993).
[27] Y. Giomataris et al., *Nucl. Instr. And Meth.,* **A376,** 29 (1996).
[28] F. Sauli, *Nucl. Instr. And Meth.,* **A386,** 531 (1997).
[29] A. Oed, *Nucl .Instr. and Meth.,* **A471,** 109 (2001).

Les détecteurs micropattern de la *Figure 2* peuvent être classés dans quatre catégories:

- les détecteurs micropistes, analogues dans leur fonctionnement aux MWPC comme les MSGC, SG[30], MGC, MSGD[31], MWD[32], MPAD[33] et les MGWC[34].

- les détecteurs à pixels (lecture 2D) comme les Micro Dot Gas Avalanche Detectors[35] (MDGAD)

- les détecteurs à trous comme les CAT[36], MGD, CPPC[37] et les GEM.

- les détecteurs fonctionnant sur le principe des plans parallèles comme les MICROMEGAS.

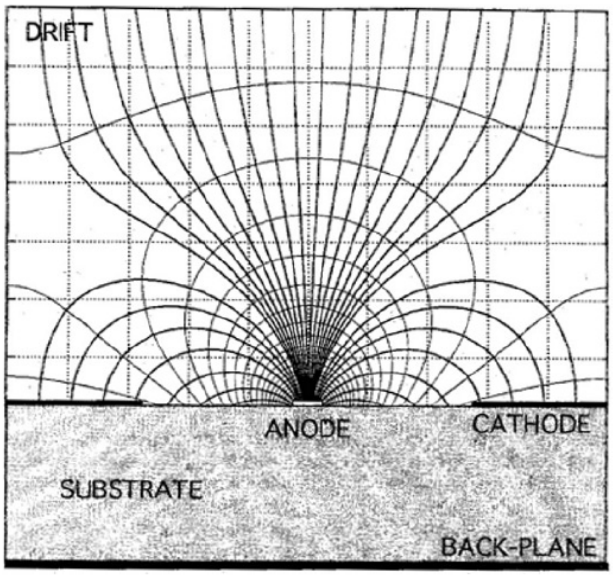

Figure 3: Lignes de champ électrique et équipotentielles dans un détecteur MSGC. La largeur de l'anode est de l'ordre de 10 μm.

VII.1. Les détecteurs de type Micropiste

Le détecteur MSGC en est exemple classique. Comme décrit précédemment, anodes et cathodes sont gravées par lithographie sur un substrat de verre de 300 μm

---

[30] G. Cicognani, et al., *Nucl. Instr. And Meth.,* **A416,** 263 (1998).
[31] J.C. Labbé, et al., *Nucl. Instr. And Meth.,* **A430,** 54 (1999).
[32] B. Adeva, et al., *Nucl. Instr. And Meth.,* **A435,** 402 (1999).
[33] P. Rehak ,et al., Proceedings of the International Workshop on MPGD, Orsay, June 1999.
[34] E. Christophel, et al., *Nucl. Instr. And Meth.,* **A398,** 195 (1997).
[35] D. Mattern, et al., *Nucl. Instr. And Meth.,* **A300,** 275 (1991).
[36] R. Bellazzin,i et al., *Nucl. Instr. And Meth.,* **A424,** 444 (1999). Et R. Bellazzini et al., *Nucl. Instr. And Meth.,* **A423,** 125(1999).
[37] H. Sakurai, et al., *Nucl. Instr. And Meth.,* **A374,** 431 (1996).

d'épaisseur. Avec des anodes de 10 μm de large gravées avec un pas de 200 μm et intercalées de cathodes de 100 μm, la résolution est au plus de 60 μm. Le volume gazeux est défini par le substrat et un plan de dérive placé 3 mm au dessus. Cette géométrie assure la formation d'un champ électrique intense à proximité de l'anode qui grâce à sa petite taille focalise les lignes de champ (voir ***Figure 3***). Les électrons primaires créés par un rayonnement externe traversant le volume de gaz sont accélérés par le champ électrique provoquant des ionisations secondaires. Au voisinage de l'anode, le phénomène d'avalanches de Townsend se produit. Les gains typiques réalisés sont de l'ordre 10^4. Plusieurs variantes de ce dispositif existent, par exemple les compteurs MGC, SG, MSGD, MWD, MPAD et les MGWC.

Les détecteurs MSGC souffrent essentiellement d'une limitation de gain due à l'accumulation de la charge sur le diélectrique: le verre. Cette accumulation de charge entraîne la réduction du champ électrique et une limitation du gain. Plusieurs solutions ont été proposées pour surmonter cette limitation. Le "coating" du verre avec des couches minces semi-conductrices, permettant un écoulement plus rapide des charges en est une. Une autre a été de réduire la surface de diélectrique entre les anodes et les cathodes. Les modèles MGC, SG, MSGD, MWD, MPAD et MGWC correspondent tous à cet objectif.

VII.2. Les détecteurs de type Microdot (Micropin)

Un détecteur microdot est une structure périodique de cathode et d'anode coaxiales. Comme pour les détecteurs micropistes, les anneaux sont déposés par lithographie sur un substrat diélectrique[35,38]. Les diamètres typiques des anneaux de la cathode et de l'anode sont 200μm et 20μm respectivement. Les gains typiques des détecteurs microdot sont de l'ordre de 10^4. Basés sur le principe des pixels, les détecteurs microdot permettent la détermination bidimensionnelle de la position (2D).

VII.3. Les détecteurs de type Compteurs À Trou (CAT et GEM)

Un détecteur CAT consiste en une feuille de diélectrique (Kapton) de 0.05-2 millimètres d'épaisseur métallisée sur les deux faces avec des trous de 0.1-2 millimètres de diamètre. Les premiers détecteurs CAT[39] ont été développés par un groupe du laboratoire LURE à Orsay. Ils ont aussi été étudiés et renommés WELL[40] par un groupe de l'université de Pise. Un détecteur WELL est constitué d'une feuille de Kapton de 50 μm d'épaisseur, métallisée sur les deux faces et "perforée" à raison d'un "puits" (la feuille de Kapton n'est pas trouée) de 35 μm de rayon tous les 120 μm. Les pistes anodes et cathodes sont gravées au préalable sur les deux faces métallisées avec un angle qui permet la détermination 2D de la position de passage des particules. La feuille est alors collée sur un support de circuit imprimé (PCB) lui assurant la rigidité mécanique. Des gains de l'ordre de 10^4 sont obtenus. Ces détecteurs présentent plusieurs avantages comparés aux détecteurs MSGC: ils sont fabriqués sur des

[38] S. Biagi et al., *Nucl. Instr. And Meth.,* **A366,** 76(1995).
[39] F. Bartol , et al., J. Phys. III, France 6 (1996)337
[40] R. Bellazzini, et al., *Nucl. Instr. And Meth.,* **A423,** 125(1999).

substrats en PCB ce qui réduit les contraintes mécaniques et le coût du détecteur. De plus la détermination bidimensionnelle de la position est possible.

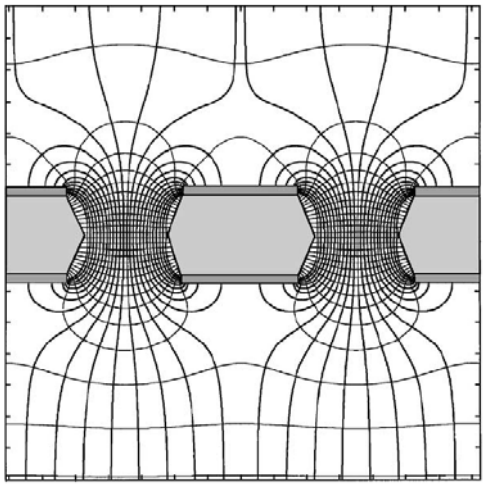

Figure 4: Lignes de champ électrique et équipotentielles dans un détecteur GEM. L'épaisseur de la feuille diélectrique (kapton) est de l'ordre de 50 à 100 μm.

Le détecteur GEM, développé par F. Sauli (voir Figure **4**), est le plus utilisé des détecteurs CAT. Il est aussi constitué d'une feuille de Kapton de 50 μm métallisée sur deux faces. Cette fois, la feuille est réellement perforée de trous de 100 μm de diamètre avec un pas de 140 μm. La feuille GEM est couplée à un plan de dérive classique ainsi qu'à un plan de lecture situé à 2-3 mm en dessous, le tout formant une enceinte étanche remplie d'un mélange de gaz. Le plan de lecture peut aussi bien être un détecteur MSGC qu'un plan PCB métallisé sur lequel est gravé un réseau de pixels pour une détermination bidimensionnelle de la position. Lorsqu'une différence de potentiel élevée est appliquée aux électrodes métalliques de la GEM, un champ électrique intense se crée à l'intérieur des trous (les lignes du champ électrique se focalisent dans chaque trou (voir Figure **4**)). L'amplification de la charge par le phénomène d'avalanche de Townsend se produit dans le voisinage du trou. Le gain mesuré est de l'ordre de 10^4. La collection du signal dans le détecteur GEM est reportée au plan de lecture, de ce fait plusieurs étages d'amplification de charge peuvent être empilés en superposant plusieurs plans de GEM au dessus du plan de lecture. Ainsi des mesures[41] effectuées avec trois plan GEM ont permis d'atteindre un gain de 10^6.

VII.4. Les détecteurs de type Plans Parallèles (MICROMEGAS)

Le détecteur micropattern le plus performant du type plans parallèles est le détecteur MICROMEGAS. L'élément principal dans ce détecteur est la grille appelée aussi "micromesh" de 3 à 5 μm d'épaisseur. Elle est tendue au dessus d'un plan de lecture en PCB métallisé, à une distance de 100μm. Le pas entre deux fils consécutifs

[41] F. Sauli, *Nucl. Instr. And Meth.,* **A477,** 1 (2002).

de la maille est de l'ordre de 50 μm. Les pistes du plan de lecture sont gravées avec un pas de 300 μm. Pour atteindre des gains typiques de 10^5, une tension de l'ordre 700 V est appliquée entre la maille et le plan de lecture. La Figure **5** représente les lignes de champ dans un détecteur MICROMEGAS. Le phénomène d'avalanche dans ce détecteur se situe entre la grille et le plan de lecture, à l'endroit où le champ électrique est le plus intense. Le principe du détecteur MICROMEGAS a été utilisé dans plusieurs applications. L'une d'entre elles est la chambre microgap à plans parallèles résistifs (MicrogapRPC). Il existe deux développements principaux dans cette direction : un détecteur "timing RPC"[42] et un détecteur RPC de haute résolution spatiale[43],[44]. Le "Timing RPC" conçu pour le TOF de l'expérience ALICE, est constitué de deux plans parallèles: un plan à une seule électrode cathode et un autre constitué de pistes anodes. Cathode et anodes ont une résistivité ρ de l'ordre de 10^9 à 10^{11} Ωcm. Le microgap ou espace entre cathode et anodes est de 100 à 400 μm, permettant de réaliser une excellente résolution temporelle de l'ordre de 50 picosecondes[42,43].

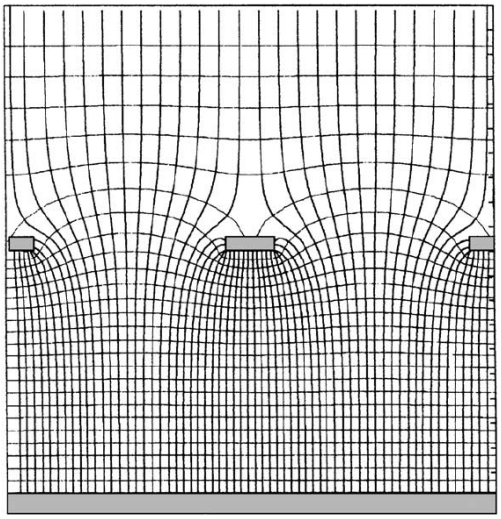

Figure 5: Lignes de champ électrique et équipotentielles dans un détecteur MICROMEGAS. La distance entre la grille et le plan de lecture est de l'ordre de 100 μm.

Les RPC de haute résolution spatiale sont quant à elles conçues avec une cathode de résistivité $\rho \sim 10^4$-$10^8 \Omega$cm (silicium, GaAs) et des anodes métalliques gravées sur un substrat en verre de résistivité $10^9 \Omega$cm, avec un pas de 50 μm. L'espace entre le plan des anodes et le plan cathode est de 100 à 400 μm, permettant de réaliser une excellente résolution spatiale, meilleure que 50 μm. Il faut souligner que ces détecteurs RPC fonctionnent à des gains et des flux équivalent à ceux des chambres à plans

[42] A. N. Akindinov, et al., *Nucl. Instr. And Meth.,***A533**, 74 (2004)
[43] P. Fonte, *IEEE Trans Nucl. ScL,* **49,** 881 (2002)
[44] I. Crotty et al., *Nucl. Instr. And Meth.,* **A505,** 203 (2003);

parallèles métalliques (PPAC). De plus, comme ils fonctionnent sans décharge, ils sont plus fiables.

VII.5. Les limitations de gain

Les détecteurs micropattern gazeux lorsqu'ils sont en régime de fonctionnement stable et optimisé, peuvent atteindre des gains maximum G_{max} de l'ordre de 10^4 à 10^5. C'est 10 à 100 fois moins que les gains obtenus avec les détecteurs à plans parallèles ou des compteurs proportionnels multifils classiques. Pourtant, ils ont été optimisés au prix de longues études systématiques des mélanges gazeux, des matériaux, et des conceptions de plus en plus complexes. Afin de comprendre cette limitation, il faut se pencher sur la physique de l'amplification des charges dans un volume gazeux. Le gain dans un détecteur gazeux est réglé par la limite dite de Reather, représentée par la zone hachurée sur la Figure **6**. Cette figure montre la variation du gain lorsque le détecteur est en régime stable (avalanche) en fonction du flux de particules ionisantes qui traversent le détecteur. Lorsque le gain du détecteur est élevé, la quantité d'ions présente dans le volume de gaz près des électrodes va modifier l'intensité du champ électrique et réduire le gain réel de fonctionnement. Cela explique la variation du gain en fonction du flux de particules chargées. Pour tous les types de détecteurs ainsi que pour la limite de Reather elle-même, le gain diminue lorsque la quantité de charge dans le gaz augmente. Pour un flux donné, la valeur du gain limite correspond au passage du régime d'avalanche au régime de décharges. Ainsi lorsque le gain augmente encore, la quantité d'ions dans le gaz forme un filament de plasma conducteur vers la cathode provoquant les décharges. Il faut cependant constater que les détecteurs micropattern gazeux sont loin de la limite de Reather. Les raisons de limitation du gain des détecteurs micropattern sont essentiellement liées aux conditions de fonctionnement pour lesquelles ils sont conçus. La première des raisons, est la recherche d'une grande granularité du détecteur pour l'adapter aux expériences de physique des particules. Le fait que les anodes et les cathodes soient rapprochées implique que le volume de gaz où se développent le champ intense et l'avalanche est réduit. L'accumulation des charges dans le volume gazeux autour des électrodes est très rapide et conduit au régime de décharge bien avant d'atteindre la limite de Reather. Pour fonctionner dans un régime stable de simples avalanches, il faut se limiter à des conditions de fonctionnement de gain plus faible. Cette raison est valable pour tous les détecteurs micropattern. On remarque cependant sur **Figure 6** que les détecteurs MICROMEGAS peuvent atteindre de meilleurs gains comparés aux autres micropattern. Ces derniers subissent une autre contrainte de conception dont les MICROMEGAS sont affranchis. C'est l'accumulation des charges en surface du diélectrique. Pour les détecteurs comme les MSGC, l'écoulement des charges sur la surface du diélectrique (le verre pour les MSGC) n'est pas optimal, cela conduit à une accumulation des charges encore plus rapide que celle due à la charge volumique. Le régime critique de décharges est atteint à des valeurs de gain encore plus faibles. Pour améliorer le fonctionnement des détecteurs micropattern gazeux construits avec des diélectriques deux solutions ont été proposées: couvrir les diélectriques avec des couches minces semi-conductrices (en passant de la résistivité de verre 10^{16} Ωcm à 10^9 Ωcm pour certains dispositifs) ou réduire la quantité de diélectrique entre les électrodes comme pour les détecteurs MGC, SG, MSGD, MWD, MPAD et MGWC. Pour les MGC, on constate que même si le régime stable se produit à un faible gain, le

fait qu'il y a moins de diélectrique entre les anodes et les cathodes permet de conserver le même gain à hauts flux. La même remarque peut être faite pour les MSGC de 1mm de pas par rapport aux MSGC de 0.2 mm. Le fonctionnement à bas flux permet aux premières de fonctionner à haut gain, mais à haut flux ce gain subit une réduction plus rapide due au fait que l'accumulation de charge se fait sur une plus grande surface de diélectrique.

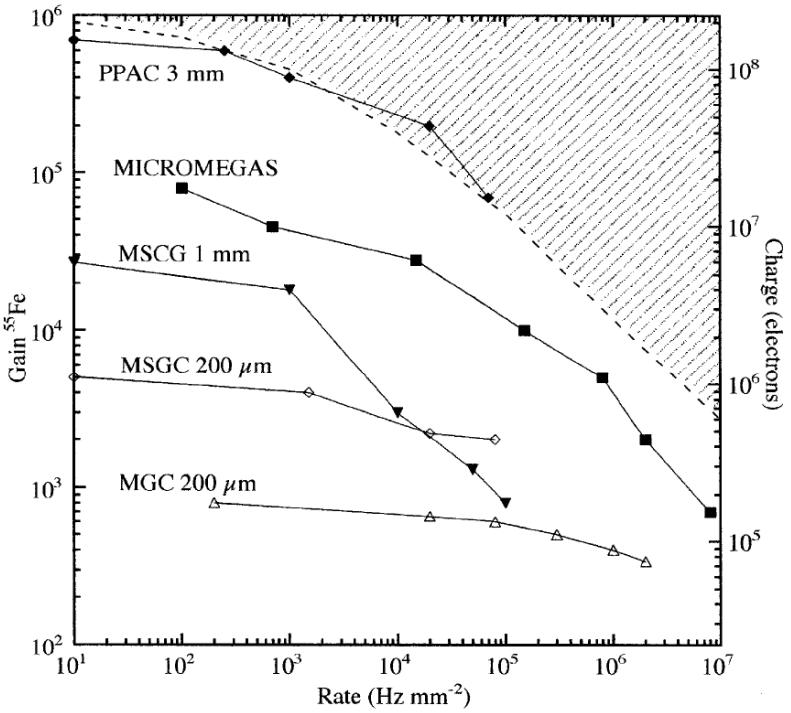

Figure 6: Gain maximum pour des conditions de fonctionnement stable en fonction du flux pour différents détecteurs micropattern gazeux. La zone hachurée correspond à la zone inaccessible par ces détecteurs.

Pourquoi dans la plupart des détecteurs micropattern décrits ici, le régime de décharges est-il à éviter? Ceci est de nouveau imposé par la nature granulaire du détecteur qui implique de très petites tailles d'électrodes. Lorsque le détecteur fonctionne dans un régime de gain élevé, il se produit des décharges entre anodes et cathodes, accélérées le plus souvent par des irrégularités dans la structure (pointes) de la cathode: des points de faiblesse se créent alors sur l'anode qui finit par rompre. Pour repousser le régime de décharges destructrices à des valeurs de gains critiques plus élevées, plusieurs solutions ont été proposées et associées telles que le recouvrement des bords de cathodes (MSGC passivés) ou l'utilisation d'électrodes résistives pour empêcher les décharges (RPC). Concernant les détecteurs GEM, le test sous des flux de l'ordre de 4 kHz/mm^2 a permis de montrer que, lorsqu'ils sont associés aux MSGC, des gains de l'ordre de 2x10^4 sont réalisables dans un régime de fonctionnement stable.

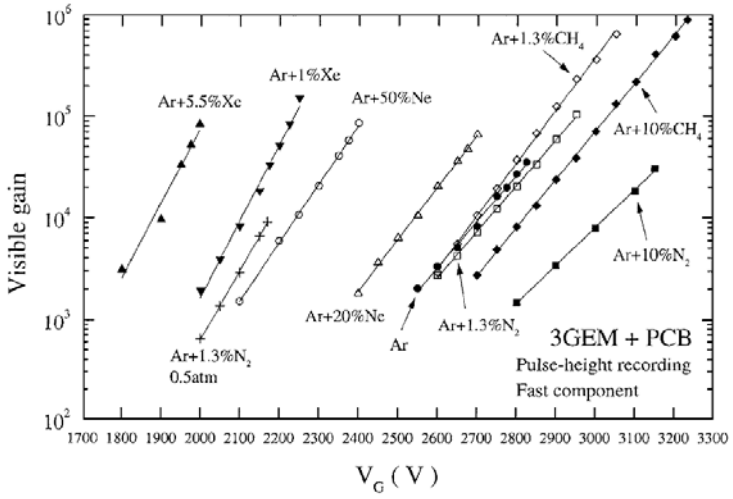

Figure 7: Gains en fonction du voltage total pour l'empilement de trois détecteurs GEM avec différents mélanges de gaz.

VII.6. Perspectives

Toutes les solutions proposées ici concourent à permettre le fonctionnement des détecteurs micropattern gazeux dans un environnement comme celui du LHC, où la granularité pour la résolution spatiale et la robustesse aux hauts flux et aux particules très ionisantes (issues des réactions nucléaires), sont nécessaires. Certaines sont néanmoins difficiles à mettre en œuvre et augmentent le coût final du détecteur. Les détecteurs micropattern gazeux les plus prometteurs aujourd'hui sont le GEM et le MICROMEGAS. L'empilement possible de plusieurs plans GEM et leur couplage à un seul plan de lecture permet d'atteindre des très forts gains jusqu'à 10^6 (voir Figure **7**), chaque étage fonctionnant avec des gains modérés loin du régime de décharges. Parmi les expériences qui ont équipé leur détecteur avec des micropattern GEM on peut citer l'expérience Hera-B[45] (physique du B avec collision d'électrons et de protons à DESY) et l'expérience COMPASS[46] (Mesure des composantes du spin du nucléon au CERN).

Les MICROMEGAS du fait de leur robustesse et de la possibilité d'une fabrication industrielle facile ont aussi été sélectionnés pour équiper plusieurs expériences telle que COMPASS et plus récemment, la TPC du détecteur proche (hors-axe) de l'expérience d'oscillations de neutrinos T2K[47] (J-PARC au Japon). Les MICROMEGAS sont aussi de très bons candidats pour calorimètre hadronique du détecteur prévu auprès du prochain accélérateur linéaire ILC[48].

Le développement des plans de lecture pour une détermination bidimensionnelle de la position a été réalisé en phase avec celui des micropatterns.

[45] T.Hott, *Nucl. Instr. And Meth.,* **A408,** 258 (1998);
[46] L. Schmitt, The COMPASS Experiment, Proceedings of ICHEP98, Vancouver,1998
[47] M. Zito, http://nuspp.in2p3.fr/TPC/temp/tpcmm26apr2006r.pdf
[48] C. Adloff, contribution to International Linear Collider (ILC) Workshop (ILC-ECFA and GDE Joint Meeting) Valencia, 6-10 November 2006

Sur la Figure **8**, une radiographie X du membre inférieur d'un petit mammifère est obtenue avec un détecteur micropattern double GEM et un plan de lecture bidimensionnelle (obtenue avec des pistes croisées) construit avec la même technologie. De nombreuses applications médicales de ce type de dispositif sont en cours de développement[49]. Dans le but d'améliorer la granularité limitée par l'encombrement de sortie des signaux, d'autres développements ont été entrepris. Le plus innovant est celui où le plan de lecture du GEM est une puce CMOS de 15x15 mm^2 composée de 105 10^3 pixels avec un pas de 50 μm, chaque pixel est relié à un amplificateur de charge et à un circuit de mise en forme[50]. Ce sont les détecteurs micropattern GEM de l'expérience XEUS (expérience ESA embarquée dans l'espace prévue pour 2015) qui en bénéficieront.

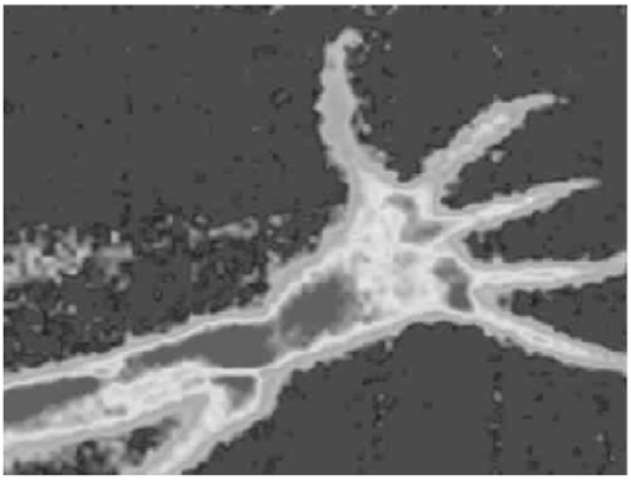

Figure 8: Radiographie X du membre inférieur d'un petit mammifère obtenue avec un détecteur micropattern double GEM et un plan de lecture bidimensionnelle.

Conclusion

Après cette expérience enrichissante dans le domaine de l'instrumentation, j'ai voulu me confronter aux analyses de données dans les expériences de physique des particules. En janvier 2001, j'ai rejoint le LAPP et la collaboration BaBar.

[49] C. Iacobaeus, et al., *Nucl. Instr. And Meth.,* **A525,** 258 (2004);
[50] R. Bellazzini, et al., *Nucl. Instr. And Meth.,* **A566,** 552 (2006);

VIII. L'expérience BaBar

Le LAPP participe à l'expérience BaBar[51] depuis la formation de la collaboration en 1993. Aujourd'hui, soixante douze instituts contribuent à BaBar (Allemagne, Italie, France, Royaume Uni, Canada, Etats-Unis, Chine, Russie, Norvège) parmi lesquels cinq laboratoires français (LAPP- Annecy, LAL Orsay, LPNHE Ecole Polytechnique Palaiseau, LPNHE Universités Paris VI et VII, CEA-DAPNIA Saclay).

La violation de CP mise en évidence pour la première fois en 1964, reste encore un phénomène difficile à étudier. Elle n'avait été observée que dans le système du K^0. Kobayashi et Maskawa ont montré que le modèle standard à trois familles de quarks prédit, par un mécanisme naturel, la violation de CP; des asymétries mesurables, liées à la violation de CP, devraient se manifester dans certaines désintégrations rares des mésons B^0 vers un état propre de CP. L'expérience BaBar, installée sur l'anneau PEP II à SLAC, étudie la violation de CP dans le système des mésons B. Les effets prédits par le modèle standard sont importants et expérimentalement mesurables. L'expérience est capable de mesurer les côtés et les angles (α, β et γ) du triangle d'unitarité (représentation graphique de la matrice CKM de mélange des quarks) dans un grand nombre de canaux, et ainsi de mettre à l'épreuve les prévisions du modèle standard. Les premières collisions $e^+ e^-$ ont été enregistrées à la fin du mois de mai 1999. Depuis cette date, les performances de l'accélérateur n'ont cessé de s'améliorer. A la fin août 2006, la luminosité intégrée enregistrée par l'expérience s'élevait à plus de 390 fb^{-1} dont 350 fb^{-1} à la résonance Y(4S) correspondant à plus de 385 millions de désintégrations $e^+e^- \rightarrow \Upsilon(4S) \rightarrow B\overline{B}$. Aux conférences de l'été 2001, BaBar avait pu présenter la première observation significative de la violation de CP dans le secteur des B, avec une mesure de $\sin(2\beta)=0.59\pm0.14(stat.)\pm0.05(syst.)$. Cet été, le résultat présenté à ICHEP2006 est affiné à $\sin(2\beta) = 0.710 \pm 0.034(stat.) \pm 0.019(syst.)$ avec une luminosité intégrée de 316 fb^{-1}. Le groupe du LAPP a construit et est responsable du système de gaz qui alimente la chambre à dérive. Il a également construit une petite chambre permettant de mesurer en ligne le gain du mélange gazeux utilisé. Il a joué un rôle important dans l'installation des différents logiciels de l'expérience au CCIN2P3.

Ce rôle s'est poursuivi jusqu'en fin 2004 avec l'importation massive des données, la transformation du CCIN2P3 en centre de calcul BaBar (Tier A) ainsi que les développements liés au projet GRID (grille de calcul) appliqué à BaBar. Depuis le démarrage de l'expérience, le groupe participe à la prise de données et à la vie de la collaboration, avec plusieurs séjours de longue durée à SLAC. C'est l'analyse des données qui est devenue l'activité la plus importante du groupe BaBar LAPP, avec la reconstruction exclusive des désintégrations hadroniques des mésons B, la reconstruction des désintégrations charmées du second méson B avec le premier méson B complètement reconstruit et la reconstruction des désintégrations rares.

Dans ce cadre, j'ai largement participé à la transformation du centre de calcul CCIN2P3 en Tier A en élaborant les outils automatiques de distribution des données. Mon activité

[51] B. Aubert *et al., Nucl. Instr. And Meth., A479, (2002)*1-116

d'analyse principale aujourd'hui concerne le volet de la reconstruction des désintégrations charmées du second méson B avec le premier méson B complètement reconstruit. C'est une méthode d'analyse originale qui permet de s'affranchir, en grande partie, du bruit de fond dans le calcul des rapports d'embranchement des désintégrations charmées du méson B. Elle a déjà permis la détermination plus précise du taux de charme dans la désintégration du méson B (Thèse de F. Couderc soutenue le 06 avril 2005). Elle permettra la détermination plus précise d'autres rapports d'embranchement tel que B en $X\pi$, en ***X Kaon*** et en ***X proton n***π. Je participe aussi à la prise de données sur site à SLAC ainsi qu'aux réunions de la collaboration qui sont au nombre de cinq par an et sont organisées soit à SLAC soit dans le pays de l'un des autres instituts de la collaboration. Elles ne nécessitent pas toujours un déplacement puisqu'elles peuvent aussi avoir lieu par téléphone.

VIII.1. Calcul et traitement des données

Dans le but de minimiser les coûts d'exploitation et de faciliter l'accès aux données, la collaboration BaBar a redéfini son modèle de calcul au cours de l'été 2000. Ce modèle repose sur une stratégie de calcul distribué ou ''multi-Tier'' similaire à celle adoptée pour les expériences LHC. Les Tier-A reçoivent une fraction importante des données dans un format détaillé, les Tier-B reçoivent l'ensemble des données dans un format réduit et les Tier-C correspondent typiquement aux universités et petits instituts travaillant localement sur un ensemble réduit de données. La collaboration BaBar a prévu 3 ou 4 Tier-A possédant tous ensemble la totalité des données détaillées. Le centre de calcul de Lyon CCIN2P3 a joué un rôle pionnier et assure depuis le début 2001 la fonction de premier Tier-A en dehors de SLAC.

J'ai été amenée à apprendre la programmation en langage PERL pour développer les outils qui permettent aujourd'hui l'extraction automatique des données et leur importation dans les différents Tier. Les données de BaBar sont réparties sur quatre grandes fédérations ou super-fédérations elles-mêmes sub-divisées en plusieurs fédérations. Deux super-fédérations sont dédiées aux données réelles (détaillées et réduites), deux autres aux données simulées (détaillées et réduites). Au fur et à mesure de l'accumulation des données, le nombre de fédérations sous-jacentes augmente. Les outils d'extraction de données que j'ai développés sont en mesure de détecter la création d'une nouvelle fédération, ou le dépôt de nouvelles données dans une fédération déjà existante. Il est possible d'extraire une base de données unique en spécifiant son numéro, comme il est possible d'extraire une fédération entière de bases de données. Les paramètres de l'extraction sont détaillés dans un fichier de configuration général. Un deuxième fichier de configuration permet de modifier ces paramètres selon les besoins de l'utilisateur ou du Tier. Ces outils offrent ainsi des fonctionnalités diverses qui permettent l'importation des données par le réseau via une simple requête envoyée par e-mail, en spécifiant un minimum de paramètres.

Depuis l'été 2001, les données du Tier-A sont automatiquement importées grâce à ce développement, et l'ensemble de la collaboration a ainsi la possibilité de calculer au CCIN2P3. Plusieurs analyses complètes ont été menées entièrement en France par des physiciens basés à l'étranger. En 2001, ce sont 15 Téra Octets(TO) de données qui ont été importées au CCIN2P3. Ce nombre s'est accru pour atteindre 100TO/an dès l'année 2003.

J'ai réalisé ce travail en collaboration avec un chercheur du LAPP, Dominique BOUTIGNY, qui m'a initiée aux technologies de pointe telles que les bases de données orientées objet (OBJECTIVITY), les systèmes de stockage hiérarchique (HPSS) et les réseaux longue distance à haut débit.

Le modèle de calcul de l'expérience BaBar évoluera naturellement vers une grille qui permettra d'exporter le code exécutable vers l'emplacement des données, en fonction de la requête de l'utilisateur.

VIII.2. Analyses

VIII.2.1. Détermination du taux de charme avec les mesures inclusives des désintégrations des mésons B^- et B^0 en mésons D et D_s et baryons charmés Λ_c et Ξ_c

Les désintégrations charmées et semi-leptoniques des mésons ***B*** ont été très étudiées dans le passé, en particulier avec les expériences du LEP et de Cornell (CLEO). Les mesures disponibles dans ces deux domaines sont devenues suffisamment précises pour les confronter aux modèles théoriques qui relient le taux de charme au taux d'embranchement semi-leptonique. Le taux de charme est le nombre moyen de quarks ***c*** et $\bar{c}$ produits par la désintégration du quark ***b*** (n_c= nombre de quarks charmés produits/nombre de désintégrations de ***B***). Le taux d'embranchement semi-leptonique est le nombre moyen d'électrons produits directement par la désintégration d'un quark ***b***. Il a été déterminé théoriquement en incluant les corrections QCD intervenant dans le calcul des masses des quarks. Le résultat dépend de l'échelle de renormalisation choisie et du rapport des masses des quarks ***c*** et ***b***. Le taux de charme déterminé à partir du taux semi-leptonique théorique s'étale sur une plage allant de 1.12 à 1.31. Si c'est la moyenne mondiale expérimentale du taux semi-leptonique qui est utilisée alors le domaine de variation du taux de charme va de 1.1±0.12 à 1.28±0.05 (la valeur du taux de désintégration semi-leptonique mesurée par BaBar est B_{sl}=10.83±0.16±0.06% (valeur en 2004) et la moyenne mondiale aujourd'hui est de B_{sl}=10.81±0.14% (incluant les valeurs à jour de BaBar)). Dans le plan (B_{sl}, n_c) l'amélioration de la précision sur la mesure des deux variables contraindra l'échelle de renormalisation et le rapport des masses de quarks ***b*** et ***c***. Elle contraindra aussi les ordres supérieurs des corrections QCD intervenant dans le calcul des masses des quarks.

Avec les mesures des rapports d'embranchement des désintégrations charmées du méson ***B***, une détermination directe du taux de charme est possible. Pour déterminer directement le taux de charme il y a deux méthodes:

- la première consiste à sommer les multiplicités de tous les hadrons charmés produits dans les désintégrations des B^0 et des B^+. Avec cette méthode, le taux de charme en $D^0 + \bar{D}^0$ est connu à 4,4%, celui en $D^{\pm}$ à 8.7%, celui en $D_s^{\pm}$ à 25%, celui en $\Lambda_c^{\pm}$ à 34% et celui en Ξ_c à 50%. De plus, les taux de charme en états charmonia ($c\bar{c}$) qui doivent être

comptés deux fois, ne sont pas connus à mieux que 20%. La somme ainsi calculée donne n_c=1.13±0.05.

- la seconde méthode utilise la notion de hadron charmé de charme anti-corrélé; il provient de la désintégration du $W^+ \to c\bar{s}$, celui de charme corrélé étant produit dans la désintégration du quark $\bar{b}$: $\bar{b} \to \bar{c} W^+$. $\mathbf{n_c}$ est égal à l'unité augmentée du taux de charme de charme anti-corrélé et diminuée du taux de transitions rares (celles qui ne donnent pas de charme et qui sont négligées). Les mesures les plus précises (avant notre analyse) du taux de charme de charme anti-corrélé donnaient la valeur 0.23, et permettaient de calculer ainsi le taux de charme total de manière indépendante : n_c = 1.23±0.04.

Les deux méthodes donnent des valeurs pour le taux de charme dans la désintégration du méson ***B*** compatibles avec les résultats de LEP et SLD (n_c =1.23±0.04). Il était toutefois nécessaire de déterminer de manière plus précise la contribution des mésons ***D*** de charme anti-corrélé car la moyenne mondiale pour le taux inclusif de ces mésons ***D*** est 8.1±2.5%. Dans BaBar, le groupe du LAPP en avait déjà mesuré une partie avec les modes de désintégration exclusifs $D\bar{D}K$, qui produisent des mésons ***D*** de charme anti-corrélé, avec un rapport d'embranchement de 3.54 ±0.51%[52].

Lorsque j'ai commencé mon travail d'analyse sur le taux de charme en collaboration avec Robert Barate et le groupe BaBar du LAL Orsay, la luminosité intégrée disponible était de 50.8 fb^{-1}. Nous voulions mesurer le taux inclusif de mésons et baryons charmés de charme anti-corrélé. La méthode consistait à reconstruire totalement un premier ***B*** et à rechercher un méson ou un baryon charmé dans le reste de l'événement, puis à étiqueter ce hadron comme charme corrélé ou comme charme anti-corrélé selon sa charge par rapport à la charge du second ***B*** qu'on appelle B_{recul}. Les mesures des taux inclusifs de hadrons charmés de charme anti-corrélé nécessitent de grands échantillons de mésons ***B.*** Notre première étude portait sur les mésons ***D*** (neutres ou chargés) pour démontrer la faisabilité de l'analyse***.*** La question des autres hadrons charmés (D_s, Λ_c ***et*** Ξ_c) a été abordée plus tard.

VIII.2.2. Etude préliminaire de la production des mésons *D* dans la désintégration des mésons *B*

Nous avons effectué deux analyses complètement indépendantes, la première au LAL et la seconde au LAPP sur un échantillon de données qui correspondait à la luminosité intégrée de 50.8 fb^{-1}.

Le groupe du LAL a construit sa propre collection réduite d'événements contenant des listes de ***B*** et de ***D*** déjà reconstruits et a utilisé simplement la corrélation de signe entre le ***B*** et le ***D***.

[52] Etude des désintégrations doublement charmées des mésons B avec l'expérience BaBar, Patrick ROBBE (BaBar LAPP Annecy)**,** Thèse de Doctorat en Sciences de l'Université de Savoie (avril 2002).

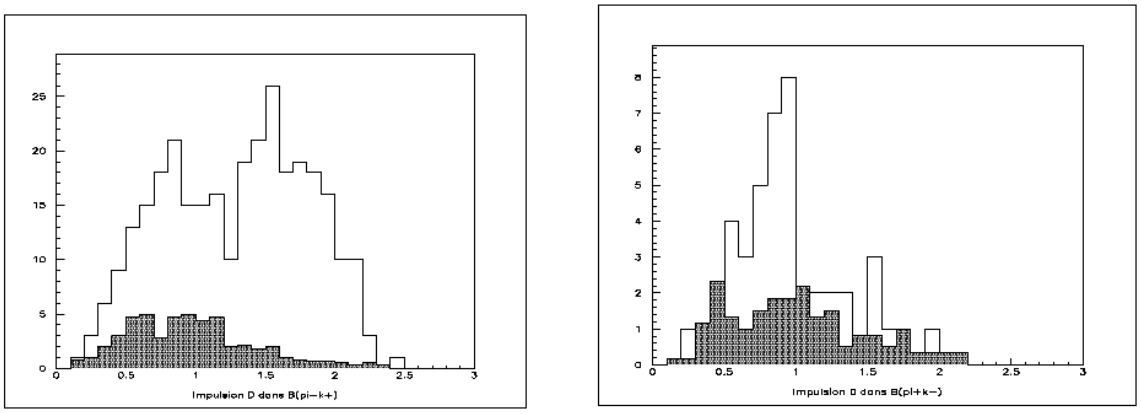

Figure 9: spectres d'impulsion dans le référentiel du B_{recul} des mésons D (reconstruits en mode $K\pi$) de charme corrélé (gauche) et charme anti-corrélé (droite) obtenus pour les données réelles et pour les B chargés (avec 50.8 fb^{-1}). Le spectre hachuré correspond au fond combinatoire.

Au LAPP, nous avons utilisé une collection déjà réduite d'événements très purs pour lesquels le premier méson B était reconstruit, les paramètres du B_{recul} sont alors calculés à partir de ceux des faisceaux et du premier *B*. J'ai ensuite reconstruit les mésons *D* dans le reste de l'événement. J'ai ainsi obtenu [53.14,54] les spectres d'impulsion des *D* de charme corrélé et charme anti-corrélé dans le référentiel du B_{recul} qui se désintègre en donnant ce *D* pour 50 fb^{-1} de données et pour les B chargés (voir *Figure 9)*. Les formes des deux spectres sont très différentes et traduisent bien la différence des processus mis en jeu. C'était la première fois que ces spectres pouvaient être obtenus avec une telle résolution (les autres mesures étaient faites dans le référentiel du *Y(4S)* et non du B_{recul}) et une telle séparation entre et charme anti-corrélé (les autres expériences utilisaient au mieux la corrélation avec le signe du lepton opposé et étaient polluées par les oscillations B^0B^0 alors que nous pouvons n'utiliser que les B chargés). Les résultats des deux analyses étaient en accord pour les rapports d'embranchement inclusifs qui ont été calculés à partir d'un signal corrigé du fond et renormalisé par l'efficacité de reconstruction du méson *D*. Cette dernière a été obtenue à partir de données simulées par Monte Carlo. Les résultats sont rapportés dans une note BaBar. A titre d'exemple, la fraction de D^0 de charme anti-corrélé a été mesurée avec une précision de 22,5% dans la désintégration d'un méson *B* chargé, démontrant la faisabilité de l'analyse.

[53] A.ZGHICHE, Présentation à la réunion de collaboration BaBar à Victoria (Canada) 6 mai 2002, http://www.slac.stanford.edu/BFROOT/www/Organization/CollabMtgs/2002/detMay2002/Tues1f/Tues1f.html. Les références 53.x se rapportent au transparent numéro x de ce fichier

[54] D meson Production in B Decays, S. PLASZCZYNSKI, M-H SCHUNE, R BARATE and A. ZGHICHE, BaBar Analysis Document BAD #407

VIII.2.3. Elargissement de la sélection des mésons B

L'analyse décrite ci-dessus souffrait de la faible statistique de mésons B complètement reconstruits. En plus de l'augmentation de statistique qui est venue avec le temps, ce nombre a pu être augmenté en relâchant les critères de sélection et en utilisant d'autres modes de désintégration. Seuls les modes de désintégration en $D^{(*)}\pi$ des mésons B ont été reconstruits dans l'échantillon initial. Nous avons décidé la production d'un nouvel échantillon de données à partir d'abord de 90 puis 230 millions d'événements $B\bar{B}$. Les critères de sélection pour le mode $D^{(*)}\pi$ ont été élargis et les modes de désintégration du méson B en $D^{(*)}\rho$ et en $D^{(*)}a_1$ ont été ajoutés. J'ai effectué cette production qui est un travail long et fastidieux. Les premières analyses du nouvel échantillon ont montré que le gain en statistique est important[55]. Une étude de la pureté de cet échantillon d'événements a été conduite en utilisant des coupures sur des variables telles que le ΔE (différence entre l'énergie reconstruite et l'énergie du faisceau) et le m_{ES} (l'énergie du faisceau est substituée à l'énergie reconstruite dans le calcul de la masse invariante) ainsi que les masses des mésons D et D^* pour effectuer une première réjection puis sur d'autres variables telles l'identification du méson K qui compose le méson $D^{(*)}$, la probabilité qu'ont les traces des composants du méson $D^{(*)}$ à constituer un vertex ou encore sur les distributions angulaires. Quatre sélections en fonction de la pureté des événements (40, 55, 70 et 80%) ont ainsi été définies permettant d'effectuer les mesures de rapports d'embranchement en fonction du fond correspondant à chaque sélection et d'optimiser les incertitudes statistiques et systématiques.

Avec l'élargissement de la sélection toutes les mesures concernant les taux inclusifs de mésons et de baryons charmés ont été effectuées avec le premier échantillon de données de 90 millions d'événements $B\bar{B}$ puis mises à jour avec celui de 230 millions d'événements $B\bar{B}$.

VIII.2.4. La production de mésons D_s par la désintégration des mésons B

Jusqu'à notre analyse, seul le rapport d'embranchement inclusif $B \to D^{\pm}_s X$ était mesuré, sans distinction entre B^0 et B^+ et entre charme corrélé et charme anti-corrélé pour le D_s. On faisait l'hypothèse que les mésons D_s ($c\bar{s}$) étaient essentiellement produits par la désintégration du W($\bar{b} \to \bar{c}W^+ \to \bar{c}c\bar{s}$) et étaient donc de charme anti-corrélé.

Notre méthode permet la détermination du rapport d'embranchement inclusif et du spectre d'impulsion du D_s en séparant charme corrélé et charme anti-corrélé. Avec un échantillon de données correspondant à la luminosité de 50.8fb^{-1}, le résultat préliminaire[55,56] obtenu pour le rapport d'embranchement inclusif de charme anti-corrélé $B^+ \to D^+_S X$ était compatible avec la moyenne mondiale. Il nécessitait cependant une plus grande statistique afin de contribuer au calcul du taux de charme.
Il est important de noter que dans cette première approche,

[55] Fabrice Couderc, Rapport de stage effectué au LAPP dans le cadre du DEA de physique théorique Rhône-Alpin (septembre 2002).
[56] http://www.slac.stanford.edu/BFROOT/www/Organization/CollabMtgs/2002/detSep2002/Wed3a/Collab-Sep02-BReco.pdf
(A. Zghiche, présentation à la réunion de collaboration BaBar, Londres, septembre 2002)

- le méson D_s n'était reconstruit que dans le mode $KK\pi$ avec un rapport d'embranchement de 4.4±1.2%, et l'efficacité de reconstruction du méson D_s a été évaluée à l'aide des données simulées comme dans le cas des mésons D.
- le bruit de fond était faible grâce à cette nouvelle méthode qui permet de s'en affranchir en grande partie.

VIII.2.5. La production de baryons Λ_c et Ξ_c par la désintégration des mésons B

Avec un nombre plus élevé de B complètement reconstruits, les mesures des taux inclusifs et des spectres d'impulsion des baryons charmés Λ_c de charme corrélé et de charme anti-corrélé dans le référentiel du B_{recul}, sont aussi possibles. J'ai présenté les résultats préliminaires de cette étude avec la statistique de la fin 2002 (82fb^{-1}~90Millions événements B$\bar{B}$) lors de la réunion de collaboration de l'expérience BaBar en février 2003[57] . J'y ai montré la contribution des baryons Λ_c de charme corrélé séparée de celle des Λ_c de charme anti-corrélé, celle-ci étant évaluée pour la première fois. Elle provient de la désintégration du méson B→ Λ_c Ξ_c comme le montre le diagramme de droite de la ***Figure 10***. Cette figure montre aussi que la production d'un baryon Λ_c de charme anti-corrélé est accompagnée de celle d'un baryon Ξ_c de charme corrélé. Le taux de production inclusif des baryons Ξ_c de charme corrélé est ainsi évalué égal au taux inclusif de production des baryons Λ_c de charme anti-corrélé. La contribution des baryons Ξ_c de charme anti-corrélé a été négligée (voir la référence). J'ai ainsi montré la faisabilité de la détermination du taux de charme dans la désintégration du méson B en mesurant les rapports d'embranchement inclusifs de production de mésons et de baryons charmés avec notre méthode.

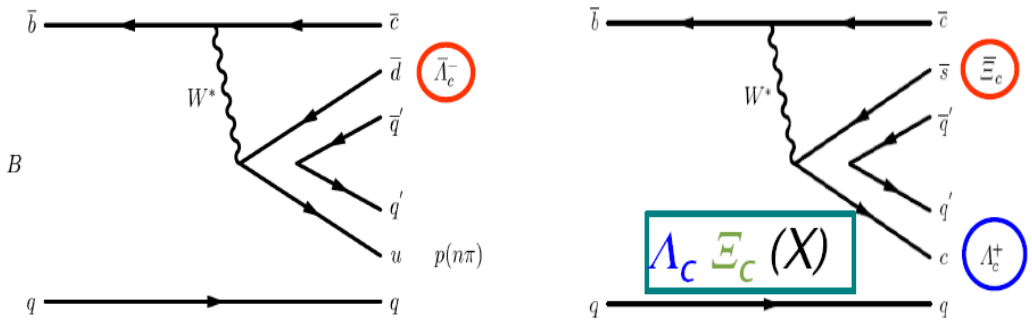

Figure 10: diagrammes de production des baryons Λ_c de charme corrélé (gauche), Λ_c de charme anti-corrélé (droit) et Ξ_c de charme corrélé(droit) par la désintégration du méson B.

57 http://www.slac.stanford.edu/BFROOT/www/Organization/CollabMtgs/2003/detFeb2003/Wed4d/zghiche.pdf (présentation à la réunion de collaboration BaBar, SLAC, février 2003)

VIII.2.6. Détermination du taux de charme avec les mesures inclusives des désintégrations des mésons B^- *et* B^0 en mésons D et D_s et baryons charmés Λ_c, *et* Ξ_c

X_c	Correlated $\mathcal{B}(B^- \to X_c X)(\%)$	Anticorrelated $\mathcal{B}(B^- \to \overline{X}_c X)(\%)$
D^0	$79.3 \pm 2.5 \pm 4.0^{+2.0}_{-1.9}$	$9.8 \pm 0.9 \pm 0.5^{+0.3}_{-0.3}$
D^+	$9.8 \pm 1.2 \pm 1.2^{+0.8}_{-0.7}$	$3.8 \pm 0.9 \pm 0.4^{+0.3}_{-0.3}$
D_s^+	$0.5 \pm 0.6 \pm 0.2^{+0.2}_{-0.1}$	$14.3 \pm 1.6 \pm 1.5^{+4.9}_{-3.0}$
	<2.2 at 90% C.L.	
Λ_c^+	$3.5 \pm 0.8 \pm 0.3^{+1.3}_{-0.8}$	$2.9 \pm 0.8 \pm 0.3^{+1.1}_{-0.6}$

Tableau 1: Contributions au taux de charme de chaque hadron X_c obtenues pour les mésons B chargés. La première colonne de résultats correspond à la contribution de charme corrélé, la seconde à celle de charme anti-corrélé. La première incertitude est statistique, la deuxième est systématique et la dernière correspond aux incertitudes sur les rapports d'embranchement des modes utilisés pour reconstruire les hadrons.

X_c	Correlated $\mathcal{B}(\overline{B}^0 \to X_c X)(\%)$	Anticorrelated $\mathcal{B}(\overline{B}^0 \to \overline{X}_c X)(\%)$
D^0	$51.1 \pm 3.1 \pm 2.5^{+1.3}_{-1.3}$	$6.3 \pm 1.9 \pm 0.5^{+0.2}_{-0.2}$
D^+	$39.7 \pm 3.0 \pm 2.8^{+2.8}_{-2.5}$	$2.3 \pm 1.8 \pm 0.3^{+0.2}_{-0.2}$
		<5.1 at 90% C.L.
D_s^+	$3.9 \pm 1.7 \pm 0.4^{+1.3}_{-0.8}$	$10.9 \pm 2.1 \pm 0.8^{+3.8}_{-2.3}$
	<8.7 at 90% C.L.	
Λ_c^+	$4.9 \pm 1.7 \pm 0.4^{+1.8}_{-1.0}$	$2.0 \pm 1.2 \pm 0.2^{+0.7}_{-0.4}$
		<3.8 at 90% C.L.

Tableau 2: Contributions au taux de charme de chaque hadron X_c obtenues pour les mésons B neutres. La première colonne de résultats correspond à la contribution de charme corrélé, la seconde à celle de charme anti-corrélé. La première incertitude est statistique, la deuxième est systématique et la dernière correspond aux incertitudes sur les rapports d'embranchement des modes utilisés pour reconstruire les hadrons.

Dans une première publication[58] avec 82 fb^{-1} de luminosité intégrée, nous avons démontré pour la première fois, la faisabilité de la mesure du taux de charme avec la méthode de reconstruction des hadrons charmés dans l'hémisphère du B_{recul} après reconstruction du premier méson B permettant l'étiquetage des hadrons charmés (mésons D et Ds et baryons Λ_c et Ξ_c, les états excités de ceux-ci étant contenus dans la mesure inclusive que nous avons effectuée) produits comme étant de charme anti-corrélé ou de charme corrélé.

Les résultats de nos mesures sont résumés dans les Tableau 1 et Tableau 2. Pour évaluer le taux de charme total, il faut rajouter la contribution des baryons Ξ_c et des états charmonia. Pour cette dernière nous avons utilisé la moyenne mondiale: 2.3±0.3 % pour la contribution corrélée et de même pour la contribution anti-corrélée. Pour la contribution de charme corrélé des baryons Ξ_c nous avons pris la valeur mesurée du taux de charme anti-corrélé des baryons Λ_c comme nous l'avons expliqué dans le chapitre VIII.2.5. La contribution des baryons Ξ_c de charme anti-corrélé a été négligée. Les Tableau 1 et Tableau 2 montrent que la contribution de charme corrélé N_c vient essentiellement des mésons D et qu'au total, elle est compatible avec l'unité:

- Pour les ***B chargés:*** $N_c = 0.983 \pm 0.030 \pm 0.046 \pm^{0.028}_{0.023}$
- Pour les ***B neutres:*** $N_c = 1.039 \pm 0.051 \pm 0.049 \pm^{0.039}_{0.031}$

Ce sont les mésons D_s qui contribuent de la manière la plus importante au taux de charme anti-corrélé $N_{\bar{c}}$, alors que leur contribution de charme corrélé est faible. Au total la contribution de charme anti-corrélé est:

- Pour les ***B chargés:*** $N_{\bar{c}} = 0.330 \pm 0.022 \pm 0.020 \pm^{0.051}_{0.031}$
- Pour les ***B neutres:*** $N_{\bar{c}} = 0.237 \pm 0.036 \pm 0.012 \pm^{0.039}_{0.024}$

La somme n_c des taux charme corrélé et anti-corrélé donne:

- Pour les ***B chargés:*** $n_c = 1.313 \pm 0.037 \pm 0.062 \pm^{0.051}_{0.042}$
- Pour les ***B neutres:*** $n_c = 1.276 \pm 0.062 \pm 0.058 \pm^{0.066}_{0.046}$

Pour tous les taux précédents, la première incertitude est statistique, la deuxième est systématique et la dernière correspond aux incertitudes sur les rapports d'embranchement des modes utilisés pour reconstruire les hadrons charmés.

Avec 82 fb^{-1} de luminosité intégrée, les taux de charmes mesurés dans BaBar étaient compatibles avec les moyennes mondiales.

La thèse[59] de F. Couderc a couvert la détermination du taux de charme avec les mesures inclusives des désintégrations des mésons B^- *et* B^0 en mésons D et D_s et baryons charmés Λ_c *et* Ξ_c et la mesure des distributions d'impulsion des hadrons charmés D, D_s et Λ_c.

Les nouveaux résultats de la détermination du taux de charme, plus précis, sont obtenus avec une luminosité intégrée de 209 fb^{-1}:

[58] BaBar Collaboration, B.~Aubert et al., PRD (70), 091106(R) (2004).
[59] Thèse de Doctorat de l'université de Savoie, F. Couderc, soutenue le 06 avril 2005.

Pour les ***B chargés***

$$N_c = 0.968 \pm 0.019 \pm 0.032 \pm {}^{0.026}_{0.022},$$
$$N_{\bar{c}} = 0.234 \pm 0.012 \pm 0.008 \pm {}^{0.016}_{0.012},$$
$$n_c = 1.202 \pm 0.023 \pm 0.040 \pm {}^{0.035}_{0.029}.$$

Pour les ***B neutres***:

$$N_c = 0.947 \pm 0.030 \pm 0.028 \pm {}^{0.035}_{0.028},$$
$$N_{\bar{c}} = 0.246 \pm 0.024 \pm 0.009 \pm {}^{0.019}_{0.014},$$
$$n_c = 1.193 \pm 0.030 \pm 0.034 \pm {}^{0.044}_{0.035}.$$

Cette étude a fait l'objet de nombreuses présentations et de deux notes internes (BAD623, BAD1234) au sein de la collaboration BaBar[60]. Les résultats seront publiés prochainement dans Phys. Rev. D[61].

[60] Parmi lesquelles
http://www.slac.stanford.edu/BFROOT/www/Organization/CollabMtgs/2004/detFeb04/Mon1a/couderc.pdf
(présentation à la réunion de collaboration BaBar, SLAC, février 2004)
http://www.slac.stanford.edu/BFROOT/www/Organization/CollabMtgs/2005/detMay05/Mon3a/couderc.pdf
(présentation à la réunion de collaboration BaBar, Elbe, mai 2005).
http://www.slac.stanford.edu/BFROOT/www/Physics/BAD/vol8/00623.012.pdf
http://www.slac.stanford.edu/BFROOT/www/Physics/BAD/vol11/01234.008.pdf

[61] **Study of Inclusive B^- and B^0 Decays to Flavor-tagged D, Ds and Λ_c**, **B. Aubert**, *et al.*, **BaBar collaboration**. Hep-ex/0606026. **Submitted to Phys.Rev. D**

VIII.2.7. Rapports d'embranchement de la désintégration du méson B dans les modes hadroniques $D^{(*,**)}\pi$ et le test de HQET

La compréhension des désintégrations hadroniques du méson ***B*** s'est améliorée ces dernières années avec le développement et l'application de la théorie effective des quarks lourds (HQET) et de la mise en place sur des bases théoriques plus solides de l'hypothèse de "factorisation"[62]. Cette dernière permet de calculer les amplitudes de désintégration hadroniques du méson ***B*** en négligeant les effets de l'interaction dans l'état final (par échange de gluons mous entre les états singlets de couleurs qui sont dans notre cas le méson ***D*** et le méson π). Dans ce cadre, le système B disposerait d'une assez grande énergie pour que le méson π produit par hadronisation du boson ***W*** s'échappe rapidement. L'amplitude de désintégration du méson ***B*** peut alors s'écrire comme le produit de deux courants hadroniques (***D***, π) indépendants.

Avec l'observation récente par les expériences BaBar et BELLE des modes supprimés de couleur (modes de classe II selon la classification de Stech et collaborateurs) de la désintégration hadronique du méson ***B*** en méson charmé ***D*** et en méson léger, la mesure précise des rapports d'embranchement des modes favorisés de couleur (classe I et III) devient importante afin de tester l'hypothèse de factorisation et le modèle HQET.

Les amplitudes des modes de désintégration du méson ***B*** en $D^{(*,**)}\pi$ s'écrivent en fonction des paramètres a_1 et a_2 de la manière suivante:

$$A(\bar{B}^0 \to D^{(*,**)+}\pi^-) = a_1 F_1 \qquad \text{(classe I)}$$

$$A(\bar{B}^0 \to D^{(*,**)0}\pi^0) = a_2 F_2 \qquad \text{(classe II)} \qquad \textbf{(Équation 1)}$$

$$A(B^- \to D^{(*,**)0}\pi^-) = a_1 F_3 + a_2 F_4 \qquad \text{(classe III)}$$

(Où les fonctions $F_{i=1,4}$ dépendent entre autres des constantes de désintégration du pion et des mésons $D^{(*,**)}$ et des facteurs de forme $f_{0,1}^{\pi B}(q^2)$.)

satisfaisant à la relation de symétrie d'isospin:

$$A(B^- \to D^{(*,**)0}\pi^-) = A(\bar{B}^0 \to D^{(*,**)+}\pi^-) - \sqrt{2}\, A(\bar{B}^0 \to D^{(*,**)0}\pi^0) \quad \textbf{(Équation 2)}$$

Elles peuvent aussi s'écrire en fonction des amplitudes des états propres d'isospin $A_{1/2}$ et $A_{3/2}$:

$$A(\bar{B}^0 \to D^{(*,**)+}\pi^-) = \sqrt{1/3}\, A_{3/2} + \sqrt{2/3}\, A_{1/2} \qquad \text{(classe I)}$$

$$A(\bar{B}^0 \to D^{(*,**)0}\pi^0) = \sqrt{2/3}\, A_{3/2} - \sqrt{1/3}\, A_{1/2} \qquad \text{(classe II)} \qquad \textbf{(Équation 3)}$$

[62] M. Neubert and B. Stech in **Heavy Flavors** edited by A.J. Buras and M. Lindner, 2nd ed. (World scientific, Singapore, 1998), hep-ph/9705292

$A(B^- \to D^{(*,**)0}\pi^-) = \sqrt{3}\, A_{3/2}$ *(classe III)*

La différence de phase forte δ s'écrit en fonction des largeurs des modes hadroniques ci-dessus (carré des amplitudes) de la manière suivante:

$$\mathbf{Cos}\ \delta = (3\,\Gamma(\bar{B}^0 \to D^{(*,**)+}\pi^-) + \Gamma(B^- \to D^{(*,**)0}\pi^-) - 6\,\Gamma(\bar{B}^0 \to D^{(*,**)0}\pi^0))/4|A_{1/2}\, A_{3/2}| \quad \textbf{(Équation 4)}$$

montrant que la mesure d'une différence de phase "forte" entre les amplitudes d'isospin I=1/2 et I=3/2 différente de zéro pourrait révéler des effets d'interaction dans l'état final comme le suggérait déjà la dernière analyse de l'expérience CLEO[63] et mesuré depuis par BaBar[64] et Belle[65].

J'ai voulu tirer avantage de notre échantillon de données et de notre méthode de reconstruction partielle de l'événement pour mesurer de manière indépendante des modèles et à plus long terme plus précise, les rapports d'embranchement du méson ***B*** dans les canaux hadroniques $D^{(*,**)}\pi$. Dans notre échantillon les caractéristiques du B_{recul} sont entièrement déterminées puisque les paramètres du faisceau sont connus avec une grande précision, et le premier méson B entièrement reconstruit. Dans les désintégrations $B \to \pi X$, l'étude de ***X*** est rendue possible sans qu'il ne soit reconstruit, seule la reconstruction du π est nécessaire. Cette dernière donne accès à l'énergie et à l'impulsion de ***X*** et donc à la masse invariante qui est la masse manquante. La mesure du rapport d'embranchement des désintégrations $B \to \pi X$ ne sera affecté ni par l'efficacité de reconstruction de ***X***, ni par la nécessité de connaître précisément ses modes de désintégration. Ce sont là les avantages que présente notre méthode par rapport à la méthode de reconstruction exclusive utilisée dans les mesures de ces rapports d'embranchement par les expériences CLEO et Belle[66] où tous les produits de désintégration des mésons B sont reconstruits dans certains de leurs modes de désintégration les plus efficaces.

J'ai étudié les désintégrations $B \to \pi X$ pour la première fois avec une simulation[53.8] Monte Carlo (~350 fb^{-1}) et avec les données réelles[53.9] (avec seulement 50.8 fb^{-1}) : les signaux D^0, D^{0*} et D^{0**} apparaissaient clairement en masse manquante au π (voir Figure 11).

Les mesures précédentes de CLEO ($B \to \pi D^{(*)}$) étaient effectuées en supposant une production égale de mésons chargés B^+ et de mésons neutres B^0 dans la désintégration du ***Y(4S)***. Elles utilisaient aussi les rapports d'embranchement connus (PDG) des désintégrations des mésons ***D***. Le calcul de la masse manquante au π (notre méthode), permet de s'affranchir de l'utilisation des rapports d'embranchement des mésons ***D e D****** puisqu'il n'est pas nécessaire de les reconstruire, ainsi que de l'incertitude avec laquelle ils sont connus. Les mésons ***D*** sont, dans notre analyse, tous comptabilisés dans le spectre de la masse manquante, quels que soient leurs modes de désintégration. Les nombres de

[63] S. Ahmed *et al.* Phys. Rev. D66 031101(R) (2002) and M.S. Alam et al. Phys. Rev. D50 43 (1994)
[64] BaBar Collaboration, B. Aubert et al., Phys. Rev. D69, 032004 (2004).
[65] Belle Collaboration, K. Abe et al., Phys. Rev. Lett.88, 052002 (2002) and S. Blyth et al., hep-ex/0607029, submitted to Phys. Rev. D
[66] Belle Collaboration, K. Abe et al.,Phys. rev. D69, 112002(2004)

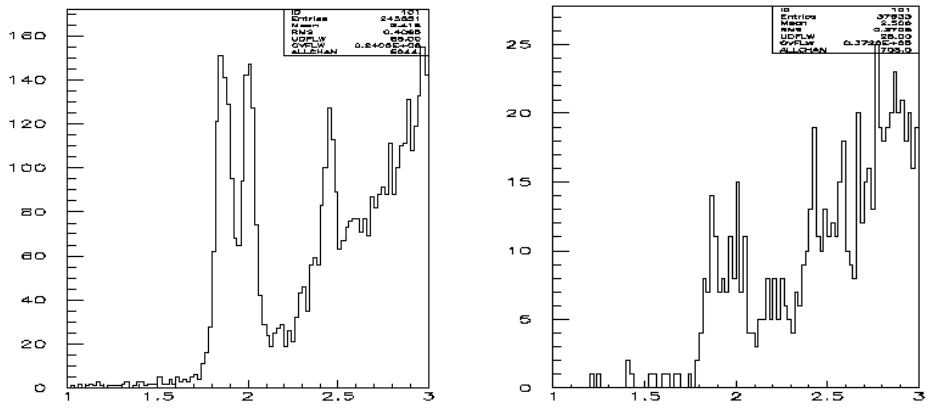

Figure 11: Distributions de masse manquante au π obtenue avec la simulation MC (gauche) et avec 50.8 fb^{-1} de données réelles de BaBar (droite).

B^0 et B^+ reconstruits étant par ailleurs connus de manière précise (avantage de la méthode) il n'est pas nécessaire non plus de faire l'hypothèse sur la production égale des B^0 et B^+. Le spectre de la masse manquante au π présente l'avantage de montrer les trois résonances ***D, D**** et ***D*** obtenues dans des conditions identiques. Il est alors possible par un simple ajustement des résonances de calculer le rapport d'embranchement total des modes de désintégration du méson $B \rightarrow D^{(**)}\pi$. L'acceptance du détecteur BaBar au π est calculée en utilisant la simulation Monte Carlo.

La Figure 12 montre la distribution de la masse manquante au pion obtenue avec la luminosité intégrée 209 fb^{-1}. Les distributions de la masse manquante pour les B_{recul} ***chargés*** et les B_{recul} ***neutres*** sont montrées sur les Figure 12(a) et Figure ***12***(b). Les données correspondent aux points avec les barres d'erreur et les différentes contributions au bruit de fond ($b\bar{b}$ et $q\bar{q}$(q=c,u,d,s)) prédites par la simulation sont représentées par les histogrammes. Lorsque le bruit de fond est soustrait, les signaux des résonances D^0, D^{0*} et D^{0**} correspondant aux B_{recul} ***chargés*** ainsi que les signaux des résonances D^+, D^{+*} et D^{+**} correspondant aux B_{recul} ***neutres*** apparaissent clairement sur les Figure 12(c) et Figure ***12***(d) respectivement. Les rapports d'embranchement sont calculés à partir des résultats des ajustements pour les résonances ***D et D****, et d'un comptage dans l'intervalle de masse de 2.2 à 2.8 GeV/c^2 pour la résonance ***D****. Les courbes d'ajustement pour les différentes composantes sont montrées sur les Figure 12(c) et **Figure *12***(d) et les résultats sont regroupés dans le Tableau 3. Ce dernier contient aussi la valeur de l'efficacité de reconstruction du pion et les rapports d'embranchement finals. Cette étude a fait l'objet de nombreuses présentations[67] lors des réunions de collaboration de BaBar, d'une note

[67] http://www.slac.stanford.edu/BFROOT/www/Organization/CollabMtgs/2004/detFeb04/Mon1a/couderc.pdf (présentation à la réunion de collaboration BaBar, SLAC, février 2004)
http://www.slac.stanford.edu/BFROOT/www/Organization/CollabMtgs/2004/detSep04/Wed2d/Wed2d.html (A. Zghiche, présentation à la réunion de collaboration BaBar, Dresde, septembre 2004)
http://www.slac.stanford.edu/BFROOT/www/Organization/CollabMtgs/2004/detDec04/Thur1a/zghiche.pdf (présentation à la réunion de collaboration BaBar, SLAC, décembre 2004)
http://www.slac.stanford.edu/BFROOT/www/Organization/CollabMtgs/2005/detMay05/Mon3a/couderc.pdf (présentation à la réunion de collaboration BaBar, Elbe, mai 2005)
http://www.slac.stanford.edu/BFROOT/www/Organization/CollabMtgs/2005/detMay05/Mon3a/zghiche.pdf (présentation à la réunion de collaboration BaBar, Elbe, mai 2005)

interne de BaBar (BAD756)[68], d'une publication à la conférence ICHEP2006 et est publiée dans la revue Phys. Rev. D[69]. Elle a montré qu'il est possible pour l'expérience BaBar de dépasser la précision actuelle en accumulant plus de statistique, aussi bien pour les modes de désintégration $B^- \rightarrow D^{0(*)}\pi^-$ que pour les modes $\bar{B}^0 \rightarrow D^{+(*)}\pi^-$. Elle a aussi montré la première mesure des rapports d'embranchement des modes $B^- \rightarrow D^{0**}\pi^-$ et $\bar{B}^0 \rightarrow D^{+**}\pi^-$.

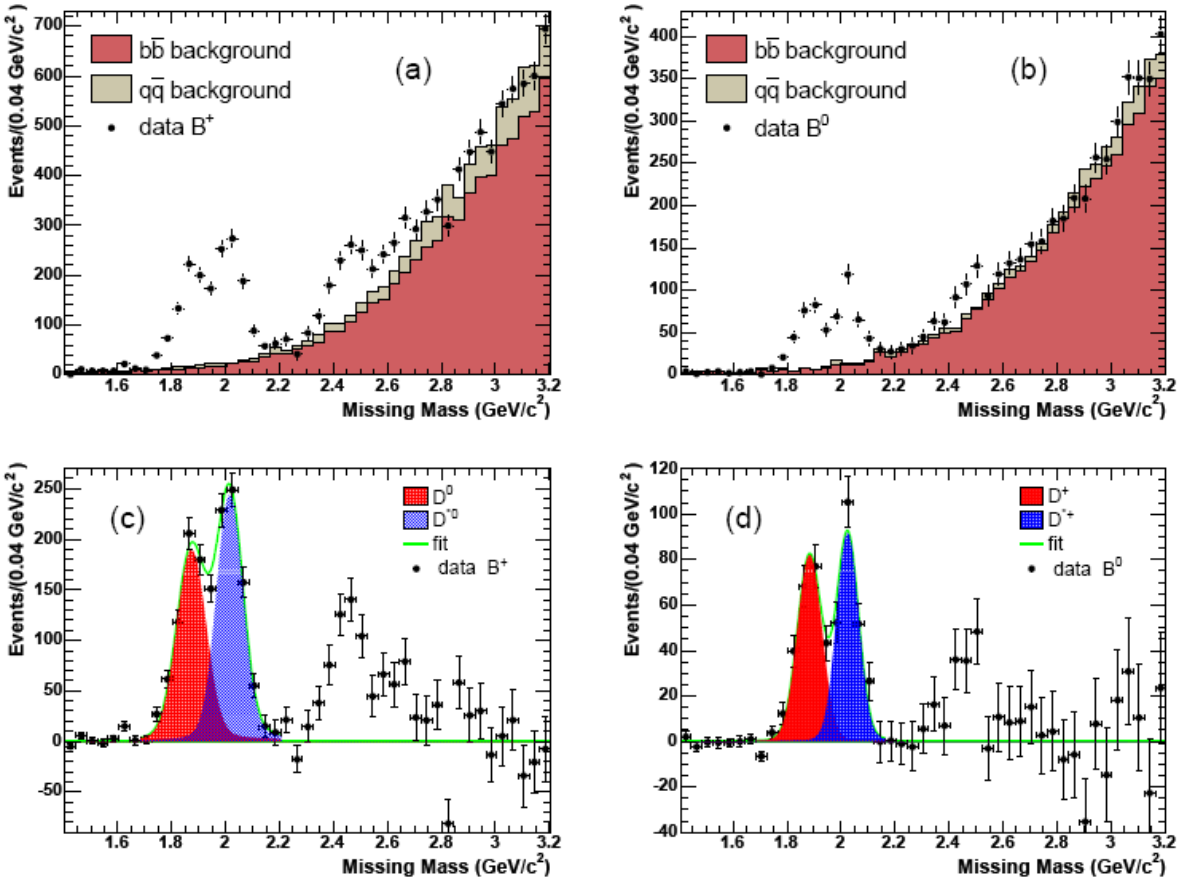

Figure 12: Haut: distribution de la masse manquante au pion obtenue pour B_{recul} chargé (a) et B_{recul} neutre (b). Les points avec les barres d'erreur correspondent aux données, les histogrammes montrent les contributions au bruit de fond (bb et qq(q=c,u,d,s)) prédits par la simulation. Bas: distribution de la masse manquante au pion après soustraction du fond pour B_{recul} chargé (c) et B_{recul} neutre (d). Les courbes montrent les ajustements pour les composants: $D\pi$ et $D^*\pi$

---

http://www.slac.stanford.edu/BFROOT/www/Organization/CollabMtgs/2005/detDec05/Thur1d/zghiche.pdf (présentation à la réunion de collaboration BaBar, SLAC, décembre 2005)
http://www.slac.stanford.edu/BFROOT/www/Organization/CollabMtgs/2006/detFeb06/Wed2/zghiche.pdf (présentation en séance plénière à la réunion de collaboration BaBar, SLAC, février 2006)
http://www.slac.stanford.edu/BFROOT/www/Organization/CollabMtgs/2006/detJun06/Thur2a/amina.pdf (présentation à la réunion de collaboration BaBar, Montréal, juin 2006)

[68] http://www.slac.stanford.edu/BFROOT/www/Physics/BAD/vol9/00756.012.pdf

[69] Measurement of the Absolute Branching Fractions B→ Dπ, D*π, D**π with a Missing Mass Method **B. Aubert**, *et al.*, **BaBar collaboration**. Hep-ex/0609033, Phys. Rev. D **74**, 111102(R) (2006)

Decay mode	Yield	Efficiency	$\mathcal{B}(10^{-3})$
$B^- \to D^0\pi^-$	677 ± 32		$4.49\pm0.21\pm0.23$
$B^- \to D^{*0}\pi^-$	774 ± 33	0.796 ± 0.007	$5.13\pm0.22\pm0.28$
$B^- \to D^{**0}\pi^-$	829 ± 78		$5.50\pm0.52\pm1.04$
$\overline{B}^0 \to D^+\pi^-$	248 ± 19		$3.03\pm0.23\pm0.23$
$\overline{B}^0 \to D^{*+}\pi^-$	245 ± 19	0.793 ± 0.007	$2.99\pm0.23\pm0.24$
$\overline{B}^0 \to D^{**+}\pi^-$	192 ± 54		$2.34\pm0.65\pm0.88$

Tableau 3: Signal, efficacités et rapports d'embranchement pour les désintégrations $B^- \to D^{0(*,**)}\pi^-$ *et* $B^0 \to D^{+(*,**)}\pi^-$.

Discussion

La mesure des rapports d'embranchement des désintégrations $B^- \to D^{0(*)}\pi^-$ et $B^0 \to D^{+(*)}\pi^-$ permet d'effectuer l'analyse en isospin afin de déterminer le rapport $A_{1/2}/\sqrt{2}A_{3/2} = 1 + O(\Lambda_{QCD}/m_b)$ ainsi que la différence de phases fortes δ. Comme souligné dans l'introduction de ce chapitre, la valeur de la phase δ lorsqu'elle est différente de zéro indiquerait le degré de non applicabilité de l'hypothèse de la factorisation et la nécessite de l'évaluation des effets de l'interaction dans l'état final. Tout comme δ, le rapport $A_{1/2}/\sqrt{2}A_{3/2}$, lorsqu'il est différent de 1, indiquerait le degré d'éloignement de la limite des quarks lourds. En utilisant la moyenne mondiale des rapports d'embranchement $B \to D^{(*)0}\pi^0$ ($0{,}291\pm0.028\times10^{-4}$ ($0{,}27\pm0.05\times10^{-4}$ pour D*)) ainsi que celle du rapport des temps de vie du B^+ et du B^0 (1.086±0.017), on obtient: $\delta = 34.2\pm1.4$ (29.1±5.2 pour D*) et $A_{1/2}/\sqrt{2}A_{3/2} = 0.84\pm0.09$ (0.73±0.12 pour D*) confirmant les mesures précédentes de BaBar ($\delta = 30.\pm5.$ (33.±5. pour D*) et $A_{1/2}/\sqrt{2}A_{3/2} = 0.69\pm0.09$ (0.76±0.08 pour D*)). D'autre part, lorsqu'une analyse des rapports d'embranchement $B \to D^{(*)}\pi$ est effectuée sans considérer les effets de l'interaction dans l'état final, les valeurs de $a_2 = 0.54\pm0.06$ (0.52±0.07 pour D*) sont obtenues. Elles sont très différentes des valeurs de l'ordre de 0.2 à 0.3 usuelles dans les calculs QCD, indiquant la nécessité d'inclure dans la description des désintégrations $B \to D^{(*)}\pi$ des corrections d'interaction dans l'état final et des contributions non factorisables. Au sein même de l'hypothèse de factorisation il ne faut pas oublier, dans les désintégrations de classe III, la contribution du diagramme d'émission des mésons D[70], qui peut très bien ne pas être négligeable. Cette contribution devrait permettre de combler une grande partie du désaccord.

Ces mesures permettent aussi de tester la symétrie de spin avec les rapports $B \to D^*\pi^-$ / $B \to D\pi^-$(voir Tableau 4). Dans le cadre de la symétrie de spin[71] ce rapport est égal à 1. Dans l'hypothèse de la factorisation[72], le rapport $B^0 \to D^{+*}\pi^-$ / $B^0 \to D^+\pi^-$ est égal à 0.96. Lorsque les contributions non factorisables sont incluses[73], le rapport pourrait se réduire à la valeur 0.83. En utilisant les constantes de désintégration obtenues par les calculs QCD sur réseau[74] la valeur attendue est 0.97 alors que le modèle Soft Collinear

[70] F. Jugeau, A. Le Yaouanc, L. Oliver, and J.-C Raynal, Phys. Rev. D 72, 094010(2005).
[71] T. Mannel et al., Phys. Lett. B259, 359 (1991).
[72] M. Neubert, W. Rieckert, B. Stech, and Q. P. Xu, in **Heavy Flavors** edited by A.J. Buras and M. Lindner, (World scientific, Singapore, 1992).
[73] B. Blok, and M. Shifman, Nuc. Phys.B389, 534 (1993).
[74] F. Jugeau, A. Le Yaouanc, L. Oliver, and J.-C Raynal, Phys. Rev. D 72, 094010(2005).

Effective Theory[75] (SCET) prédit 1.0. Pour le rapport $B^- \to D^{0*}\pi^- / B^- \to D^0\pi^-$, les valeurs 1.05 et 1.0 sont respectivement prédites par les calculs utilisant des constantes de désintégration provenant de QCD sur réseau et SCET.

$$\mathcal{B}(B^- \to D^{*0}\pi^-)/\mathcal{B}(B^- \to D^0\pi^-) = 1.14 \pm 0.07 \pm 0.04,$$
$$\mathcal{B}(B^- \to \text{“}D^{**0}\text{”}\pi^-)/\mathcal{B}(B^- \to D^0\pi^-) = 1.22 \pm 0.13 \pm 0.23,$$
$$\mathcal{B}(\overline{B}^0 \to D^{*+}\pi^-)/\mathcal{B}(\overline{B}^0 \to D^+\pi^-) = 0.99 \pm 0.11 \pm 0.08,$$
$$\mathcal{B}(\overline{B}^0 \to \text{“}D^{**+}\text{”}\pi^-)/\mathcal{B}(\overline{B}^0 \to D^+\pi^-) = 0.77 \pm 0.22 \pm 0.29.$$

Tableau 4: rapports des rapports d'embranchement mesurés

La mesure pour la première fois des rapports d'embranchement absolus des désintégrations $B \to D^{**}\pi^-$, permettra aussi de donner quelques éléments de test des règles de somme de QCD. Dans notre mesure le D** est la superposition de quatre excitations orbitales (L=1), regroupées en deux états étroits de spin 3/2 et deux états larges de spin 1/2 (voir **Figure 13**). La contribution des états de spin 3/2 est prédite, à partir de règles de somme exactes de la QCD, plus élevée que celle des états de spin 1/2. Dans le cas des désintégrations semi-leptoniques, certaines mesures montrent une contribution des états de spin 1/2 anormalement élevée et supérieure à celle des états de spin 3/2. En effet, l'expérience DELPHI mesure une contribution semi-leptonique de spin 1/2 un ordre de grandeur supérieure à celle prédite par les modèles et en contradiction avec les règles de somme. C'est ce qui est appelé le puzzle 1/2-3/2 dans la référence[76]. Dans le cas des désintégrations hadroniques du B en D** π , les auteurs de[68], calculent des contributions de spin 3/2 supérieures à celles de spin 1/2 dans le cas des désintégrations de classe I . Ils prédisent cependant des contributions des états de spin 1/2 et des états de spin 3/2 comparables dans le cas de la désintégration hadronique de classe III (cas des mésons B chargés). C'est le cas où le diagramme d'émission des mésons D^{**0} deviendrait important.

Une solution proposée au puzzle 1/2-3/2 dans la référence[73] est que dans les semi-leptoniques d'autres excitations que les résonances D** ½ aient été mal interprétées comme les résonances larges D** de spin ½. Une telle solution impliquerait que ces résonances apparaissent dans le spectre de masse invariante à des masses supérieures à celles des D**. Comparons donc le spectre de masse manquante (Figure 12(d)) obtenu dans le cas des mésons B neutres (classe I) à celui obtenu avec les mésons B chargés (classe III-Figure 12(c)) . La résonance D** dans le spectre des B neutres semble plus étroite, contenant essentiellement des contributions de spin 3/2. La résonance D** dans le spectre des B chargés se présente comme une superposition des contributions larges (spin 1/2) et des contributions étroites (spin 3/2). Ceci est en accord qualitatif avec le résultat de BELLE et l'analyse de Jugeau et al[68] . Regardons ensuite s'il y a des traces d'autres excitations que les D**. On s'attend à ce que de telles excitations se désintègrent en un pion et un $D^{(*)}$. Ceci

[75] S. Mantry, D. Pirjol, and I. W. Stewart, Phys. Rev. D68, 114009 (2003).
[76] I.I. Bigi *et al.* , hep-ph/0512270

a été étudié dans la Figure 14 où la masse manquante à un seul π a été obtenue à partir des données dans le cas des mésons B chargés avec les conditions suivantes:

- qu'il existe un deuxième pion de même charge que le premier pour une première cascade du D** vers le D* (voir figure), et que la masse manquante aux deux pions satisfasse: $1.85<MM(2\pi)<2.15$ GeV/c^2.
- qu'il existe un troisième pion de charge opposée aux deux premiers pour une deuxième cascade vers le méson D satisfaisant: $MM(2\pi)-MM(3\pi)<0.150$ GeV/c^2.

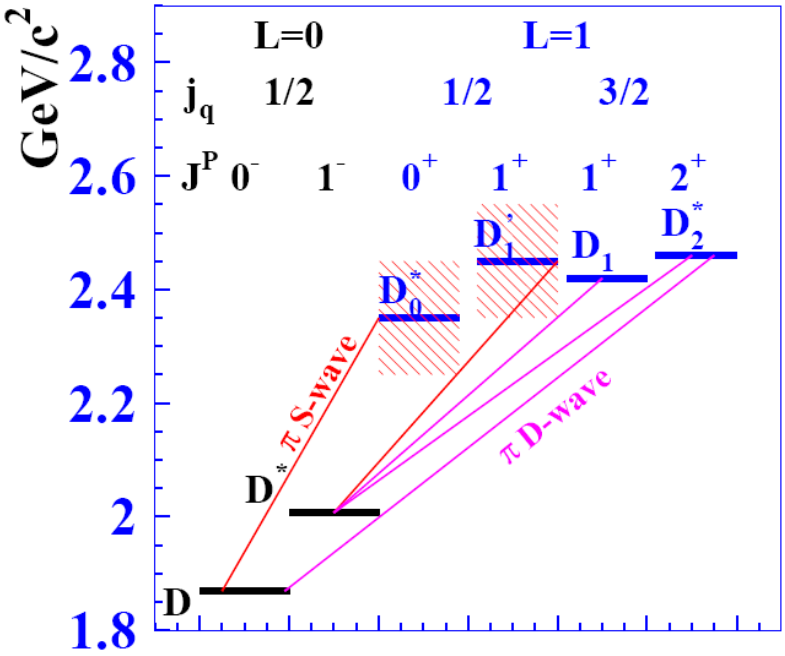

Figure 13 : spectroscopie des états excités des mésons D. Les lignes représentent les transitions à un pion possibles.

La Figure 14 montre la superposition de deux états étroits correspondant au D_1 et D_2^* et un troisième, large correspondant au D_1'. L'ajustement de la distribution de masse manquante est effectué en considérant une contribution égale de D_1' et de $D_1+D_2^*$. Cette figure montre aussi que les contributions des états excités au-delà de 2.8 GeV/c^2 sont négligeables. Par conséquent cette courbe ne soutient pas l'hypothèse de l'effet d'excitations plus élevées dans le cas des désintégrations non-leptoniques. Elle semble confirmer que D, D* et D** saturent pratiquement tout le spectre en masse manquante.

La multiplication de la luminosité intégrée cumulée par BaBar par un facteur 4 (luminosité attendue fin 2008) permettra une meilleure modélisation et une possible séparation des états excités D**.

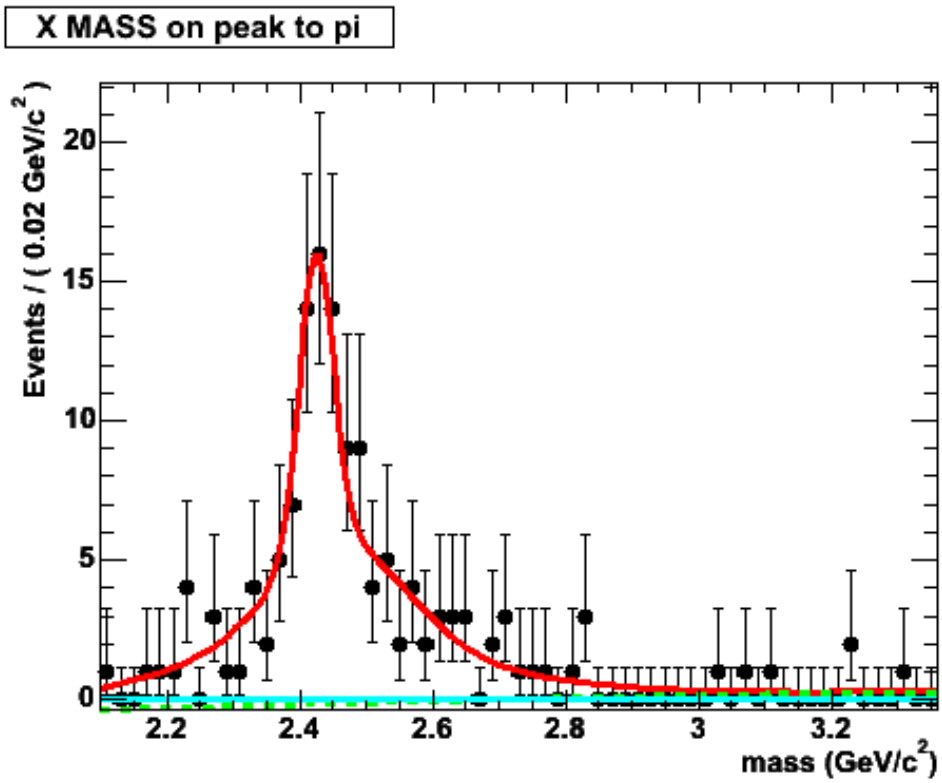

Figure 14: Spectre brut de la distribution de la masse manquante à un pion (données B chargés) avec deux autres pions requis dans l'événement permettant la double cascade du D** au D* puis au D. L'ajustement est effectué en supposant des contributions égales de D_1' et de (D_1 + D_2*).

VIII.3. Perspectives d'analyse

Détermination de rapports d'embranchement absolus $D_s \to \Phi\pi$ et $\Lambda_c \to pK\pi$

La détermination des rapports d'embranchement absolus des désintégrations $D_s \to \Phi\pi$ ***(3.6±0.9%)*** et $\Lambda_c \to pK\pi$ ***(5.0±1.3 %)*** est importante pour la normalisation de nombreuses désintégrations ayant le méson D_s ou le baryon Λ_c dans l'état final. L'incertitude avec laquelle ils sont connus reste une limitation systématique pour les mesures de précision.

La méthode originale de la masse manquante, développée ici, a permis de mesurer des taux de branchement exclusifs $B^+ \to D^+_S{}^{(*)} X$ où X peut être un méson D^0 ou un D^{0*} en utilisant 50.8 fb^{-1} de luminosité[53.18], seule la reconstruction du méson D_S est nécessaire. Elle a permis aussi la mesure du rapport d'embranchement $B \to DD_s$[53.17] en reconstruisant les mésons D, donnant accès au rapport d'embranchement du mode $D_s \to \Phi\pi$. En effet, en mesurant le nombre total de D_s par masse manquante au D, il suffit de reconstruire dans le même échantillon d'événements, tous les $D_s \to \Phi\pi$, et d'appliquer l'efficacité de reconstruction déterminée par Monte Carlo. D. del Re a mené cette analyse à son terme dans BaBar[77]. Pour une luminosité intégrée de 209fb^{-1}, on mesure la valeur 4.58±0.48±0.68 % pour le rapport d'embranchement du $D_s \to \Phi\pi$.

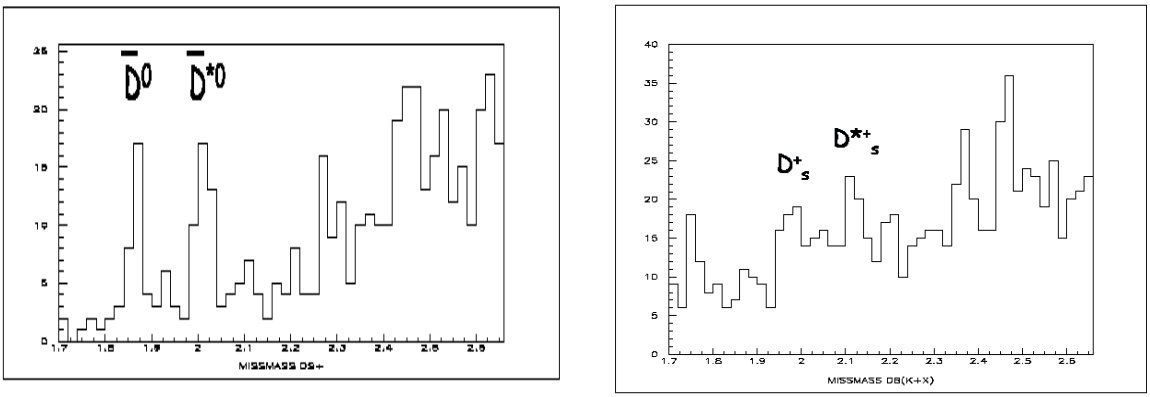

Figure 15: Distributions de masse manquante au méson D_s[53.18] (gauche) et au méson D[53.17] (droite) obtenue avec une simulation MC et une luminosité de 350 fb^{-1}.

De même, il serait intéressant, de mesurer le rapport d'embranchement absolu du mode de désintégration du baryon $\Lambda_c \to pK\pi$, car non seulement 30% de l'incertitude

[77] **Study of B --> $D^{(*)}D_{s(J)}{}^{(*)}$ Decays and Measurement of Ds^- and $D_{sJ}(2\,460)^-$ Branching Fractions** **The BABAR Collaboration, B. Aubert, et al,** Phys.Rev. D74 (2006) 031103

sur le rapport d'embranchement est due aux modèles théoriques pour les processus de production mais les autres modes de désintégration du baryon Λ_c sont mesurés par rapport à celui-ci. Le but serait donc d'abord de mesurer le nombre de baryons Λ_c produits dans la désintégration des mésons chargés $B^+ \rightarrow \Lambda_c\, p\pi^+$ (en effectuant la masse manquante à $p\pi^+$) puis comme pour le D_s, de reconstruire dans le même échantillon tous les baryons $\Lambda_c \rightarrow pK\pi$. J'ai montré[53.3] sur une simulation qu'il est possible de reconstruire les baryons Λ_c par masse manquante au système $p\pi$ dans BaBar, avec une résolution de 17MeV/c^2 (voir Figure 16). L'accroissement du nombre de mésons B permettrait aussi de reconstruire les autres baryons charmés, tels que les Σ_c et les Ξ_c [53.5].

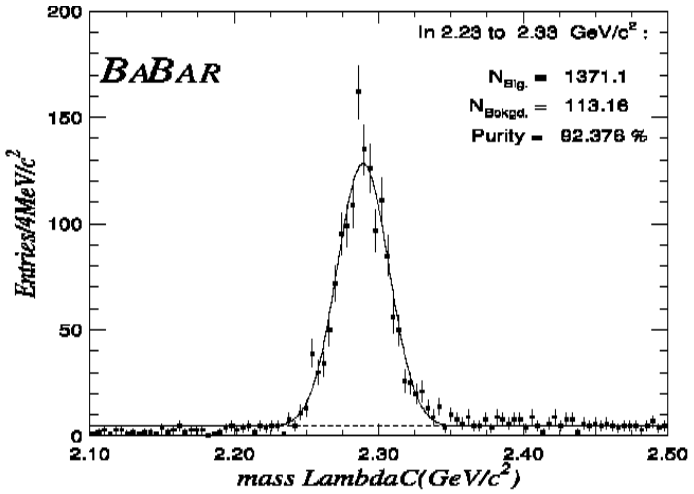

Figure 16 : Distribution de masse manquante au système $p\pi$ obtenue avec une simulation MC ne contenant que le signal. La résolution de la résonance Λ_c ainsi obtenue est de 17 MeV/c^2.

La méthode de la masse manquante a aussi été utilisée dans BaBar pour mesurer le spectre du charmonium en calculant la masse manquante au méson K[78].

Ce programme de recherche n'est possible que parce que l'expérience BaBar est une usine à B. En effet, les centaines de millions de paires $B\bar{B}$ produites permettent d'étudier des modes de désintégration à faible taux d'embranchement. La méthode de la masse manquante permet elle, de s'affranchir en grande partie du fond combinatoire qui pollue toute reconstruction directe des mésons et des baryons charmés, ce qui la rend compétitive pour les analyses décrites.

[78]Measurements of the Absolute Branching Fractions of $B^{\pm} \rightarrow K^{\pm} X_{c\bar{c}}$, **B. Aubert**, *et al.*, **BaBar collaboration**, Phys. Rev. Lett. 96, 052002 (2006)

IX. Conclusion

Au cours de mon implication dans les développements de détecteurs pour CMS, j'ai très activement dirigé les équipes d'ingénieurs et de techniciens à l'IPHC (ex-IReS) de Strasbourg. C'est ainsi que nous avons monté une salle blanche où des détecteurs MSGC étaient qualifiés après réception avec un système de pointes qui permettait le repérage des courts-circuits et des pistes interrompues. C'est aussi dans cette salle que l'électronique frontale était "bondée" (soudure par ultrasons). Cette salle était également utilisée pour l'assemblage final du détecteur et pour les premiers tests sous tension. J'ai aussi contribué à monter le banc de "tests cosmiques" où le détecteur une fois assemblé était graduellement mis sous tension pour arriver aux valeurs nominales. La mesure du gain était alors effectuée et le détecteur qualifié. Durant mon séjour à l'IPHC, j'ai été responsable de toutes les mesures effectuées en "cosmiques" sur les bancs de tests et sous faisceaux au CERN et au PSI.

Dans BaBar, outre ma participation à l'élaboration des outils de transfert des données au Tier-A du centre de calcul CCIN2P3 de Lyon et à la qualification des données pour le groupe d'analyse Exclusive B Decays to Charm "BRECO", j'ai essentiellement contribué à la thèse de F. Couderc en explorant la méthode de reconstruction partielle des événements et en démontrant la faisabilité de la mesure du taux de charme. Tout en contribuant à cette étude, j'ai entièrement effectué l'analyse et conduit à la publication de la mesure des taux d'embranchement de désintégrations hadroniques du méson B en $D^{(*,**)}\pi$ avec la méthode originale de la masse manquante.

De la mesure de sections efficaces dans le domaine de la physique nucléaire, jusqu'aux analyses dans le domaine de la physique du B et de la violation de CP, mon parcours dans la recherche m'a permis de traiter des thématiques très diverses. Dans ce rapport j'ai mis l'accent sur ma contribution à deux aspects importants de la physique expérimentale d'aujourd'hui, les développements de détecteurs pour les expériences de physique des hautes énergies, CMS au LHC et l'analyse des données dans une expérience de physique des particules, BaBar.

Publications avec contribution personnelle très importante

1. **Deep Inelastic Scattering in the Distorted Wave Born Approximation : An AnalyticApproach.**
   M. Traini (Trento U.) , S. Turck-Chieze, A. Zghiche (Saclay) . **Phys.Rev.C38:2799-2812,1988**
2. **Longitudinal and transverse responses in quasi-elastic electron scattering from Pb-208 and He-4.**
   A. Zghiche *et al.*, Apr 1993. 69pp. **Nucl.Phys.A572:513-559,1994, Erratum-ibid.A584:757,1995**
3. **Spin-Exchange Optical Pumping as a Source of Spin-Polarized Atomic Deuterium**
   A. Zghiche *et al.*, **contribution aux Proceedings du Workshop on Polarized Gas Targets for Storage Rings, Heidelberg, 1991, eds. H.G.Gaul, E.Steffens, and K.Zapfe, MPI fur Kernphysik (1991)**
4. **Spin-Exchange Optical Pumping as a Source of Spin-Polarized Atomic Deuterium**
   K.P. Coulter *et al.* **Phys. Rev. Lett. 68:174-177,1992**
5. **An Active storage cell for a polarized gas internal target.**
   K.P. Coulter *et al.* **Nucl.Instrum.Meth.A350:423-429,1994**
6. **η - 4He quasibound states.** N. Willis *et al.* **Phys.Lett.B406(1997)14-17**

7. **Coulomb distortion measurements by comparing electron and positron quasi-elastic scattering off C-12 and Pb-208.**
   P. Gueye *et al.* 1999. 9pp. **Phys.Rev.C60:044308,1999**
8. **Test of a CMS MSGC tracker prototype in a high intensity hadron beam.**
   D. Abbaneo *et al.* 1998. Prepared for 7th Pisa Meeting on Advanced Detectors: Frontier Detectors for Frontier Physics, La Biodola, Isola d'Elba, Italy, 25-31 May 1997. **Nucl.Instrum.Meth.A409:37-42,1998**
9. **Comparative studies of MSGC and MSGC-GEM detectors.**
   Y. Benhammou *et al.* **Nucl.Instrum.Meth.A419:400-404,1998**
10. **Large scale test of wedge shaped microstrip gas counters.**
    M. Ackermann *et al.* **Nucl.Instrum.Meth.A436:313-325,1999**
11. **A study of various coatings for MSGCs.**
    V. Mack, J.C. Fontaine, D. Huss (Haute Alsace U., GRPHE) , J.M. Brom, A. Zghiche (Strasbourg, CRN) , J. Schunck . 1999.
    Nucl.Instrum.Meth.A423:369-375,1999
12. **Study of the ABC enhancement in the polarized d d ---> alpha X**0 reaction.**
    R. Wurzinger *et al.* , **Phys.Lett.B445:423-427,1999**
13. **Status report on Micro Strip Gas Chambers**.A. Zghiche (for the CMS Tracker Collaboration).**Proceedings of the International Europhysics Conference on High Energy Physics 99 (page:1012), Tempere, Finland, 15-21 July 1999**
14. **Beam test results of a wedge-shaped MSGC + GEM detector at CERN.**
    Y. Benhammou *et al.*, **Nucl.Instrum.Meth.A441:452-458,2000**
15. **First Results of Micromegas detector with fast integrated electronics, F. Jeanneau etal., Nucl.Instrum.Meth.A450:313-32,2000**
16. **Robustness test of a system of MSGC+GEM detectors at the cyclotron facility of the Paul Scherrer institute.**
    M. Ageron *et al.*, **Nucl.Instrum.Meth.A471:380-391,2001**
17. **Test of the CMS Microstrip Silicon tracker readout and control system.**
    A. Zghiche *for the CMS TRACKER collaboration.* **Nucl.Instrum.Meth.A461:470-473,2001**Prepared for 8th Pisa Meeting on Advanced Detector: Frontier Detectors for Frontier Physics, La Biodola, Isola d'Elba, Italy, 21-25May 2000.
18. **Experimental and simulation study of the behaviour and operation modes of MSGC + GEM detectors.**
    M. Ageron *et al.* 2002. **Nucl.Instrum.Meth.A489:121-139,2002**
19. **Measurement of the Branching Fractions for Inclusive Decays B^- and B^0 to Flavor-tagged D, Ds and Λ_c, B. Aubert, *et al.* , BaBar collaboration. Phys.Rev. D70 (2004) 091106**
20. **Hadronic B decays at BaBar, A. Zghiche** (for the **BaBar collaboration**).**Proceedings of the 12th International QCD Conference, 4-8th July 2005 Montpellier (France)**
21. **Study of Inclusive B^- and B^0 Decays to Flavor-tagged D, Ds and Λ_c**
    B. Aubert, *et al.*, BaBar collaboration. Hep-ex/0606026. **Submitted to Phys.Rev. D**

22. **Measurement of the Absolute Branching Fractions B→ Dπ, D*π, D**π with a Missing Mass Method** **B. Aubert**, *et al.*, **BaBar collaboration**. Hep-ex/0609033, Phys. Rev. D **74**, 111102(R) (2006)

Nombre d'articles significatifs dans des revues à comité de lecture : 19

Nombre total d'articles publiés dans des revues à comité de lecture:220

Nombre d'organisations de congrès de recherche : 3

- **Réunions de collaboration "Trajectographe Avant de CMS", à l' IPHC (ex-IReS) en 1996 et à Colmar en 1998**

- **Les Journées Jeunes Chercheurs, La-Roche-en-Ardennes (30/11-5/12 2003): organisation de la session " Mesures de précision en physique des particules"**

- **Les journées de prospectives du LAPP (mars 2004): responsable du groupe "physique du B"**
- **Organisatrice de la session Physique du B des RENCONTRES DE MORIOND: Electroweak Interactions and Unified Theories du 11 - 18 mars 2006.**

Nombre de communications dans des congrès internationaux : 8

- **Fourth Students' Workshop on Electromagnetic Interactions, Bosen (Germany): "Transverse and Longitudinal separation of the quasi-elastic scattering cross section of electrons on ^{208}Pb"**

- **4th Workshop on Perspectives in Nuclear Physics at Intermediate Energies: ICTP, Trieste, Italy-May 8-12, 1989: "Transverse and Longitudinal separation of the quasi-elastic scattering cross section of electrons on ^{208}Pb"**
- **"Nucleons in Nuclei: What's new?" 1990 Gordon Conference on Photonuclear Reactions, Août 06-10, 1990, Tilton School, Tilton, New Hampshire: "Transverse and Longitudinal separation of the quasi- elastic scattering cross section of electrons on ^{208}Pb"**

- **Workshop on Polarized Gas Targets for Storage Rings, Heidelberg, 1991, eds. H.G. Gaul, E. Steffens, and K. Zapfe, MPI fur Kernphysik(1991): "Spin-Exchange Optical Pumping as a Source of Spin-Polarized Atomic Deuterium"**

- **"International Europhysics Conference on High Energy Physics 99", Tempere, Finland, 15-21 July 1999: "Status report on Micro Strip Gas Chambers "**

- **"8th Pisa meeting on advanced Detectors", La Biodola, Isola d'Elba, Italy 21-27,2000 : "Test of the CMS Microstrip silicon tracker readout and control system" Nucl.Instr.Meth.A 461 (2001) 470-473**

- **Journées Jeunes Chercheurs, La-Roche-en-Ardennes (30/11-5/12 2003): "Mesures de précision en physique des particules"**

- **QCD2005, 12th International QCD Conference, 4-8th July 2005 Montpellier (France) :"Hadronic B decays at BaBar"**

Autres Communications dans le cadre des réunions des groupes de travail

- **Nombreuses communications lors des réunions de collaboration "Trajectographe Avant de CMS" au CERN-**
- **Genève, Aachen, Bruxelles, Karlsruhe, Lyon et Strasbourg entre 1995 et 2000 (à raison de 2 à 3 communications**
- **par an).**
- **Les réunions de collaboration BaBar (SLAC-San Francisco): nombreuses communications**
  - **Groupe "Computing" pour l'importation des données BaBar au centre de calcul ccin2p3 de Lyon.**
  - **Groupe d'analyse BRECO**
  - **Présentation en réunion plénière**

Nombre de communications dans des congrès nationaux : 5

- **The ELFE Project an Electron Laboratory for Europe Physics with a 15-30 GeV high intensity continuous beam electron accelerator, Clermont-Ferrand, Juillet 1992, " Hadronization in nuclear matter "**

- **Les 7èmes Journées d'Etudes SATURNE 29/01/1996 - 02/02/1996 Ramatuelle France: "Les états quasi-liés η-^{4}He et l'effet ABC"**

- **Les journées CMS-France à Saline Royale d'Arc et Senans 1997: "Rapport d'étape sur le trajectographe gazeux à Micro-Pistes de CMS"**

- **Workshop SOCLE (Séminaire Orienté vers une Contribution au Linéaire à Electron) du 26 au 28 janvier 1999: Détecteurs de traces gazeux et électronique associée sous forte irradiation: le cas de CMS**

- **Les journées de prospectives du LAPP (mars 2004): exposé de synthèse sur les prospectives de la physique du B**
- **Les journées de prospectives du LAPP (mars 2004): participation au travail de prospective sur la physique des neutrinos**

Séminaires

- **"Coulomb Sum Rule from the Transverse-Longitudinal Response functions of ^{208}Pb(e,e')", Université de Trento, Italie (1988)**

- **"La Séparation Transverse-Longitudinale de la Section Efficace ^{208}Pb(e,e') et la Règle de Somme Coulombienne", DPhN/BE, CEA-Saclay, France (1989)**

- **"Coulomb Sum Rule from the Transverse-Longitudinal Response functions of ^{208}Pb(e,e')", Physics Division, Argonne National Laboratory, Chicago, USA (1990)**

- **"Coulomb Sum Rule from the Transverse-Longitudinal Response functions of ^{208}Pb(e,e')", Budker Institute of Nuclear physics, Novosibirsk, Russie (1990)**

- **"Coulomb Sum Rule from the Transverse-Longitudinal Response functions of ^{208}Pb(e,e')", Caltech, USA (1991)**

- **"Le Pouvoir d'Analyse Tensoriel T_{20} mesuré avec une cible polarisée de deutérium à VEPP-3", Laboratoire National Saturne, CEA-Saclay, France (1991)**

- **"Le Pouvoir d'Analyse Tensoriel T_{20} mesuré avec une cible polarisée de deutérium à VEPP-3", IReS, Strasbourg, France (1992)**

- **"Les états quasi-liés η-^{4}He et l'effet ABC", IReS, Strasbourg, France (1995)**

- **" Les détecteurs Micro-pistes gazeux ", LAPP, Annecy-le-Vieux, France (2000)**

Séjours à l'étranger

- **Séjour Post-doctoral, 1989-1991, Argonne National Laboratory (ANL) et Fermi National Laboratory (FNAL), USA.**
- **Associée scientifique au CERN, 1999-2000, expérience CMS au LHC, groupe "trajectographe", CERN, Genève, Suisse**

Autres responsabilités scientifiques:

- **Porte-parole de l'expérience "Diffusion Quasi-Elastique d'électrons et de positrons sur des cibles de ^{12}C et ^{208}Pb", à l'accélérateur linéaire d'électrons de Saclay (ALS) (1990)**
- **Co-porte-parole de l'expérience "Mesure de la Masse Manquante dans la réaction ^{2}H(^{2}H,α)X au seuil de production du η", à Saturne, Saclay (LNS) (1993)**
- **Au Laboratoire National Saturne co-responsable de l'écriture du programme d'acquisition du détecteur SPES III, étendu par la suite aux autres détecteurs de Saturne.**
- **Dans l'expérience BaBar**
    - **co-responsable de l'importation des données au centre de calcul ccin2p3 de Lyon, entre 2001 et 2003.**
    - **responsabilité de la vérification de la qualité des données pour le groupe BRECO. J'occupe cette fonction depuis juillet 2005.**

Diffusion de l'information scientifique

La fête de la science 2002: Poster BaBar
La fête de la Science 2004: conceptrice et responsable stand "création de particules" dans le parcours: " visiteur particule".
La fête de la science 2006 : conceptrice et responsable du stand "Plongée au cœur de la matière dans le parcours: "visiteur chercheur".

Résumé

Les détecteurs gazeux à micropistes (MSGC) ont fait l'objet d'un vaste programme de recherche et développement dans le but de les qualifier pour équiper le trajectographe de l'expérience Compact Muon Solenoid (CMS) installée sur l'un des 4 points d'interaction du collisionneur proton proton de 14 TeV: le Large Hadron Collider (LHC) en construction au CERN. Les points étudiés les plus critiques pour que les MSGC et leurs variantes telles que les grilles de multiplication d'électrons (GEM) fonctionnent dans l'environnement difficile du LHC sont: la tenue aux flux de particules très ionisantes, le vieillissement dû aux radiations ainsi que la rapidité du signal pour un déclenchement à 40 MHz. Les paramètres importants pour l'optimisation du gain de ces détecteurs sont le mélange de gaz, la résistivité des substrats qui constituent le support des détecteurs et le métal des pistes. L'étude de ces paramètres a permis de définir le détecteur gazeux qui assure une stabilité de fonctionnement avec un gain constant pendant dix ans de collisions LHC. Il se compose de deux étages de multiplication d'électrons dans le gaz (amplification), associant un détecteur MSGC à un détecteur GEM.

L'expérience BaBar, installée sur l'anneau PEP II à SLAC, a été conçue pour étudier la violation de CP dans le système des mésons B. Les premières collisions $e^+ e^-$ ont été enregistrées en mai 1999. En août 2006, la luminosité intégrée enregistrée par l'expérience s'élevait à plus de 390 fb^{-1} dont 350 fb^{-1} à la résonance Y(4S) correspondant à plus de 385 millions de désintégrations $e^+ e^- \rightarrow Y(4S) \rightarrow BB$. Dès les conférences de l'été 2001, la collaboration BaBar avait pu présenter la première observation significative de la violation de CP dans le secteur des B. Avec l'accumulation des données, la précision statistique de cette mesure s'est améliorée de plus qu'un facteur 4 et la précision systématique de près d'un facteur 3. Le grand nombre de désintégrations BB permet aussi de construire un échantillon de données où un premier méson B est totalement reconstruit. Les paramètres du second *B* sont alors calculés à partir de ceux des faisceaux et du premier *B.* Grâce à cet échantillon, la détermination du nombre de charme moyen (le nombre de quarks c produits dans les désintégrations des mésons B) avec les mesures inclusives des désintégrations des mésons B^- *et* B^0 en mésons *D* et D_s et baryons charmés Λ_c a pu être effectuée séparément pour les mésons B chargés et neutres en s'affranchissant d'un grand nombre d'hypothèses ainsi que des erreurs systématiques qui en découlent. Avec le même échantillon de données, la mesure des rapports d'embranchement des modes $B^- \rightarrow D^{0(*,**)}\pi^-$ et $B^0 \rightarrow D^{+(*,**)}\pi^-$ a été effectuée avec une méthode originale dans BaBar, celle de la masse manquante. Dans le système du second B, les rapports d'embranchement ont été mesurés en calculant la masse manquante au π^-, qui est le module du quadrivecteur impulsion manquant (les quadrivecteurs impulsion du Y(4S), du premier méson B et du π^- étant déterminés). Ceci a permis d'améliorer la précision de la mesure en réduisant la contribution des incertitudes systématiques. Cette mesure ainsi que la mesure du taux de charme permettent respectivement de contraindre l'hypothèse de la factorisation dans les calculs de la Heavy Quark Effective Theory (HQET), et les paramètres de la chromodynamique quantique (QCD), tels que le rapport des masses des quarks et l'échelle de renormalisation.

Abstract

The Compact Muon Solenoid (CMS) is one of the two detectors, designed for the search of the HIGGS boson at the Large Hadron Collider (LHC), to operate late 2007 at CERN. Micro Strip Gas Counters (MSGC) have been extensively studied to qualify as part of the CMS tracker. When exposed to highly ionizing particles and to high rates of incident particles, MSGCs have shown a good behavior allowing them to cope with the LHC environment. Similar micropattern gaseous detectors such as Gas Electron Multiplier (GEM) and Micro Mesh gas detectors (MicroMegas) are developed to be used in high energy physics.

BaBar, the detector for the SLAC PEP-II asymmetric e+e- B Factory operating at the Υ(4S) resonance, was designed to allow comprehensive studies of CP-violation in B-meson decays. First observation of CP violation has been realized in 2001. Since then an impressive amount of B decays measurements has been performed. Among those, we present here the branching fraction measurements of charged and neutral B decays to $D\pi$-, $D^*\pi$-, and $D^{**}\pi$- with a missing mass method, based on a sample of 231 million $\Upsilon(4S) \rightarrow B\bar{B}$ pairs. In order to do this, one of the B mesons is fully reconstructed and the "recoil" one decays to a reconstructed charged pion and a companion charmed meson identified by its recoil mass, inferred by kinematics. The same sample is used to reconstruct charmed mesons (D, Ds) and baryons (Λ_c) in the "recoil side" allowing the measurement of the charm number in the B decays.

Les annexes

Annexe 1: Measurement of the Absolute Branching Fractions $B \rightarrow D\pi$, $D^*\pi$, $D^{**}\pi$ with a Missing Mass Method B. Aubert, *et al.*, BaBar collaboration. Hep-ex/0609033, et publié dans Phys. Rev. D 74, 111102(R) (2006)

Annexe 2: BAD756, BaBar Document Analysis, measurement of the Absolute Branching Fractions $B \rightarrow D\pi$, $D^*\pi$, $D^{**}\pi$ with a Missing Mass Method, F. Couderc et A. Zghiche. Description détaillée de l'analyse

Annexe 3: Study of Inclusive B^- and B^0 Decays to Flavor-tagged D, Ds and Λ_c B. Aubert, *et al.,* BaBar collaboration. Hep-ex/0606026. Submitted to Phys.Rev. D

Annexe 4: Hadronic B decays at BaBar, A. Zghiche (for the BaBar collaboration).Proceedings of the 12th International QCD Conference, 4-8th July 2005 Montpellier (France)

Annexe 5: Measurement of the Branching Fractions for Inclusive Decays B^- and B^0 to Flavor-tagged D, Ds and Λ_c, B. Aubert, *et al.* , BaBar collaboration. Phys.Rev. D70 (2004) 091106

Annexe 6: liste complète des publications dans des journaux avec comité de lecture

BABAR-PUB-06/057
SLAC-PUB-12107

Measurement of the Absolute Branching Fractions $B \to D\pi, D^*\pi, D^{**}\pi$ with a Missing Mass Method

B. Aubert,[1] M. Bona,[1] D. Boutigny,[1] F. Couderc,[1] Y. Karyotakis,[1] J. P. Lees,[1] V. Poireau,[1] V. Tisserand,[1] A. Zghiche,[1] E. Grauges,[2] A. Palano,[3] J. C. Chen,[4] N. D. Qi,[4] G. Rong,[4] P. Wang,[4] Y. S. Zhu,[4] G. Eigen,[5] I. Ofte,[5] B. Stugu,[5] G. S. Abrams,[6] M. Battaglia,[6] D. N. Brown,[6] J. Button-Shafer,[6] R. N. Cahn,[6] E. Charles,[6] M. S. Gill,[6] Y. Groysman,[6] R. G. Jacobsen,[6] J. A. Kadyk,[6] L. T. Kerth,[6] Yu. G. Kolomensky,[6] G. Kukartsev,[6] G. Lynch,[6] L. M. Mir,[6] T. J. Orimoto,[6] M. Pripstein,[6] N. A. Roe,[6] M. T. Ronan,[6] W. A. Wenzel,[6] P. del Amo Sanchez,[7] M. Barrett,[7] K. E. Ford,[7] T. J. Harrison,[7] A. J. Hart,[7] C. M. Hawkes,[7] A. T. Watson,[7] T. Held,[8] H. Koch,[8] B. Lewandowski,[8] M. Pelizaeus,[8] K. Peters,[8] T. Schroeder,[8] M. Steinke,[8] J. T. Boyd,[9] J. P. Burke,[9] W. N. Cottingham,[9] D. Walker,[9] D. J. Asgeirsson,[10] T. Cuhadar-Donszelmann,[10] B. G. Fulsom,[10] C. Hearty,[10] N. S. Knecht,[10] T. S. Mattison,[10] J. A. McKenna,[10] A. Khan,[11] P. Kyberd,[11] M. Saleem,[11] D. J. Sherwood,[11] L. Teodorescu,[11] V. E. Blinov,[12] A. D. Bukin,[12] V. P. Druzhinin,[12] V. B. Golubev,[12] A. P. Onuchin,[12] S. I. Serednyakov,[12] Yu. I. Skovpen,[12] E. P. Solodov,[12] K. Yu Todyshev,[12] M. Bondioli,[13] M. Bruinsma,[13] M. Chao,[13] S. Curry,[13] I. Eschrich,[13] D. Kirkby,[13] A. J. Lankford,[13] P. Lund,[13] M. Mandelkern,[13] R. K. Mommsen,[13] W. Roethel,[13] D. P. Stoker,[13] S. Abachi,[14] C. Buchanan,[14] S. D. Foulkes,[15] J. W. Gary,[15] O. Long,[15] B. C. Shen,[15] K. Wang,[15] L. Zhang,[15] H. K. Hadavand,[16] E. J. Hill,[16] H. P. Paar,[16] S. Rahatlou,[16] V. Sharma,[16] J. W. Berryhill,[17] C. Campagnari,[17] A. Cunha,[17] B. Dahmes,[17] T. M. Hong,[17] D. Kovalskyi,[17] J. D. Richman,[17] T. W. Beck,[18] A. M. Eisner,[18] C. J. Flacco,[18] C. A. Heusch,[18] J. Kroseberg,[18] W. S. Lockman,[18] G. Nesom,[18] T. Schalk,[18] B. A. Schumm,[18] A. Seiden,[18] P. Spradlin,[18] D. C. Williams,[18] M. G. Wilson,[18] J. Albert,[19] E. Chen,[19] A. Dvoretskii,[19] F. Fang,[19] D. G. Hitlin,[19] I. Narsky,[19] T. Piatenko,[19] F. C. Porter,[19] A. Ryd,[19] G. Mancinelli,[20] B. T. Meadows,[20] K. Mishra,[20] M. D. Sokoloff,[20] F. Blanc,[21] P. C. Bloom,[21] S. Chen,[21] W. T. Ford,[21] J. F. Hirschauer,[21] A. Kreisel,[21] M. Nagel,[21] U. Nauenberg,[21] A. Olivas,[21] W. O. Ruddick,[21] J. G. Smith,[21] K. A. Ulmer,[21] S. R. Wagner,[21] J. Zhang,[21] A. Chen,[22] E. A. Eckhart,[22] A. Soffer,[22] W. H. Toki,[22] R. J. Wilson,[22] F. Winklmeier,[22] Q. Zeng,[22] D. D. Altenburg,[23] E. Feltresi,[23] A. Hauke,[23] H. Jasper,[23] J. Merkel,[23] A. Petzold,[23] B. Spaan,[23] T. Brandt,[24] V. Klose,[24] H. M. Lacker,[24] W. F. Mader,[24] R. Nogowski,[24] J. Schubert,[24] K. R. Schubert,[24] R. Schwierz,[24] J. E. Sundermann,[24] A. Volk,[24] D. Bernard,[25] G. R. Bonneaud,[25] E. Latour,[25] Ch. Thiebaux,[25] M. Verderi,[25] P. J. Clark,[26] W. Gradl,[26] F. Muheim,[26] S. Playfer,[26] A. I. Robertson,[26] Y. Xie,[26] M. Andreotti,[27] D. Bettoni,[27] C. Bozzi,[27] R. Calabrese,[27] G. Cibinetto,[27] E. Luppi,[27] M. Negrini,[27] A. Petrella,[27] L. Piemontese,[27] E. Prencipe,[27] F. Anulli,[28] R. Baldini-Ferroli,[28] A. Calcaterra,[28] R. de Sangro,[28] G. Finocchiaro,[28] S. Pacetti,[28] P. Patteri,[28] I. M. Peruzzi,[28,*] M. Piccolo,[28] M. Rama,[28] A. Zallo,[28] A. Buzzo,[29] R. Contri,[29] M. Lo Vetere,[29] M. M. Macri,[29] M. R. Monge,[29] S. Passaggio,[29] C. Patrignani,[29] E. Robutti,[29] A. Santroni,[29] S. Tosi,[29] G. Brandenburg,[30] K. S. Chaisanguanthum,[30] M. Morii,[30] J. Wu,[30] R. S. Dubitzky,[31] J. Marks,[31] S. Schenk,[31] U. Uwer,[31] D. J. Bard,[32] W. Bhimji,[32] D. A. Bowerman,[32] P. D. Dauncey,[32] U. Egede,[32] R. L. Flack,[32] J. A. Nash,[32] M. B. Nikolich,[32] W. Panduro Vazquez,[32] P. K. Behera,[33] X. Chai,[33] M. J. Charles,[33] U. Mallik,[33] N. T. Meyer,[33] V. Ziegler,[33] J. Cochran,[34] H. B. Crawley,[34] L. Dong,[34] V. Eyges,[34] W. T. Meyer,[34] S. Prell,[34] E. I. Rosenberg,[34] A. E. Rubin,[34] A. V. Gritsan,[35] A. G. Denig,[36] M. Fritsch,[36] G. Schott,[36] N. Arnaud,[37] M. Davier,[37] G. Grosdidier,[37] A. Höcker,[37] F. Le Diberder,[37] V. Lepeltier,[37] A. M. Lutz,[37] A. Oyanguren,[37] S. Pruvot,[37] S. Rodier,[37] P. Roudeau,[37] M. H. Schune,[37] A. Stocchi,[37] W. F. Wang,[37] G. Wormser,[37] C. H. Cheng,[38] D. J. Lange,[38] D. M. Wright,[38] C. A. Chavez,[39] I. J. Forster,[39] J. R. Fry,[39] E. Gabathuler,[39] R. Gamet,[39] K. A. George,[39] D. E. Hutchcroft,[39] D. J. Payne,[39] K. C. Schofield,[39] C. Touramanis,[39] A. J. Bevan,[40] F. Di Lodovico,[40] W. Menges,[40] R. Sacco,[40] G. Cowan,[41] H. U. Flaecher,[41] D. A. Hopkins,[41] P. S. Jackson,[41] T. R. McMahon,[41] S. Ricciardi,[41] F. Salvatore,[41] A. C. Wren,[41] D. N. Brown,[42] C. L. Davis,[42] J. Allison,[43] N. R. Barlow,[43] R. J. Barlow,[43] Y. M. Chia,[43] C. L. Edgar,[43] G. D. Lafferty,[43] M. T. Naisbit,[43] J. C. Williams,[43] J. I. Yi,[43] C. Chen,[44] W. D. Hulsbergen,[44] A. Jawahery,[44] C. K. Lae,[44] D. A. Roberts,[44] G. Simi,[44] G. Blaylock,[45] C. Dallapiccola,[45] S. S. Hertzbach,[45] X. Li,[45] T. B. Moore,[45] S. Saremi,[45] H. Staengle,[45] R. Cowan,[46] G. Sciolla,[46] S. J. Sekula,[46] M. Spitznagel,[46] F. Taylor,[46] R. K. Yamamoto,[46] H. Kim,[47] S. E. Mclachlin,[47] P. M. Patel,[47] S. H. Robertson,[47] A. Lazzaro,[48] V. Lombardo,[48] F. Palombo,[48] J. M. Bauer,[49] L. Cremaldi,[49] V. Eschenburg,[49]

R. Godang,[49] R. Kroeger,[49] D. A. Sanders,[49] D. J. Summers,[49] H. W. Zhao,[49] S. Brunet,[50] D. Côté,[50] M. Simard,[50] P. Taras,[50] F. B. Viaud,[50] H. Nicholson,[51] N. Cavallo,[52,†] G. De Nardo,[52] F. Fabozzi,[52,†] C. Gatto,[52] L. Lista,[52] D. Monorchio,[52] P. Paolucci,[52] D. Piccolo,[52] C. Sciacca,[52] M. A. Baak,[53] G. Raven,[53] H. L. Snoek,[53] C. P. Jessop,[54] J. M. LoSecco,[54] T. Allmendinger,[55] G. Benelli,[55] L. A. Corwin,[55] K. K. Gan,[55] K. Honscheid,[55] D. Hufnagel,[55] P. D. Jackson,[55] H. Kagan,[55] R. Kass,[55] A. M. Rahimi,[55] J. J. Regensburger,[55] R. Ter-Antonyan,[55] Q. K. Wong,[55] N. L. Blount,[56] J. Brau,[56] R. Frey,[56] O. Igonkina,[56] J. A. Kolb,[56] M. Lu,[56] R. Rahmat,[56] N. B. Sinev,[56] D. Strom,[56] J. Strube,[56] E. Torrence,[56] A. Gaz,[57] M. Margoni,[57] M. Morandin,[57] A. Pompili,[57] M. Posocco,[57] M. Rotondo,[57] F. Simonetto,[57] R. Stroili,[57] C. Voci,[57] M. Benayoun,[58] H. Briand,[58] J. Chauveau,[58] P. David,[58] L. Del Buono,[58] Ch. de la Vaissière,[58] O. Hamon,[58] B. L. Hartfiel,[58] Ph. Leruste,[58] J. Malclès,[58] J. Ocariz,[58] L. Roos,[58] G. Therin,[58] L. Gladney,[59] M. Biasini,[60] R. Covarelli,[60] C. Angelini,[61] G. Batignani,[61] S. Bettarini,[61] F. Bucci,[61] G. Calderini,[61] M. Carpinelli,[61] R. Cenci,[61] F. Forti,[61] M. A. Giorgi,[61] A. Lusiani,[61] G. Marchiori,[61] M. A. Mazur,[61] M. Morganti,[61] N. Neri,[61] E. Paoloni,[61] G. Rizzo,[61] J. J. Walsh,[61] M. Haire,[62] D. Judd,[62] D. E. Wagoner,[62] J. Biesiada,[63] N. Danielson,[63] P. Elmer,[63] Y. P. Lau,[63] C. Lu,[63] J. Olsen,[63] A. J. S. Smith,[63] A. V. Telnov,[63] F. Bellini,[64] G. Cavoto,[64] A. D'Orazio,[64] D. del Re,[64] E. Di Marco,[64] R. Faccini,[64] F. Ferrarotto,[64] F. Ferroni,[64] M. Gaspero,[64] L. Li Gioi,[64] M. A. Mazzoni,[64] S. Morganti,[64] G. Piredda,[64] F. Polci,[64] F. Safai Tehrani,[64] C. Voena,[64] M. Ebert,[65] H. Schröder,[65] R. Waldi,[65] T. Adye,[66] N. De Groot,[66] B. Franek,[66] E. O. Olaiya,[66] F. F. Wilson,[66] R. Aleksan,[67] S. Emery,[67] A. Gaidot,[67] S. F. Ganzhur,[67] G. Hamel de Monchenault,[67] W. Kozanecki,[67] M. Legendre,[67] G. Vasseur,[67] Ch. Yèche,[67] M. Zito,[67] X. R. Chen,[68] H. Liu,[68] W. Park,[68] M. V. Purohit,[68] J. R. Wilson,[68] M. T. Allen,[69] D. Aston,[69] R. Bartoldus,[69] P. Bechtle,[69] N. Berger,[69] R. Claus,[69] J. P. Coleman,[69] M. R. Convery,[69] M. Cristinziani,[69] J. C. Dingfelder,[69] J. Dorfan,[69] G. P. Dubois-Felsmann,[69] D. Dujmic,[69] W. Dunwoodie,[69] R. C. Field,[69] T. Glanzman,[69] S. J. Gowdy,[69] M. T. Graham,[69] P. Grenier,[69] V. Halyo,[69] C. Hast,[69] T. Hryn'ova,[69] W. R. Innes,[69] M. H. Kelsey,[69] P. Kim,[69] D. W. G. S. Leith,[69] S. Li,[69] S. Luitz,[69] V. Luth,[69] H. L. Lynch,[69] D. B. MacFarlane,[69] H. Marsiske,[69] R. Messner,[69] D. R. Muller,[69] C. P. O'Grady,[69] V. E. Ozcan,[69] A. Perazzo,[69] M. Perl,[69] T. Pulliam,[69] B. N. Ratcliff,[69] A. Roodman,[69] A. A. Salnikov,[69] R. H. Schindler,[69] J. Schwiening,[69] A. Snyder,[69] J. Stelzer,[69] D. Su,[69] M. K. Sullivan,[69] K. Suzuki,[69] S. K. Swain,[69] J. M. Thompson,[69] J. Va'vra,[69] N. van Bakel,[69] M. Weaver,[69] A. J. R. Weinstein,[69] W. J. Wisniewski,[69] M. Wittgen,[69] D. H. Wright,[69] A. K. Yarritu,[69] K. Yi,[69] C. C. Young,[69] P. R. Burchat,[70] A. J. Edwards,[70] S. A. Majewski,[70] B. A. Petersen,[70] C. Roat,[70] L. Wilden,[70] S. Ahmed,[71] M. S. Alam,[71] R. Bula,[71] J. A. Ernst,[71] V. Jain,[71] B. Pan,[71] M. A. Saeed,[71] F. R. Wappler,[71] S. B. Zain,[71] W. Bugg,[72] M. Krishnamurthy,[72] S. M. Spanier,[72] R. Eckmann,[73] J. L. Ritchie,[73] A. Satpathy,[73] C. J. Schilling,[73] R. F. Schwitters,[73] J. M. Izen,[74] X. C. Lou,[74] S. Ye,[74] F. Bianchi,[75] F. Gallo,[75] D. Gamba,[75] M. Bomben,[76] L. Bosisio,[76] C. Cartaro,[76] F. Cossutti,[76] G. Della Ricca,[76] S. Dittongo,[76] L. Lanceri,[76] L. Vitale,[76] V. Azzolini,[77] N. Lopez-March,[77] F. Martinez-Vidal,[77] Sw. Banerjee,[78] B. Bhuyan,[78] C. M. Brown,[78] D. Fortin,[78] K. Hamano,[78] R. Kowalewski,[78] I. M. Nugent,[78] J. M. Roney,[78] R. J. Sobie,[78] J. J. Back,[79] P. F. Harrison,[79] T. E. Latham,[79] G. B. Mohanty,[79] M. Pappagallo,[79] H. R. Band,[80] X. Chen,[80] B. Cheng,[80] S. Dasu,[80] M. Datta,[80] K. T. Flood,[80] J. J. Hollar,[80] P. E. Kutter,[80] B. Mellado,[80] A. Mihalyi,[80] Y. Pan,[80] M. Pierini,[80] R. Prepost,[80] S. L. Wu,[80] Z. Yu,[80] and H. Neal[81]

(The *BABAR* Collaboration)

[1] *Laboratoire de Physique des Particules, IN2P3/CNRS et Université de Savoie, F-74941 Annecy-Le-Vieux, France*
[2] *Universitat de Barcelona, Facultat de Fisica, Departament ECM, E-08028 Barcelona, Spain*
[3] *Università di Bari, Dipartimento di Fisica and INFN, I-70126 Bari, Italy*
[4] *Institute of High Energy Physics, Beijing 100039, China*
[5] *University of Bergen, Institute of Physics, N-5007 Bergen, Norway*
[6] *Lawrence Berkeley National Laboratory and University of California, Berkeley, California 94720, USA*
[7] *University of Birmingham, Birmingham, B15 2TT, United Kingdom*
[8] *Ruhr Universität Bochum, Institut für Experimentalphysik 1, D-44780 Bochum, Germany*
[9] *University of Bristol, Bristol BS8 1TL, United Kingdom*
[10] *University of British Columbia, Vancouver, British Columbia, Canada V6T 1Z1*
[11] *Brunel University, Uxbridge, Middlesex UB8 3PH, United Kingdom*
[12] *Budker Institute of Nuclear Physics, Novosibirsk 630090, Russia*
[13] *University of California at Irvine, Irvine, California 92697, USA*
[14] *University of California at Los Angeles, Los Angeles, California 90024, USA*
[15] *University of California at Riverside, Riverside, California 92521, USA*
[16] *University of California at San Diego, La Jolla, California 92093, USA*
[17] *University of California at Santa Barbara, Santa Barbara, California 93106, USA*
[18] *University of California at Santa Cruz, Institute for Particle Physics, Santa Cruz, California 95064, USA*

[19] California Institute of Technology, Pasadena, California 91125, USA
[20] University of Cincinnati, Cincinnati, Ohio 45221, USA
[21] University of Colorado, Boulder, Colorado 80309, USA
[22] Colorado State University, Fort Collins, Colorado 80523, USA
[23] Universität Dortmund, Institut für Physik, D-44221 Dortmund, Germany
[24] Technische Universität Dresden, Institut für Kern- und Teilchenphysik, D-01062 Dresden, Germany
[25] Laboratoire Leprince-Ringuet, CNRS/IN2P3, Ecole Polytechnique, F-91128 Palaiseau, France
[26] University of Edinburgh, Edinburgh EH9 3JZ, United Kingdom
[27] Università di Ferrara, Dipartimento di Fisica and INFN, I-44100 Ferrara, Italy
[28] Laboratori Nazionali di Frascati dell'INFN, I-00044 Frascati, Italy
[29] Università di Genova, Dipartimento di Fisica and INFN, I-16146 Genova, Italy
[30] Harvard University, Cambridge, Massachusetts 02138, USA
[31] Universität Heidelberg, Physikalisches Institut, Philosophenweg 12, D-69120 Heidelberg, Germany
[32] Imperial College London, London, SW7 2AZ, United Kingdom
[33] University of Iowa, Iowa City, Iowa 52242, USA
[34] Iowa State University, Ames, Iowa 50011-3160, USA
[35] Johns Hopkins University, Baltimore, Maryland 21218, USA
[36] Universität Karlsruhe, Institut für Experimentelle Kernphysik, D-76021 Karlsruhe, Germany
[37] Laboratoire de l'Accélérateur Linéaire, IN2P3/CNRS et Université Paris-Sud 11,
Centre Scientifique d'Orsay, B.P. 34, F-91898 ORSAY Cedex, France
[38] Lawrence Livermore National Laboratory, Livermore, California 94550, USA
[39] University of Liverpool, Liverpool L69 7ZE, United Kingdom
[40] Queen Mary, University of London, E1 4NS, United Kingdom
[41] University of London, Royal Holloway and Bedford New College, Egham, Surrey TW20 0EX, United Kingdom
[42] University of Louisville, Louisville, Kentucky 40292, USA
[43] University of Manchester, Manchester M13 9PL, United Kingdom
[44] University of Maryland, College Park, Maryland 20742, USA
[45] University of Massachusetts, Amherst, Massachusetts 01003, USA
[46] Massachusetts Institute of Technology, Laboratory for Nuclear Science, Cambridge, Massachusetts 02139, USA
[47] McGill University, Montréal, Québec, Canada H3A 2T8
[48] Università di Milano, Dipartimento di Fisica and INFN, I-20133 Milano, Italy
[49] University of Mississippi, University, Mississippi 38677, USA
[50] Université de Montréal, Physique des Particules, Montréal, Québec, Canada H3C 3J7
[51] Mount Holyoke College, South Hadley, Massachusetts 01075, USA
[52] Università di Napoli Federico II, Dipartimento di Scienze Fisiche and INFN, I-80126, Napoli, Italy
[53] NIKHEF, National Institute for Nuclear Physics and High Energy Physics, NL-1009 DB Amsterdam, The Netherlands
[54] University of Notre Dame, Notre Dame, Indiana 46556, USA
[55] Ohio State University, Columbus, Ohio 43210, USA
[56] University of Oregon, Eugene, Oregon 97403, USA
[57] Università di Padova, Dipartimento di Fisica and INFN, I-35131 Padova, Italy
[58] Laboratoire de Physique Nucléaire et de Hautes Energies,
IN2P3/CNRS, Université Pierre et Marie Curie-Paris6,
Université Denis Diderot-Paris7, F-75252 Paris, France
[59] University of Pennsylvania, Philadelphia, Pennsylvania 19104, USA
[60] Università di Perugia, Dipartimento di Fisica and INFN, I-06100 Perugia, Italy
[61] Università di Pisa, Dipartimento di Fisica, Scuola Normale Superiore and INFN, I-56127 Pisa, Italy
[62] Prairie View A&M University, Prairie View, Texas 77446, USA
[63] Princeton University, Princeton, New Jersey 08544, USA
[64] Università di Roma La Sapienza, Dipartimento di Fisica and INFN, I-00185 Roma, Italy
[65] Universität Rostock, D-18051 Rostock, Germany
[66] Rutherford Appleton Laboratory, Chilton, Didcot, Oxon, OX11 0QX, United Kingdom
[67] DSM/Dapnia, CEA/Saclay, F-91191 Gif-sur-Yvette, France
[68] University of South Carolina, Columbia, South Carolina 29208, USA
[69] Stanford Linear Accelerator Center, Stanford, California 94309, USA
[70] Stanford University, Stanford, California 94305-4060, USA
[71] State University of New York, Albany, New York 12222, USA
[72] University of Tennessee, Knoxville, Tennessee 37996, USA
[73] University of Texas at Austin, Austin, Texas 78712, USA
[74] University of Texas at Dallas, Richardson, Texas 75083, USA
[75] Università di Torino, Dipartimento di Fisica Sperimentale and INFN, I-10125 Torino, Italy
[76] Università di Trieste, Dipartimento di Fisica and INFN, I-34127 Trieste, Italy
[77] IFIC, Universitat de Valencia-CSIC, E-46071 Valencia, Spain
[78] University of Victoria, Victoria, British Columbia, Canada V8W 3P6
[79] Department of Physics, University of Warwick, Coventry CV4 7AL, United Kingdom

[80] University of Wisconsin, Madison, Wisconsin 53706, USA
[81] Yale University, New Haven, Connecticut 06511, USA

(Dated: September 20, 2006)

We present branching fraction measurements of charged and neutral B decays to $D\,\pi^-$, $D^*\,\pi^-$ and $D^{**}\pi^-$ with a missing mass method, based on a sample of 231 million $\Upsilon(4S) \to B\overline{B}$ pairs collected by the *BABAR* detector at the PEP-II e^+e^- collider. One of the B mesons is fully reconstructed and the other one decays to a reconstructed charged π and a companion charmed meson identified by its recoil mass, inferred by kinematics. Here D^{**} refers to the sum of all the non-strange charm meson states with masses in the range $2.2 - 2.8$ GeV/c^2. We measure the branching fractions:

$$\begin{aligned}
\mathcal{B}(B^- \to D^0\pi^-) &= (4.49 \pm 0.21 \pm 0.23) \times 10^{-3} \\
\mathcal{B}(B^- \to D^{*0}\pi^-) &= (5.13 \pm 0.22 \pm 0.28) \times 10^{-3} \\
\mathcal{B}(B^- \to D^{**0}\pi^-) &= (5.50 \pm 0.52 \pm 1.04) \times 10^{-3} \\
\mathcal{B}(\overline{B}^0 \to D^+\pi^-) &= (3.03 \pm 0.23 \pm 0.23) \times 10^{-3} \\
\mathcal{B}(\overline{B}^0 \to D^{*+}\pi^-) &= (2.99 \pm 0.23 \pm 0.24) \times 10^{-3} \\
\mathcal{B}(\overline{B}^0 \to D^{**+}\pi^-) &= (2.34 \pm 0.65 \pm 0.88) \times 10^{-3}
\end{aligned}$$

and the ratios:

$$\begin{aligned}
\mathcal{B}(B^- \to D^{*0}\pi^-)/\mathcal{B}(B^- \to D^0\pi^-) &= 1.14 \pm 0.07 \pm 0.04 \\
\mathcal{B}(B^- \to D^{**0}\pi^-)/\mathcal{B}(B^- \to D^0\pi^-) &= 1.22 \pm 0.13 \pm 0.23 \\
\mathcal{B}(\overline{B}^0 \to D^{*+}\pi^-)/\mathcal{B}(\overline{B}^0 \to D^+\pi^-) &= 0.99 \pm 0.11 \pm 0.08 \\
\mathcal{B}(\overline{B}^0 \to D^{**+}\pi^-)/\mathcal{B}(\overline{B}^0 \to D^+\pi^-) &= 0.77 \pm 0.22 \pm 0.29
\end{aligned}$$

The first uncertainty is statistical and the second is systematic.

PACS numbers: 13.25.Hw, 12.15.Hh, 11.30.Er

Our understanding of hadronic B-meson decays has improved considerably during the past few years with the development of the Heavy Quark Effective Theory (HQET) [1, 2] and the Soft Collinear Effective Theory (SCET) [3, 4]. In these models, and in the framework of the factorization hypothesis [4, 5], the amplitude of the $B \to D^{(*)}\pi$ two-body decay carries information about the difference δ between the strong-interaction phases of the two isospin amplitudes $A_{1/2}$ and $A_{3/2}$ that contribute [6, 7]. A non-zero value of δ provides a measure of the departure from the heavy-quark limit and the importance of the final-state interactions in the $D^{(*)}\pi$ system. With the measurements by the *BABAR* [8] and BELLE [9] experiments of the color-suppressed B decay $\overline{B}^0 \to D^{(*)0}\pi^0$ providing evidence for a sizeable value of δ, an improved measurement of the color-favored decay amplitudes ($B^- \to D^{(*)0}\pi^-$ and $\overline{B}^0 \to D^{(*)+}\pi^-$) is of renewed interest. In addition, the study of B decays into D, D^*, and D^{**} mesons will allow tests of the spin symmetry [10, 11, 12, 13] imbedded in HQET and of non-factorizable corrections [14] that have been assumed to be negligible in the case of the excited states D^{**} [15].

In this paper we present new measurements of the branching fractions for the decays $B^- \to D^0\,\pi^-$, $D^{*0}\,\pi^-$, $D^{**0}\pi^-$, and $\overline{B}^0 \to D^+\,\pi^-$, $D^{*+}\,\pi^-$, $D^{**+}\pi^-$ [16], based on a missing mass method previously used by *BABAR* [17]. Here D^{**} refers to the sum of all the non-strange charm meson states with masses in the range $2.2 - 2.8$ GeV/c^2. This analysis uses $\Upsilon(4S) \to B\overline{B}$ events in which a B^+ or a B^0 meson, denoted $B_{\rm reco}$, decays into a hadronic final state and is fully reconstructed. The decays of the recoiling $\overline{B}$ into a charged pion and a charmed meson, *i.e.* $\overline{B} \to \pi^- X$, are studied. The charged pion is reconstructed and the mass of the $X = D, D^*, D^{**}$ is inferred from the kinematics of the two body B decay. This method, unlike the previous exclusive measurements [18, 19], does not assume that the $\Upsilon(4S)$ decays into B^+ and B^0 with equal rates, nor does it rely on the D, D^*, or D^{**} decay branching fractions.

The measurements presented here are based on a sample of 231 million $B\overline{B}$ pairs (210 fb^{-1}) recorded at the $\Upsilon(4S)$ resonance with the *BABAR* detector at the PEP-II asymmetric-energy B factory at SLAC. The *BABAR* detector is described in detail elsewhere [20]. Charged-particle trajectories are measured by a 5-layer double-sided silicon vertex tracker (SVT) and a 40-layer drift chamber (DCH), both operating in a 1.5-T solenoidal magnetic field. Charged-particle identification is provided by the average energy loss (dE/dx) in the tracking devices and by an internally reflecting ring-imaging Cherenkov detector. Photons are detected by a CsI(Tl) electromagnetic calorimeter. Muons are identified by the instrumented magnetic-flux return (IFR). We use Monte Carlo (MC) simulations of the *BABAR* detector based on GEANT4 [21] to optimize selection criteria and determine selection efficiencies.

We reconstruct B^+ and B^0 decays ($B_{\rm reco}$) in the modes $B^+ \to \overline{D}^{(*)0}\pi^+$, $\overline{D}^{(*)0}\rho^+$, $\overline{D}^{(*)0}a_1^+$, and $B^0 \to D^{(*)-}\pi^+$,

$D^{(*)-}\rho^+$, $D^{(*)-}a_1^+$. $\overline{D}^0$ candidates are reconstructed in the $K^+\pi^-$, $K^+\pi^-\pi^0$, $K^+\pi^-\pi^+\pi^-$, and $K^0_S\pi^+\pi^-$ decay channels, while D^- candidates are reconstructed in the $K^+\pi^-\pi^-$ and $K^0_S\pi^-$ modes, and K^0_S mesons are reconstructed to $\pi^+\pi^-$. D^* candidates are reconstructed in the $D^{*-} \to \overline{D}^0\pi^-$ and $\overline{D}^{*0} \to \overline{D}^0\pi^0$ decay modes. A 3σ cut is applied on the D meson mass m_D (and on the D^*-D mass difference Δm_{D^*}) where $\sigma = \sigma_{m_D}(\sigma_{\Delta m_{D^*}})$ is the resolution on m_D (Δm_{D^*}) and is determined from data. A vertex fit is performed on D (D^*) with the mass constrained to the nominal value [22]. Two nearly independent variables are defined to identify the fully reconstructed B candidates kinematically. The first one is the beam-energy substituted mass, $m_{\rm ES} = \sqrt{(s/2 + \mathbf{p}_i\cdot\mathbf{p}_B)^2/E_i^2 - \mathbf{p}_B^2}$, where $\mathbf{p}_B$ is the $B_{\rm reco}$ momentum and $(E_i, \mathbf{p}_i)$ is the four-momentum of the initial e^+e^- system, both measured in the laboratory frame. The invariant mass of the initial e^+e^- system is $\sqrt{s}$. The second variable is $\Delta E = E_B^* - \sqrt{s}/2$, where E_B^* is the $B_{\rm reco}$ candidate energy in the center-of-mass frame. To define the $B_{\rm reco}$ sample (Fig. 1), we require $|\Delta E| < n\,\sigma_{\Delta E}$, where the measured resolutions $\sigma_{\Delta E}$ range from 12 to 35 MeV and $n = 2$ or 3, both depending on the $B_{\rm reco}$ mode. The $B_{\rm reco}$ candidate multiplicity is 1.4 for data as well as for the MC simulation sample. For events with more than one candidate, we select the $B_{\rm reco}$ with the best χ^2 defined with the variables m_D, Δm_{D^*}, and ΔE. The MC simulation shows that the recoil variables are reconstructed well within their experimental resolution when using this selection.

The number of $B_{\rm reco}$ is extracted from the $m_{\rm ES}$ spectra (Fig. 1) in the $5.27 - 5.29$ GeV/c^2 signal region. The $m_{\rm ES}$ distribution is fit to the sum of a broad combinatorial background and a narrow signal in the mass interval $5.21 - 5.29$ GeV/c^2. The combinatorial background is described by an empirical phase-space threshold function [23] and the signal with a Crystal Ball function [24] which is a Gaussian function centered at the B meson mass modified to account for photon radiation energy-loss. All parameters for the functions describing the $B_{\rm reco}$ signal and background distributions are determined from data. The measured yields of reconstructed B^+ and B^0 candidates, $N_{B^+} = 189474 \pm 7487$ and $N_{B^0} = 103169 \pm 3303$, are obtained by subtracting the fitted and the peaking (described below) backgrounds from the total number of events found in the signal region. These $B_{\rm reco}$ numbers serve as the normalization of all branching fraction measurements reported in this paper. The error is dominated by the systematic uncertainties due to the fit of the combinatorial background and to the determination of the peaking background. We assign 2.3% uncertainty to N_{B^+} and 1.8% to N_{B^0} as a fit uncertainty, obtained by varying the lower boundary of the fit interval from 5.20 to 5.23 GeV/c^2. The contamination of misreconstructed B^0 events in the B^+ signal (and vice-versa) induces a peaking background near the

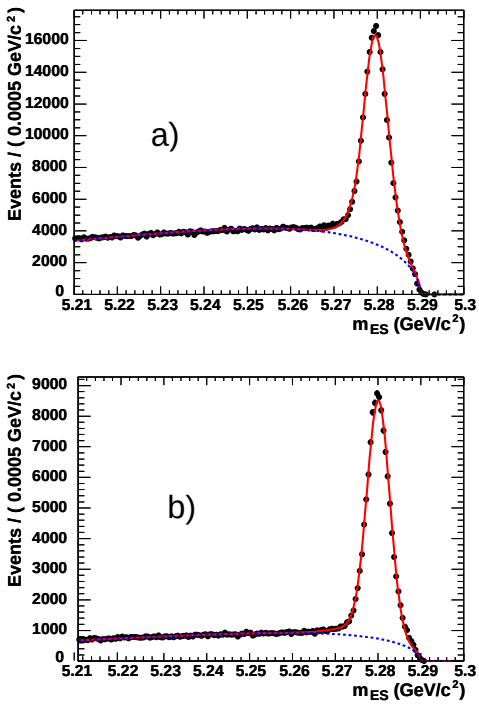

FIG. 1: $m_{\rm ES}$ spectra of reconstructed (a) B^+ and (b) B^0 candidates. The solid curve is the sum of the fitted signal and background whereas the dashed curve is the background component only.

B mass. From the MC simulation, the fraction of B^0 events in the reconstructed B^+ signal sample is found to be $(3.2 \pm 3.2_{\rm syst.})\%$ and the fraction of B^+ events in the reconstructed B^0 signal sample $(2.8 \pm 2.8_{\rm syst.})\%$. A 100% systematic uncertainty is conservatively assigned to these numbers taking into account the possible differences in the reconstruction efficiency in data and MC, as well as the branching fraction uncertainties for those B decay modes contributing to the peaking background. The total systematic uncertainties on N_{B^+} and N_{B^0} are 3.9% and 3.2%, respectively.

In the decay $\Upsilon(4S) \to B_{\rm reco}\overline{B}_{X\pi}$ where $\overline{B}_{X\pi}$ is the recoiling $\overline{B}$ which decays into π^-X, the invariant mass of the X system is derived from the missing 4-momentum p_X applying energy-momentum conservation:

$$p_X = p_{\Upsilon(4S)} - p_{B_{\rm reco}} - p_{\pi^-}.$$

The 4-momentum of the $\Upsilon(4S)$, $p_{\Upsilon(4S)}$, is computed from the beam energies and p_{π^-} and $p_{B_{\rm reco}}$ are the measured 4-momenta of the pion and of the reconstructed $B_{\rm reco}$, respectively. The $B_{\rm reco}$ energy is constrained by the beam energies. The $\overline{B} \to D\pi^-$, $\overline{B} \to D^*\pi^-$, or $\overline{B} \to D^{**}\pi^-$ signal yields peak at the D, D^*, and D^{**} masses in the missing mass spectrum, respectively.

The pion candidates, chosen among the tracks that do not belong to the $B_{\rm reco}$, are required to have produced at

least 12 DCH hits. For the charged $B_{\rm reco}$, the pion candidate has the opposite sign to the $B_{\rm reco}$. For neutral $B_{\rm reco}$, because of the $B^0-\overline{B}^0$ mixing, the corresponding requirement is not applied. Muon tracks are rejected using the IFR information, electrons tracks using the energy loss in the SVT and the DCH, or the ratio of the candidate's EMC energy deposition to its momentum (E/p). Protons and kaons are rejected based on informations from the DIRC and energy loss in the SVT and the DCH. The rejection efficiency is 97% and there is no peaking trend in the missing mass distribution from remaining kaons, protons, muons, or electrons. The pion reconstruction efficiency is determined from the MC simulation and reported in Table I.

The signal yields for the different decay modes are extracted from the missing mass spectra. The data distributions and the $b\overline{b}$ and the $q\overline{q}$ ($q = c, u, d, s$) background expectations are shown in Figs. 2(a) and 2(b). The shape of the background is taken from MC and the normalization is scaled to match the data in the sideband region $2.8 - 3.2$ GeV/c^2. The error on the background normalization is 2%. This is determined using the statistical errors of MC and data samples. The background subtracted missing mass distributions are shown in Figs. 2(c) and 2(d).

The $D\pi$ and $D^*\pi$ signal yields are extracted by a χ^2 fit to the background subtracted missing mass distribution in the range $1.65 - 2.20$ GeV/c^2. The $D\pi$ and $D^*\pi$ components are each modeled by a sum of two Gaussian functions, to account for tails in the mass distributions. The parameters are $m_i^{D^{(*)}}$ and $\sigma_i^{D^{(*)}}$ for the D and D^* resonances, where the index $i = 1, 2$ corresponds to the first and second Gaussian. In the fit, the central values m_i^D and the σ_i^D are free parameters, while for the D^* the variances are constrained by the ratios $\sigma_i^{D^*}/\sigma_i^D = 0.900 \pm 0.015$, as determined from MC simulation, while the central values differences $m_i^{D^*} - m_i^D$ are fixed to 0.1421 GeV/c^2 and to 0.1406 GeV/c^2 for B^+ and B^0, respectively, corresponding to the world average D and D^* mass differences [22].

The D^{**} yields are defined as the excess of candidates in the missing mass range $2.2 - 2.8$ GeV/c^2, and the $\overline{B} \to D^{**}\pi^-$ branching fractions refer to the contributions of all non-strange charm meson states in the same region. The range is chosen in order to maximize the acceptance to the four P-wave D^{**} states predicted by the theory given the 34 MeV/c^2 mass resolution, determined from MC simulation, in the same region. The well-known narrow D_1 and D_2^* states [22] are fully contained in this range, and more than 90% of the broad D_0 and D_1', are covered if measured masses and widths [25, 26] are used. The event yields, the efficiencies, and the resulting branching fractions are reported in Table I.

The uncertainty related to π reconstruction efficiency is due to the MC sample statistics and the systematic uncertainty on track reconstruction and particle identification algorithms. The uncertainty due to the yield extraction is estimated by fitting the MC sample. The difference between the MC and the data fitted yields is found to be consistent with zero and the statistical errors are taken as a systematic error. We evaluate the uncertainty on the missing mass resolution in the $D\pi$ and $D^*\pi$ yield extraction by varying by one standard deviation the ratio $\sigma_i^{D^*}/\sigma_i^D$ while $\sigma_2^{D^*}$ and $m_2^{D^*}$ are let free. The difference in the yield is taken as systematic uncertainty. The uncertainty related to the subtraction of the background is determined by varying the branching fraction of the different background components within the uncertainties of the most recent measurements [22] and taking into account the error on the background normalization. Due to the threshold shape of some of the background components and the fast varying combinatorial background, $B \to D^{**}\pi$ branching fractions have larger systematic errors than $B \to D\pi$ and $B \to D^*\pi$ branching fractions. The summary of these systematic uncertainties is reported in Table II.

TABLE I: Signal yields, efficiencies and branching fractions for $\overline{B} \to D\pi^-$, $\overline{B} \to D^*\pi^-$ and $\overline{B} \to D^{**}\pi^-$. The first error is statistical except for the efficiencies for which it is mainly systematic. The second error on the branching fractions is systematic. The $\overline{B} \to D^{**}\pi^-$ branching fractions are given for the $2.2 - 2.8$ GeV/c^2 mass range which in addition to the P-wave states may include some yet unknown charm meson states.

Decay mode	Yield	Efficiency	$\mathcal{B}(10^{-3})$
$B^- \to D^0\pi^-$	677 ± 32		4.49±0.21±0.23
$B^- \to D^{*0}\pi^-$	774 ± 33	0.796±0.007	5.13±0.22±0.28
$B^- \to D^{**0}\pi^-$	829 ± 78		5.50±0.52±1.04
$\overline{B}^0 \to D^+\pi^-$	248 ± 19		3.03±0.23±0.23
$\overline{B}^0 \to D^{*+}\pi^-$	245 ± 19	0.793±0.007	2.99±0.23±0.24
$\overline{B}^0 \to D^{**+}\pi^-$	192 ± 54		2.34±0.65±0.88

Using the measured branching fractions we compute the following ratios:

$$\mathcal{B}(B^- \to D^{*0}\pi^-)/\mathcal{B}(B^- \to D^0\pi^-) = 1.14 \pm 0.07 \pm 0.04,$$
$$\mathcal{B}(B^- \to D^{**0}\pi^-)/\mathcal{B}(B^- \to D^0\pi^-) = 1.22 \pm 0.13 \pm 0.23,$$
$$\mathcal{B}(\overline{B}^0 \to D^{*+}\pi^-)/\mathcal{B}(\overline{B}^0 \to D^+\pi^-) = 0.99 \pm 0.11 \pm 0.08,$$
$$\mathcal{B}(\overline{B}^0 \to D^{**+}\pi^-)/\mathcal{B}(\overline{B}^0 \to D^+\pi^-) = 0.77 \pm 0.22 \pm 0.29.$$

The first uncertainty is statistical and the second is systematic. In addition to the cancellation of many of the systematic errors, the ratios are insensitive to the absolute normalization scale.

In summary, we have measured the branching fractions for the decays $B^- \to D^0\pi^-$, $B^- \to D^{*0}\pi^-$, $B^- \to D^{**0}\pi^-$, $\overline{B}^0 \to D^+\pi^-$, $\overline{B}^0 \to D^{*+}\pi^-$, and $\overline{B}^0 \to D^{**+}\pi^-$, using a missing mass method. This measurement does not assume that the $\Upsilon(4S)$ decays into B^+

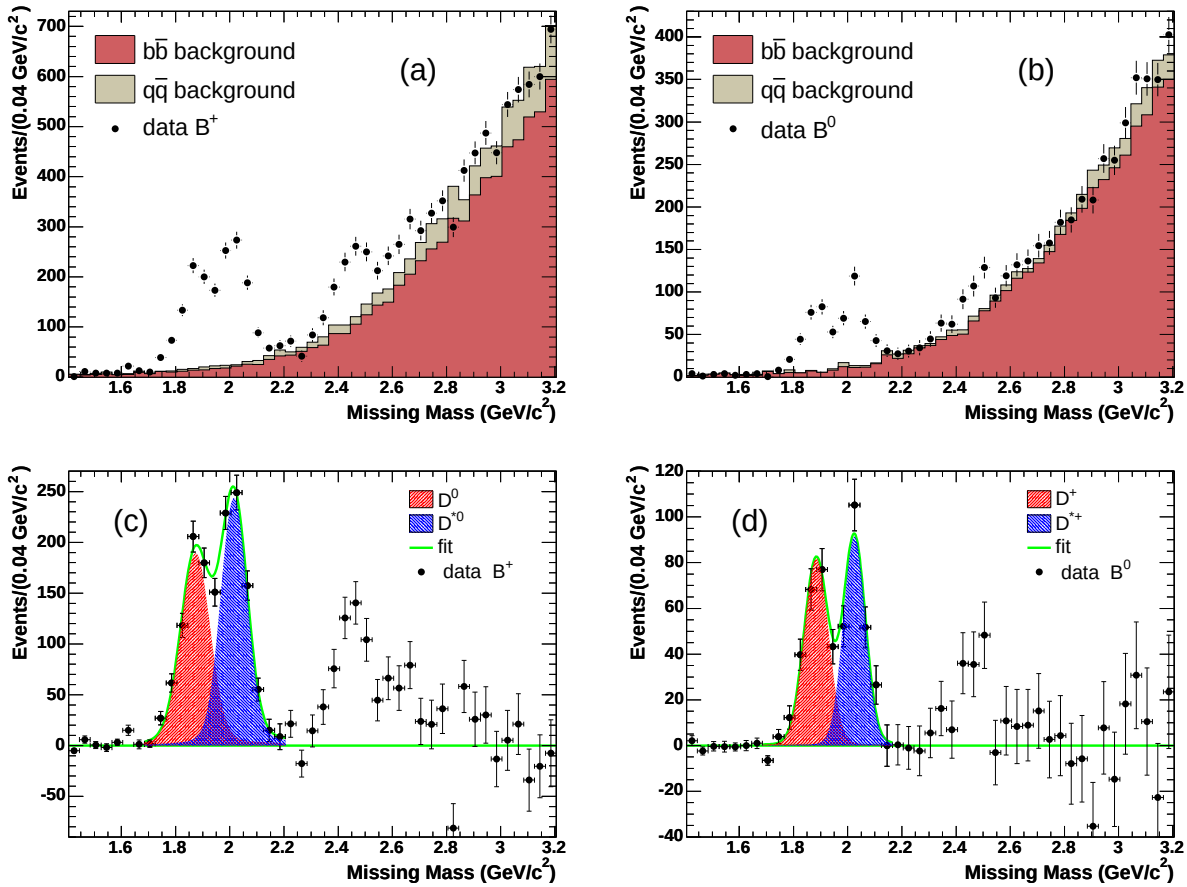

FIG. 2: Top: missing mass distributions obtained in the recoil of B^+ (a) and B^0 (b). The points with error bars show the data and the histograms show the background contributions ($b\overline{b}$ and $q\overline{q}$ ($q = c, u, d, s$)) predicted by the MC simulation. Bottom: background-subtracted missing mass spectra for B^+ (c) and B^0 (d). The curves show the result of the fits to the $D\pi$ and $D^*\pi$ components.

TABLE II: Total relative systematic uncertainties for the branching fractions $\mathcal{B}(B^- \to (D^0,\ D^{*0},\ D^{**0})\pi^-)$ and $\mathcal{B}(\overline{B}^0 \to (D^+,\ D^{*+},\ D^{**+})\pi^-)$.

Syst. Source	$B^- \to D^0\pi^-$	$B^- \to D^{*0}\pi^-$	$B^- \to D^{**0}\pi^-$	$\overline{B}^0 \to D^+\pi^-$	$\overline{B}^0 \to D^{*+}\pi^-$	$\overline{B}^0 \to D^{**+}\pi^-$
N_B	3.9%	3.9%	3.9%	3.2%	3.2%	3.2%
Efficiency	0.9%	0.9%	0.9%	0.9%	0.9%	0.9%
Yield extraction	2.7%	2.7%	5.1%	5.4%	5.1%	5.9%
Missing mass resolution	0.9%	0.8%	-	1.9%	1.1%	-
Background subtraction	1.6%	2.3%	17.7%	3.7%	5.4%	37.1%
Total	5.2%	5.4%	18.9%	7.6%	8.2%	37.7%

and B^0 with equal rates, nor does it rely on the D, D^*, or D^{**} intermediate branching fractions. The results for $\mathcal{B}(B \to D\pi^-)$ and $\mathcal{B}(B \to D^*\pi^-)$ are compatible with previous world averages [22]. We have extracted a new result for $\mathcal{B}(B \to D^{**}\pi^-)$ branching fractions where D^{**} excited states correspond to the yield measured in the mass range $2.2 - 2.8$ GeV/c^2. The isospin study [6, 7] will become competitive with the exclusive measurements [19] if the statistical error is reduced by a factor of 2. With regard to spin symmetry, the values measured for the ratios $\mathcal{B}(B^- \to D^{*0}\pi^-)/\mathcal{B}(B^- \to D^0\pi^-)$ and $\mathcal{B}(\overline{B}^0 \to D^{*+}\pi^-)/\mathcal{B}(\overline{B}^0 \to D^+\pi^-)$ are close to 1, as predicted by different theoretical models [10, 11, 12, 13, 14], and their precision is comparable or better than the current world averages [22].

We are grateful for the extraordinary contributions of

our PEP-II colleagues in achieving the excellent luminosity and machine conditions that have made this work possible. The success of this project also relies critically on the expertise and dedication of the computing organizations that support *BABAR*. The collaborating institutions wish to thank SLAC for its support and the kind hospitality extended to them. This work is supported by the US Department of Energy and National Science Foundation, the Natural Sciences and Engineering Research Council (Canada), Institute of High Energy Physics (China), the Commissariat à l'Energie Atomique and Institut National de Physique Nucléaire et de Physique des Particules (France), the Bundesministerium für Bildung und Forschung and Deutsche Forschungsgemeinschaft (Germany), the Istituto Nazionale di Fisica Nucleare (Italy), the Foundation for Fundamental Research on Matter (The Netherlands), the Research Council of Norway, the Ministry of Science and Technology of the Russian Federation, Ministerio de Educación y Ciencia (Spain), and the Particle Physics and Astronomy Research Council (United Kingdom). Individuals have received support from the Marie-Curie IEF program (European Union) and the A. P. Sloan Foundation.

* Also with Università di Perugia, Dipartimento di Fisica, Perugia, Italy
† Also with Università della Basilicata, Potenza, Italy

[1] M. Beneke *et al.*, Nucl. Phys. **B591**, 313 (2000).
[2] M. Neubert and B. Stech in *Heavy Flavors* edited by A.J. Buras and M. Lindner, 2nd ed. (World scientific, Singapore, 1998).
[3] C.W. Bauer, D. Pirjol, and I. W. Stewart, Phys. Rev. D **65**, 054022 (2002).
[4] C.W. Bauer, D. Pirjol, and I. W. Stewart, Phys. Rev. Lett. **87**, 201806 (2001).
[5] M. Bauer, B. Stech, M. Wirbel, Z. Phys. C **34**, 103 (1987).
[6] J.L. Rosner, Phys. Rev. D **60**, 074029 (1999).
[7] C. W. Chiang and J.L. Rosner, Phys. Rev. D **67**, 074013 (2003).
[8] *BABAR* Collaboration, B. Aubert *et al.*, Phys. Rev. D **6**, 032004 (2004).
[9] Belle Collaboration, K. Abe *et al.*, Phys. Rev. Lett. **88**, 052002 (2002).
[10] T. Mannel *et al.* , Phys. Lett. B **259**, 359 (1991).
[11] M. Neubert, W. Rieckert, B. Stech, and Q. P. Xu, in *Heavy Flavors* edited by A.J. Buras and M. Lindner, (World scientific, Singapore, 1992).
[12] S. Mantry, D. Pirjol, and I. W. Stewart, Phys. Rev. D **68**, 114009 (2003).
[13] F. Jugeau, A. Le Yaouanc, L. Oliver, and J.-C Raynal, Phys. Rev. D **72**, 094010(2005).
[14] B. Blok, and M. Shifman, Nucl. Phys. **B389**, 534 (1993).
[15] M. Neubert, Phys. Lett. B **418**, 173 (1998).
[16] Charge conjugate relations are assumed throughout this paper.
[17] *BABAR* Collaboration, B. Aubert *et al.*, Phys. Rev. Lett. **96**, 052002 (2006).
[18] S. Ahmed *et al.* , Phys. Rev. D **66**, 031101(R) (2002) and M.S. Alam *et al.* , Phys. Rev. D **50**, 43(1994).
[19] G. Calderini, *BABAR* Collaboration, XXXIII International Conference on High Energy Physics (ICHEP'06), Moscow, 26 July - 2 August, 2006.
[20] *BABAR* Collaboration, B. Aubert *et al.*, Nucl. Instr. Meth. A **479**,1 (2002).
[21] GEANT4 Collaboration, S. Agostinelli *et al.* Nucl. Instrum. Methods Phys Res. Sect. A **506**, 250 (2003).
[22] W.-M. Yao *et al.* (Particle Data Group Collaboration), J. Phys. **G33**, 1, (2006).
[23] ARGUS Collaboration, H. Albrecht *et al.*, Z. Phys. C **48**, 543 (1990).
[24] CRYSTAL BALL collaboration, T. Skwarnicki, DESY F31-86-02, J. E. Gaiser *et al.*, Phys. Rev. D **34**, 711 (1986).
[25] Belle Collaboration, K.Abe *et al.*, Phys. Rev. D **69**, 112002 (2004).
[26] FOCUS Collaboration, J. M. Link *et al.*, Phys. Lett. B **586**, 11 (2004).

BABAR Analysis Document #756, Version 12 July 6th, 2006

Measurement of the Branching Fraction for $B^-(B^0) \to D^0(D^+)\pi^-$, $B^-(B^0) \to D^{*0}(D^{*+})\pi^-$ and $B^-(B^0) \to D^{**0}(D^{**+})\pi^-$ with a missing mass method

F. Couderc and A.Zghiche

Abstract

We present a measurement of the branching fractions for the decays $B^- \to D^0\ \pi^-$, $D^{*0}\ \pi^-$, $D^{**0}\pi^-$ and $\bar{B}^0 \to D^+\ \pi^-$, $D^{*+}\ \pi^-$, $D^{**+}\pi^-$ using a missing mass method. The results are based on $\Upsilon(4S)$ decays in $B\bar{B}$ pairs. One of the B mesons is fully reconstructed and the other one decays to a charmed meson and a π^-. Only the π^- is reconstructed and the mass and momentum of the associated charmed particle is inferred by kinematics. The analysis is based on a sample of 231 million $B\bar{B}$ events recorded with the *BABAR* detector at the $\Upsilon(4S)$ resonance. We measure:

$$\begin{aligned}
\mathcal{B}(B^- \to D^0\pi^-) &= (4.49 \pm 0.21 \pm 0.23) \times 10^{-3} \\
\mathcal{B}(B^- \to D^{*0}\pi^-) &= (5.13 \pm 0.22 \pm 0.28) \times 10^{-3} \\
\mathcal{B}(B^- \to D^{**0}\pi^-) &= (5.50 \pm 0.52 \pm 1.04) \times 10^{-3} \\
\mathcal{B}(\bar{B}^0 \to D^+\pi^-) &= (3.00 \pm 0.23 \pm 0.23) \times 10^{-3} \\
\mathcal{B}(\bar{B}^0 \to D^{*+}\pi^-) &= (2.97 \pm 0.23 \pm 0.24) \times 10^{-3} \\
\mathcal{B}(\bar{B}^0 \to D^{**+}\pi^-) &= (2.32 \pm 0.65 \pm 0.88) \times 10^{-3}
\end{aligned}$$

Contents

1 Introduction

The understanding of hadronic B-meson decays has improved considerably during the past few years with the development of the Heavy Quark Effective Theory (HQET)[1],[2] and Soft Collinear Effective Theory (SCET) [3]. Neglecting the Final State Interactions in the framework of the so-called "Factorization" hypothesis, the two body charmed meson B decay($B \to DX$) amplitudes can be calculated as a product of two hadronic currents.

With the recent measurement by *BABAR*[4] and BELLE [5] experiments of the color suppressed charmed meson B decay $\bar{B}^0 \to D^0\pi^0$, the precise measurement of the color favored charmed meson B decay amplitudes $B^- \to D^0\pi^-$and $B^0 \to D^-\pi^+$regains interest. It will give access to the strong phase difference δ, between the isospin amplitudes I=1/2 and I=3/2. δ is expressed as a function of the charmed meson B decay widths[6], providing the opportunity to test the factorization hypothesis and the HQET model. In addition, the study of the charmed meson B decay into the excited states D^*, D^{**} will respectively allow the test of the spin symmetry [8] imbedded in HQET and the size of the non-factorized corrections assumed to be negligible in the case of the excited states D^{**} [9].

The branching fraction for the charged B decay mode $B^- \to D^0\pi^-$has been recently updated by CLEO-II [7, 10] as $\mathcal{B}(B^- \to D^0\pi^-) = (4.98 \pm 0.29) \times 10^{-3}$, while the $B^- \to D^{*0}\pi^-$ branching fraction is still not known with a precision better than 10% ($\mathcal{B}(B^- \to D^{*0}\pi^-) = (4.6 \pm 0.4) \times 10^{-3}$)[10]. The branching fractions of the corresponding B^0 decay modes are indicated in Table 1. All these branching fractions are calculated assuming equal production of B^+ and B^0 at the $\Upsilon(4S)$ and using the PDG values of the $D^0 \to K^-\,\pi^+$ branching fraction, the $\mathcal{B}(D^0 \to K^-\,\pi^+\,\pi^0)/\mathcal{B}(D^0 \to K^-\,\pi^+)$, $\mathcal{B}(D^0 \to K^-\,\pi^+\,\pi^-\,\pi^+)/\mathcal{B}(D^0 \to K^-\,\pi^+)$ branching fraction ratios and their errors. In addition, for the $B^- \to D^{*0}\pi^-$mode, the absolute $\mathcal{B}(D^{*0} \to D^0\pi^0)$ is also used. B decays into $\bar{D}^{**}\pi^+$ modes have also been recently measured by Belle, for both the narrow $\bar{D}_1$, $\bar{D}_2^*$ and the wide $\bar{D}_0^*$ and $\bar{D}_1'$ states, for different decay modes of the $\bar{D}^{**}$. These measurements have typically a $10-20\%$ statistical precision and are summarized in Table 1. The sum of the product of the B branching fractions times the $\bar{D}^{**}$ sub-decay branching fractions for the different $\bar{D}^{**}\pi^+$ modes experimentally reconstructed is approximately 1 to 2 $\times 10^{-3}$.

In this document, we will present the measurement of the branching fractions for the decays $\bar{B}^0(B^-) \to D^+(D^0)\pi^-$, $\bar{B}^0\,(B^-) \to D^{*+}(D^{0*})\pi^-$ and $\bar{B}^0\,(B^-) \to D^{**+}(D^{0**})\pi^-$, using an original method in which the associated B^0 or B^+ mesons are reconstructed through their decays $B \to \bar{D}^{(*)}\pi^+$, $B \to \bar{D}^{(*)}\rho^+$ and $B \to \bar{D}^{(*)}a_1^+$. The recoil B^- momentum and energy are precisely known and the missing mass to the π^- is performed. The D^0, D^{*0} and D^{**0} meson counting is made by a fit of the corresponding missing mass, hence, there is no need to use the D, D^* or D^{**} meson intermediate branching fractions to calculate the B decay branching fractions. In addition, the total number of reconstructed B^+ or B^0 is known with good precision as a result of the reconstruction itself, therefore, the assumption of equal production of B^0 and B^+ is no more necessary in this analysis. As a B-factory, *BABAR* is able to reconstruct a large number of B mesons making the method not only model independent but statistically competitive as well.

As the event reconstruction is described in detail elsewhere [13], we will focus on showing the signal yield and discussing the possibility to extract it with a good precision. Indeed, the major issue in this method is the proper description of the background. The ef-

ficiency studies as well as the study of the systematic uncertainties will also be discussed. Finally, we will show the measured branching fractions.

	$\mathcal{B}(B^0)$, 10^{-4}	$\mathcal{B}(B^+)$, 10^{-4}
$\mathcal{B}(B \to \bar{D}\pi^+)$	(27.6 ± 2.5) [10]	(49.8 ± 2.9) [10]
$\mathcal{B}(B \to \bar{D}^*\pi^+)$	(27.6 ± 2.1) [10]	(46 ± 4) [10]
$\mathcal{B}(B \to \bar{D}_0^*\pi^+)\mathcal{B}(\bar{D}_0^* \to \bar{D}\pi^-)$	< 1.2 [11]	$(6.1 \pm 0.6 \pm 0.9 \pm 1.6)$[11]
$\mathcal{B}(B \to \bar{D}_1'\pi^+)\mathcal{B}(\bar{D}_1' \to \bar{D}^*\pi^-)$	< 0.7 [11]	$(5.0 \pm 0.4 \pm 1.0 \pm 0.4)$[11]
$\mathcal{B}(B \to \bar{D}_1\pi^+)\mathcal{B}(\bar{D}_1 \to \bar{D}^*\pi^-)$	$(3.68 \pm 0.60^{+0.71\ +0.65}_{-0.40\ -0.30})$[11]	$(6.8 \pm 0.7 \pm 1.3 \pm 0.3)$[11]
$\mathcal{B}(B \to \bar{D}_1\pi^+)\mathcal{B}(\bar{D}_1 \to \bar{D}\pi^+\pi^-)$	$(0.89 \pm 0.15 \pm 0.17^{+0.0}_{-0.27})$[12]	$(1.85 \pm 0.29 \pm 0.35^{+0.0}_{-0.44})$[12]
$\mathcal{B}(B \to \bar{D}_2^*\pi^+)\mathcal{B}(\bar{D}_2^* \to \bar{D}\pi^-)$	$(3.08 \pm 0.33 \pm 0.09^{+0.15}_{-0.02})$[11]	$(3.4 \pm 0.3 \pm 0.6 \pm 0.4)$[11]
$\mathcal{B}(B \to \bar{D}_2^*\pi^+)\mathcal{B}(\bar{D}_2^* \to \bar{D}^*\pi^-)$	$(2.45 \pm 0.42^{+0.35\ +0.39}_{-0.45\ -0.17})$[11]	$(1.8 \pm 0.3 \pm 0.3 \pm 0.2)$[11]

Table 1: *Existing measurements of the branching-fraction products for $B \to \bar{D}\pi^+$, $\bar{D}^*\pi^+$ and $\bar{D}^{**}\pi^+$*

2 Data and Monte-Carlo samples

This analysis is based on the full Run1 to Run4 data sample. We use the skim BSemiExcl, processed with release 14. The analysis is performed over a total luminosity of $209\,fb^{-1}$, corresponding to 230 million $B\bar{B}$ pairs. We also use the generic $B^+\,B^-$, $B^0\,\bar{B}^0$, $c\bar{c}$ and $q\bar{q}$ Monte-Carlo samples summarized in Table 2, and select the Monte-Carlo events from the skim BSemiExcl. We also use a large statistics sample of cocktail Monte-Carlo $B \to \bar{D}X$, with $\bar{D}$ decaying only to reconstructible modes, to compute the reconstruction efficiencies. This sample is described in Table 3 for the different decay modes and the different run periods.

type	N_{evt} (10^6)	equiv.int. luminosity (fb^-1)
$B^+\,B^-$	377.0	718.2
$B^0\,\bar{B}^0$	353.4	673.2
$c\bar{c}$	176.9	136.1
$q\bar{q}$	513.3	245.6

Table 2: *Generic Monte-Carlo samples used in this analysis*

N_{evts} (10^6)	Run1	Run2	Run3	Run4
$B^0 \to \bar{D}^{(*)-}X$	2.01	5.36	2.38	19.33
$B^+ \to \bar{D}^{(*)0}\pi^+$	0.60	2.00	0.84	2.84
$B^+ \to \bar{D}^{(*)0}\rho^+/a_1^+$	0.71	2.40	0.98	3.41

Table 3: *Number of events from the different "cocktail" Monte-Carlo samples used in this analysis.*

3 Selection of the fully reconstructed B sample

3.1 Introduction

The selection of the fully reconstructed B^0 and B^+ samples is described in [13]. The following hadronic B decay modes are used:

- $B^+ \to \bar{D}^0\pi^+$, $\bar{D}^{*0}\pi^+$, $\bar{D}^0\rho^+$, $\bar{D}^{*0}\rho^+$, $\bar{D}^0 a_1^+$ and $\bar{D}^{*0}a_1^+$
- $B^0 \to D^-\pi^+$, $D^{*-}\pi^+$, $D^-\rho^+$, $D^{*-}\rho^+$, $D^- a_1^+$ and $D^{*-}a_1^+$

where the $\bar{D}$ and $\bar{D}^*$ meson decay modes used for reconstructing the B's are:

- $\bar{D}^0 \to K^+\pi^-$, $K^+\pi^-\pi^0$, $K^+\pi^-\pi^+\pi^-$, $K_S^0\pi^+\pi^-$.
- $D^- \to K^+\pi^-\pi^-$
- $D^{*-} \to \bar{D}^0\pi^-$
- $D^{*0} \to D^0\pi^0$ and $D^{*0} \to D^0\gamma$.

  The $D^{*0} \to D^0\gamma$ channel was used to reconstruct charged B up to version5 of BAD756. The systematic uncertainty associated to the B counting while using this channel was 5.%. It decreases to only 2.3% if this channel is not used. The final systematic uncertainty is reduced as well, by 26.%. The statistical uncertainty on the final result is enhanced by only 13.% (the total charged B number is reduced by 21.%).

  In this version of the BAD the results will be given considering only D^{*0} reconstructed into D^0 π^0.

Two nearly independent variables are defined to identify the B-meson candidates kinematically: the energy-substituted B mass $m_{\rm ES} = \sqrt{(s/2 + \mathbf{p_0}\cdot\mathbf{p_B})^2/(\mathrm{E}_0^2 - \mathrm{p}_\mathrm{B}^2)}$ where the subscripts 0 and B refer to the e^+e^- system and the B candidate respectively; and $\Delta E = E_B^* - \sqrt{s}/2$, where E_B^* is the B candidate energy in the center-of-mass frame. A cut at $\pm 3\sigma_{\Delta E}$, which can be tightened to improve the purity of the B sample for some of the modes, is applied on ΔE. The number of B events is estimated from a fit to the $m_{\rm ES}$ spectrum in the mass range 5.27-5.29 GeV/c^2 after the ΔE cut. The purity of the signal (fraction of correctly reconstructed B's over the total number of events selected) depends on the cuts applied to define the signal region in the ($m_{\rm ES}$, ΔE) plane, as well as on the cuts on the masses of the reconstructed $\bar{D}$ and $\bar{D}^*$ mesons, on the K meson identification criteria used and on the $\bar{D}$ meson track vertexing probabilities and angular distributions. In the analysis described in Ref.[13], four (two) different level of cuts on these variables have been tuned to define B^+ (B^0) samples of different purities. In this analysis, we will use the loose $B+$ and the tight B^0 selections of Ref. [13], which give B purities of 50% or better.

The selection code is run for one B charge at a time thus, each one of the four samples B^+, B^-, B^0 and $\bar{B}^0$ is built separately. In case of multiple B candidates, only one B candidate is allowed per event. The criteria for selecting the best candidate, described in [13], is based first on the purity of the B modes and then on a χ^2 built from the D and

D^* masses, and from ΔE. Studies on Monte-Carlo signal samples have shown that in case of multiple candidates, this algorithm chooses the correct B candidate 80 % of the time. The B^+ and B^- (B^0 and $\bar{B}^0$) candidates are then summed in a single charged (neutral) B sample. The data $m_{\rm ES}$ spectra of the charged (neutral) B candidates are shown in Fig.1 (Fig.2), separately for each B submode.

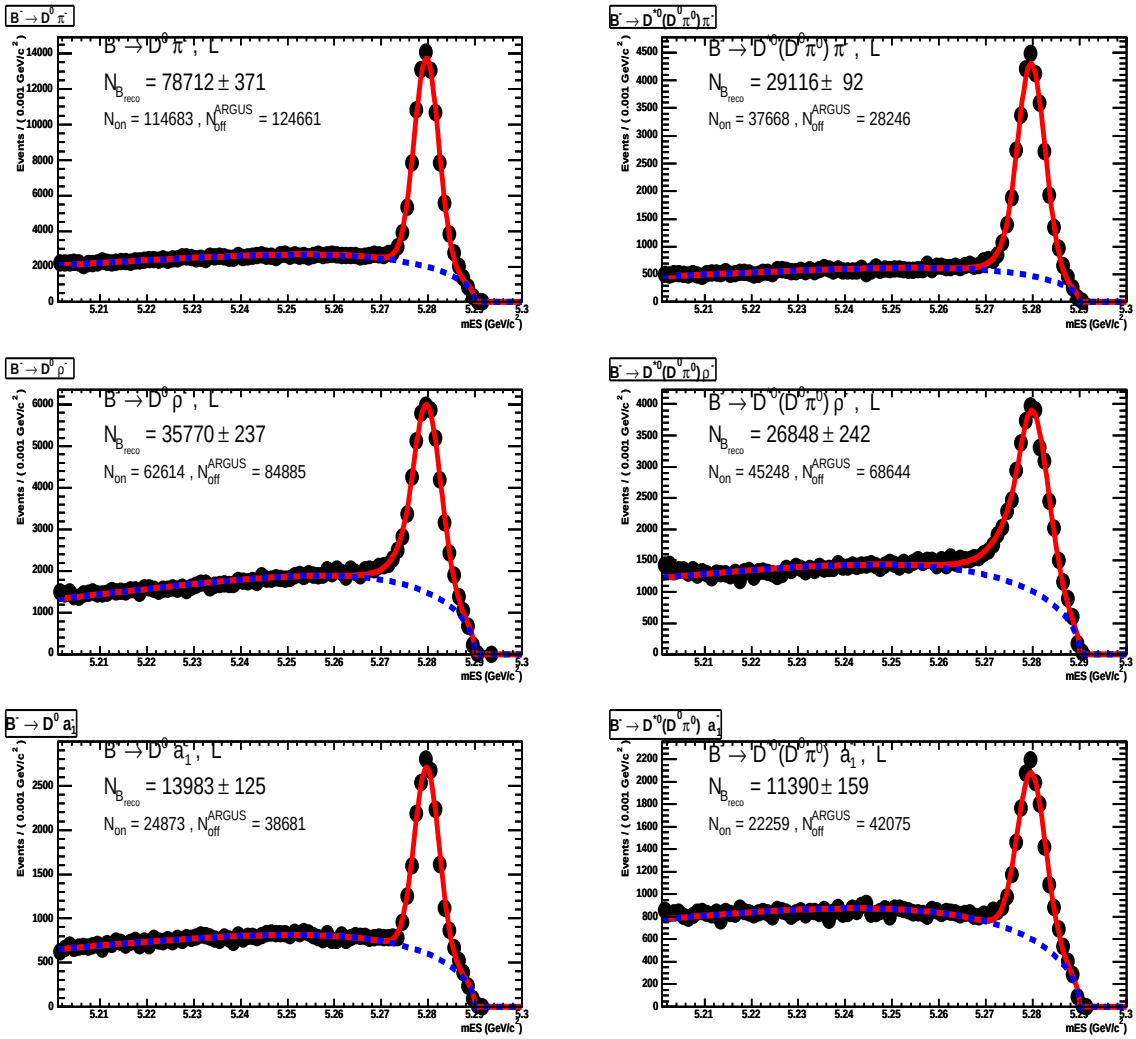

Figure 1: *The data $m_{\rm ES}$ spectra of the selected $B^{\pm}$ candidates, fitted separately for each of the reconstructed modes. Left column: D^0X. Right column: $D^{*0}X$ ($D^{*0} \to D^0\pi^0$). with $X = \pi$ (top), $X = \rho$ (middle), $X = a_1$ (bottom). $N_{B_{reco}}$ is obtained by counting the yield of B after subtraction of the Argus contribution in the $m_{\rm ES}$ range: 5.27-5.29 GeV/c^2. N_{on} is the total yield in the same range. N_{off}^{Argus} is the Argus yield in the $m_{\rm ES}$ range:5.20-5.26 GeV/c^2.*

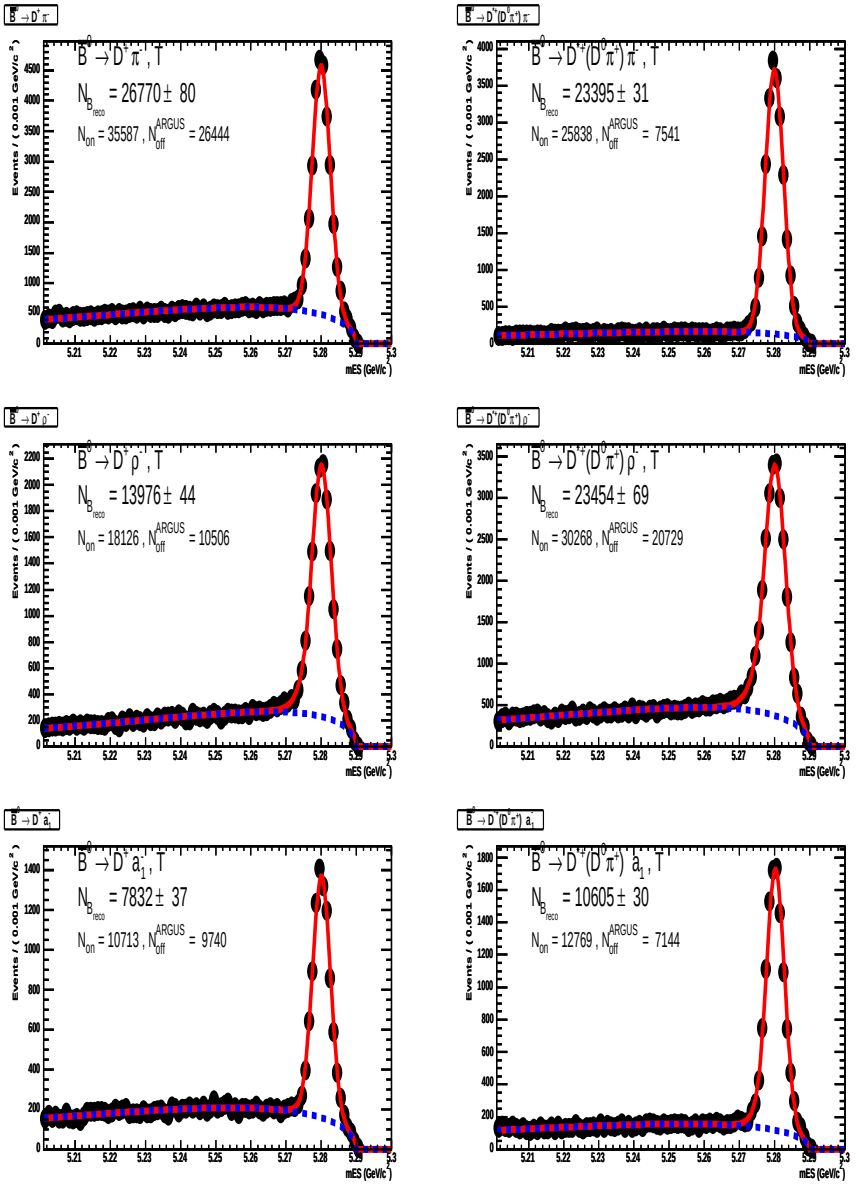

Figure 2: *The data $m_{\rm ES}$ spectra of the selected B^0 and $\bar{B}^0$ candidates, fitted separately for each of the reconstructed modes. Left column: $D^- X$. Right column: $D^{*-} X$ ($D^{*-} \to \bar{D}^0\pi^-$), with $X = \pi$ (top), $X = \rho$ (middle), $X = a_1$ (bottom). $N_{B_{reco}}$ is obtained by counting the yield of B after subtraction of the Argus contribution in the $m_{\rm ES}$ range: 5.27-5.29 GeV/c^2. N_{on} is the total yield in the same range. N_{off}^{Argus} is the Argus yield in the $m_{\rm ES}$ range:5.20-5.26 GeV/c^2.*

3.2 $m_{\rm ES}$ spectrum fitting procedure

The total number of fully reconstructed charged or neutral B-mesons is extracted performing a binned maximum likelihood fit to the $m_{\rm ES}$ distributions. Each of the different B

submodes is fitted separately. The signal distribution is parameterized as a two-gaussian or a Crystal Ball function. The final fitted B number is not affected by the choice of either signal parametrization . The combinatorial background is parameterized as an Argus threshold function[16]. As a first iteration of the $m_{\rm ES}$ fit, the semi-leptonic data (for which a muon or an electron with a momentum higher than $1.3\,{\rm GeV}/c^2$ is requested in the B_{recoil} side, this leads to the purification of the sample) are used to determine the mean value of $m_{\rm ES}$ and to keep it fixed in the final hadronic decay $m_{\rm ES}$ fit. The Argus function parameter is left floating in the fit, while the end point on $m_{\rm ES}$ is fixed to $5.29\,{\rm GeV}/c^2$. All the selection criteria are detailed in BAD623 [13] and BAD1234 [14]. The final yield reported in this analysis is obtained with a selection close to the Loose purity of BAD623 [13] and BAD1234 [14] for charged B and to the Tight purity for B^0.

3.3 Generic Monte-Carlo

In order to check the $m_{\rm ES}$ distribution fit procedure, we have run the B selection and $m_{\rm ES}$ fits separately on the B^+ B^-, B^0 $\bar{B}^0$, $c\bar{c}$ and $q\bar{q}$ Monte Carlo samples, and on the total. In addition, the generic Monte Carlo simulation enabled the determination of the amount of peaking backgrounds. These two subjects are discussed in the following sections 3.4 and 3.5.

3.4 Data

The results of the fits for the $m_{\rm ES}$ spectra of the different B modes are shown in Fig.1 (B^+) and Fig.2(B^0), separately for each B submode. The B event yields in the signal box $5.27 < m_{\rm ES} < 5.29\,{\rm GeV}/c^2$ are estimated by summing the number of events fitted for the individual B modes, corrected from events with $m_{\rm ES} < 5.27\,{\rm GeV}/c^2$. For the $209\,fb^{-1}$ of data luminosity, the B meson selection and reconstruction method led to a fitted number of $195818 \pm 549(stat.) \pm 4503(syst.)$ charged B candidates and $106032 \pm 128 \pm 1908$ neutral B candidates. The statistic uncertainty on the yield is given on the fit of the background whilst the systematic one is determined varying the start point of the Argus fit in the range [5.20-5.23]. This study has been performed for both Generic MC and data. Less than 1% variation of the generated yield is due the variation of the Argus function fit start point. In the data, the variation of the yield for B^+ and B^0 was found to be equal to 2.3% and 1.8% respectively. We assign these values as systematic uncertainties on the B counting (see appendix A for details).

3.5 Peaking background

In our analysis, the contamination of misreconstructed B^0 events in the B^+ signal (and vice-versa) induces a background which peaks near the B mass. From the Monte Carlo simulation, the fraction of B^0 events in the reconstructed B^+ signal sample is found to be $c_0 = 0.032 \pm 0.032(syst.)$, and the fraction of B^+ events in the reconstructed B^0 signal sample $c_+ = 0.028 \pm 0.028(syst.)$ (see Appendix A.2 for details). The systematic uncertainties assigned to these numbers are conservative, they take into account the possible differences in reconstructing real and simulated events, as well as branching fraction uncertainties for those B decay modes contributing to the wrong charge contamination. Thus,

in the data, the total number of reconstructed charged B to be used in the determination of the branching fractions becomes $189474 \pm 549(stat.) \pm 7467(syst.)$ after subtraction of the peaking background and with a total systematic uncertainty of 3.9%, as a result of the sum in quadrature of the fit and the peaking systematic uncertainties. Similarly, the number of true B^0 events in the B^0 sample becomes $103169 \pm 128 \pm 3301$ with a total systematic uncertainty of 3.2% as detailed in Table 4.

B meson	B final number	Peaking value$(\% \pm \%)$	fit syst. $(\%)$ uncertainty	total B counting syst.$(\%)$
B^-	$189474 \pm 549 \pm 7467$	3.2 ± 3.2	2.3	3.9
B^0	$103169 \pm 128 \pm 3301$	2.7 ± 2.7	1.8	3.2

Table 4: *Systematic uncertainties on the B counting from the peaking background and the B $m_{\rm ES}$ distribution fit.*

4 Missing mass reconstruction

4.1 Overview

The goal of the analysis described in this document is the reconstruction of the missing particle X in the reaction $e^+e^- \to \Upsilon(4S) \to B_1B_2$ where B_1 is a fully reconstructed B meson (B_{full}) and $B_2 \to X\pi^-$ is the recoiling $\bar{B}$ (B_{recoil}). Only the π^- is reconstructed in the decay $B_2 \to X\pi^-$. The 4-vector of X is constrained by the energy-momentum conservation: $Q_\mu^{(X)} = Q_\mu^{(\Upsilon(4S))} - Q_\mu^{(B_1)} - Q_\mu^{(\pi^-)}$, where $Q_\mu^{(B_1)}$ is already constrained and $Q_\mu^{(\Upsilon(4S))} = Q_\mu^{(e^+)} + Q_\mu^{()}$. This allows to compute the mass $M(X)$ of the missing particle X as the length of the 4-vector $Q_\mu^{(X)}$. Decays like $\bar{B} \to D\pi^-$, $\bar{B} \to D^*\pi^-$, $\bar{B} \to D^{**}\pi^-$ will appear as peaks at the D, D^* or D^{**} masses in the *missing mass to* π^- spectrum $MM(\pi)$. This allows to compute the branching fraction for those modes:

$$\mathcal{B}(\bar{B} \to (D, D^*, D^{**})\pi^-) = \frac{N_{MM}(D, D^*, D^{**})}{\varepsilon(D, D^*, D^{**}) \times N_{B_1}}, \tag{1}$$

where $N_{MM}(D, D^*, D^{**})$ is the number of events reconstructed at the D, D^* or D^{**} mass, $\varepsilon(D, D^*, D^{**})$ is the reconstruction efficiency for that mode and N_{B_1} is the number of fully reconstructed $\bar{B}$ mesons (either charged or neutrals, corrected from the cross-feed between B^- and $\bar{B}^0$ modes). We will describe in the following how the efficiency $\varepsilon(D, D^*, D^{**})$ and the signal yields $N_{MM}(D, D^*, D^{**})$ are determined. The analysis is run separately for each B_{full} charge (B or $\bar{B}$), the pion charge of B_{recoil} is correlated correspondingly for the B^+ sample and left uncorrelated for the B^0 sample.

4.2 The π selection

The missing mass is performed to a pion in the recoil system. This π is selected among all the charged tracks reconstructed as GoodTrackLoose. Four vetoes are applied to this pion to find it among kaons, electrons, muons and protons and therefore to reduce the combinatorial background. The π is identified as not being a kaon by the Tight kaon veto, nor an electron or a muon by the VeryTight veto, nor a proton by the Tight veto. In the Fig. 3, are reported the total background from generic MC when neither veto is applied, and are superimposed the backgrounds when electrons, muons and protons are vetoed. Proton veto does not improve the combinatorial background, but muon and electron vetoes are efficient. In section 5, the Fig. 8 where the background components are drawn, shows that very negligible amount of electrons and muons have been missed by the vetoes. These cuts have an overall efficiency on the signal of 97%.

A separate charge analysis is performed in order to avoid a bias in the B selection. For the charged B sample, B^+ and B^- are run separately, same for the neutral B sample, where B^0 and $\bar{B}^0$ are run separately. Four samples are obtained this way, then charged B samples are summed apart from neutral B samples. When the B^+ (B^-) is reconstructed , only $\pi^-(\pi^+)$ are selected and when a B^0 ($\bar{B}^0$) is selected, no correlation is required on the pion charge thus allowing the reconstruction of B^0 B^0 and $\bar{B}^0$ $\bar{B}^0$ mixed events in addition to B^0 $\bar{B}^0$ events. The efficiency of the reconstruction of the π for each of these cases (charged and neutral B_{full}), is discussed in the following subsection.

4.3 Reconstruction efficiencies

To measure the branching fraction $\mathcal{B}(\bar{B} \to (D, D^*, D^{**})\pi^-)$, we need to determine the missing mass reconstruction efficiency ε, which is basically given by the π^- track reconstruction efficiency. This question is addressed here, using the Monte Carlo simulation of signal events (cocktail MC). A sample of cocktail MC events six times larger than the data sample has been used. The π^- track reconstruction efficiency is computed as a ratio of the reconstructed π number N^{π}_{reco} to the generated one N^{π}_{gene} .

We will describe in the following how N^{π}_{gene} is obtained through MC matching, how N^{π}_{reco} is computed through pion reconstruction and performing the *missing mass to* π^- and finally we will compute the efficiency.

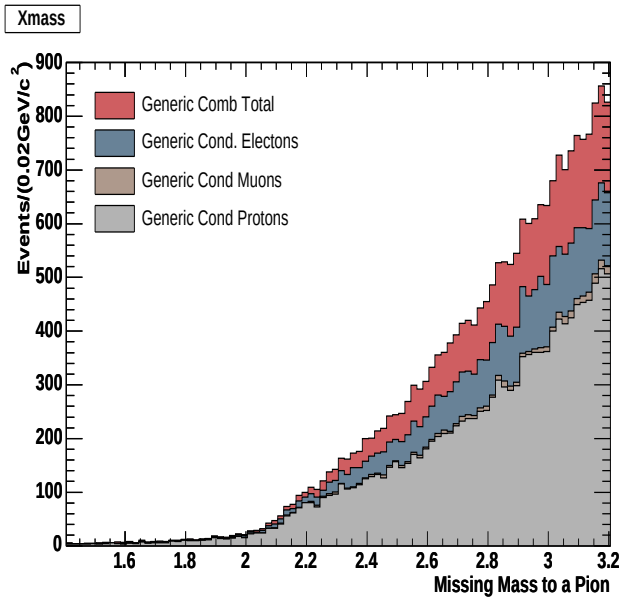

Figure 3: *The effect of electron, muon and proton vetoes on the missing mass to* π^- *distribution from charged B Generic MC background. The Kaon veto is applied to all histograms on this figure. The grey filled histogram corresponds to all vetoes, then each veto is retired individually to show its efficiency*

4.3.1 Determination of N^{π}_{gene} with Monte Carlo Matching

To obtain N^{π}_{gene} , we first perform the reconstruction and the selection of one B as B_{full} . The matching of this B_{full} to the generated one is done with the difference of the momentum of each, as described in Appendix A.2 (momentum difference not larger than $0.206\,\mathrm{GeV}/c^2$). Once B_{full} is matched, we look into the MC truth block for the other B (B_{recoil}) and count the number of generated π, N^{π}_{gene} , as those produced in one of the B_{recoil} decays $D\,\pi^-$, $D^*\,\pi^-$ or $D^{**}\,\pi^-$.

4.3.2 Determination of N^{π}_{reco} computing the *missing mass to* π^-

The reconstructed number of pions N^{π}_{reco} , is determined from selected pions as described above in subsection 4.2. Once such a pion is selected, the missing mass to it is computed in the B_{recoil} system. In addition to the previous selection criteria, in the MC truth block the event must contain a π whose mother particle is a B. A truth variable is then defined such that the decay mode of this MC B_{recoil} is one of those we study ($D\,\pi^-$, $D^*\,\pi^-$ or $D^{**}\,\pi^-$). The missing mass is plotted with a cut using the truth variable as shown in Figs. 4 and 5 for B^+ and B^0 respectively. N^{π}_{reco} is determined from this plot by counting the events in the range defined for the fit.

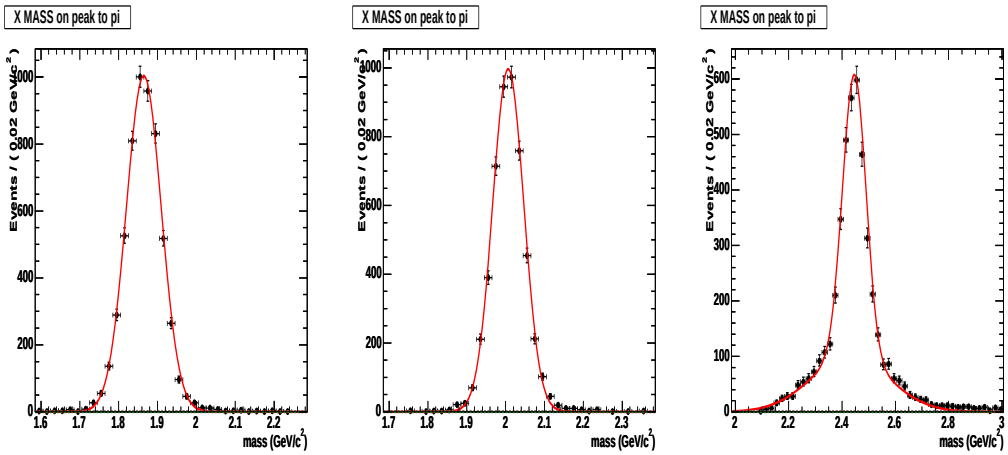

Figure 4: *Separate fit of the missing mass to* π^- *distribution for each resonance, conditioned with the MC truth for charged B signal MC.*

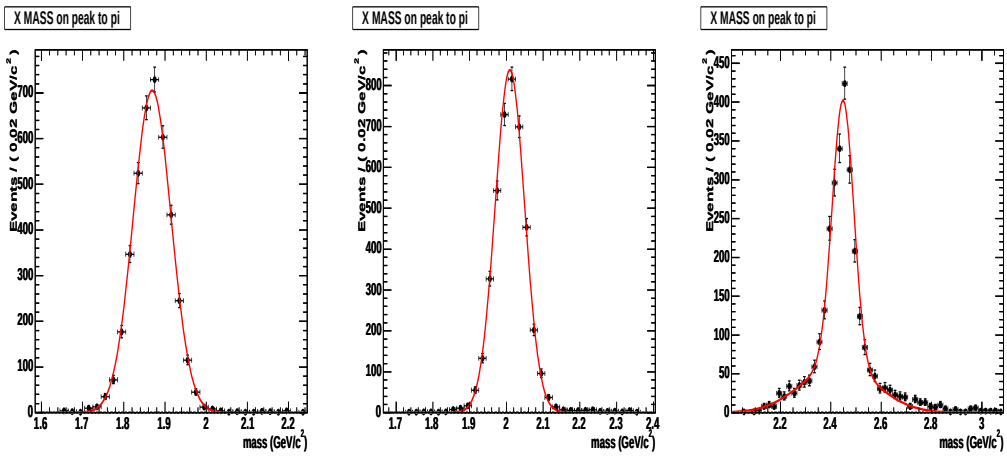

Figure 5: *Separate fit of the missing mass to* π^- *distribution for each resonance, conditioned with the MC truth for* B^0 *signal MC.*

4.3.3 Determination of the efficiency

The pion reconstruction efficiency is computed as the ratio of N^{π}_{reco} to N^{π}_{gene} . A tracking efficiency correction is applied to take into account the running conditions (correction tables provided for each high voltage of the drift chamber by the tracking group task force [27]). An average depending on the data luminosity for each high voltage period is performed. For the particle identification corrections, the PID tweaking has also been applied (recipes from [28]). Table 5 and Table 6 summarize the π track efficiency values obtained from signal MC for the B^+ and B^0 samples respectively. They show the raw and corrected efficiency values. The π reconstruction efficiency is comparable between the different resonances. The uncertainty on the efficiency value is equal to 0.007 for both B^+ and B^0 samples. It is obtained from the statistic uncertainty from the cocktail MC sample and the systematic uncertainties due to tracking efficiency (0.8% per track) and identification (0.2% per veto). This systematic uncertainty is added quadratically to the other contributions determined all through this analysis (see section 6.4). The efficiency mean value is 0.796 ± 0.007 and 0.793 ± 0.007 for B^+ and B^0 samples respectively.

D resonance	N^{π}_{gene}	N^{π}_{reco}	raw eff. $\varepsilon \pm \sigma$	corr. eff.$\varepsilon \pm \sigma$
$D^0\ \pi^-$	8230	6633	0.8060 ± 0.0035	0.797 ± 0.007
$D^{*0}\ \pi^-$	7208	5821	0.8070 ± 0.0037	0.798 ± 0.007
$D^{**0}\pi^-$	6542	5246	0.8010 ± 0.039	0.792 ± 0.007
Mean value				0.796 ± 0.007

Table 5: *Raw and corrected π^- reconstruction efficiencies for the $B^- \to D^0\pi^-$, $D^{*0}\pi^-$ and $D^{**0}\pi^-$ decay modes, as computed from the cocktail MC sample.*

D resonance	N^{π}_{gene}	N^{π}_{reco}	raw eff. $\varepsilon \pm \sigma$	corr. eff.$\varepsilon \pm \sigma$
$D^+\ \pi^-$	5387	4358	0.8089 ± 0.0043	0.799 ± 0.008
$D^{*+}\ \pi^-$	4835	3877	0.8019 ± 0.0046	0.792 ± 0.008
$D^{**+}\pi^-$	4337	3463	0.7985 ± 0.0049	0.788 ± 0.008
Mean value				0.793 ± 0.007

Table 6: *π^- reconstruction efficiencies for the $B^0 \to D^+\pi^-$, $D^{*+}\pi^-$ and $D^{**+}\pi^-$ decay modes, as computed from the Signal MC sample.*

5 Signal Yield

In the previous sections, B_{full} has been defined as the fully reconstructed B-meson, and B_{recoil} as the recoil B-meson for which momentum and energy are precisely determined after the selection of the "best-B_{full}" candidate. In our analysis, the signal is obtained by computing the missing mass in the B_{recoil} system. We use the MC generic simulation to determine the combinatorial background and subtract it from the data missing mass distribution. We are then able to measure the signal yield of $\bar{B}^0(B^-) \rightarrow D^+(D^0)\pi^-$, $\bar{B}^0(B^-) \rightarrow D^{*+}(D^{*0})\pi^-$ and $\bar{B}^0(B^-) \rightarrow D^{**+}(D^{**0})\pi^-$. Both charged and neutral B yields will be discussed in the next subsections.

5.1 Signal Yield

To extract the ($B^- \rightarrow D^0\pi^-$, $B^- \rightarrow D^{*0}\pi^-$ and $B^- \rightarrow D^{**0}\pi^-$) and ($\bar{B}^0 \rightarrow D^+\pi^-$, $\bar{B}^0 \rightarrow D^{*+}\pi^-$ and $\bar{B}^0 \rightarrow D^{**+}\pi^-$) branching fractions, the B^+ (B^0) data missing mass distribution will be analyzed using the generic MC as a model for the background component of the distribution. The generic MC components $b\bar{b}$, $c\bar{c}$, $q\bar{q}$ and the B^0 (B^+) peaking background have been normalized to the data B^+ (B^0) reconstructed number corresponding to $209 fb^{-1}$ luminosity. They have been reported on Figs. 6 and 7 together with the total *missing mass to* π^- distribution from the data.

5.1.1 Background components of the missing mass distribution

The $b\bar{b}$ background contribution has been split in its different components shown in Fig. 8. This figure shows that electron and muon contributions are negligible, thanks to the electron and muons veto applied on the pion reconstruction and selection (section 4.2). It also shows that the most important contribution comes from the polynomial combinatorial background (any other pions which do not originate from the processes listed on the Fig. 8). A close look to the mass range 2.0-2.8 GeV/c^2, reveals that the second most important $b\bar{b}$ background comes from pions originating from the ρ decays of $B^- \rightarrow D^0\rho^-$ and $B^- \rightarrow D^{*0}\rho^-$ processes. The Fig. 9 shows that the $B^- \rightarrow D^0\rho^-$ and $B^- \rightarrow D^{*0}\rho^-$ backgrounds have a sigmoid shape which is responsible of some kind of a shoulder around 2.1 GeV/c^2 of the Fig. 8. This shoulder appears also clearly in Fig. 6 and Fig. 7, where the generic MC background is superimposed to the data missing mass distribution.

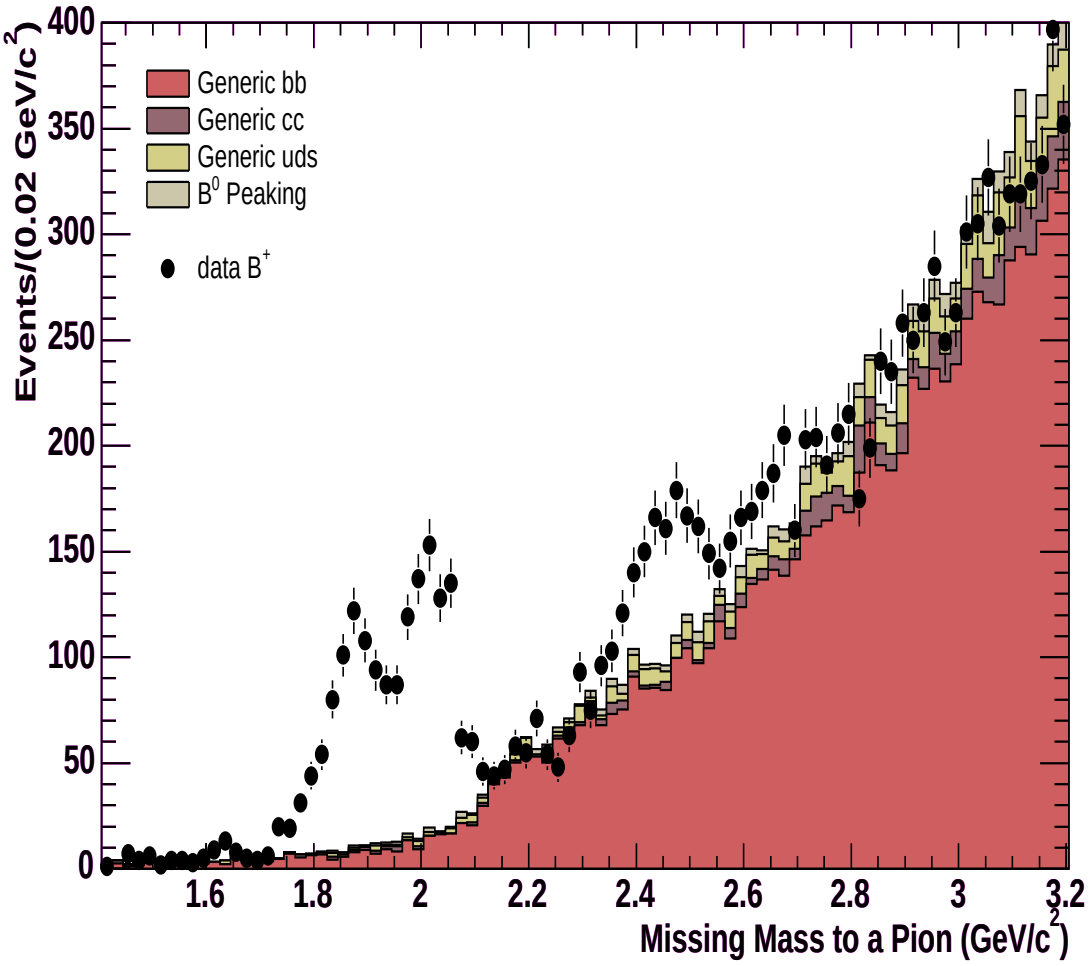

Figure 6: *Missing mass distribution obtained with total charged B data ($209\,fb^{-1}$). Superimposed to data are the generic MC contributions from $b\bar{b}$, $c\bar{c}$ and $q\bar{q}$, as well as the B^0 peaking normalized to the data B_{full} number.*

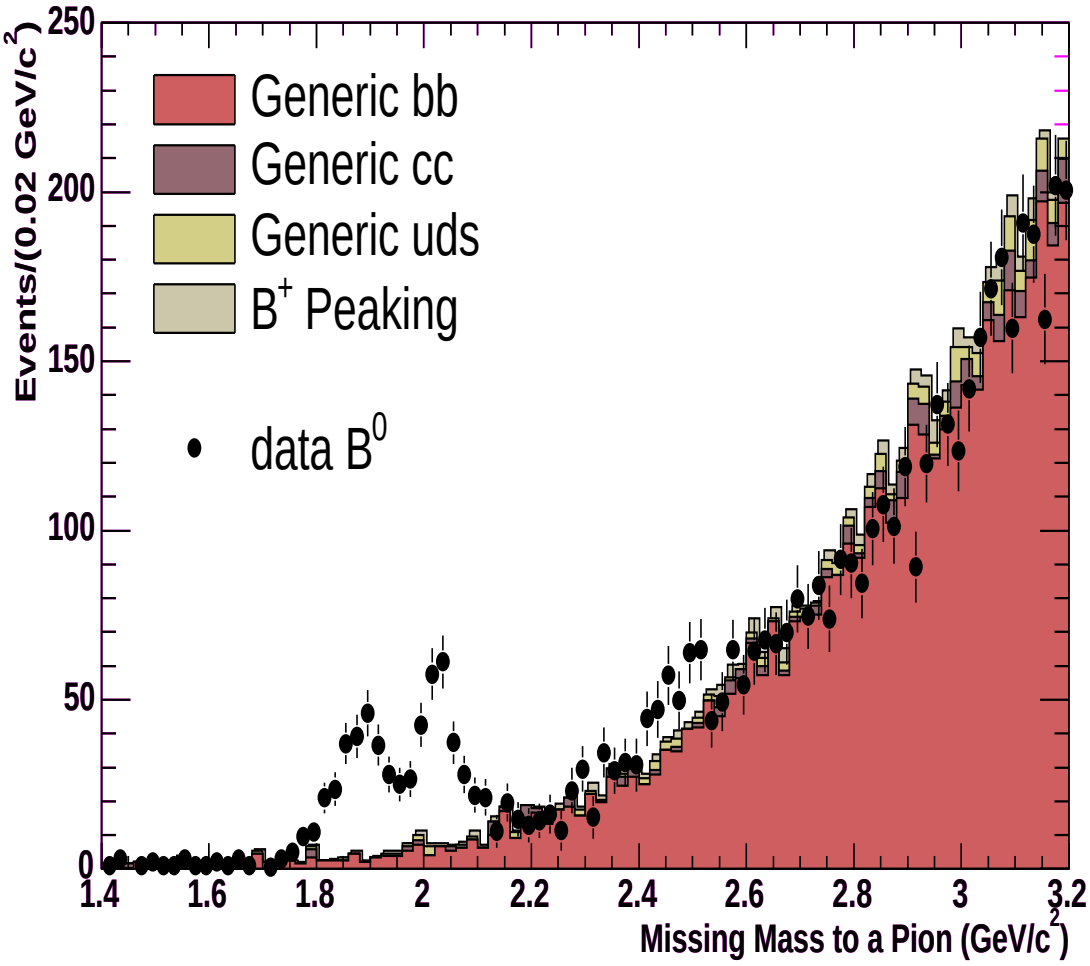

Figure 7: *Missing mass distribution obtained with total charged B data ($209 fb^{-1}$). Superimposed to data are the generic MC contributions from $b\bar{b}$, $c\bar{c}$ and $q\bar{q}$, as well as the B^+ peaking normalized to the data B_{full} number.*

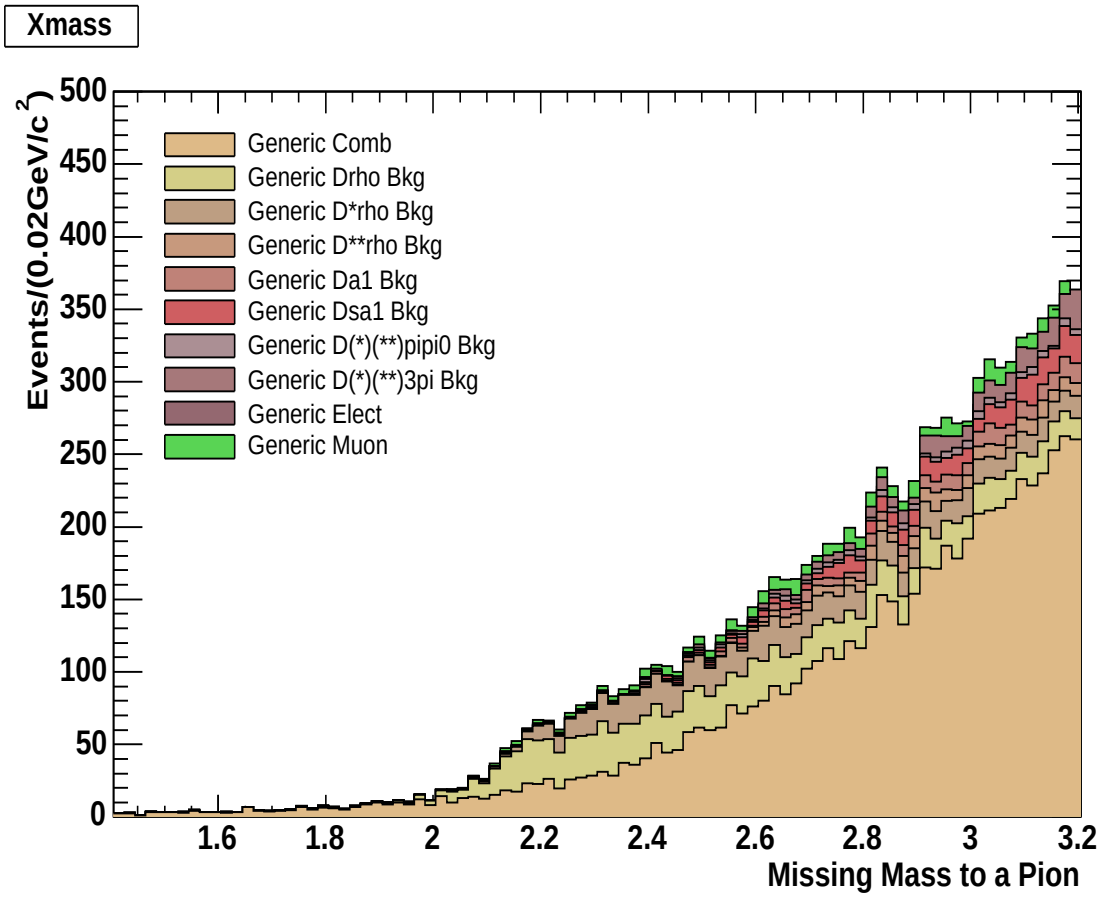

Figure 8: *Missing mass distribution of the normalized generic MC contributions from $b\bar{b}$ The list of the different components is given on the figure.*

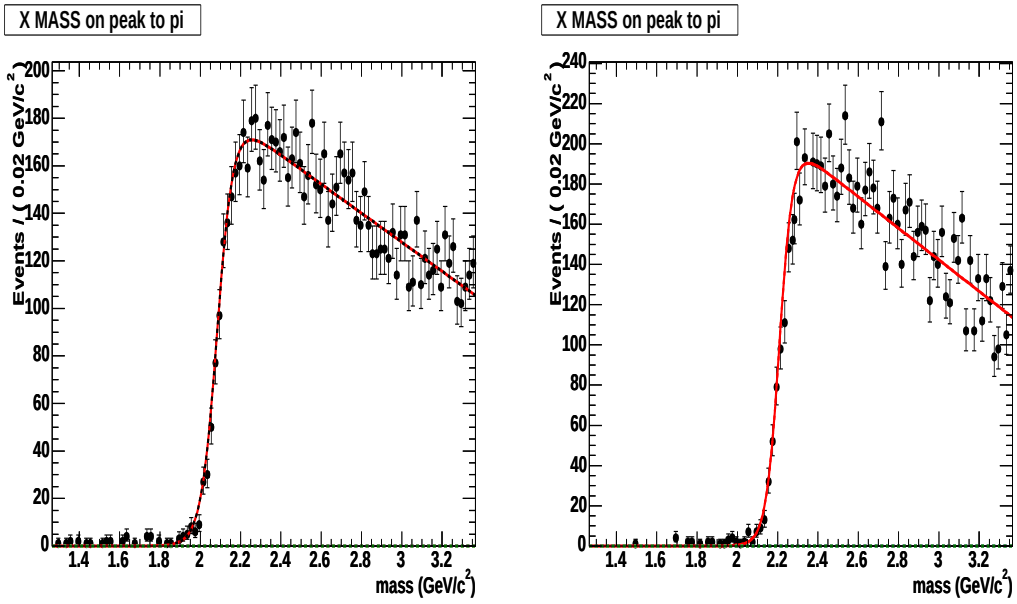

Figure 9: *Fit of* $B^- \rightarrow D^0\rho^-$ *and* $B^- \rightarrow D^{*0}\rho^-$ *, combinatorial background contributions to the missing mass to* π^- *distribution from signal MC*

5.1.2 Procedure for extraction of the missing mass signal Yield

To take into account the particular shape of the $B^- \rightarrow D^0\rho^-$ ($\bar{B}^0 \rightarrow D^+\rho^-$) and $B^- \rightarrow D^{*0}\rho^-$ ($\bar{B}^0 \rightarrow D^{*+}\rho^-$) background components in the B^+ (B^0) signal, and to estimate their systematic uncertainties contribution, we have defined a three step procedure to apply to the data in order to extract the yield.

- Step-1
  The $B^- \rightarrow D^0\rho^-$ ($\bar{B}^0 \rightarrow D^+\rho^-$) and $B^- \rightarrow D^{*0}\rho^-$ ($\bar{B}^0 \rightarrow D^{*+}\rho^-$) background components are subtracted from the B^+ (B^0) missing mass distribution. Their systematic uncertainty contributions will be estimated independently as will discussed in section 6.3.

- Step-2
  In addition to the normalization to the same number of B_{recoil} as in the data, we applied a correction factor on the MC background to take into account the discrepancy between the data and the Monte Carlo in the missing mass range 2.8-3.2 GeV/c^2. This ratio was found equal to 0.970 ± 0.020 for B^+ and 0.890 ± 0.025 for B^0 sample. The missing mass distributions, after background subtraction, are shown on Figs. 10 and 11 for B^+ and B^0 respectively. In order to estimate the systematic uncertainty due to this normalization, the normalization factor can be varied within one standard deviation as will be shown in section 6.3.

- Step-3
  Once the generic MC background distribution is renormalized, it is subtracted from

the data and the missing mass distribution of Figs. 12 and 13 are obtained for B^+ and B^0 respectively.

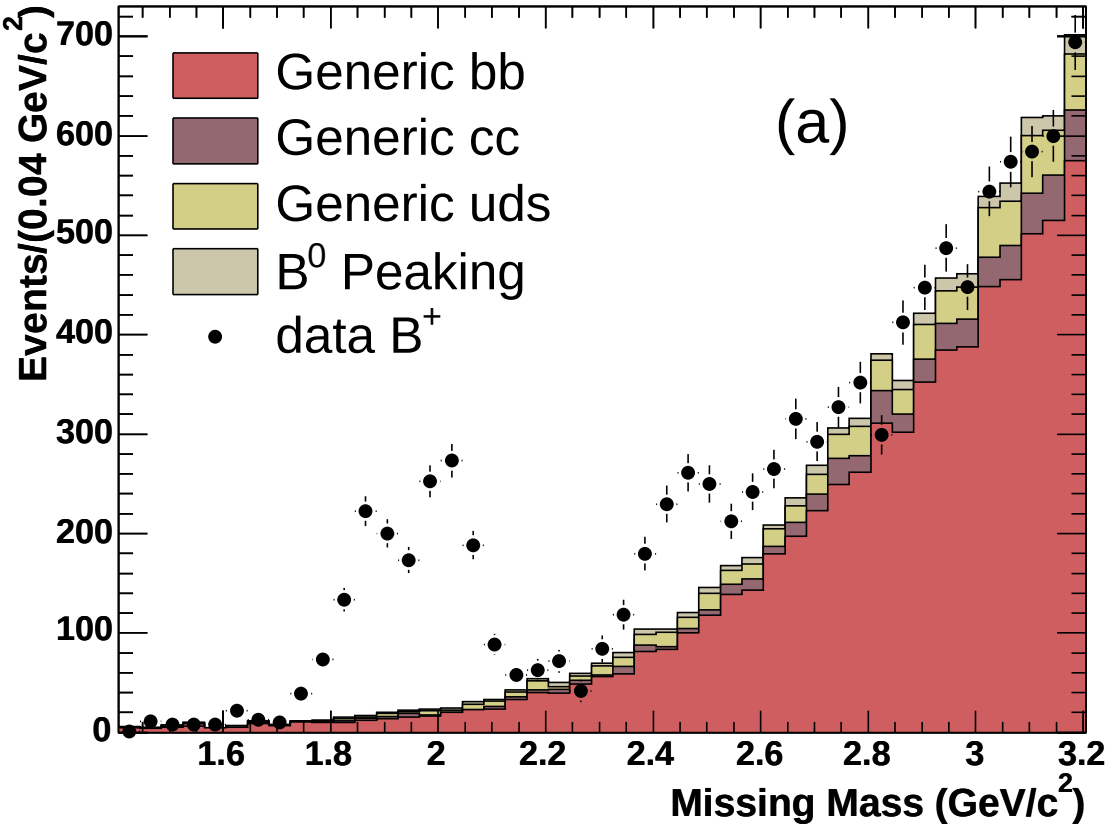

Figure 10: *Missing mass distribution obtained with total charged B data ($209\,fb^{-1}$). Superimposed to data are the normalized generic MC contributions from $b\bar{b}$ (without the $B^- \to D^0\rho^-$ and $B^- \to D^{*0}\rho^-$ contrib.), $c\bar{c}$ and $q\bar{q}$, as well as the B^0 peaking.*

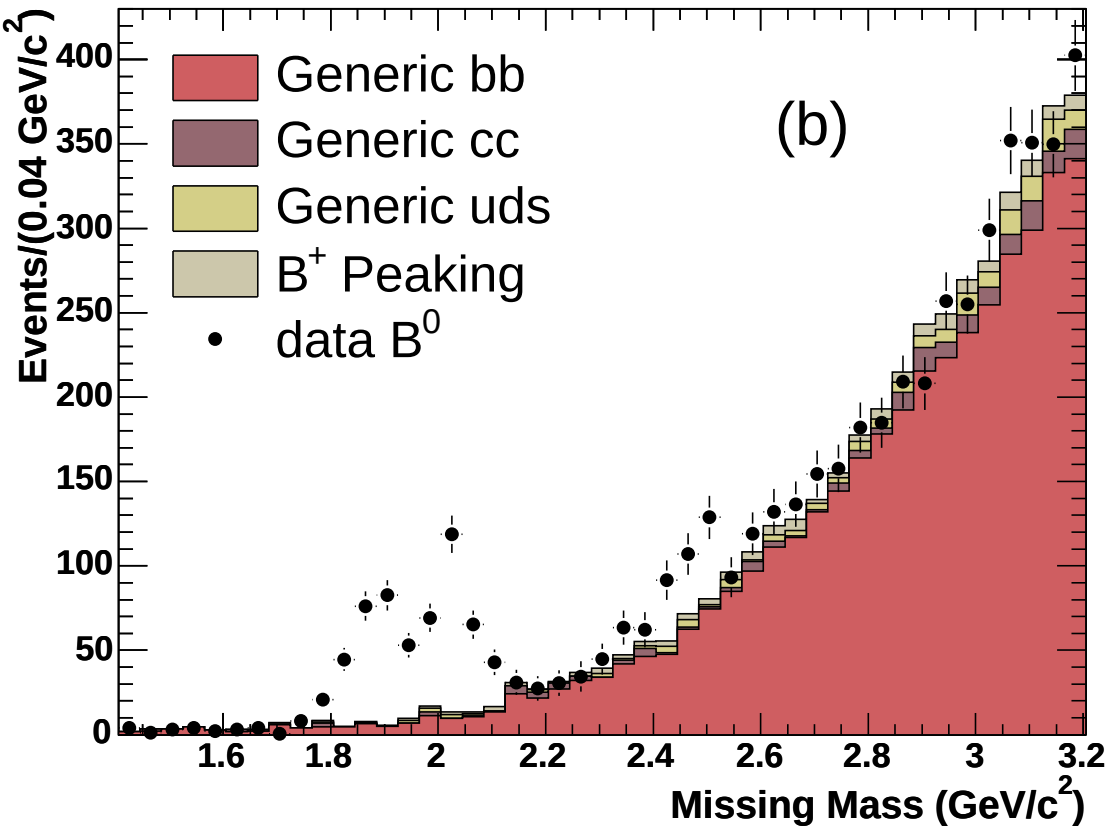

Figure 11: *Missing mass distribution of the neutral B data ($209\,fb^{-1}$). Superimposed to data are the normalized generic MC contributions from $b\bar{b}$ (without the $\bar{B}^0 \to D^+\rho^-$ and $\bar{B}^0 \to D^{*+}\rho^-$ contrib.), $c\bar{c}$ and $q\bar{q}$, as well as the B^+ peaking.*

5.2 Signal Yield Fit With A Double Gaussian

We have fitted the missing mass spectrum of Figs. 12 and 13, with a double gaussian for each of the D and D^* resonances. The second gaussian, centered at a higher mass, accounts for the tail of the missing mass distribution. The parameters of the first gaussian are σ_1^D and m_1^D for the D resonance and $\sigma_1^{D^*}$ and $m_1^{D^*}$ for the D^* resonance. Those of the second gaussian are σ_2^D and m_2^D for the D resonance and $\sigma_2^{D^*}$ and $m_2^{D^*}$ for the D^* resonance.

In the fit, the central values m_1^D and m_2^D and the widths σ_1^D and σ_2^D of the double gaussian which fits the D mass distribution have been left floating. We fixed the mass difference $m_1^{D^*} - m_1^D$ (and $m_2^{D^*} - m_2^D$) to 0.1421 GeV/c^2 and to 0.1406 GeV/c^2 respectively for B^+ and B^0. We also fixed the ratios $\sigma_1^{D^*}/\sigma_1^D$ and $\sigma_2^{D^*}/\sigma_2^D$ to 0.900($\pm$0.015) for both B^+ and B^0. This ratio has been determined using the Monte carlo simulation (see appendix C for details). For the D^{**} peak, the yield has been obtained by counting the

candidates in excess in the $2.2-2.8$ GeV/c^2 missing mass range. The D^0 and D^+ fitted parameters are compared to the Monte Carlo simulated ones in Tables 8 and 10.

The choice of the double gaussian is discussed in appendix B. As shown in this appendix, the χ^2 of the binned fit with a double gaussian pdf is better than the binned fit with a single one.

D resonance	2-Gauss.N^{π}_{fit}	stat. fit err.(%)
D^0	677±32	4.7%
D^{*0}	774±33	4.2%
D^{**0}	829±78	9.4%

Table 7: *Yield N^{π}_{fit} for D^0, D^{*0} and D^{**0} with corresponding statistical uncertainties as fitted in Fig. 12. Each resonance peak is fitted by a double gaussian pdf. The D^{**0}yield is obtained from counting.*

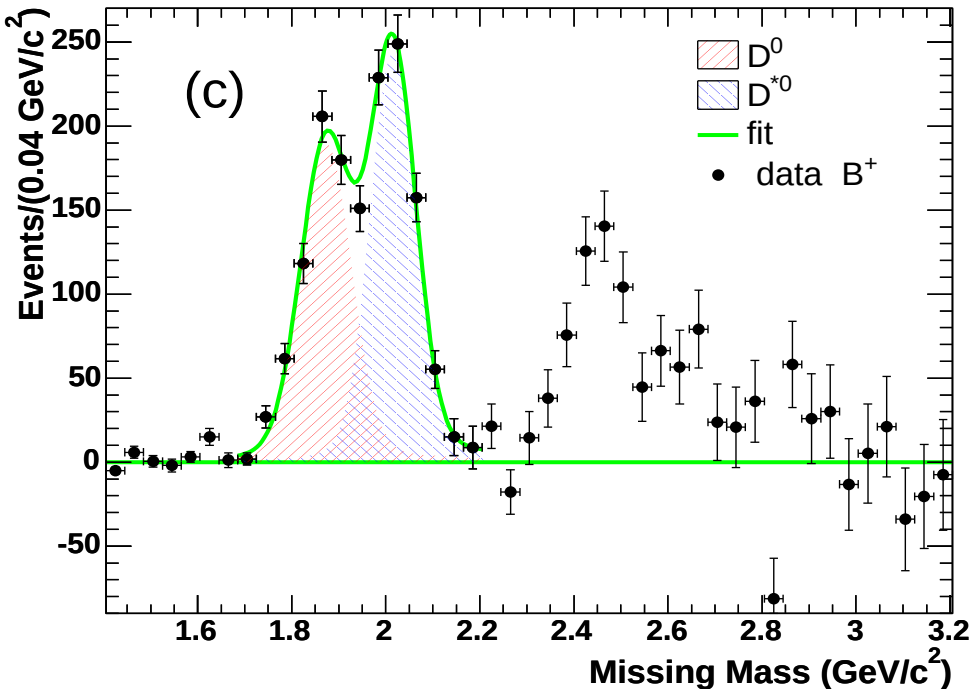

Figure 12: *Missing mass distribution of the charged B data ($209\,fb^{-1}$),obtained after subtraction of the contribution of the total normalized generic MC background. Each resonance peak is fitted by a double gaussian pdf. The D^{**0}yield is obtained from counting.*

Parameters (GeV/c^2)	MC constrained fit param.	data constr. param. fit
σ_1^D	0.0472±0.0016	0.0500±0.0021
σ_2^D	0.150±0.041	0.200±0.11
$mass_1^D$	1.8649±0.0013	1.8715±0.0024
$mass_2^D$	1.94±0.13	2.01±0.12

Table 8: *Comparison between the double gaussian generic MC fit parameters (column1) and the data fit parameters (column2) with the constraints set for both the first and the second gaussian, for the B^+ sample.*

D resonance	2-Gauss.N_{fit}^{π} (mixed data)	stat. fit err.(%)
D^+	248±19	7.7%
D^{*+}	245±19	7.7%
D^{**+}	192±54	28.1%

Table 9: *Yield N_{fit}^{π} for D^+, D^{*+} and D^{**+} with corresponding statistical uncertainties as fitted in figure 13. Each resonance peak is fitted by a double gaussian pdf. The D^{**+} yield is obtained from counting.*

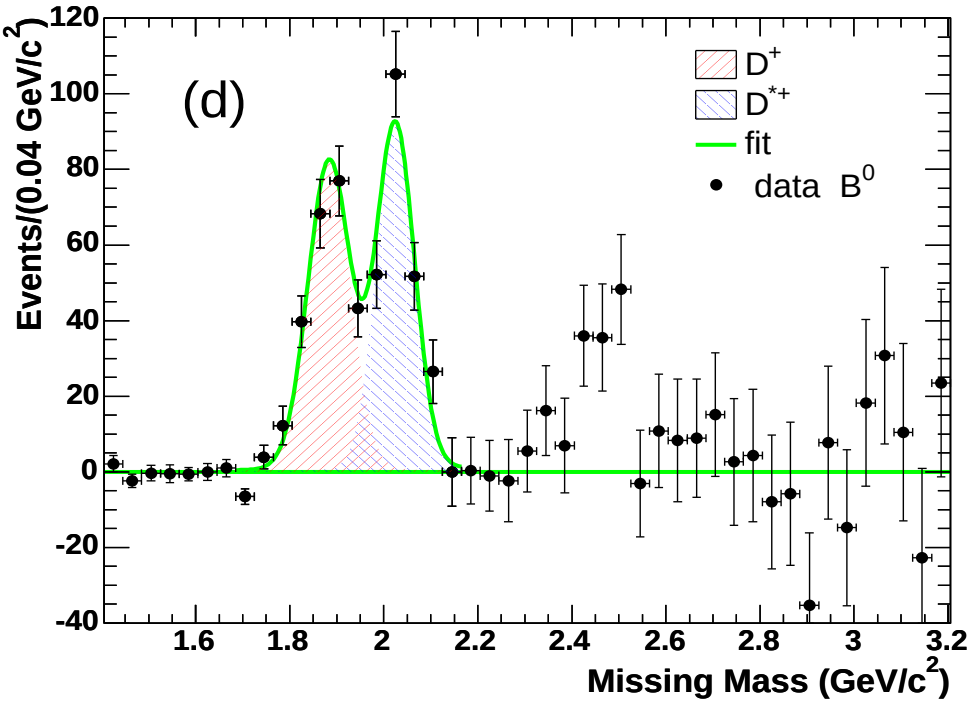

Figure 13: *Missing mass distribution of the neutral B data ($209\,fb^{-1}$) obtained after subtraction of the contribution of the total normalized generic MC background. Each resonance peak is fitted by a double gaussian pdf. The D^{**+} yield is obtained from counting.*

Parameters (GeV/c^2)	MC constrained fit param.	data constr. fit param.
σ_1^D	0.0437±0.0019	0.0442±0.0030
σ_2^D	0.134±0.028	0.160±0.094
$mass_1^D$	1.8719±0.0022	1.8835±0.0036
$mass_2^D$	1.93±0.12	1.93±0.13

Table 10: *Comparison between the double gaussian generic MC fit parameters (column1) and the data fit parameters (column2) with the constraints set for both the first and the second gaussian for the B^0 sample.*

6 Systematic Studies

In this analysis, systematic uncertainties come mainly from the B_{full} selection and counting, the subtraction of the generic MC background to extract the yield from the missing mass distribution and also from the π track reconstruction efficiency determination. Each item will be detailed in the following subsections.

6.1 B_{full} selection systematic uncertainty

The B_{full} selection procedure described in section 3 may introduce a bias in the determination of $N_{B_{full}}$. Monte Carlo samples are useful to check if such a bias has been introduced in our analysis. This is by computing the MC branching ratio $\mathcal{B}_C$ for each resonance and comparing it to the nominal $\mathcal{B}_G$ values (those used to generate the MC samples). $\mathcal{B}_C$ is obtained using N^{π}_{gene} defined in section 4. The B_{full} number defined in section 3 in the other hand, is not obtained performing a fit to the $m_{\rm ES}$ distribution (where many uncertainties may add) but by counting. To do this counting, a B_{full} momentum matching to the MC truth block is performed as described in appendix A.2. The difference between $\mathcal{B}_C$ and the nominal $\mathcal{B}_G$, if any, should give part of the systematic uncertainty induced by the selection and the counting of the B_{full} . Tables 11 and 12 compare the branching ratio obtained from the signal MC sample for charged B and neutral B respectively. Discrepancies of less than 2.5% and 4.5% have been obtained for B^+ and B^0 respectively. They are considered compatible with zero within the uncertainty due to the statistics of the Monte Carlo sample. As systematic uncertainty of the reconstruction method we take the value of the Monte Carlo statistic uncertainty.

D resonance	MC $\mathcal{B}_G$	calculated $\mathcal{B}_C$	Deviation from $\mathcal{B}_G$
D^0	0.0053	0.00520 ± 0.00010	$1.9\% \pm 1.9\%$
D^{*0}	0.0046	0.00450 ± 0.00010	$2.2\% \pm 2.2\%$
D^{**0}	0.0041	0.00410 ± 0.00010	$0.0\% \pm 2.4\%$

Table 11: *D^0, D^{*0} and D^{**0} calculated branching ratio from charged B signal Monte Carlo with corresponding statistic uncertainty and induced systematic uncertainty on the data.*

D resonance	MC $\mathcal{B}_G$	calculated $\mathcal{B}_C$	deviation from $\mathcal{B}_G$
D^+	0.0030	0.00290 ± 0.00010	$3.4\% \pm 3.4\%$
D^{*+}	0.0027	0.00260 ± 0.00010	$3.8\% \pm 3.8\%$
D^{**+}	0.0024	0.00230 ± 0.00010	$4.3\% \pm 4.3\%$

Table 12: *D^+, D^{*+} and D^{**+} calculated branching ratio from B^0 signal Monte Carlo with corresponding statistic uncertainty and induced systematic uncertainty on the data.*

6.2 B_{full} counting systematic uncertainty

There are additional contributions to be considered as systematic uncertainty in the $N_{B_{full}}$ counting. They come from the fit of the B_{full} $m_{\rm ES}$ distribution and the peaking background correction. Adding quadratically the fit and the peaking components, the final systematic uncertainties on N_{B^+} and N_{B^0} are found to be 3.9% and 3.2% respectively. These values are summarized in Table 4 of section 3.5.

6.3 Systematic uncertainty on the D resonances yield determination

The final numbers $N_{MM}(D, D^*, D^{**})$ of the events reconstructed at the D, D^* or D^{**} mass are obtained from the missing mass distribution, after subtraction of the generic MC background normalized to the number of reconstructed B and to the background in the missing mass range: 2.8-3.2 GeV/c^2 (see section 5). The final systematic uncertainty due to generic MC subtraction has been computed using four contributions detailed in Table 13 and 14 for B^+ and B^0 respectively. These contributions are determined as follows:

- Normalization contribution
  This first contribution called Norm in Tables 13 and 14 is obtained by varying the normalization factor of the generic MC [for B^+ (0.97 ± 0.02)] and [for B^0 (0.89 ± 0.025)] by one standard deviation. The induced difference in the yield is taken as systematic uncertainty on the final Branching fractions.

- The $B^- \to D^0\rho^-$ (for B^+) and $\bar{B}^0 \to D^+\rho^-$ (for B^0) contribution
  The background contribution $B^- \to D^{*0}\rho^-$ ($\bar{B}^0 \to D^{*+}\rho^-$ for B^0) is subtracted from the data and the MC missing mass distributions, in order to study the $B^- \to D^0\rho^-$ ($\bar{B}^0 \to D^+\rho^-$) component systematics (by opposition to the analysis procedure described in section 5.1.1 , where both are subtracted). A variation of one standard deviation of the branching fractions of $B^- \to D^0\rho^-$($\bar{B}^0 \to D^+\rho^-$)from the PDG values [10], is then performed. The induced variation on the yields of $B^- \to D^0\pi^-$, $B^- \to D^{*0}\pi^-$ and $B^- \to D^{**0}\pi^-$ ($\bar{B}^0 \to D^+\pi^-$, $\bar{B}^0 \to D^{*+}\pi^-$ and $\bar{B}^0 \to D^{**+}\pi^-$) are considered as the systematic uncertainties to apply to the final branching fractions and reported in the second line of Tables 13 and 14.

- The $B^- \to D^{*0}\rho^-$ (for B^+) and $\bar{B}^0 \to D^{*+}\rho^-$ (for B^0) contribution
  The same procedure is applied to the combinatorial background component of pions produced in $B^- \to D^{*0}\rho^-$ decays ($\bar{B}^0 \to D^{*+}\rho^-$ for B^0). They are kept in the missing mass distribution to be studied while the $B^- \to D^0\rho^-$ ($\bar{B}^0 \to D^+\rho^-$) are subtracted. A variation of one standard deviation of the branching fractions of $B^- \to D^{*0}\rho^-$ ($\bar{B}^0 \to D^{*+}\rho^-$) from the PDG values [10], is then performed. The induced variation on the yields of $B^- \to D^0\pi^-$, $B^- \to D^{*0}\pi^-$ and $B^- \to D^{**0}\pi^-$ ($\bar{B}^0 \to D^+\pi^-$, $\bar{B}^0 \to D^{*+}\pi^-$ and $\bar{B}^0 \to D^{**+}\pi^-$) are considered as the systematic uncertainties to apply to the final branching fractions and reported in the third line of Tables 13 and 14.

- The MC statistical error propagation
  Part of the systematic uncertainties on the yield determination are due to the background subtraction, and are estimated via error propagation of the MC background statistic uncertainties. These are reported in the fifth line of Tables 13 and 14.

Adding in quadrature the three first lines we obtain the total MC background renormalization systematic uncertainty reported in the fourth line of Tables 13 and 14. The total MC background systematic uncertainties are reported in the last line. These tables show negligible effect of the variation of the generic MC background on $B^- \to D^0\pi^-$, $B^- \to D^{*0}\pi^-$ $\bar{B}^0 \to D^+\pi^-$ and $\bar{B}^0 \to D^{*+}\pi^-$. As much as 18% systematic uncertainty is due to the subtraction of the generic MC background in the measurement of the $B^- \to D^{**0}\pi^-$ branching fraction and up to 37% on the measurement of the $\bar{B}^0 \to D^{**+}\pi^-$ branching fraction. Only the total systematic uncertainty is reported in Table 19 (for B^+) and Table 21 (for B^0).

Syst. Source	$B^- \to D^0\pi^-$	$B^- \to D^{*0}\pi^-$	$B^- \to D^{**0}\pi^-$
Norm	0.3%	0.3%	5.0%
$B^- \to D^0\rho^-$	0.3%	0.1%	6.6%
$B^- \to D^{*0}\rho^-$	0.2%	0.2%	14.0%
MC Background renorm. Total	0.5%	0.4%	16.3%
MC statistical propagation	1.6%	2.3%	7.1%
MC Backgr. total syst.	1.6%	2.3%	17.7%

Table 13: *Breakdown of systematic uncertainties due to Generic MC background subtraction for Charged B. Lines 1, 2 and 3 are added in quadrature and reported in line 4. Lines 4 and 5 are then added in quadrature to compute the total systematic uncertainty.*

Syst. Source data with mixing	$\bar{B}^0 \to D^+\pi^-$	$\bar{B}^0 \to D^{*+}\pi^-$	$\bar{B}^0 \to D^{**+}\pi^-$
Norm	0.2%	0.2%	19.9%
$\bar{B}^0 \to D^+\rho^-$	0.2%	1.0%	18.8%
$\bar{B}^0 \to D^{*+}\rho^-$	0.%	0.%	12.6%
Total MC Background norm.	0.5%	1.%	31.1%
MC statistical propagation	3.7%	5.3%	21.7%
MC Backgr. total syst.	3.7%	5.4%	37.1%

Table 14: *Breakdown of systematic uncertainties due to Generic MC background subtraction for B^0. Lines 1, 2 and 3 are added in quadrature and reported in line 4. Lines 4 and 5 are then added in quadrature to compute the total systematic uncertainty.*

6.4 Systematic uncertainties from π reconstruction efficiency

The π reconstruction efficiency has been determined in section 4.3 with a statistical uncertainty (see raw efficiency in table 5 and table 6). The corresponding relative uncertainty will be added quadratically as systematic uncertainty to take into account the uncertainty due to the efficiency determination. The systematic uncertainty due to the track efficiency has also to be taken into account. For a GoodTrackLoose track, the track efficiency relative uncertainty is 0.8% per track. As for the kaon veto on the pion, the systematic

uncertainty is estimated to 0.2% per veto corresponding to 10% of the rate misidentification of the KTight selector (the total for the four vetoes used in our analysis and added quadratically is then 0.4%). The uncertainties on the corrected efficiency of table 5 and table 6 take into account these different components.

6.5 Fit bias systematic uncertainties determined from generic MC

In appendix-B section B.1 and section B.3 we have repeated the analysis procedure on the generic Monte Carlo, for both B^+ and B^0 samples. It was aimed to determine whether the fit procedure induces a bias in the yield determination. The study has shown that the difference between the generated yield and the fitted yield should be added as a systematic uncertainty. The D^{**} yield is obtained by counting the excess between 2.2 and 2.8 GeV/c^2, it is also compared to the D^{**} generated one. Table 15 displays the determined uncertainty values for both B^+ and B^0 yields extracted from tables 27 and 32.

B mode	syst. err.(%)
$B^- \rightarrow D^0\pi^-$	1.9%
$B^- \rightarrow D^{*0}\pi^-$	1.5%
$B^- \rightarrow D^{**0}\pi^-$	4.5%
$\bar{B}^0 \rightarrow D^+\pi^-$	4.2%
$\bar{B}^0 \rightarrow D^{*+}\pi^-$	3.4%
$\bar{B}^0 \rightarrow D^{**+}\pi^-$	4.0%

Table 15: *Systematic uncertainties from the fit bias determined on generic Monte Carlo for both B^+ and B^0 samples. The D^{**} yield obtained by counting the excess between 2.2 and 2.8 GeV/c^2 is compared to the generated one.*

6.6 Fit bias systematic uncertainties determined from data

In appendix-B section B.2 and section B.4, we have performed a fit using a double gaussian pdf for each resonance on both B^+ and B^0 samples. The parameters of the first gaussian where constrained in the following way: the mass difference of the two resonances D^0 and D^{*0} (or D^+ and D^{*+}) is fixed to 0.1421 GeV/c^2 (0.1406 GeV/c^2) while the mass value is left floating, the ratio of the resolutions of D^0 (D^+) and D^{*0} (D^{*+}) is fixed to 0.90 as determined from the signal MC and discussed in appendix C, the value of the D^0 (D^+) peak resolution is left floating. The second gaussian parameters were either constrained the same way or left floating. The yields obtained whether constraining the second gaussian parameters or not were compared and the difference is taken as a systematic uncertainty. Table 16 displays the determined uncertainty values on both B^+ and B^0 data yields, extracted from Tables 28 and 33.

B mode	syst. err.(%)
$B^- \to D^0\pi^-$	0.7%
$B^- \to D^{*0}\pi^-$	0.6%
$B^- \to D^{**0}\pi^-$	-%
$\bar{B}^0 \to D^+\pi^-$	1.9%
$\bar{B}^0 \to D^{*+}\pi^-$	0.8%
$\bar{B}^0 \to D^{**+}\pi^-$	-%

Table 16: *Fit bias systematic uncertainties determined on data for both B^+ and B^0 samples. $D^{**}$is not fitted.*

6.7 D and D^* missing mass resolution ratio systematic uncertainties

In order to determine the yields from the missing mass spectra we have performed a fit, using a double gaussian pdf for each resonance on both B^+ and B^0 samples. To constrain the fit we have used a ratio R of the resolution of the D^* resonance over the resolution of the D resonance. This ratio has been determined equal to 0.90 ± 0.15 in the appendix C. The effect on the yield of the variation of R by one standard deviation has been shown negligible in appendix C. Table 17 summarize the determined uncertainty values on both B^+ and B^0 data yields, extracted from tables 38 and 39.

B mode	syst. err.(%)
$B^- \to D^0\pi^-$	0.6%
$B^- \to D^{*0}\pi^-$	0.5%
$B^- \to D^{**0}\pi^-$	-%
$\bar{B}^0 \to D^+\pi^-$	0.4%
$\bar{B}^0 \to D^{*+}\pi^-$	0.8%
$\bar{B}^0 \to D^{**+}\pi^-$	-%

Table 17: *Systematic uncertainties due to one standard deviation variation on the ratio R (constrained fit parameter), determined on data for both B^+ and B^0 samples. $D^{**}$is not fitted.*

6.8 Selection of the the pion of the Highest momentum

To reduce the combinatorial background, a study of the effect of selecting only one pion to perform the *missing mass to* π^- distribution has been performed. The pion is selected to be the one of the highest momentum as already discussed in the efficiency study section [4.3]. This criterium is applied to the pion in addition to the all other criteria discussed in section [4.3]. This study is reported in Appendix E in section E.2 and has shows no improvement in the significance of the result using this cut while additional systematic uncertainties have to be taken into account. This cut will not be used in this analysis and no systematic uncertainty is therefore considered.

7 Branching Fractions

The branching fractions are reported in table 18 for charged B branching fractions and in table 20 for B^0.
The breakdown of the systematic errors applied to each resonance is summarized in table 19 for charged B branching fractions and in table 21 for B^0.

7.1 Charged B Branching Fractions and systematic uncertainties breakdown

The branching fractions of the decays $B^- \rightarrow D^0\pi^-$, $B^- \rightarrow D^{*0}\pi^-$ and $B^- \rightarrow D^{**0}\pi^-$ are compared to the PDG updated values in Table 18. The D^0 , D^{*0} and D^{**0} yields have been taken from Table 7. The pion reconstruction efficiency is taken from table 5 (corrected values). The total number of B_{recoil} comes from Table 4. The measured $B^- \rightarrow D^0\pi^-$ branching fraction shows a discrepancy of about $10.\% \pm 9.\%$ when compared to the CLEO-II value [7], [10], whilst the $B^- \rightarrow D^{*0}\pi^-$ branching fraction shows a discrepancy of $11.\% \pm 11.\%$ with CLEO-II [10]. Both previous branching fraction are compatible with CLEO-II [10]. The branching fraction of the $\bar{B}^0 \rightarrow D^{**+}\pi^-$ decay is a new measurement.

D resonance	measured $\mathcal{B}$	PDG $\mathcal{B}$
$B^- \rightarrow D^0\pi^-$	$4.49\pm0.21\pm0.23 \times 10^{-3}$	$4.98\pm0.29 \times 10^{-3}$
$B^- \rightarrow D^{*0}\pi^-$	$5.13\pm0.22\pm0.28 \times 10^{-3}$	$4.6\pm0.4 \times 10^{-3}$
$B^- \rightarrow D^{**0}\pi^-$	$5.50\pm0.52\pm1.04 \times 10^{-3}$	-

Table 18: *Measured branching fractions $\mathcal{B}(B^- \rightarrow (D^0, D^{*0}, D^{**0})\pi^-)$ from B_{full} selection(RUN1-4) of total luminosity of $209\,fb^{-1}$. The D^0 , D^{*0} and D^{**0} yields have been taken from Table 7. The pion reconstruction efficiency is taken from Table 5 (corrected values). The total number of B_{recoil} comes from table 4.*

The breakdown of the systematic uncertainties applied to the branching fractions of table 18 are summarized in table 19. In this analysis, it is the systematic uncertainty coming from the generic MC background subtraction which is the most important.

Syst. Source	$B^- \to D^0\pi^-$	$B^- \to D^{*0}\pi^-$	$B^- \to D^{**0}\pi^-$
N_B (table 4)	3.9%	3.9%	3.9%
Efficiency (table 5)	0.9%	0.9%	0.9%
$\mathcal{B}$(signal MC on $\mathcal{B}$table 11)	1.9%	2.2%	2.4%
MC Background (table 13)	1.6%	2.3%	17.7%
MC Fit Bias (table 15)	1.9%	1.5%	4.5%
Data Fit Bias (table 16)	0.7%	0.6%	-%
Ratio R (table 17)	0.6%	0.5%	-%
TOTAL	5.2%	5.4%	18.9%

Table 19: *Breakdown of systematic errors applied to the branching fractions $\mathcal{B}(B^- \to (D^0, D^{*0}, D^{**0})\pi^-)$.*

7.2 Neutral B Branching Fractions and systematic uncertainties breakdown

The branching fraction of the decays $\bar{B}^0 \to D^+\pi^-$ $\bar{B}^0 \to D^{*+}\pi^-$ and $\bar{B}^0 \to D^{**+}\pi^-$ are reported and compared to the PDG values in table 20. The D^+ , D^{*+} and D^{**+} yields have been taken from table 9. The pion reconstruction efficiency is taken from table 6 (corrected values). The total number of B_{recoil} comes from table 4. The B^0 branching fraction of the decay $\bar{B}^0 \to D^{**+}\pi^-$is measured for the first time. The branching fraction $\mathcal{B}(\bar{B}^0 \to D^+\pi^-)$ is found compatible with the CLEO-II measurement [10] by $9.\% \pm 14.\%$, and $\mathcal{B}(\bar{B}^0 \to D^{*+}\pi^-)$ is found compatible as well, with the CLEO measurement [10] by $9.\% \pm 13.\%$, all these are compatible within one standard deviation.

D resonance	measured $\mathcal{B}$	PDG $\mathcal{B}$
$\bar{B}^0 \to D^+\pi^-$	$3.00 \pm 0.23 \pm 0.23 \times 10^{-3}$	$2.76 \pm 0.25 \times 10^{-3}$
$\bar{B}^0 \to D^{*+}\pi^-$	$2.97 \pm 0.23 \pm 0.24 \times 10^{-3}$	$2.76 \pm 0.21 \times 10^{-3}$
$\bar{B}^0 \to D^{**+}\pi^-$	$2.32 \pm 0.65 \pm 0.88 \times 10^{-3}$	-

Table 20: *Measured branching fractions $\mathcal{B}(\bar{B}^0 \to (D^+, D^{*+}, D^{**+})\pi^-)$ from B_{full} selection(RUN1-4) of total luminosity of $209\,fb^{-1}$. The D^+ , D^{*+} and D^{**+} yields have been taken from table 9 thus including the mixing data. The pion reconstruction efficiency is taken from table 6 (corrected values). The total number of B_{recoil} comes from table 4.*

The breakdown of the systematic uncertainties applied to the branching fractions of table 20 are summarized in table 21. The most important contribution to the systematic uncertainties is the uncertainty due to the generic MC background subtraction.

Syst. Source	$\bar{B}^0 \to D^+\pi^-$	$\bar{B}^0 \to D^{*+}\pi^-$	$\bar{B}^0 \to D^{**+}\pi^-$
N_B (table 4)	3.2%	3.2%	3.2%
Efficiency (table 6)	0.9%	0.9%	0.9%
$\mathcal{B}$(signal MC on $\mathcal{B}$table 12)	3.4%	3.8%	4.3%
MC Background (table 14)	3.7%	5.4%	37.1%
MC Fit Bias (table 15)	4.2%	3.4%	4.0%
Data Fit Bias (table 16)	1.9%	0.8%	-%
Ratio R (table 17)	0.4%	0.8%	-%
TOTAL	7.6%	8.2%	37.7%

Table 21: *Breakdown of systematic uncertainties applied to the branching fractions* $\mathcal{B}(\bar{B}^0 \to (D^+, D^{*+}, D^{**+})\pi^-)$

7.3 Branching fraction ratios

The ratio of B branching fractions obtained for the ratios $B^- \to D^{*0}\pi^- / B^- \to D^0\pi^-$ and $B^- \to D^{**0}\pi^- / B^- \to D^0\pi^-$ are shown in the table 22 for charged B data and in table 23 for B^0. The systematic uncertainties on these ratios come only from the subtraction of the generic MC background and the fit bias.

$B^- \to D^{*0}\pi^- / B^- \to D^0\pi^-$	1.14$\pm$ 0.07 (stat.) $\pm$ 0.04(syst.)
$B^- \to D^{**0}\pi^- / B^- \to D^0\pi^-$	1.22 $\pm$ 0.13 (stat.) $\pm$0.23(syst.)

Table 22: *ratio of branching fractions* $B^- \to D^{*0}\pi^- / B^- \to D^0\pi^-$ *and* $B^- \to D^{**0}\pi^- / B^- \to D^0\pi^-$

$\bar{B}^0 \to D^{*+}\pi^- / \bar{B}^0 \to D^+\pi^-$	0.99$\pm$ 0.11 (stat.) $\pm$0.08 (syst.)
$\bar{B}^0 \to D^{**+}\pi^- / \bar{B}^0 \to D^+\pi^-$	0.77$\pm$ 0.22 (stat.) $\pm$0.29 (syst.)

Table 23: *ratio of branching fractions* $\bar{B}^0 \to D^{*+}\pi^- / \bar{B}^0 \to D^+\pi^-$ *and* $\bar{B}^0 \to D^{**+}\pi^- / \bar{B}^0 \to D^+\pi^-$

8 Conclusion

A new measurement of $\mathcal{B}(B^- \rightarrow D^0\pi^-)$ and $\mathcal{B}(B^- \rightarrow D^{*0}\pi^-)$ branching fractions has been performed with an original method. 189k charged B meson and 103k B^0 out of 230 M $B\bar{B}$ pairs have been fully reconstructed into a set of hadronic decay modes. Momentum and energy of the recoil B become precisely known and the *missing mass to* π^- distribution can be derived. The $B^- \rightarrow D^0\pi^-$ branching fraction, $\mathcal{B}(B^- \rightarrow D^0\pi^-) = 4.49 \pm 0.21 \pm 0.23 \times 10^{-3}$ ($4.49 \pm 0.31 \times 10^{-3}$-if the uncertainties are added quadratically) is compatible with the value of CLEO-II [7], [10]. The $B^- \rightarrow D^{*0}\pi^-$ measured branching fraction, $\mathcal{B}(B^- \rightarrow D^{*0}\pi^-) = 5.13 \pm 0.22 \pm 0.28 \times 10^{-3}$ ($5.13 \pm 0.36 \times 10^{-3}$) is also compatible with the previous CLEO-II measurement [10] and is measured with a slightly better precision. We also measure $B^- \rightarrow D^{**0}\pi^-$ branching fraction, $\mathcal{B}(B^- \rightarrow D^{**0}\pi^-) = 5.50 \pm 0.52 \pm 1.04 \times 10^{-3}$ ($5.50 \pm 1.16 \times 10^{-3}$).
In addition, the ratio $\mathcal{B}(B^- \rightarrow D^{*0}\pi^-)$ / $\mathcal{B}(B^- \rightarrow D^0\pi^-)$ is found to be $1.14 \pm 0.07(stat.) \pm 0.04(syst.)$ while $\mathcal{B}(B^- \rightarrow D^{**0}\pi^-)$ / $\mathcal{B}(B^- \rightarrow D^0\pi^-)$ is $1.22 \pm 0.13(stat.) \pm 0.23(syst.)$. The B^0 branching fractions, $\mathcal{B}(\bar{B}^0 \rightarrow D^+\pi^-) = 3.00 \pm 0.23 \pm 0.23 \times 10^{-3}$ ($3.00 \pm 0.32 \times 10^{-3}$) and $\mathcal{B}(\bar{B}^0 \rightarrow D^{*+}\pi^-) = 2.97 \pm 0.23 \pm 0.24 \times 10^{-3}$($2.97 \pm 0.33 \times 10^{-3}$) are compatible with the CLEO-II measurement [10] . $\mathcal{B}(\bar{B}^0 \rightarrow D^{**+}\pi^-)$ is measured for the first time: $(\bar{B}^0 \rightarrow D^{**+}\pi^-) = 2.32 \pm 0.65 \pm 0.88 \times 10^{-3}$($2.32 \pm 1.09 \times 10^{-3}$). The ratio $\mathcal{B}(\bar{B}^0 \rightarrow D^{*+}\pi^-)/\mathcal{B}(\bar{B}^0 \rightarrow D^+\pi^-)$ is measured to be equal to $0.99 \pm 0.11(stat.) \pm 0.08(syst.)$ and the ratio $\mathcal{B}(\bar{B}^0 \rightarrow D^{**+}\pi^-)/ \mathcal{B}(\bar{B}^0 \rightarrow D^+\pi^-) = 0.77 \pm 0.22(stat.) \pm 0.29(syst.)$. To calculate these branching fractions no assumption on equal production of B^+ and B^0 at the $\Upsilon(4S)$ is necessary with this method as it is the case for CLEO-II analysis [10] where is embedded a theoretical assumption on the number of charged B mesons in comparison to neutral B. The branching fractions of the decays $B^- \rightarrow D^0\pi^-$and $B^- \rightarrow D^{*0}\pi^-$measured with this method are also independent from the values of the $D^0 \rightarrow K^-\ \pi^+$ branching fraction and the $\mathcal{B}(D^0 \rightarrow K^-\ \pi^+\ \pi^0)/\mathcal{B}(D^0 \rightarrow K^-\ \pi^+)$, $\mathcal{B}(D^0 \rightarrow K^-\ \pi^+\ \pi^-\ \pi^+)/\mathcal{B}(D^0 \rightarrow K^-\ \pi^+)$ branching fraction ratios and their errors . In addition, to compute $B^- \rightarrow D^{*0}\pi^-$branching fraction, the absolute value of the branching $\mathcal{B}(D^{*0} \rightarrow D^0\pi^0)$ is not needed. The precision obtained in the measurement of the ratios $\mathcal{B}(\bar{B}^0 \rightarrow D^{*+}\pi^-)/\mathcal{B}(\bar{B}^0 \rightarrow D^+\pi^-)$ and $\mathcal{B}(B^- \rightarrow D^{*0}\pi^-)$ / $\mathcal{B}(B^- \rightarrow D^0\pi^-)$ can also be emphasized.

A Appendix : $m_{\rm ES}$ distributions (B^+ and B^0 Generic MC)

A.1 Check of the fitted yields in the generic Monte-Carlo

We have checked the yield extraction procedure and the amount of peaking backgrounds by running separately the B selection and $m_{\rm ES}$ fits on the B^+ B^-, B^0 $\bar{B}^0$, $c\bar{c}$ and $q\bar{q}$ Monte-Carlos samples, and on the total.

A.2 Charged B yields and peaking background in the B^+ B^- Monte-Carlo

The real signal from generic B^+ B^- contribution is contaminated by the reconstruction of neutral B as charged B. This so called ¨B^0peaking background ¨ can be estimated by running the B^+ B^- reconstruction analysis on the B^0 $\bar{B}^0$ sample. Fig.14 shows the contribution for each individual B^+ reconstructed mode of the B^0 peaking. It is worth to emphasize at this point that the most important contribution is seen for the right column: $D^{*0}X$ ($D^{*0} \rightarrow D^0\pi^0$) for which it is easy to associate a soft neutral pion with the D^0 meson to make a D^{*0} meson and therefore a charged B. In this method, the association criteria for the generic MC has been tuned such as the Argus-shaped background is reproduced by non-associated B. It is what is shown in Fig.14 where the green points correspond to not-associated B^+ and agree with the Argus fit of the background. The criterium is defined by the difference between the momentum of the reconstructed B^+ and the one of the true B in the event. A reconstructed B^+ is considered matched if the difference is less than $0.206\,\mathrm{GeV}/c^2$. The number of wrongly reconstructed B^+ is then extracted by two means: first by counting the matched B^+, and second by fitting the $m_{\rm ES}$ distribution. No difference between the two evaluations of peaking background have been observed. The peaking background obtained by the fit has been determined to be 3.2% of the fitted B^+ number. As much as 3.2% of the final data fitted B^+ number has therefore to be subtracted, and a systematic uncertainty of 3.2% has to be quadratically added to the total systematic uncertainty on the determination of the final number of reconstructed B^+.

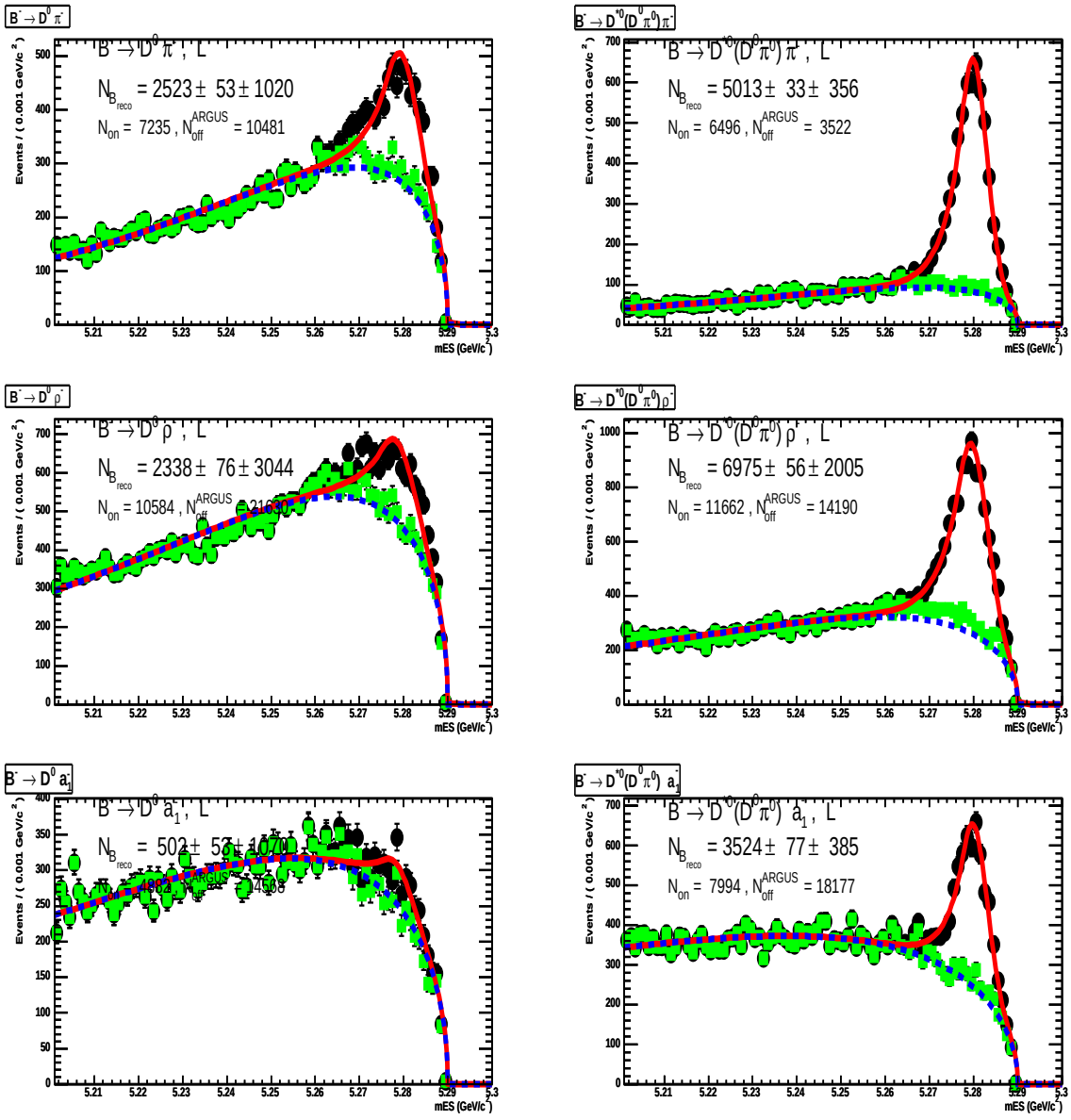

Figure 14: *The Generic $m_{\rm ES}$ spectra of the selected B^0 candidates reconstructed as $B^{\pm}$, fitted separately for each of the reconstructed modes. The green points correspond to not-associated B^+ and are shown to match to the Argus-shaped background. The fitted B^+ number is comparable to the counted number and corresponds to a peaking of about* $3.2\% \pm 3.2\%$. *$N_{B_{reco}}$ is obtained by counting the yield of B after subtraction of the Argus contribution in the $m_{\rm ES}$ range: 5.27-5.29* GeV/c^2. *N_{on} is the total yield in the same range. N_{off}^{Argus} is the Argus yield in the $m_{\rm ES}$ range:5.20-5.26* GeV/c^2.

A.2.1 The B^+ m_{ES} spectra in the $c\bar{c}$ Monte-Carlo

No peaking contribution is expected from the $c\bar{c}$ combinatorial as shown by the m_{ES} distribution in Fig.15, for each B^+ decay mode. It shows a complete superimposition of the $c\bar{c}$ m_{ES} distribution to the not-associated reconstructed B^+ (green points) and the Argus fit of the spectrum.

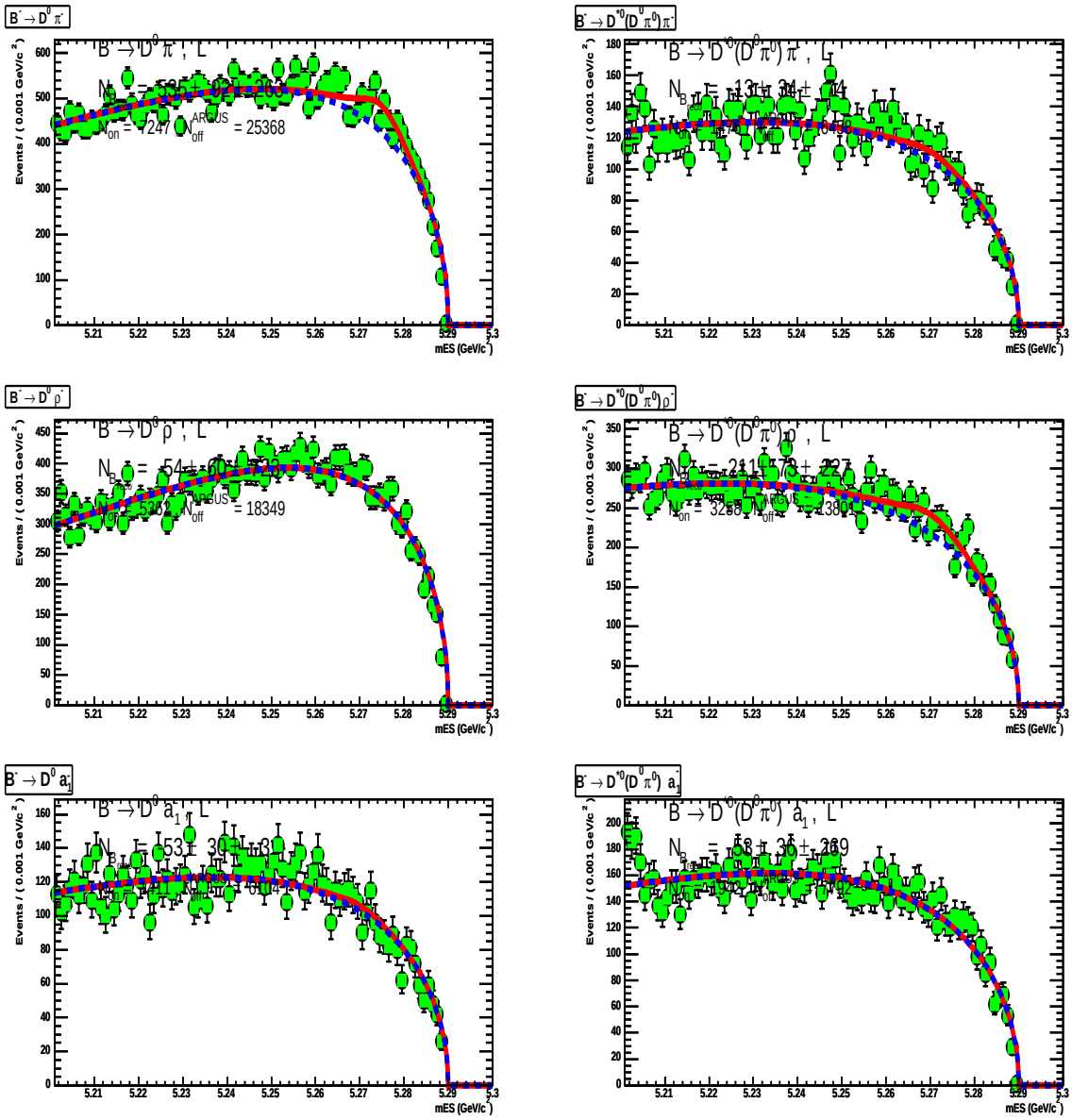

Figure 15: *The Generic m_{ES} spectra of the $c\bar{c}$ candidates reconstructed as $B^{\pm}$, fitted separately for each of the reconstructed modes. The green points correspond to not-associated B and are shown to superimpose to the Argus-shaped background as well as to $c\bar{c}$ m_{ES} distribution(black points)*

A.2.2 The B^+ m_{ES} spectra in the $q\bar{q}$ Monte-Carlo

The same procedure has been applied to $q\bar{q}$ Generic MC. m_{ES} spectra for each B^+ decay mode have been extracted and are shown in figure16 where as seen for $c\bar{c}$ distribution , a complete superimposition of the $q\bar{q}$ m_{ES} distribution to the not-associated B^+ (green points) and the Argus fit of the spectrum is demonstrated. As expected, there is no peaking contribution from $q\bar{q}$.

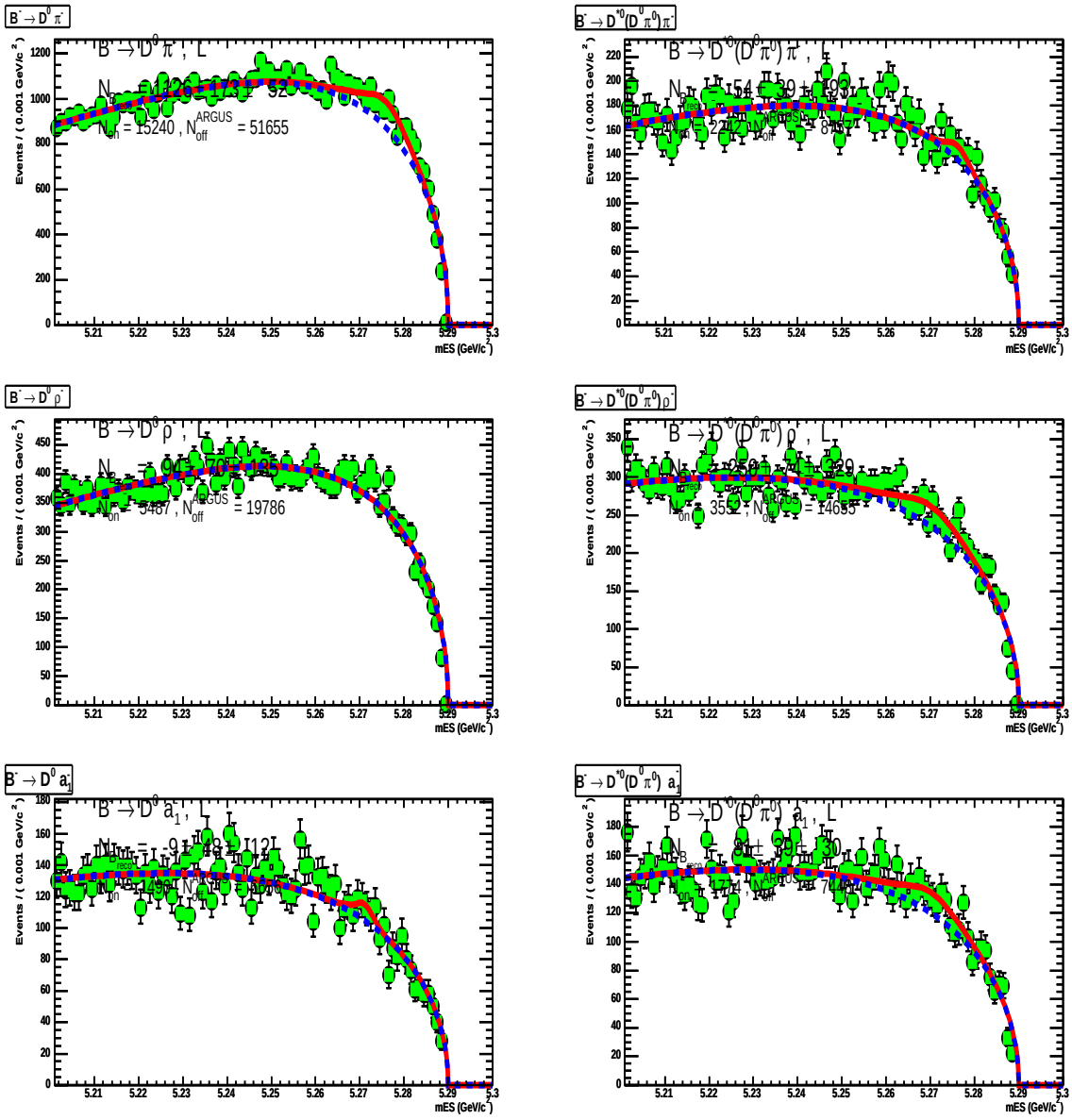

Figure 16: *The Generic m_{ES} spectra of the $q\bar{q}$ candidates reconstructed as $B^{\pm}$, fitted separately for each of the reconstructed modes. The green points correspond to not-associated B^+ and are shown to superimpose to the Argus-shaped background as well as to $q\bar{q}$ m_{ES} distribution(black points)*

A.3 Neutral B yields and peaking background in the $B^0\ \bar{B}^0$ Monte-Carlo

The procedure described in the subsection A.2 has been applied to the neutral B. The real signal from generic $B^0\ \bar{B}^0$ contribution is contaminated by the reconstruction of charged B as neutral B. This so called "B^+ peaking background" has been estimated running the $B^0\ \bar{B}^0$ reconstruction analysis on the $B^+\ B^-$ sample. Figure 17 shows the contribution for each individual B^0 reconstructed mode of the B^+ peaking. The value of the B^+ peaking background has been evaluated with the same two methods as for the B^0 peaking background and found to be $2.7 \pm 2.7\%$. Thus as much as 2.7% of the final data fitted B^0 number has to be subtracted from the latter, and a systematic uncertainty of 2.7% has to be quadratically added to the total systematic uncertainty on the determination of the final number of reconstructed B^0.

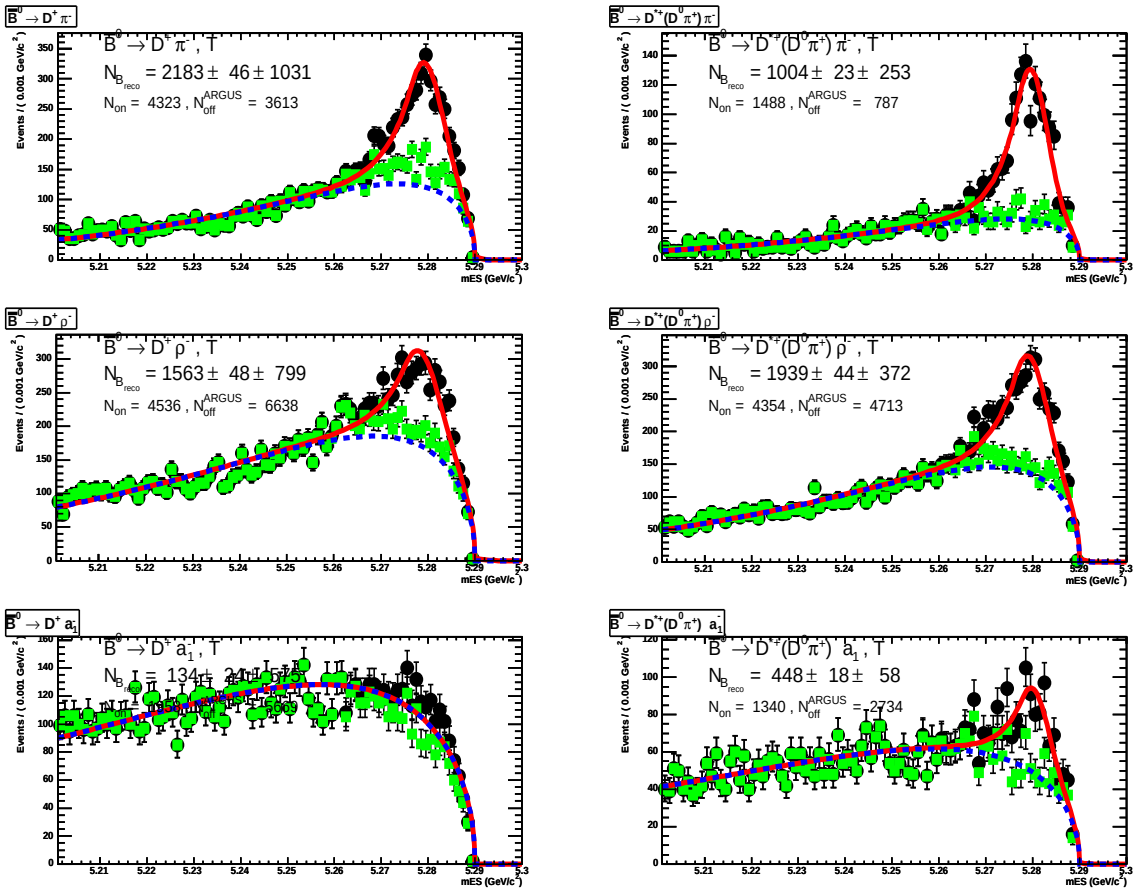

Figure 17: *The Generic $m_{\rm ES}$ spectra of the selected $B^{\pm}$ candidates reconstructed as B^0, fitted separately for each of the reconstructed modes. The green points correspond to not-associated B^0 and are shown to superimpose to the Argus-shaped background. The fitted B^0 number is comparable to the counted number and corresponds to a peaking of* $2.7\% \pm 2.7\%$. *$N_{B_{reco}}$ is obtained by counting the yield of B after subtraction of the Argus contribution in the $m_{\rm ES}$ range: 5.27-5.29* GeV/c^2. *N_{on} is the total yield in the same range. N_{off}^{Argus} is the Argus yield in the $m_{\rm ES}$ range:5.20-5.26* GeV/c^2.

A.3.1 The B^0 $m_{\rm ES}$ distribution in the $c\bar{c}$ Monte-Carlo

No peaking contribution is expected from the $c\bar{c}$ combinatorial as shown in Fig.18 by the $m_{\rm ES}$ distribution for each B^0 decay mode. It shows as well a complete superimposition of the $c\bar{c}$ $m_{\rm ES}$ distribution to the not-associated reconstructed B^0 (green points) and the Argus fit of the spectrum.

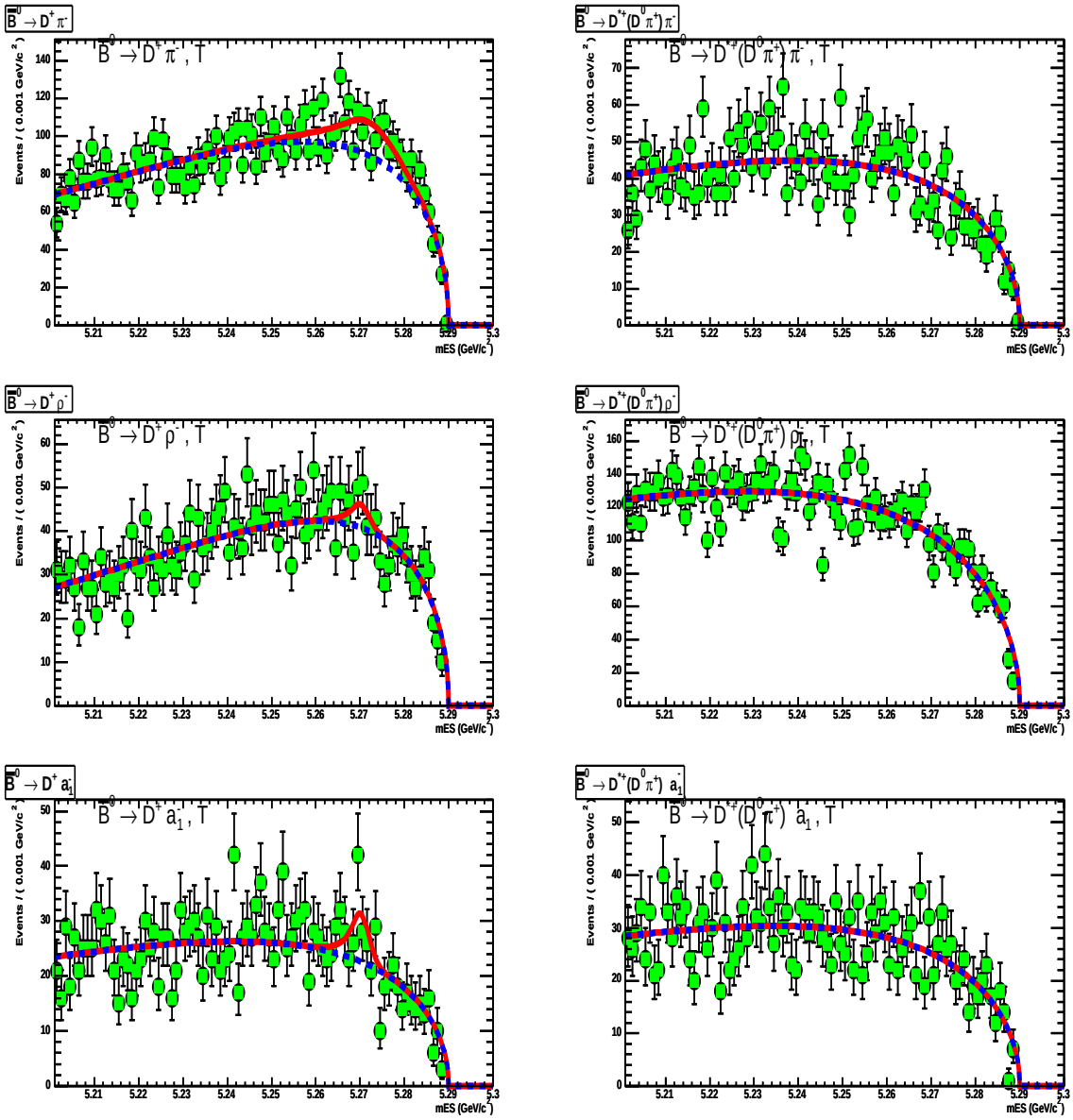

Figure 18: *The Generic m_{ES} spectra of the $c\bar{c}$ candidates reconstructed as B^0, fitted separately for each of the reconstructed modes. The green points correspond to not-associated B^0 and are shown to superimpose to the Argus-shaped background as well as to $c\bar{c}$ m_{ES} distribution(black points)*

A.3.2 The B^0 m_{ES} distribution in the $q\bar{q}$ Monte-Carlo

The same procedure has been applied to $q\bar{q}$ Generic MC. m_{ES} spectra for each B^0 decay mode have been extracted and are shown in figure19 where as seen for $c\bar{c}$ distribution ,a complete superimposition of the $q\bar{q}$ m_{ES} distribution to the not-associated B^0 (green points) and the Argus fit of the spectrum is demonstrated. As expected, there is no peaking

contribution from $q\bar{q}$.

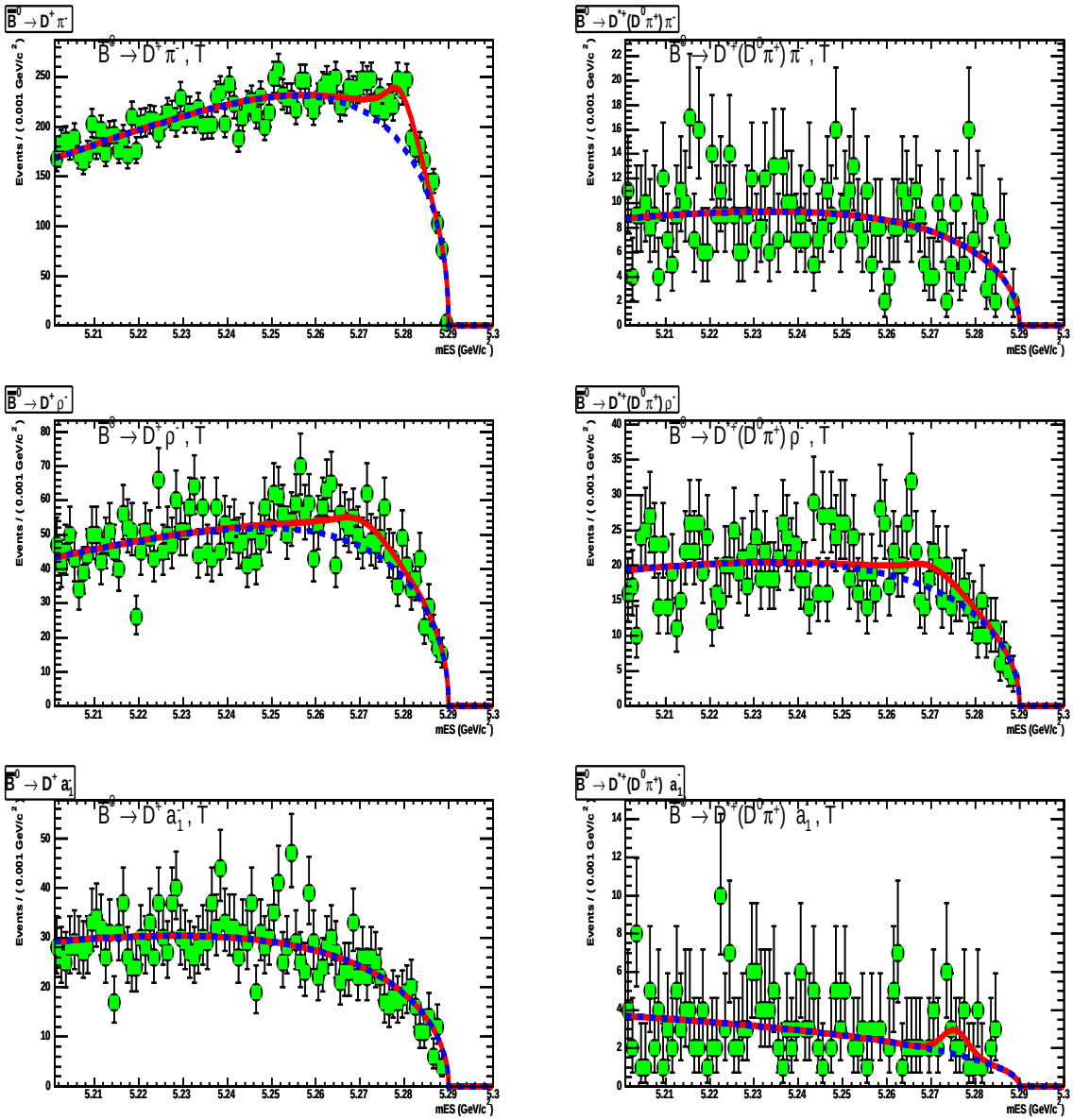

Figure 19: *The Generic $m_{\rm ES}$ spectra of the $q\bar{q}$ candidates reconstructed as B^0, fitted separately for each of the reconstructed modes. The green points correspond to not-associated B^0 and are shown to superimpose to the Argus-shaped background as well as to $q\bar{q}$ $m_{\rm ES}$ distribution(black points)*

A.4 B yields in the sum of B^+ B^-, B^0 $\bar{B}^0$, $c\bar{c}$ and $q\bar{q}$ MC

Using generic MC, it is possible to study the variation induced by the fit method in the determination of the final number of reconstructed B. The most important parameter in the

fit of the Argus-shaped background of the m_{ES} distribution appeared to be the background lower fit limit. The study of the variation of the lower limit has shown that 3.0% discrepancy could be measured if the lower fit limit is varied from 5.2 to 5.23 GeV/c^2 for the charged B and 1.8% for the neutral B generic MC samples. The study has also shown that if the D^{*0} ($D^{*0} \rightarrow D^0\gamma$) X decay modes are excluded from the fit, this discrepancy reduces to less than 1% for the charged B. The same behavior has been studied and observed in the data. For the charged B, we fixed the lower fit limit of the Argus-shaped background distribution to 5.22 GeV/c^2 and evaluated the uncertainty due to this effect, on the final reconstructed B to 2.3.0%, whilst the 1.8% systematic uncertainty has been kept for the neutral B.

B Appendix : The Analysis Method

This annexe is aimed to check the method used in our analysis to determine the signal yield and the final branching fractions and extract the systematic uncertainties. In order to determine the background in the data, we use the shape of the generic Monte Carlo background scaled to the data missing mass distribution in the mass range 2.8-3.2 GeV/c^2. The resulting background subtracted missing mass distribution is fitted in the mass range 1.65-2.2 GeV/c^2, in order to extract the yield of $D\pi$ and $D^*\pi$ B decays. The $D^{**}\pi$ yield is obtained by counting the signal excess in the 2.2-2.8 GeV/c^2 mass range.

B.1 Fit Of The Generic MC Charged B missing mass distribution

In order to determine the final systematic error due to the fit procedure bias, if any, we have applied the whole procedure on the charged B generic Monte Carlo sample. The final missing mass distribution obtained after subtraction of the MC background is shown in figure 20. The fit of the distribution is performed with one gaussian pdf for each resonance (D and D^*). The results are compared in table 24. The performance of the fit is poor with a χ^2 of 118 even if the result of the fit is compatible with the generated values reported as Truth MC in the table.

In order to improve the quality of the fit, the $D\pi$ and $D^*\pi$ components are described with a double gaussian, where the second one accounts for the tail of the missing mass distribution. The parameters of the first gaussian are σ_1^D and m_1^D for the D resonance and $\sigma_1^{D^*}$ and $m_1^{D^*}$ for the D^* resonance. Those of the second gaussian are σ_2^D and m_2^D for the D resonance and $\sigma_2^{D^*}$ and $m_2^{D^*}$ for the D^* resonance. In the fit, the central values m_1^D and m_2^D and the widths σ_1^D and σ_2^D of the double gaussian which fits the D mass distribution are left floating. We fix the ratios $\sigma_1^{D^*}/\sigma_1^D$ and $\sigma_2^{D^*}/\sigma_2^D$ to 0.900($\pm$0.015), determined by the MC simulation(appendix C). We also fix the mass difference $m_1^{D^*} - m_1^D$ (and $m_2^{D^*} - m_2^D$) to 0.1421 GeV/c^2. For the D^{**} peak, the yield is obtained by counting the candidates in excess in the $2.2 - 2.8$ GeV/c^2 missing mass range.

The results of the fit have been reported in table 25 and shown in figure 21. This time the χ^2 is 23. The parameters are displayed in table 30. This fit provides the value of the ratio f12 of the second gaussian yield over the first one. its values were found similar whether the fit is performed with $\sigma_2^{D^*}$ and $m_2^{D^*}$ fixed or floating, and it was averaged to $(17.4 \pm 5.5)\%$.

The difference between the yield obtained when $\sigma_2^{D^*}$ and $m_2^{D^*}$ are left floating (table 26) and the yield when they are constrained (table 25), is reported in table 27 and will be taken as part of the systematic uncertainty due to the fit bias. The discrepancy between the generated yield and the fitted yield when the $\sigma_2^{D^*}$ and $m_2^{D^*}$ are left floating will be the second part of the systematic error due to the fit bias. The yield difference as well as the final systematic uncertainties are determined and reported in table 27.

In conclusion, the double gaussian pdf for each resonance is well suited to perform better χ^2 fits of the missing mass distributions. The ratio f12 of the two gaussian yields has been determined to be $(17.4 \pm 5.5)\%$ for the charged B sample. The other parameters are displayed in table 30. While fitting the data with a double gaussian pdf, this parameter

can be left floating and the yield difference when$\sigma_2^{D^*}$ and $m_2^{D^*}$ are floating or not, should be added as a fit systematic uncertainty.

D resonance	Truth MC	N_{fit}^{π} (1 Gauss.)	fit err.(%)	$\|\|1 - TruthMC / N_{fit}^{\pi}\|\|$(%)
D^0	2501	2470±58	2.3%	1.2%
D^{*0}	2318	2260±56	2.5%	2.6%
D^{**0}	2096	2196 ± 122 (c)	5.5%	4.5%

Table 24: *comparison between the generated yield Truth MC and MC N_{fit}^{π} (obtained from the fit) for D^0, D^{*0} and D^{**0} with corresponding uncertainties as fitted in figure 20. The fit is performed considering only one gaussian pdf for each resonance. The mass difference of the two resonances D^0 and D^{*0} is fixed to* 0.1421 GeV$/c^2$ *while the mass value is left floating. The ratio of the resolutions of D^0 and D^{*0} is fixed to 0.90 as determined from the signal MC and discussed in appendix C. The value of the D^0 peak resolution is left floating. The D^{**0} yield is obtained from counting.*

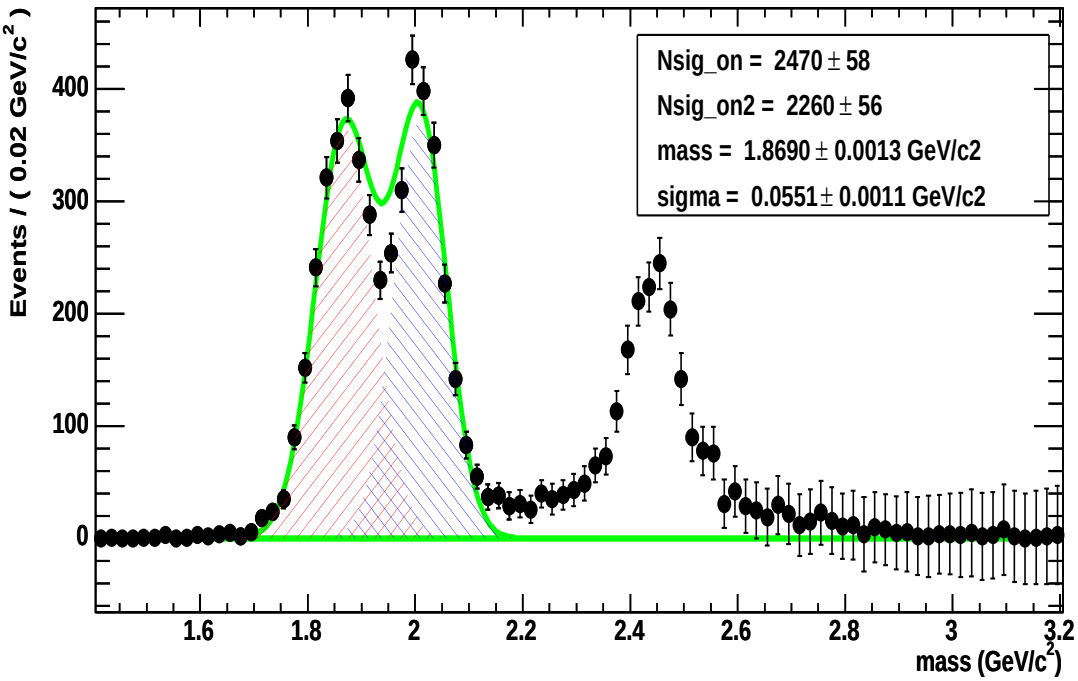

Figure 20: *Missing mass distribution from charged B generic MC, with the subtraction of the generic combinatorial background. The fit is performed considering only one gaussian pdf for each resonance. The mass difference of the two resonances D^0 and D^{*0} is fixed to* $0.1421\ \mathrm{GeV}/c^2$ *while the mass value is left floating. The ratio of the resolutions of D^0 and D^{*0} is fixed to 0.90 as determined from the signal MC and discussed in appendix C. The value of the D^0 peak resolution is left floating. The D^{**0} yield is obtained from counting (c).*

D resonance	Truth MC	N^{π}_{fit} (2 gauss. fix.)	fit err.(%)	$\|1 - TruthMC / N^{\pi}_{fit}\|$(%)
D^0	2501	2564±64	2.5%	2.5%
D^{*0}	2318	2269±62	2.3%	2.1%

Table 25: *Comparison between the generated yield Truth MC and MC N^{π}_{fit} (obtained from the fit) for D^0, D^{*0} and D^{**0} with corresponding uncertainties as fitted in figure 21. The fit is performed considering a double gaussian pdf for each resonance with $\sigma_2^{D^*}$ and $m_2^{D^*}$ fixed.*

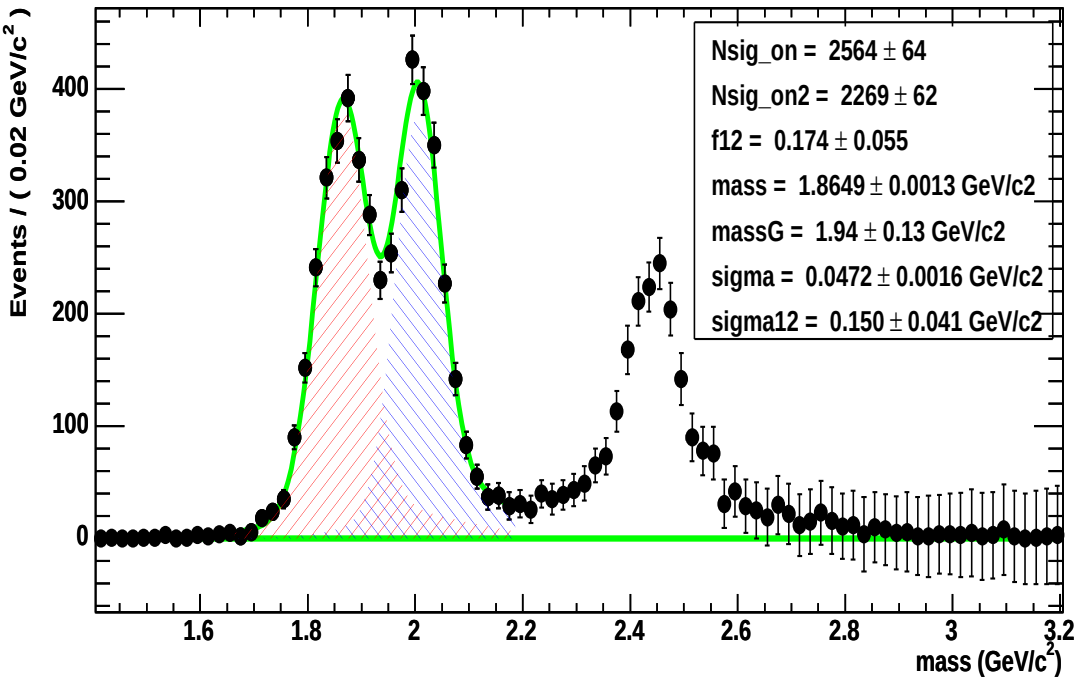

Figure 21: *Missing mass distribution from charged B generic MC, with the subtraction of the generic combinatorial background. The fit is performed considering a double gaussian pdf for each resonance with fixed* $\sigma_2^{D^*}$ *and* $m_2^{D^*}$*. The* D^{**0} *yield is obtained from counting .*

D resonance	Truth MC	N_{fit}^{π} (2 gauss. free)	fit err.(%)	$\|1 - TruthMC / N_{fit}^{\pi}\|$(%)
D^0	2501	2544±65	2.5%	1.7%
D^{*0}	2318	2292±63	2.7%	1.1%

Table 26: *Comparison between the generated yield Truth MC and MC* N_{fit}^{π} *(obtained from the fit) for* D^0*,* D^{*0} *and* D^{**0} *with corresponding uncertainties as fitted in figure 21. The fit is performed considering a double gaussian pdf for each resonance with* $\sigma_2^{D^*}$ *and* $m_2^{D^*}$ *floating.*

D resonance	fixed param. fit (2 Gauss.)	free fit (2 Gauss.)	$\|1 - fixed / free\|$(%)	syst. err.(%)
D^0	2564±64	2544±65	0.8%	1.9%
D^{*0}	2269±62	2292±63	1.0%	1.5%

Table 27: *Comparison between MC fitted yields with a double gaussian pdf for each resonance: (column 1)* $\sigma_2^{D^*}$ *and* $m_2^{D^*}$ *are fixed, (column 2)*$\sigma_2^{D^*}$ *and* $m_2^{D^*}$ *are floating.*

B.2 Fit Of The Charged B Data

The double gaussian fit has been applied to the data. Table 28 shows the fitted yields obtained with $\sigma_2^{D^*}$ and $m_2^{D^*}$ fixed (and floating. The fraction of the second gaussian f12 is left floating. The systematic uncertainty could be determined as the difference between the "free double Gaussian" fit yield and the "constrained double gaussian" yield. Table 30 gathers and allows to compare the data fit parameters obtained in each case to the Monte Carlo fit parameters. It shows that the discrepancy between the peak resolution has been reduced compared to the one Gaussian pdf fit values (Table 29), while the shift in the cental value of the resonance shows very little improvement.

D resonance	1-G. fit	2-G. fixed fit	2-G. free fit	$\|1 - fixed / free\|$(%)	syst. err.(%)
D^0	667±32	677±32	672±31	0.7%	0.7%
D^{*0}	770 ±33	774±33	779±33	0.6%	0.6%
D^{**0}	829± 78 (c)	-	-	-	-%

Table 28: *Comparison between data fitted yields. (Column 1) fit with one gaussian, (second column) double gaussian fit with* $\sigma_2^{D^*}$ *and* $m_2^{D^*}$ *fixed, (third column) double gaussian fit with* $\sigma_2^{D^*}$ *and* $m_2^{D^*}$ *floating. The* D^{**0} *yield is obtained from counting (c).*

D resonance	fitted mass(GeV/c^2)	fitted resolution.(GeV/c^2)
D^0	1.8736±0.0025	0.0575±0.0021
D^0 from MC	1.8646	0.0450±0.0006

Table 29: D^0 *mass and resolution obtained from the one gaussian fit.*

Parameters (GeV/c^2)	MC fit param.	data fixed param. fit	data free fit
σ_D (1^{st} Gauss.)	0.0472±0.0016	0.0500±0.0021	0.0512±0.0018
σ_D (2^{nd} Gauss)	0.150±0.041	0.200±0.11	0.200±0.06
σ_{D^*} (2^{nd} Gauss)	-	-	0.080±0.11
$mass_D$ (1^{st} Gauss.)	1.8649±0.0013	1.8715±0.0024	1.8720±0.0022
$mass_D$ (2^{nd} Gauss)	1.94±0.13	2.01±0.12	1.93±0.15
$mass_{D^*}$ (2^{nd} Gauss)	-	-	2.2±0.11
f12(%)	17.4±5.5	9.0±3.5	4.6±1.1

Table 30: *Comparison between (column 1) the double gaussian generic MC fit parameters and (column2) the data fit parameters of the double gaussian pdf with $\sigma_2^{D^*}$ and $m_2^{D^*}$ fixed and (column 3) with $\sigma_2^{D^*}$ and $m_2^{D^*}$ floating, for the B^+ sample.*

B.3 Fit Of The Generic MC Neutral B

In order to determine the systematic uncertainty due to the fit bias for the neutral B branching fractions, the same study has been performed. The neutral B sample including the mixing $B^0\,B^0$ and $\bar{B}^0\,\bar{B}^0$ events has been used. The single gaussian fit yields are displayed in table 31 and compared to the MC truth yield. The double gaussian fit parameters are displayed in table 35. Table 32 displays the yields obtained with the double gaussian fit compared to the MC truth yield. The systematic uncertainties are computed comparing the truth values to the fitted values. The f12 fraction is found equal to $(14.0 \pm 4.2)\%$. The χ^2 of the single gaussian fit was determined equal to 36 while the double gaussian fit one was better and equal to 17.

D resonance	Truth MC	N^{π}_{fit} (1 Gauss.)	fit err.(%)	$\|1 - TruthMC / N^{\pi}_{fit}\|$(%)
D^{+}	609	614±28	4.5%	0.8%
D^{*+}	545	532±26	4.9%	2.4%
D^{**+}	550	573 ± 84 (c)	14.6%	4.0%

Table 31: *Comparison between the generated yield Truth MC and MC N^{π}_{fit} (obtained from the fit) for D^{+}, D^{*+} and D^{**+} . The fit is performed considering only one gaussian pdf for each resonance. The mass difference of the two resonances D^{+} and D^{*+} is fixed to* 0.1406 GeV/c^2 *while the mass value is left floating. The ratio of the resolutions of D^{+} and D^{*+} is fixed to 0.90 as determined from the signal MC and discussed in appendix C. The value of the D^{+} peak resolution is left floating. The D^{**+} yield is obtained from counting (c).*

D resonance	MC Truth	fixed param. fit (2 Gauss.)	free fit (2 Gauss.)	$\|1 - fixed / free\|$(%)	syst. err.(%)
D^{+}	609	634±30	636±65	0.3%	4.2%
D^{*+}	545	528±28	527±63	0.2%	3.4%

Table 32: *Comparison between (column1) the generated yield and (column 2) the double gaussian fit with $\sigma_2^{D^*}$ and $m_2^{D^*}$ fixed and (column 3) the double gaussian fit with $\sigma_2^{D^*}$ and $m_2^{D^*}$ floating.*

B.4 Fit Of The Neutral B Data

The double gaussian fit has been applied to the neutral B data. Table 33 shows the fitted yields obtained when $\sigma_2^{D^*}$ and $m_2^{D^*}$ are left floating and when they are constrained. The fraction of the second gaussian f12 is left floating. The systematic uncertainty could be determined as the difference between the "free double Gaussian " fit yield and the "constrained double gaussian" yield. Table 35 gathers and allows to compare the data fit parameters obtained in each case to the Monte Carlo fit parameters. It shows that the discrepancy between the peak resolution has been reduced compared to the one Gaussian pdf fit values (Table 34), while the shift in the cental value of the resonance shows very little improvement.

D resonance	1-G. fit	2-G.fixed fit	2-G.free fit	$\|\|1 - fixed / free\|\|(\%)$	syst. err.(%)
D^+	241 $\pm$19	248$\pm$19	253$\pm$24	1.9%	1.9%
D^{*+}	238 $\pm$19	245$\pm$19	243$\pm$24	0.8%	0.8%
D^{**+}	192$\pm$54 (c)	-	-	-	-%

Table 33: *Comparison between data fitted yields, (column 1) fit with one gaussian, (column2) double gaussian fit with $\sigma_2^{D^*}$ and $m_2^{D^*}$ fixed, (column 3) double gaussian fit with $\sigma_2^{D^*}$ and $m_2^{D^*}$ floating. The D^{**+} yield is obtained from counting (c).*

D resonance	fitted mass(GeV/c^2)	fitted resolution.(GeV/c^2)
D^+	1.8802$\pm$0.0037	0.0491$\pm$0.0038
D^+ from MC	1.869	0.0450$\pm$0.0006

Table 34: *D^+ mass and resolution obtained from the one gaussian fit.*

Parameters (GeV/c^2)	MC fit param.	data fixed param. fit	data free fit
σ_D (1^{st} Gauss.)	0.0437$\pm$0.0019	0.0442$\pm$0.0030	0.0384$\pm$0.0063
σ_D (2^{nd} Gauss)	0.134$\pm$0.028	0.160$\pm$0.094	0.122$\pm$0.033
σ_{D^*} (2^{nd} Gauss)	-	-	0.080$\pm$0.023
$mass_D$ (1^{st} Gauss.)	1.8719$\pm$0.0022	1.8835$\pm$0.0036	1.8828$\pm$0.0038
$mass_D$ (2^{nd} Gauss)	1.93$\pm$0.12	1.93$\pm$0.13	1.93$\pm$0.11
$mass_{D^*}$ (2^{nd} Gauss)	-	-	2.06$\pm$0.14
f12(%)	13.4$\pm$2.8	13.9$\pm$6.6	36.0$\pm$14.0

Table 35: *Comparison between (column 1)the double gaussian generic MC fit parameters and (column 2) the data fit parameters a double gaussian with $\sigma_2^{D^*}$ and $m_2^{D^*}$ fixed and (column 3) double gaussian fit with $\sigma_2^{D^*}$ and $m_2^{D^*}$ floating, for the B^0 sample.*

C Appendix : Resolution in the Missing Mass

This annexe is aimed to validate the fit constraints used in our analysis to determine the signal yield and the final branching fractions. It is based on Monte Carlo sample. It will show that it is correct to use the D and D^* MC fitted resolution ratio R to constrain the fit of the data missing mass spectrum.

A study has been performed in order to evaluate the uncertainties on the ratio R, other than the MC statistical uncertainty. Thus, effects such as the variation of the resolution width, or the central value of the resonance mass have been investigated. The difference in the evaluation of this ratio R, using the fit of the MC missing mass spectra in section C.1 or using the center of mass momentum resolution and its kinematic relation to the missing mass C.2, will also be added to the final value of the systematic uncertainty on R. We will also show in section 6 that one standard deviation variation of R has negligible effect on the final branching fractions . The systematic uncertainty on the branching fraction due to this will be added to the final result.

C.1 Evaluation of the D and D^* resolutions' ratio from missing mass spectra

In the following section, we will show that the resolution of resonances fitted from the missing mass spectra varies as a function of the missing mass value or the center of mass momentum p^* value. We will first display a profile of the missing mass resolution, to give a rough sight on the variation of the resolution. We will next fit the resolution for different missing mass ranges and compare D and D^* resolutions obtained here figure 25 and figure 26 to those obtained from missing mass spectra figure 23.

Figure 22 shows the profile of the difference between monte carlo generated missing mass and the monte carlo reconstructed missing mass. It is the spread of this difference (Y-axis) for a given range of the generated missing mass (X-axis). The profile shows that the spread of the missing mass difference is larger when the missing missing mass is lower. We thus expect that the resolution of the D resonance to be larger than the resolution of the D^* resonance. The fitted resolution values obtained for each missing mass range of the profile of figure 22 are gathered in the table 36 and the fits are shown in the following set of figures 24-33. The ratio R of D^* over D is obtained from the fitted resolution values (12) and (1) of table 36 and is 0.907 ± 0.006. The one determined directly from the MC missing mass spectra of figure 23 is 0.90 ± 0.013. The two numbers are compatible. Since the ratio R obtained from the missing mass fit is directly related to our analysis, we use this one to constrain the fit of the data. We will evaluate the total uncertainty on this ratio in the following sections.

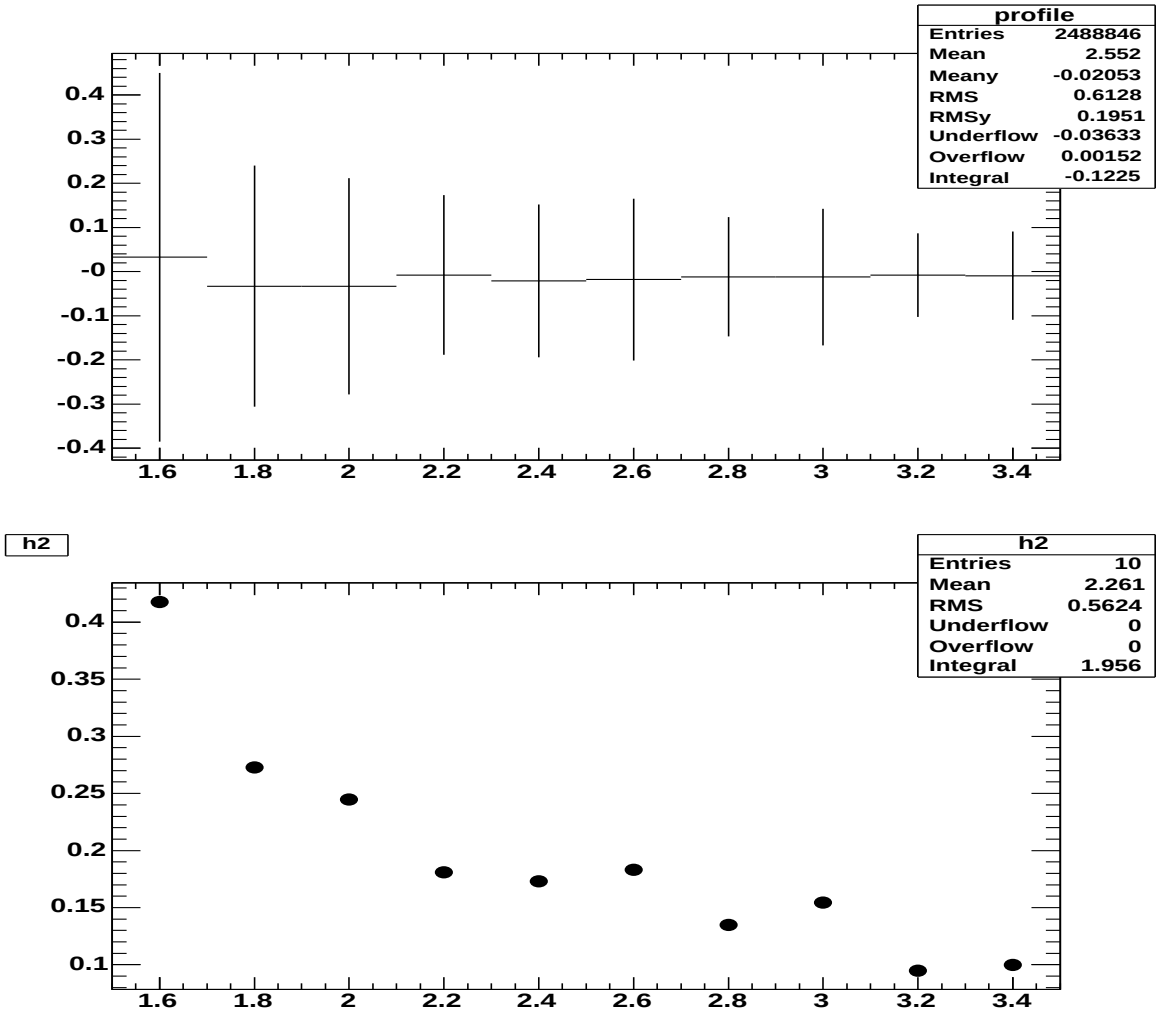

Figure 22: *Profile of the missing mass resolution as a function of the missing mass range from charged B monte carlo (top plot) . Variation of the spread of the profile as a function of the missing mass range (bottom plot).*

missing mass range (GeV/c^2)	fitted resolution.(GeV/c^2)	ratio
1.5-1.7	0.0521±0.0028	
1.7-1.9	0.0516±0.00023(1)	
1.9-2.1	0.0468±0.00022(2)	(2)/(1)=0.907±0.006
2.1-2.3	0.0411±0.00007	
2.3-2.5	0.0360±0.0002	
2.5-2.7	0.0317±0.0002	
2.7-2.9	0.0266±0.0002	
2.9-3.1	0.0245±0.00015	
3.1-3.3	0.0215±0.00010	
3.3-3.5	0.0183±0.00009	

Table 36: *resolution and ratio obtained from the fit shown in figure 24-33.*

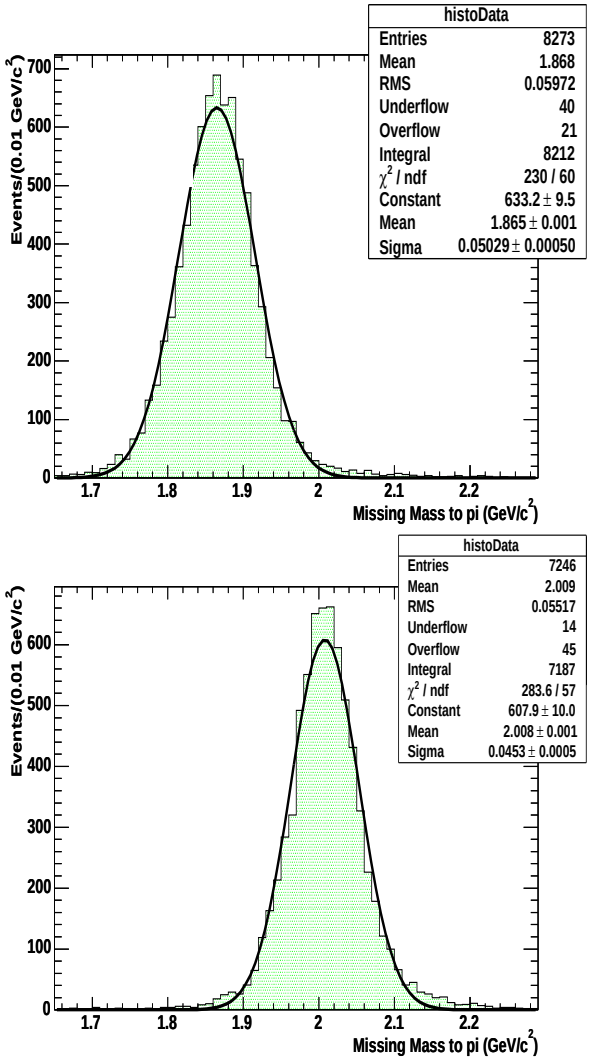

Figure 23: *Fit of the missing mass for the D resonance (top)and for the D^* resonance (bottom)*

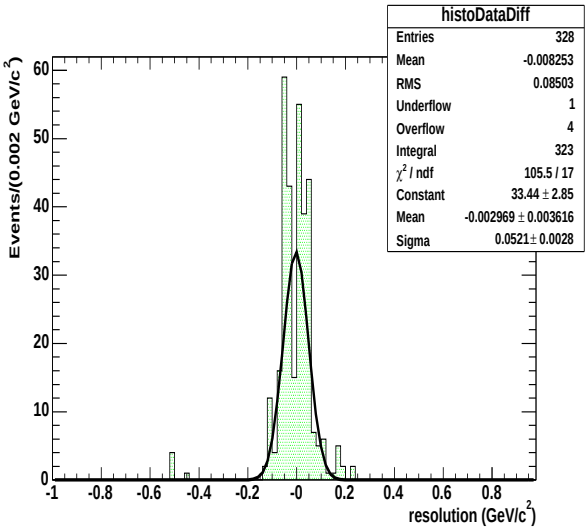

Figure 24: *Fit of the missing mass resolution for the range 1.5-1.7* GeV/c^2 *of table 36*

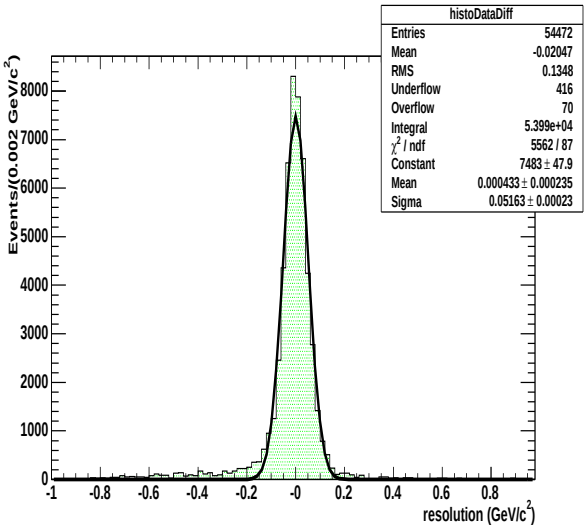

Figure 25: *Fit of the missing mass resolution for the range 1.7-1.9* GeV/c^2 *of table 36*

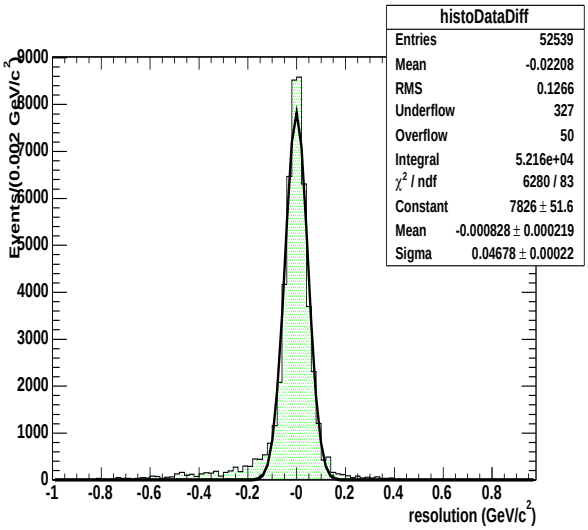

Figure 26: *Fit of the missing mass resolution for the range 1.9-2.1* GeV/c^2 *of table 36*

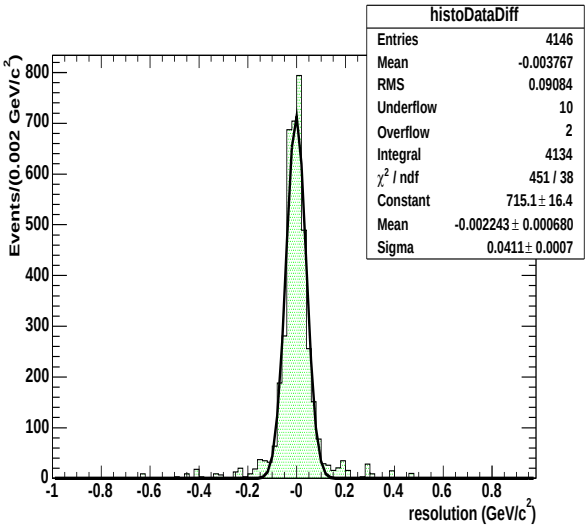

Figure 27: *Fit of the missing mass resolution for the range 2.1 -2.3* GeV/c^2 *of table 36*

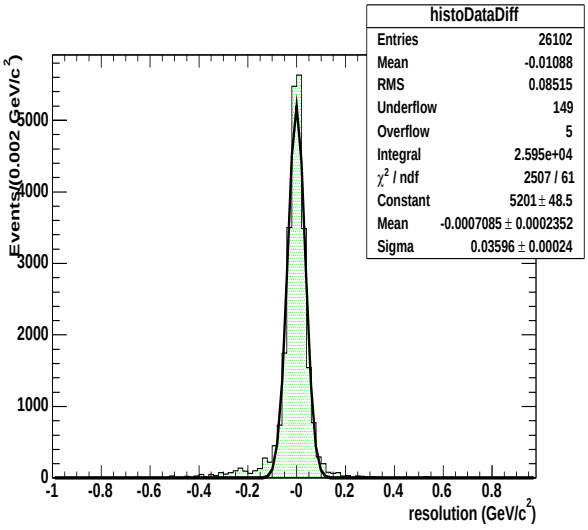

Figure 28: *Fit of the missing mass resolution for the range 2.3 -2.5* GeV/c^2 *of table 36*

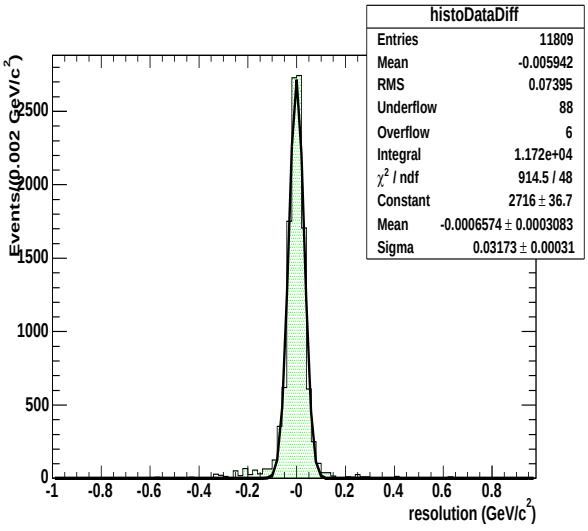

Figure 29: *Fit of the missing mass resolution for the range 2.5 -2.7* GeV/c^2 *of table 36*

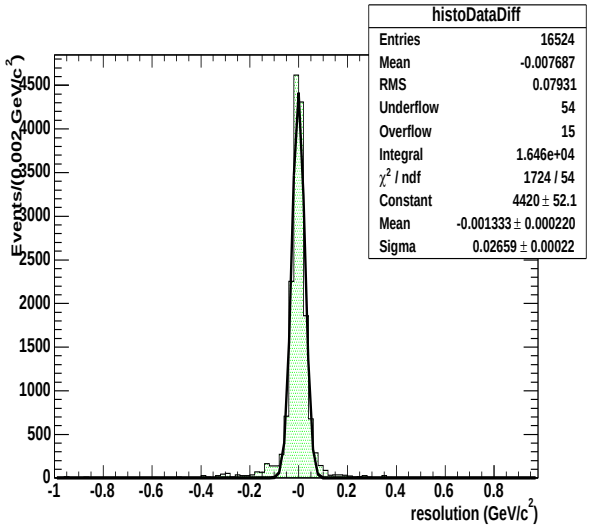

Figure 30: *Fit of the missing mass resolution for the range 2.7-2.9* GeV/c^2 *of table 36*

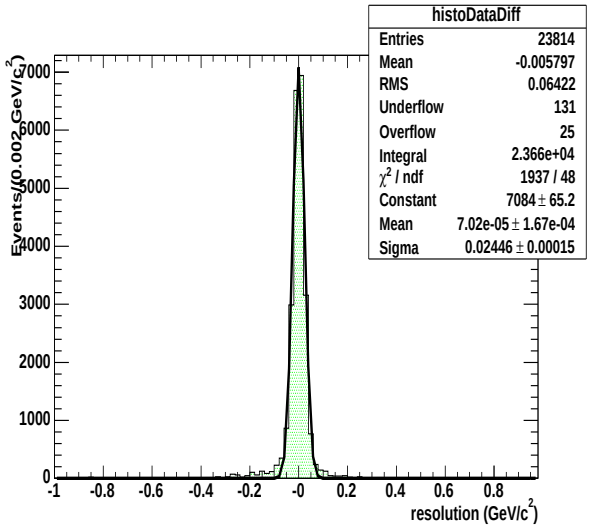

Figure 31: *Fit of the missing mass resolution for the range 2.9-3.1* GeV/c^2 *of table 36*

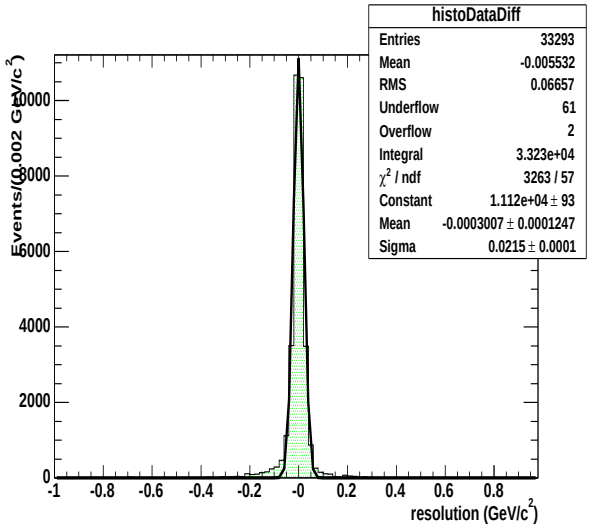

Figure 32: *Fit of the missing mass resolution for the range 3.1-3.3* GeV/c^2 *of table 36*

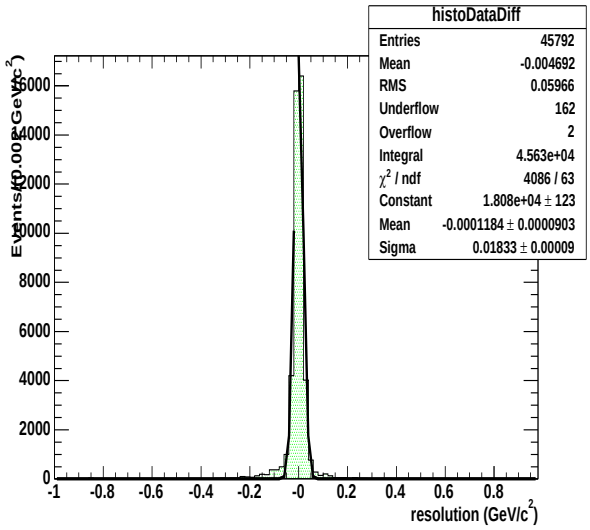

Figure 33: *Fit of the missing mass resolution for the range 3.3-3.5* GeV/c^2 *of table 36*

C.2 Evaluation of the mass resolution ratio R as a function of the center of mass momentum resolution

The missing mass as a function of the center of mass momentum of the pion, its mass and the B mass, is written

$$m_X^2 = m_B^2 + m_\pi^2 - 2m_B\sqrt{m_\pi^2 + p_\pi^{*2}} \tag{2}$$

We have evaluated the effect of the center of mass momentum p^* resolution on the missing mass resolution. According to [17] the momentum resolution $\Delta p^*/p^*$ varies as a function of the particle momentum. For a particle of a transverse momentum of the order of 2 GeV/c the resolution is of the order of 0.71%. In our case, the missing mass ranges from 1.8 to 2.10 GeV/c^2 and the p^* ranges from 2.1 to 2.4 GeV/c. The missing mass resolution for the D resonance is of the order of 0.050 GeV/c^2. The corresponding $\Delta p^*/p^*$ resolution value is 0.78%. With this value of the momentum resolution we have calculated the spread of the the resonance peaks in the missing mass spectra. Table 37 shows the variation of the missing mass spread as a function of the missing mass value. Thus for a momentum resolution of 0.78%, the spread varies from an average value of 0.05 GeV/c^2 to 0.025 GeV/c^2. The ratio of the spread of D^* over D is equal to 0.9080.

We find for the third time the same ratio and we conclude that the ratio of the resolution of D^* over D resonances is equal to 0.90 ± 0.013 determined from the MC missing mass spectra. The uncertainty is only from the MC statistics. An additional uncertainty coming from the difference of the two values we have obtained (0.008) can be considered. In that case, the ratio is determined to be 0.90 ± 0.015.

C.3 Evaluation of the systematic uncertainties on the mass resolution ratio R

C.3.1 Impact of a shift in the missing mass value

A shift of 0.010 GeV/c^2 of the central value of the resonance in the missing mass spectrum has been applied to evaluate the variation of the resonances' ratio R. We found a ratio equal to 0.9082 to be compared to 0.9080. If the shift is of 0.020 GeV/c^2, the ratio value is 0.9084. Thus, the shift of the fitted central values induces a negligible effect on the ratio R.

C.3.2 Impact of a the missing mass width value on R

We also varied the spread of the resonance up to 0.130 GeV/c^2 corresponding to a $\Delta p^*/p^*$ value of 2.%. We obtained for the highest value we considered (0.130 GeV/c^2), a ratio of 0.9074. We conclude that there is no additional uncertainty to consider. Any tail could also be taken into account with this large spread value without modifying the mass resolution ratio.

C.3.3 Impact of the B momentum reconstruction on the missing mass resolution

In order to check that the mass resolution ratio in only due to the pion momentum resolution, we computed the missing mass using the reconstructed B momentum and the generated pion momentum. The red histogram in figure 34, shows that the resolution of the D and D^* resonances are similar. In a second step, we computed the missing mass using the reconstructed pion momentum, and overlayed the resulting histograms (blue for the D resonance and green for D^*) on the first one in figure 34. We observe a width difference between these histograms (blue is wider than green) and confirm that the mass resonance ratio is a result of the pion momentum reconstruction.

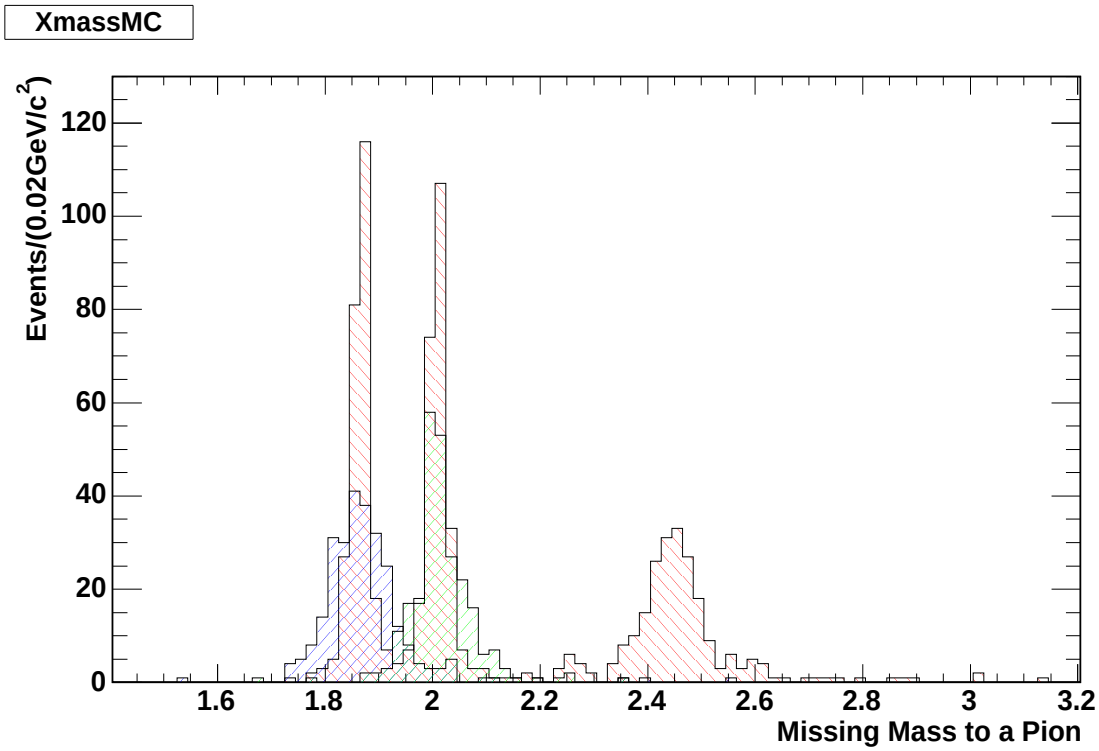

Figure 34: *Comparison between the missing mass distribution from neutral B generic MC computed with the reconstructed B momentum and the generated pion (red) and the one computed with the reconstructed parameters for both the B and the pion (blue for the D resonance and green for D^*).*

C.3.4 Impact of the Beam energy on the missing mass resolution

We have checked the effect on the missing mass, of the error on the beam energy. We observed no shift of the central value of the missing mass when the beam energy (in fact its the *B* momentum) is varied by 1 MeV (or 2 MeV) and only a maximum widening of the of the resolution by 1 MeV (or 2 MeV).

C.4 Systematic uncertainty on the yield due to the mass resolution ratio R

The effect, on the yield and the final branching fractions, of the variation of one standard deviation of the mass resolution ratio R is negligible as displayed in tables 38 and 39. These tables also show that the variation of the ratio R has a negligible effect on the *D* and D^* yield ratio. The systematic uncertainty due to R will be considered in section 6 and added to the final systematic uncertainties.

p^* range (GeV/c)	miss. mass MM	MM spread(GeV/c^2)	ratio
D range			
2.3078	1.8646		
2.2898(-$\Delta p^*/p^*$)	1.9148	0.0502	
2.3258(+$\Delta p^*/p^*$)	1.8130	-0.0516	
		((1)mean=0.05089)	
D^* range			
2.2556	2.0067		
2.2380(-$\Delta p^*/p^*$)	2.0524	0.0457	
2.2732(+$\Delta p^*/p^*$)	1.9600	-0.0467	
		((2)mean=0.04621)	(2)/(1)=0.9080
D^{**} range			
2.0911	2.4000		
2.0748(-$\Delta p^*/p^*$)	2.4355	0.0355	
2.1074(+$\Delta p^*/p^*$)	2.363.9	-0.0361	
background range			
1.7835	3.0000		
1.7695(-$\Delta p^*/p^*$)	3.0243	0.0243	
1.7974(+$\Delta p^*/p^*$)	2.9755	-0.0245	

Table 37: *Resolution (spread) and ratio obtained from the determination of the missing mass spread for* $\Delta p^*/p^* = 0.78\%$

D resonance	R=0.9	R=0.915	R=0.885	syst. err.(%)
D^0	677 $\pm$32	673$\pm$30	679$\pm$30	0.6%
D^{*0}	774 $\pm$33	778$\pm$30	772$\pm$30	0.5%
D^0 and D^{*0} yield ratio	1.143 $\pm$0.073	1.156$\pm$0.068	1.137$\pm$0.067	

Table 38: *Effect on the charged B data fitted yield of the variation of the ratio R by one standard deviation*

D resonance	R=0.9	R=0.915	R=0.885	syst. err.(%)
D^+	248±19	247±18	249±18	0.4%
D^{*+}	245 ±19	246±19	243±19	0.8%
D^+ and D^{*+} yield ratio	0.988 ±0.108	0.996±0.106	0.976±0.104	

Table 39: *Effect on the neutral B data fitted yield of the variation of the ratio R by one standard deviation*

D Appendix : Pion multiplicity in the Monte carlo and the Data

In this annexe, the pion multiplicity is compared between data and monte carlo.

Figures 35 and 36 show the profile of the pion multiplicity as a function of the missing mass. The multiplicity is quite constant versus the *missing mass to* π^- and quite similar between MC and data as viewed in the top plots of both figures. The mean value of the multiplicity is 1.047 for the data and 1.054 for the monte carlo. The bottom plots show the spread of the multiplicity which is also similar for data and MC and about 0.22. It is thus, quite reasonable to compare the generic monte carlo combinatorial background to the data one.

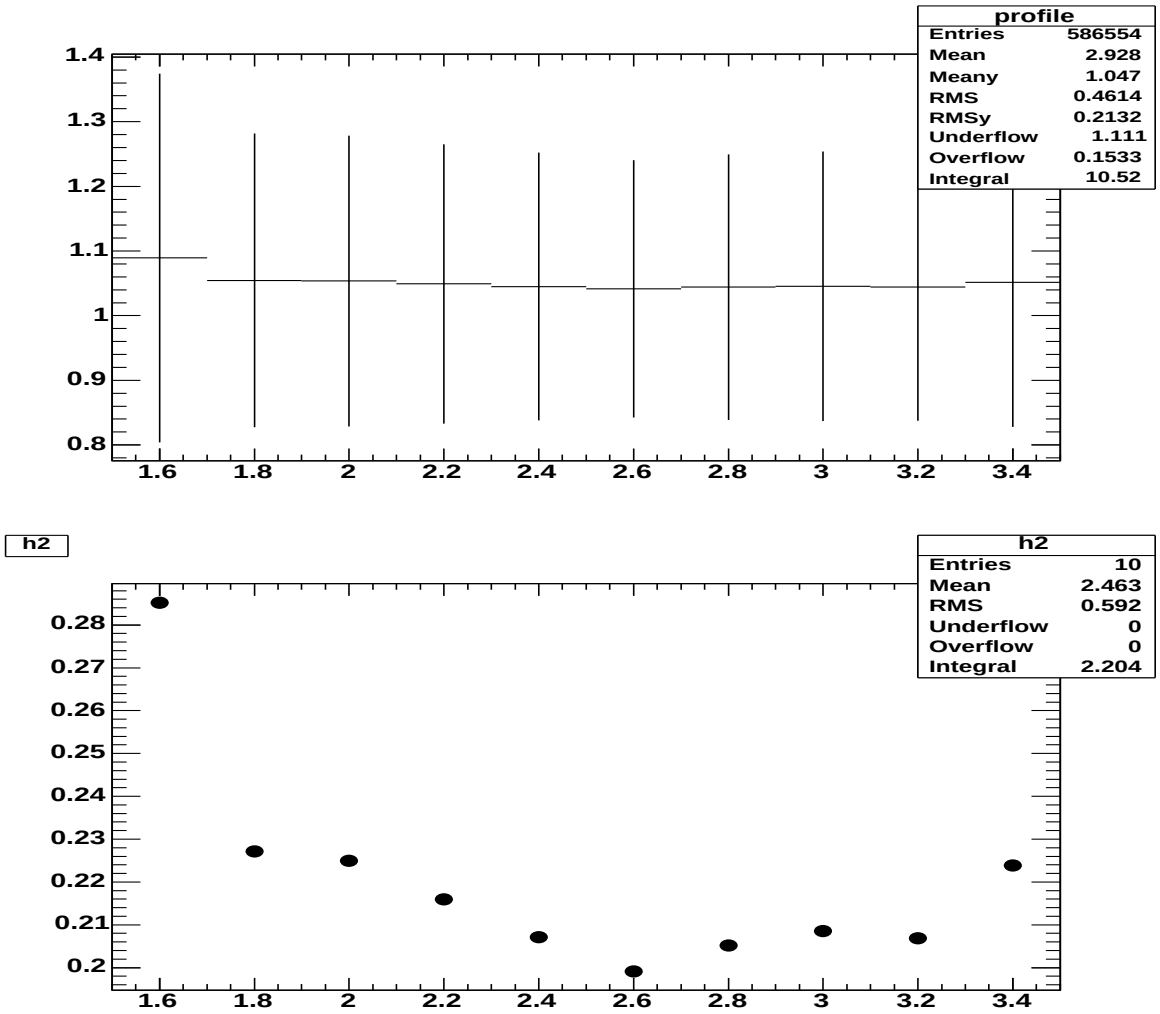

Figure 35: *(Top plot) Profile of the pion multiplicity of the data as a function of the missing mass range. (Bottom plot) Variation of the spread of the profile as a function of the missing mass range.*

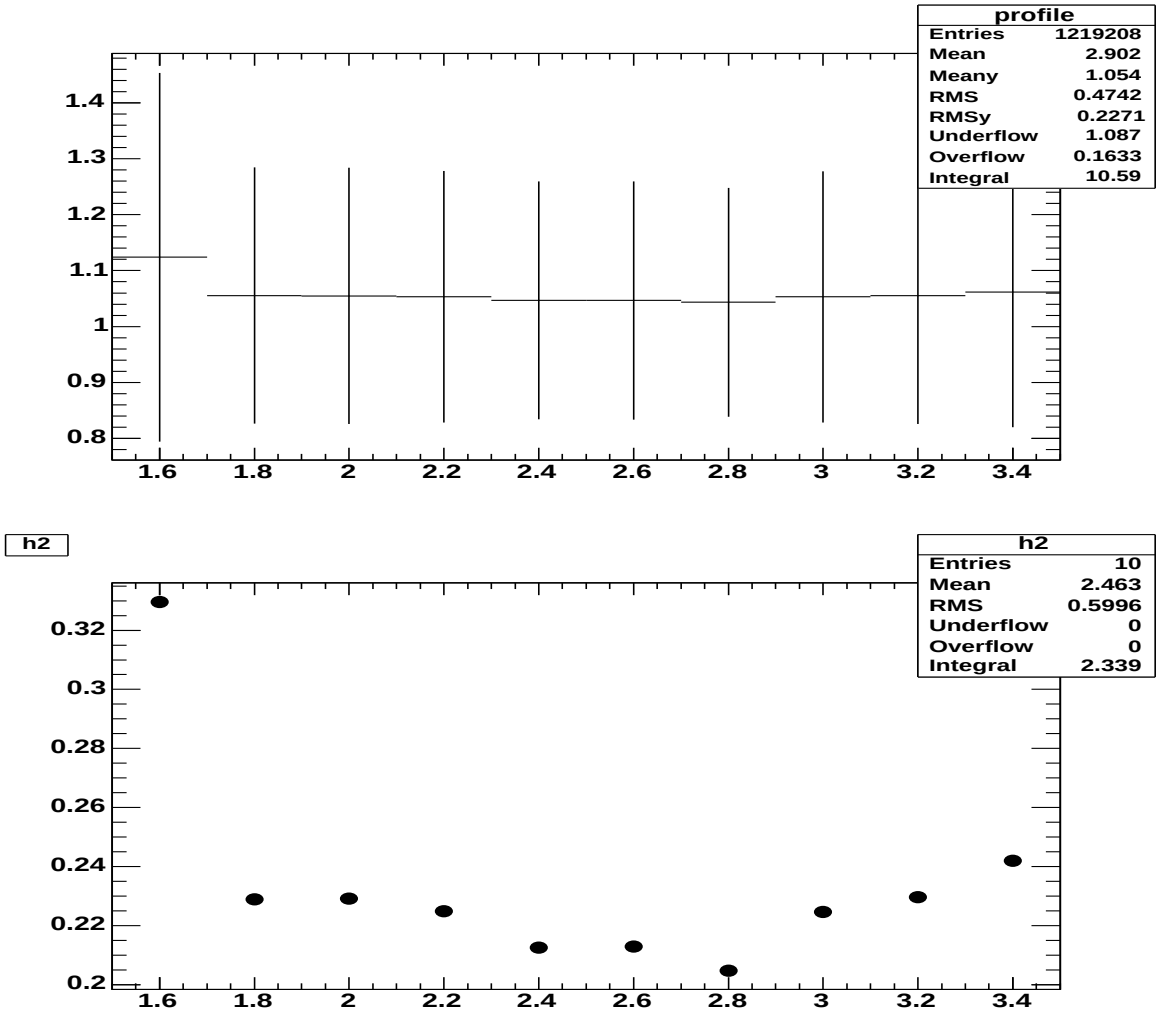

Figure 36: *Profile of the pion multiplicity as a function of the missing mass range, from charged B generic monte carlo (top plot) . Variation of the spread of the profile as a function of the missing mass range (bottom plot).*

For the events that have two pions candidates, figure 37 shows that the *missing mass to* π^- distribution of the wrong pions is pushed at the high values of the missing mass (top plot), so very negligible contamination is expected in the resonance mass region. This distribution has been obtained with cocktail MC which luminosity is about 6 times the data. This figure (bottom plot) shows also, the difference between the reconstructed missing mass and the generated one in the missing mass range 1.6-3. GeV/c^2. There is negligible amount of events close to zero (for 6 times the data luminosity) to be compared to about 17500 cocktail MC reconstructed events, which confirms the top plot conclusions. Therefore,for the data, no peaking from the wrong pion is expected in the resonance missing mass region .

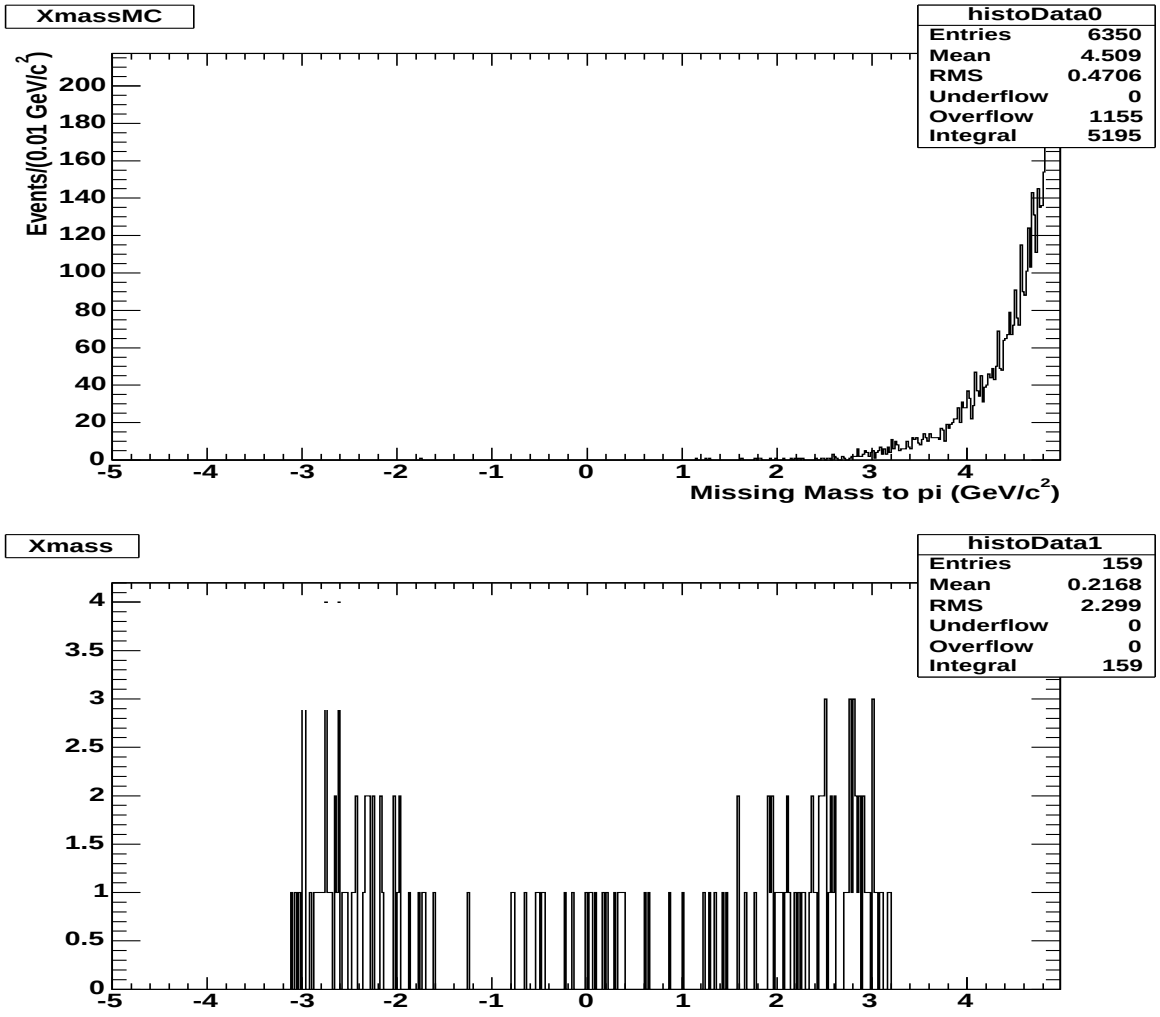

Figure 37: *Missing mass distribution obtained with the wrong pion when the candidate multiplicity is 2, obtained from charged B cocktail monte carlo (top plot) . Missing mass difference between data and MC for the wrong pion for the missing mass range 1.6-3.* GeV/c^2 *(bottom plot).*

E Appendix : Study Of The Highest Momentum Pion Cut

The effect on the yield significance, of a cut on the combinatorial pions used to calculate the missing mass distribution, is studied in this appendix. The cut is aimed to select the right pion, by choosing the one which has the highest center of mass momentum.

E.1 Charged *B* Yield With The Highest Momentum Pion

To reduce the combinatorial background, a study of the effect of selecting only one pion to build the missing mass distribution, has been performed. The pion is selected to be the one of the highest momentum. This criterion is applied to the pion in addition to the all other criteria discussed in section [4.3]. Figure 38 shows that this selection has a negligible effect on the background underneath D^0 and D^{*0} resonances. It reduces the background by 10% in the missing mass region beyond 2.2 GeV/c^2 where the D^{**0} resonance is expected to contribute.

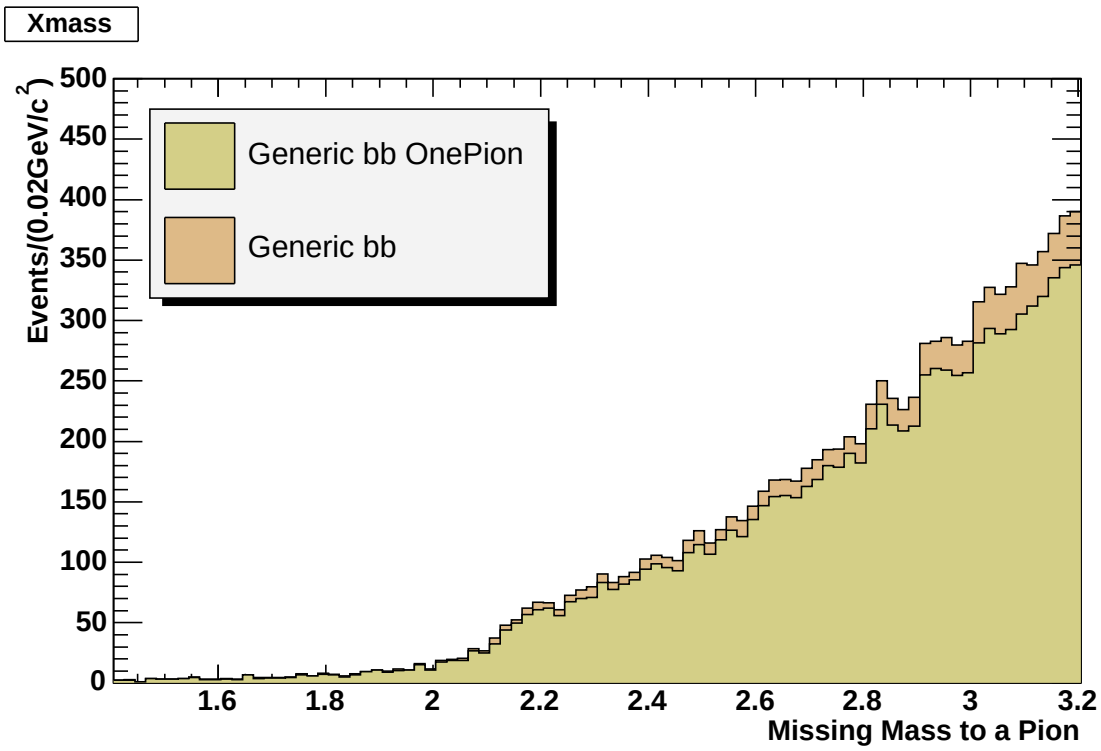

Figure 38: *Missing mass distribution of the $b\bar{b}$ component of the charged B generic MC, with and without the π momentum selection.*

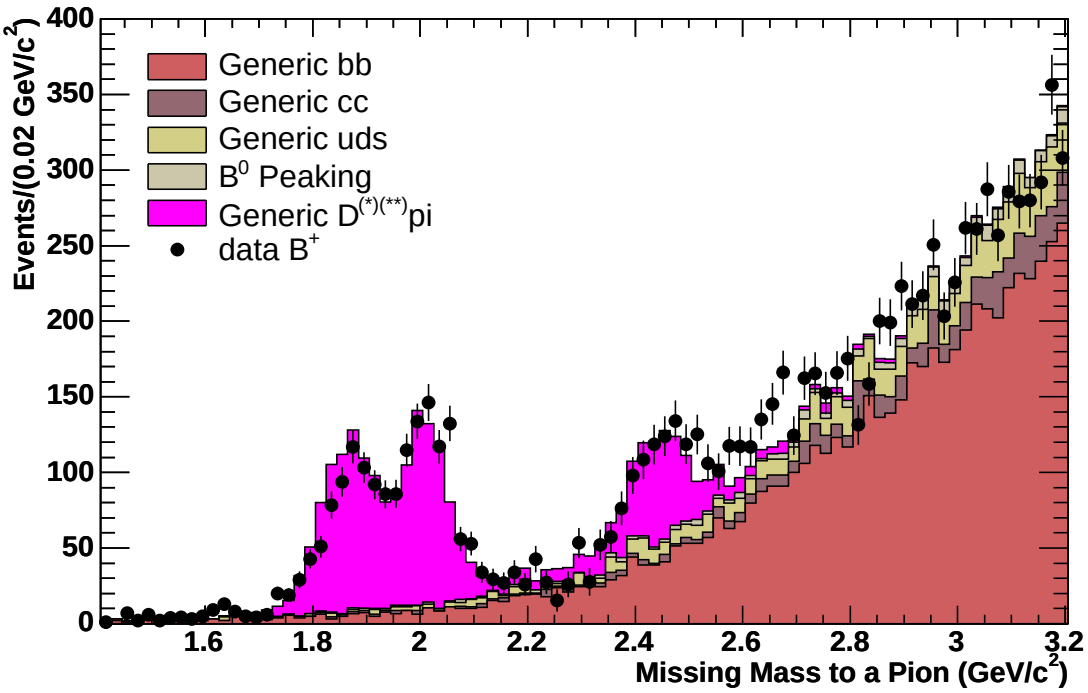

Figure 39: *missing mass distribution obtained with total charged B data, with a total luminosity of* $209 fb^{-1}$*, are superimposed to the data, the normalized generic MC contributions from* $b\bar{b}$ *(*$B^- \rightarrow D^0\rho^-$ *and* $B^- \rightarrow D^{*0}\rho^-$ *background components are subtracted from the data and the MC distributions),* $c\bar{c}$ *and* $q\bar{q}$*, as well as the* B^0 *peaking. The resonance contribution from truth generic MC is also superimposed. Only one pion per event, the one of the highest momentum value is selected to perform the missing mass to* π^- *distributions.*

The same procedure described in section 5.1.2 has been applied to extract the D^0 , D^{*0} and D^{**0} yields. The highest momentum pion missing mass distribution of the data superimposed to the total generic MC background is reported on figure 39. The corresponding subtracted (from normalized generic MC background with a factor of 0.93 ± 0.02) and fitted *missing mass to* π^- distribution is reported in figure 40. The fit results are given in table 40 and compared to the MC values. According to procedure of section 5.1.2, $B^- \rightarrow D^0\rho^-$and $B^- \rightarrow D^{*0}\rho^-$background components are subtracted from the data and the MC distributions. The final D^0 , D^{*0} and D^{**0} yield is given in table 41.

The Branching fractions computed with the two sets of yields of table 7 and table 41 are compatible within the statistical uncertainties. The final branching fractions are computed using the yield of table 7 and using the π reconstruction efficiencies from the tables 5-a.

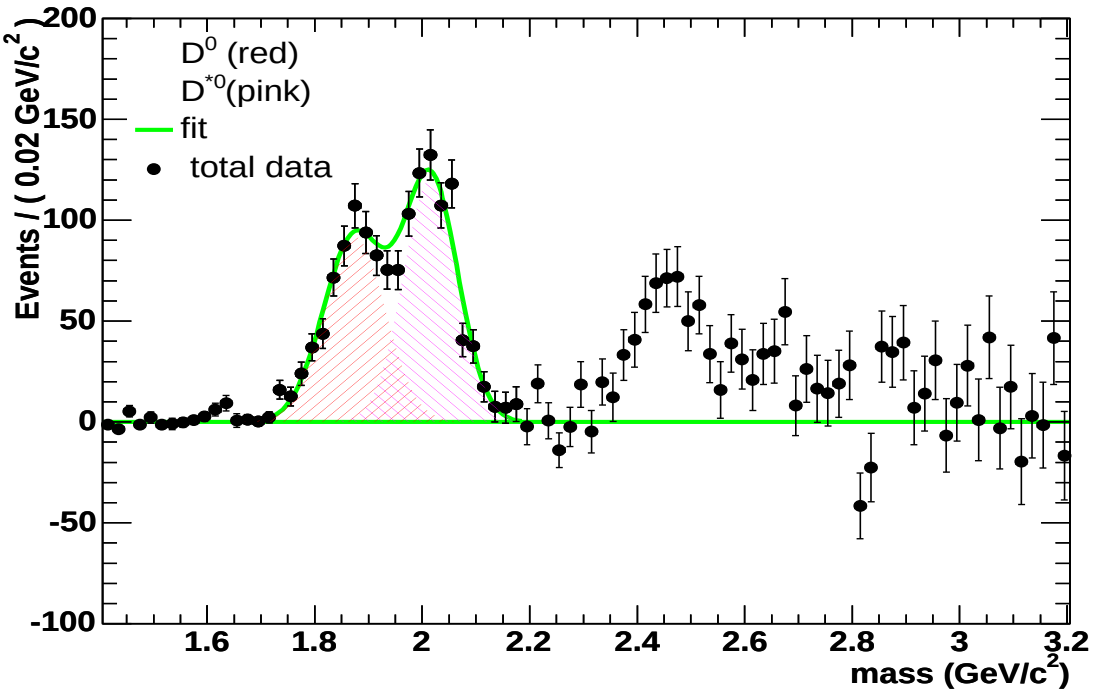

Figure 40: *Missing mass distribution of the charged B data for a total luminosity of* $209 fb^{-1}$. *This distribution has been obtained after subtraction of the contribution of the total normalized generic MC background. The* χ^2 *binned fit for* D^0 *and* D^{*0} *resonances has been performed fixing the mass difference of the two resonances* D^0 *and* D^{*0} *to* 0.1421 GeV/c^2 *while the* D^0 *mass value is floating. The ratio of the resolutions of* D^0 *and* D^{*0} *has been fixed to 0.90 as determined in appendix C. The value of the* D^0 *peak resolution has been let floating. The* D^{**0}*yield is obtained from counting. The result of the fit of* D^0 *and* D^{*0} *resonances is shown in table 40. Only one pion per event, the one of the highest momentum value is selected to perform the missing mass to* π^- *distributions.*

D resonance	fitted mass(GeV/c^2)	fitted resolution.(GeV/c^2)
D^0	1.8736±0.0025	0.0575±0.0021
D^0 from MC	1.8646	0.0450±0.0006

Table 40: D^0 *mass and resolution obtained from the fit shown in figure 40.*

D resonance	N^{π}_{fit}	stat. fit err.(%)
D^0	647$\pm$32	4.9%
D^{*0}	755$\pm$33	4.4%
D^{**0}	764$\pm$77	10.1%

Table 41: *Yield N^{π}_{fit} for D^0, D^{*0} and D^{**0} with corresponding statistical uncertainties as fitted in figure 40. The χ^2 binned fit for D^0 and D^{*0} resonances has been performed fixing the mass difference of the two resonances D^0 and D^{*0} to* 0.1421 GeV/c^2 *while the D^0 mass value is floating. The ratio of the resolutions of D^0 and D^{*0} has been fixed to 0.90 as determined in appendix C. The value of the D^0 peak resolution has been left floating. The D^{**0} yield is obtained from counting. The result of the fit of the D^0 and the D^{*0} resonances is shown in table 40 . Only one pion per event, the one of the highest momentum value is selected to perform the missing mass to π^- distributions.*

The yields obtained using the highest momentum cut have slightly worse statistical significance when compared to the yields obtained without this cut as shown in table 42. The comparison of the systematic uncertainties of table 43 shows that they are similar wheter the cut is applied or not. Nevertheless, this cut induces additional systematic uncertainties, in particular when considered for the D^{**0}resonance. Keeping the multiple candidate events does not induce any bias as shown in appendix D, where the multiplicity of pion candidates in the event has been found low and about 1.05. In addition, in the multiple candidate events, the wrong candidate does not induce any signal in the resonance mass region. Thus, and due to the fact that the highest momentum pion cut induces only additional systematic errors without improving the statistical significance, it will not be used in the final result.

D resonance with the cut	Signal	Background	Stat. Significance
D^0	2403	305	46.2
D^{*0}	2239	1029	39.1
D^{**0}	2014	10873	17.7
D resonance without the cut	Signal	Background	Stat. Significance
D^0	2501	352	46.8
D^{*0}	2318	1048	39.9
D^{**0}	2096	11124	18.2

Table 42: *Statistical significance for D^0, D^{*0} and D^{**0} obtained from generic MC with the highest momentum cut compared to the significance obtained without the cut.*

Syst. Source	$B^- \rightarrow D^0\pi^-$	$B^- \rightarrow D^{*0}\pi^-$	$B^- \rightarrow D^{**0}\pi^-$
MC Backgr. total syst. without the cut	1.6%	2.3%	17.7%
MC Backgr. total syst. with the cut	2.0%	2.0%	17.0%

Table 43: *Comparison of systematic uncertainties due to Generic MC background subtraction for B^+ data with and without the cut to select the highest momentum pion.*

E.2 Neutral B Yield With The Highest Momentum Pion

To reduce the combinatorial background, the same study of the effect of selecting only one pion to calculate the *missing mass to* π^- distribution has been performed on the B^0 data. The pion is selected to be the one of the highest momentum as already discussed in the efficiency study section [4.3]. This criterium is applied to the pion in addition to the all other criteria discussed in section [4.3]. Figure 41 shows that this selection has a negligible effect on the background underneath D^+ and D^{*+} resonances. It reduces the background by 10% in the missing mass region beyond 2.2 GeV/c^2 where the D^{**+} resonance is expected to contribute.

The figure 42 shows the highest momentum pion missing mass distribution obtained with the total neutral B data with no mixing, with a total luminosity of $209\,fb^{-1}$. Superimposed to data, are the normalized generic MC contributions from $b\bar{b}$, $c\bar{c}$ and $q\bar{q}$, as well as the charged B peaking. The resonance contribution from truth generic MC is also superimposed. According to procedure of section 5.1.2, $\bar{B}^0 \rightarrow D^+\rho^-$ and $\bar{B}^0 \rightarrow D^{*+}\rho^-$ background

components are subtracted from the data and the MC distributions.

The normalization factor have been computed as the ratio : data to generic MC in the missing mass range of 2.8-3.2 GeV/c^2 and found equal to 0.83 ± 0.03.

The generic MC background is normalized and subtracted from the data. The figure 43, shows the subtracted missing mass distribution, where D^+ and D^{*+} are fitted with a double gaussian pdf.The average and the resolution of the gaussian of the D^+ missing mass have been left floating in the fit while, the D^+-D^{*+} mass difference and the ratio D^{*+}/D^+ of the missing mass resolution have been fixed to 0.1406 GeV/c^2 and 0.90 respectively, as determined from the signal MC in appendix C. The fit results are given in table 44 and compared to the MC values. The D^{**+} resonance has not been fitted: the yield is only counted as all the excess between 2.2 and 2.8 GeV/c^2. The number N^{π}_{fit} for D^+, and D^{*+} resonances, and N^{π}_{count} for D^{**+} are reported in table 45.

The Branching fractions computed with the two sets of yields of table 9 and table 45 are compatible within the statistical uncertainties. It is the result of table 9, that will be used as default to compute the final B^0 branching fractions.

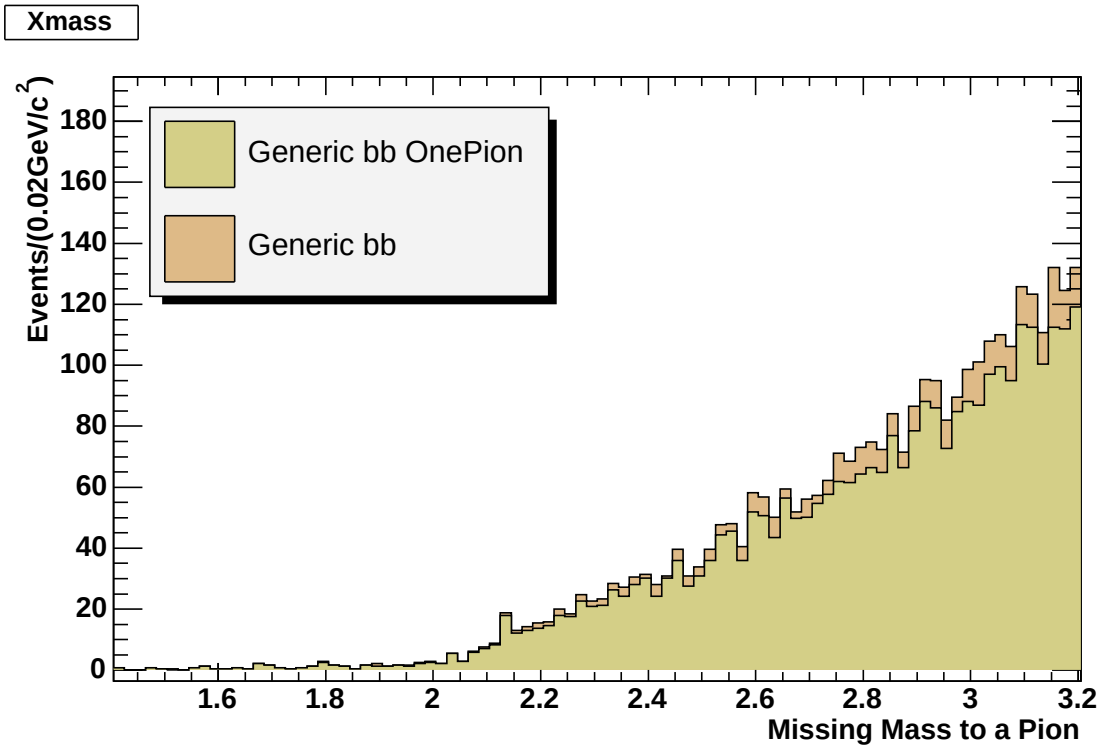

Figure 41: *Missing Mass distribution of the $b\bar{b}$ component of the neutral B generic MC, with and without the π momentum selection.*

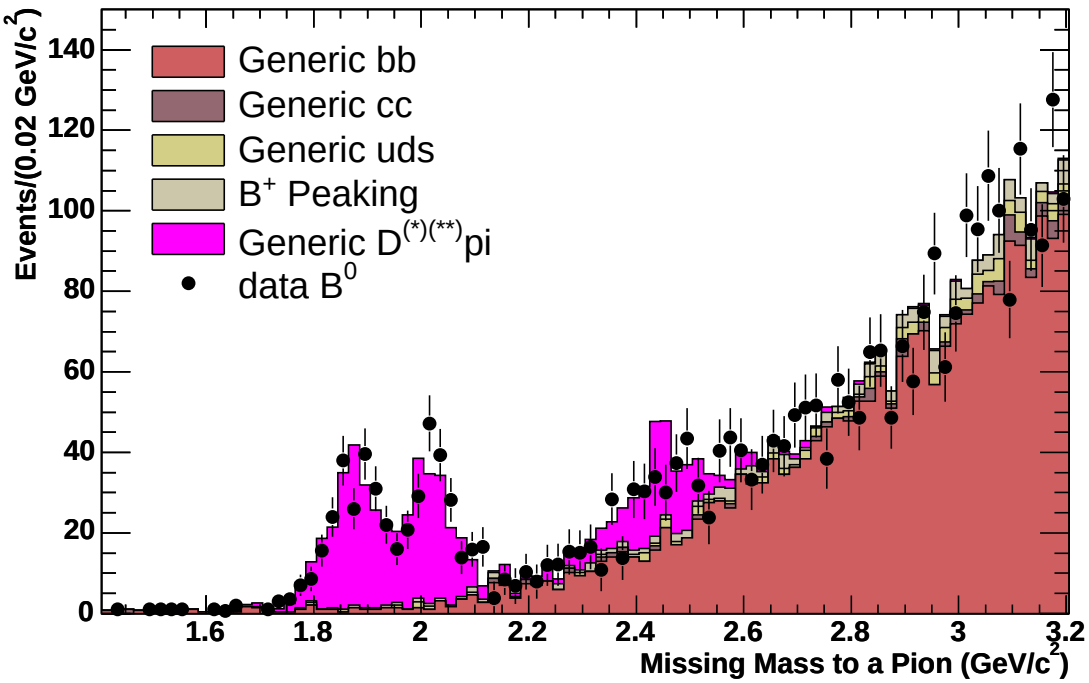

Figure 42: *Missing mass distribution obtained with total neutral B data, with a total luminosity of* $209\,fb^{-1}$*, Superimposed to data are the normalized generic MC contributions from* $b\bar{b}$*,* $c\bar{c}$ *and* $q\bar{q}$*, as well as the* B^0 *peaking. The resonance contribution from truth generic MC is also superimposed. Only one pion per event, the one of the highest momentum value is selected to perform the missing mass to* π^- *distributions.*

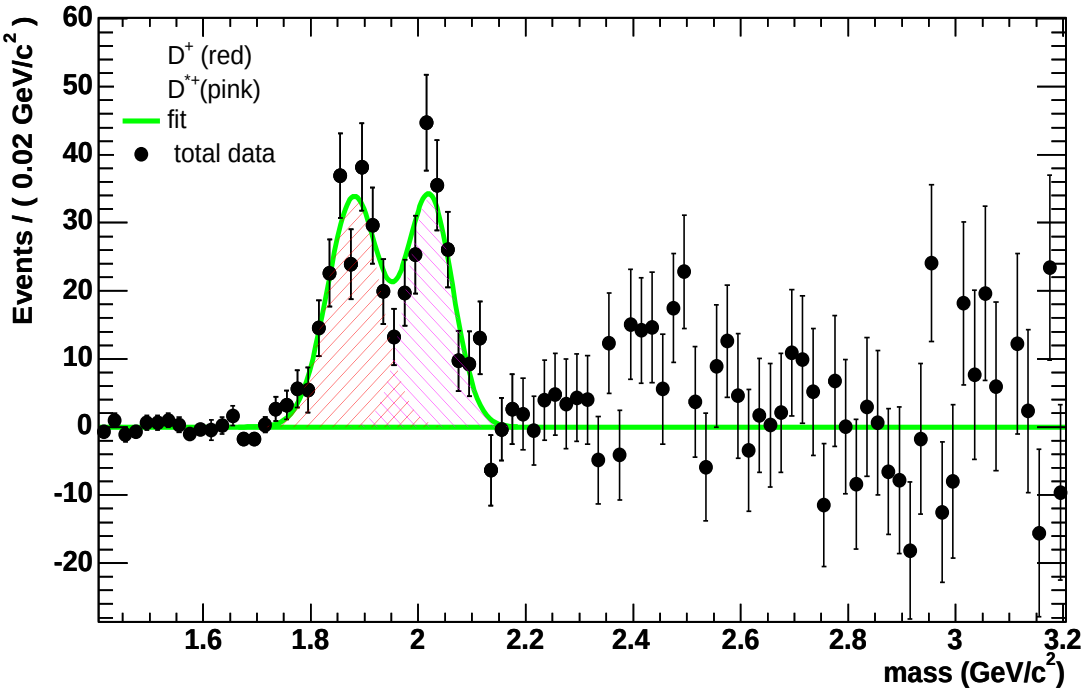

Figure 43: *missing mass distribution of the neutral B data for a total luminosity of* $209\,fb^{-1}$. *This distribution has been obtained after subtraction of the contribution of the total normalized generic MC background. The* χ^2 *binned fit for* D^+ *and* D^{*+} *resonances has been performed fixing the mass difference of the two resonances* D^+ *and* D^{*+} *to* 0.1406 GeV$/c^2$ *while the* D^+ *mass value is floating. The ratio of the resolutions of* D^+ *and* D^{*+} *has been fixed to 0.90 as determined in appendix C. The value of the* D^+ *peak resolution has been let floating. The* D^{**+} *yield is obtained from counting. The result of the fit of* D^+ *and* D^{*+} *is shown in table 44. Only one pion per event, the one of the highest momentum value is selected to perform the missing mass to* π^- *distributions.*

D resonance	fitted mass(GeV$/c^2$)	fitted resolution.(GeV$/c^2$)
D^+	1.8802 ± 0.0037	0.0491 ± 0.0038
D^+ from MC	1.869	0.0450 ± 0.0006

Table 44: D^+ *mass and resolution obtained from the fit shown in figure 43.*

D resonance	N^{π}_{fit}	stat. fit err.(%)
D^{+}	207 $\pm$16	7.7%
D^{*+}	184 $\pm$ 16	8.7%
D^{**+}	159 $\pm$ 44	27.7%

Table 45: *Yield N^{π}_{fit} for D^{+}, D^{*+} and D^{**+} with corresponding statistical uncertainties as fitted in figure 43. The χ^2 binned fit for D^{+} and D^{*+} resonances has been performed fixing the mass difference of the two resonances D^{+} and D^{*+} to* 0.1406 GeV/c^2 *while the D^{+} mass value is floating. The ratio of the resolutions of D^{+} and D^{*+} has been fixed to 0.90 as determined in appendix C. The value of the D^{+} peak resolution has been let floating. The D^{**+} yield is obtained from counting. The result of the fit for D^{+} and D^{*+} is shown in table 44 . Only one pion per event, the one of the highest momentum value is selected to perform the missing mass to π^{-} distributions.*

The yields obtained using the highest momentum cut have similar statistical significance when compared to the yields obtained without this cut. This cut only induces additional systematic uncertainties in particular when considered for the D^{**+}resonance. Keeping the multiple candidate events does not induce any bias as shown in appendix D, where the multiplicity of pion candidates in the event has been found low and about 1.05. In addition, in the multiple candidate events, the wrong candidate does not induce any signal in the resonance mass region. Thus, and due to the fact that the highest momentum pion cut induces only additional systematic errors without improving the statistical significance, it will not be used in the final result.

List of Figures

References

[1] M. Beneke *et al.*, Nucl. Phys. **B591**,313(2000).

[2] M. Neubert and B.stech in *Heavy Flavors* edited by A.J. Buras ad M. Lindner, 2nd ed. (World scientific, Singapor,1998).

[3] C.W. Bauer *et al.* , Phys. Rev. Lett. **87**,201806(2001).

[4] *BABAR* Collaboration, B. Aubert *et al.*,Phys. Rev. D **69**,032004 (2004).

[5] Belle Collaboration,k.Abe *et al.*,hep-ex/0409004.

[6] J.L. Rosner, Phys. Rev. D **60**, 074029(1999).

[7] S. Ahmed *et al.* , Phys. Rev. D **66**, 031101(R) (2002).

[8] T. Mannel *et al.* , Phys. Lett. B **259**, 359(1991).

[9] M. Neubert, Phys. Lett. B **418**, 173 (1998).

[10] Particle Data Group, S. Eidelman *et al.*, Phys. Lett. B **592**, 1(2004).

[11] Belle Collaboration,k.Abe *et al.*,Phys. Rev. D **69**, 112002(2004).

[12] Belle Collaboration,k.Abe *et al.*,Phys. Rev. Lett. **94**,221805(2005).

[13] F. Couderc *et al.*, BAD623.*BABAR* Collaboration, B. Aubert *et al.*,Phys. Rev. D **70**, 091106(R) (2004).

[14] F. Couderc *et al.*, BAD1234.

[15] Particle Data Group, D.E. Groom *et al.*, Eur. Phys. Jour. C **15**, 1 (2000)

[16] ARGUS Collaboration, H. Albrecht *et al.*,Phys. Lett. B **185**, 218 (1987), Phys. Lett. B **241**, 278 (1990).

[17] *BABAR* Collaboration, B. Aubert *et al.*, Nucl. Instr. Meth. A **479**, 1 (2002).

[18] G.C. Fox and S. Wolfram, Nucl. Phys. B **149**, 413 (1979).

[19] ARGUS Collaboration, H. Albrecht *et al.*, Phys. Lett. B **241**, 278 (1990).

[20] The Geant4 Collaboration, CERN preprint CERN-IT-2002-003, submitted to Nucl. Instrum. Methods.

[21] S. Godfrey and N. Isgur Phys. Rev. D **32**, 189(1985).

[22] M. Di Pierro and E. Eichten Phys. Rev. D **64**, 114004(2001) , hep-ph 0104208.

[23] D. Ebert et al. PRD 57 (1998) 5663, err. Phys. Rev. D **59**, 019902(1999) , hep-ph 9712318.

[24] P.R. Page Phys. Rev. D **60**, 057501(1999) , hep-ph 9809575.

[25] D. Melikhov and O. Pene Phys. Lett. B **446**, 336 (1999) , hep-ph 9809308.

[26] F.E. Close and E.S. Swanson hep-ph 0505206.

[27] T. Allmendinger, E. Varnes, http://www.slac.stanford.edu/BFROOT/www/Physics/ TrackEfficTaskForce/ TrackingTaskForce-2004.html

[28] T.Brandt,http://www.slac.stanford.edu/BFROOT/www/Physics/Tools/Pid/PidOnMc/pidonmc.html

BABAR-PUB-06/020
SLAC-PUB-11898

Study of Inclusive B^- and $\overline{B}^0$ Decays to Flavor-Tagged D, D_s and Λ_c^+

B. Aubert, R. Barate, M. Bona, D. Boutigny, F. Couderc,
Y. Karyotakis, J. P. Lees, V. Poireau, V. Tisserand, and A. Zghiche
Laboratoire de Physique des Particules, F-74941 Annecy-le-Vieux, France

E. Grauges
Universitat de Barcelona Fac. Fisica. Dept. ECM Avda Diagonal 647, 6a planta E-08028 Barcelona, Spain

A. Palano and M. Pappagallo
Università di Bari, Dipartimento di Fisica and INFN, I-70126 Bari, Italy

J. C. Chen, N. D. Qi, G. Rong, P. Wang, and Y. S. Zhu
Institute of High Energy Physics, Beijing 100039, China

G. Eigen, I. Ofte, and B. Stugu
University of Bergen, Institute of Physics, N-5007 Bergen, Norway

G. S. Abrams, M. Battaglia, D. N. Brown, J. Button-Shafer, R. N. Cahn, E. Charles, C. T. Day, M. S. Gill,
Y. Groysman, R. G. Jacobsen, J. A. Kadyk, L. T. Kerth, Yu. G. Kolomensky, G. Kukartsev, G. Lynch,
L. M. Mir, P. J. Oddone, T. J. Orimoto, M. Pripstein, N. A. Roe, M. T. Ronan, and W. A. Wenzel
Lawrence Berkeley National Laboratory and University of California, Berkeley, California 94720, USA

M. Barrett, K. E. Ford, T. J. Harrison, A. J. Hart, C. M. Hawkes, S. E. Morgan, and A. T. Watson
University of Birmingham, Birmingham, B15 2TT, United Kingdom

K. Goetzen, T. Held, H. Koch, B. Lewandowski, M. Pelizaeus, K. Peters, T. Schroeder, and M. Steinke
Ruhr Universität Bochum, Institut für Experimentalphysik 1, D-44780 Bochum, Germany

J. T. Boyd, J. P. Burke, W. N. Cottingham, and D. Walker
University of Bristol, Bristol BS8 1TL, United Kingdom

T. Cuhadar-Donszelmann, B. G. Fulsom, C. Hearty, N. S. Knecht, T. S. Mattison, and J. A. McKenna
University of British Columbia, Vancouver, British Columbia, Canada V6T 1Z1

A. Khan, P. Kyberd, M. Saleem, and L. Teodorescu
Brunel University, Uxbridge, Middlesex UB8 3PH, United Kingdom

V. E. Blinov, A. D. Bukin, V. P. Druzhinin, V. B. Golubev, A. P. Onuchin,
S. I. Serednyakov, Yu. I. Skovpen, E. P. Solodov, and K. Yu Todyshev
Budker Institute of Nuclear Physics, Novosibirsk 630090, Russia

D. S. Best, M. Bondioli, M. Bruinsma, M. Chao, S. Curry, I. Eschrich, D. Kirkby,
A. J. Lankford, P. Lund, M. Mandelkern, R. K. Mommsen, W. Roethel, and D. P. Stoker
University of California at Irvine, Irvine, California 92697, USA

S. Abachi and C. Buchanan
University of California at Los Angeles, Los Angeles, California 90024, USA

S. D. Foulkes, J. W. Gary, O. Long, B. C. Shen, K. Wang, and L. Zhang
University of California at Riverside, Riverside, California 92521, USA

H. K. Hadavand, E. J. Hill, H. P. Paar, S. Rahatlou, and V. Sharma
University of California at San Diego, La Jolla, California 92093, USA

J. W. Berryhill, C. Campagnari, A. Cunha, B. Dahmes, T. M. Hong, D. Kovalskyi, and J. D. Richman
University of California at Santa Barbara, Santa Barbara, California 93106, USA

T. W. Beck, A. M. Eisner, C. J. Flacco, C. A. Heusch, J. Kroseberg, W. S. Lockman, G. Nesom, T. Schalk, B. A. Schumm, A. Seiden, P. Spradlin, D. C. Williams, and M. G. Wilson
University of California at Santa Cruz, Institute for Particle Physics, Santa Cruz, California 95064, USA

J. Albert, E. Chen, A. Dvoretskii, D. G. Hitlin, I. Narsky, T. Piatenko, F. C. Porter, A. Ryd, and A. Samuel
California Institute of Technology, Pasadena, California 91125, USA

R. Andreassen, G. Mancinelli, B. T. Meadows, and M. D. Sokoloff
University of Cincinnati, Cincinnati, Ohio 45221, USA

F. Blanc, P. C. Bloom, S. Chen, W. T. Ford, J. F. Hirschauer, A. Kreisel, U. Nauenberg, A. Olivas, W. O. Ruddick, J. G. Smith, K. A. Ulmer, S. R. Wagner, and J. Zhang
University of Colorado, Boulder, Colorado 80309, USA

A. Chen, E. A. Eckhart, A. Soffer, W. H. Toki, R. J. Wilson, F. Winklmeier, and Q. Zeng
Colorado State University, Fort Collins, Colorado 80523, USA

D. D. Altenburg, E. Feltresi, A. Hauke, H. Jasper, and B. Spaan
Universität Dortmund, Institut für Physik, D-44221 Dortmund, Germany

T. Brandt, V. Klose, H. M. Lacker, W. F. Mader, R. Nogowski, A. Petzold, J. Schubert, K. R. Schubert, R. Schwierz, J. E. Sundermann, and A. Volk
Technische Universität Dresden, Institut für Kern- und Teilchenphysik, D-01062 Dresden, Germany

D. Bernard, G. R. Bonneaud, P. Grenier,* E. Latour, Ch. Thiebaux, and M. Verderi
Ecole Polytechnique, LLR, F-91128 Palaiseau, France

D. J. Bard, P. J. Clark, W. Gradl, F. Muheim, S. Playfer, A. I. Robertson, and Y. Xie
University of Edinburgh, Edinburgh EH9 3JZ, United Kingdom

M. Andreotti, D. Bettoni, C. Bozzi, R. Calabrese, G. Cibinetto, E. Luppi, M. Negrini, A. Petrella, L. Piemontese, and E. Prencipe
Università di Ferrara, Dipartimento di Fisica and INFN, I-44100 Ferrara, Italy

F. Anulli, R. Baldini-Ferroli, A. Calcaterra, R. de Sangro, G. Finocchiaro, S. Pacetti, P. Patteri, I. M. Peruzzi,† M. Piccolo, M. Rama, and A. Zallo
Laboratori Nazionali di Frascati dell'INFN, I-00044 Frascati, Italy

A. Buzzo, R. Capra, R. Contri, M. Lo Vetere, M. M. Macri, M. R. Monge, S. Passaggio, C. Patrignani, E. Robutti, A. Santroni, and S. Tosi
Università di Genova, Dipartimento di Fisica and INFN, I-16146 Genova, Italy

G. Brandenburg, K. S. Chaisanguanthum, M. Morii, and J. Wu
Harvard University, Cambridge, Massachusetts 02138, USA

R. S. Dubitzky, J. Marks, S. Schenk, and U. Uwer
Universität Heidelberg, Physikalisches Institut, Philosophenweg 12, D-69120 Heidelberg, Germany

W. Bhimji, D. A. Bowerman, P. D. Dauncey, U. Egede, R. L. Flack, J. R. Gaillard, J .A. Nash, M. B. Nikolich, and W. Panduro Vazquez
Imperial College London, London, SW7 2AZ, United Kingdom

X. Chai, M. J. Charles, U. Mallik, N. T. Meyer, and V. Ziegler
University of Iowa, Iowa City, Iowa 52242, USA

J. Cochran, H. B. Crawley, L. Dong, V. Eyges, W. T. Meyer, S. Prell, E. I. Rosenberg, and A. E. Rubin
Iowa State University, Ames, Iowa 50011-3160, USA

A. V. Gritsan
Johns Hopkins Univ. Dept of Physics & Astronomy 3400 N. Charles Street Baltimore, Maryland 21218

M. Fritsch and G. Schott
Universität Karlsruhe, Institut für Experimentelle Kernphysik, D-76021 Karlsruhe, Germany

N. Arnaud, M. Davier, G. Grosdidier, A. Höcker, F. Le Diberder, V. Lepeltier, A. M. Lutz, A. Oyanguren,
S. Pruvot, S. Rodier, P. Roudeau, M. H. Schune, A. Stocchi, W. F. Wang, and G. Wormser
Laboratoire de l'Accélérateur Linéaire, IN2P3-CNRS et Université Paris-Sud 11,
Centre Scientifique d'Orsay, B.P. 34, F-91898 ORSAY Cedex, France

C. H. Cheng, D. J. Lange, and D. M. Wright
Lawrence Livermore National Laboratory, Livermore, California 94550, USA

C. A. Chavez, I. J. Forster, J. R. Fry, E. Gabathuler, R. Gamet, K. A. George,
D. E. Hutchcroft, D. J. Payne, K. C. Schofield, and C. Touramanis
University of Liverpool, Liverpool L69 7ZE, United Kingdom

A. J. Bevan, F. Di Lodovico, W. Menges, and R. Sacco
Queen Mary, University of London, E1 4NS, United Kingdom

C. L. Brown, G. Cowan, H. U. Flaecher, D. A. Hopkins, P. S. Jackson, T. R. McMahon, S. Ricciardi, and F. Salvatore
University of London, Royal Holloway and Bedford New College, Egham, Surrey TW20 0EX, United Kingdom

D. N. Brown and C. L. Davis
University of Louisville, Louisville, Kentucky 40292, USA

J. Allison, N. R. Barlow, R. J. Barlow, Y. M. Chia, C. L. Edgar,
M. P. Kelly, G. D. Lafferty, M. T. Naisbit, J. C. Williams, and J. I. Yi
University of Manchester, Manchester M13 9PL, United Kingdom

C. Chen, W. D. Hulsbergen, A. Jawahery, C. K. Lae, D. A. Roberts, and G. Simi
University of Maryland, College Park, Maryland 20742, USA

G. Blaylock, C. Dallapiccola, S. S. Hertzbach, X. Li, T. B. Moore, S. Saremi, H. Staengle, and S. Y. Willocq
University of Massachusetts, Amherst, Massachusetts 01003, USA

R. Cowan, K. Koeneke, G. Sciolla, S. J. Sekula, M. Spitznagel, F. Taylor, and R. K. Yamamoto
Massachusetts Institute of Technology, Laboratory for Nuclear Science, Cambridge, Massachusetts 02139, USA

H. Kim, P. M. Patel, C. T. Potter, and S. H. Robertson
McGill University, Montréal, Québec, Canada H3A 2T8

A. Lazzaro, V. Lombardo, and F. Palombo
Università di Milano, Dipartimento di Fisica and INFN, I-20133 Milano, Italy

J. M. Bauer, L. Cremaldi, V. Eschenburg, R. Godang, R. Kroeger,
J. Reidy, D. A. Sanders, D. J. Summers, and H. W. Zhao
University of Mississippi, University, Mississippi 38677, USA

S. Brunet, D. Côté, M. Simard, P. Taras, and F. B. Viaud
Université de Montréal, Physique des Particules, Montréal, Québec, Canada H3C 3J7

H. Nicholson
Mount Holyoke College, South Hadley, Massachusetts 01075, USA

N. Cavallo,[‡] G. De Nardo, D. del Re, F. Fabozzi,[‡] C. Gatto, L. Lista, D. Monorchio, D. Piccolo, and C. Sciacca
Università di Napoli Federico II, Dipartimento di Scienze Fisiche and INFN, I-80126, Napoli, Italy

M. Baak, H. Bulten, G. Raven, and H. L. Snoek
NIKHEF, National Institute for Nuclear Physics and High Energy Physics, NL-1009 DB Amsterdam, The Netherlands

C. P. Jessop and J. M. LoSecco
University of Notre Dame, Notre Dame, Indiana 46556, USA

T. Allmendinger, G. Benelli, K. K. Gan, K. Honscheid, D. Hufnagel, P. D. Jackson,
H. Kagan, R. Kass, T. Pulliam, A. M. Rahimi, R. Ter-Antonyan, and Q. K. Wong
Ohio State University, Columbus, Ohio 43210, USA

N. L. Blount, J. Brau, R. Frey, O. Igonkina, M. Lu, R. Rahmat, N. B. Sinev, D. Strom, J. Strube, and E. Torrence
University of Oregon, Eugene, Oregon 97403, USA

F. Galeazzi, A. Gaz, M. Margoni, M. Morandin, A. Pompili,
M. Posocco, M. Rotondo, F. Simonetto, R. Stroili, and C. Voci
Università di Padova, Dipartimento di Fisica and INFN, I-35131 Padova, Italy

M. Benayoun, J. Chauveau, P. David, L. Del Buono, Ch. de la Vaissière, O. Hamon,
B. L. Hartfiel, M. J. J. John, Ph. Leruste, J. Malclès, J. Ocariz, L. Roos, and G. Therin
Universités Paris VI et VII, Laboratoire de Physique Nucléaire et de Hautes Energies, F-75252 Paris, France

P. K. Behera, L. Gladney, and J. Panetta
University of Pennsylvania, Philadelphia, Pennsylvania 19104, USA

M. Biasini, R. Covarelli, and M. Pioppi
Università di Perugia, Dipartimento di Fisica and INFN, I-06100 Perugia, Italy

C. Angelini, G. Batignani, S. Bettarini, F. Bucci, G. Calderini, M. Carpinelli, R. Cenci, F. Forti, M. A. Giorgi,
A. Lusiani, G. Marchiori, M. A. Mazur, M. Morganti, N. Neri, E. Paoloni, G. Rizzo, and J. Walsh
Università di Pisa, Dipartimento di Fisica, Scuola Normale Superiore and INFN, I-56127 Pisa, Italy

M. Haire, D. Judd, and D. E. Wagoner
Prairie View A&M University, Prairie View, Texas 77446, USA

J. Biesiada, N. Danielson, P. Elmer, Y. P. Lau, C. Lu, J. Olsen, A. J. S. Smith, and A. V. Telnov
Princeton University, Princeton, New Jersey 08544, USA

F. Bellini, G. Cavoto, A. D'Orazio, E. Di Marco, R. Faccini, F. Ferrarotto, F. Ferroni, M. Gaspero,
L. Li Gioi, M. A. Mazzoni, S. Morganti, G. Piredda, F. Polci, F. Safai Tehrani, and C. Voena
Università di Roma La Sapienza, Dipartimento di Fisica and INFN, I-00185 Roma, Italy

M. Ebert, H. Schröder, and R. Waldi
Universität Rostock, D-18051 Rostock, Germany

T. Adye, N. De Groot, B. Franek, E. O. Olaiya, and F. F. Wilson
Rutherford Appleton Laboratory, Chilton, Didcot, Oxon, OX11 0QX, United Kingdom

S. Emery, A. Gaidot, S. F. Ganzhur, G. Hamel de Monchenault,
W. Kozanecki, M. Legendre, B. Mayer, G. Vasseur, Ch. Yèche, and M. Zito
DSM/Dapnia, CEA/Saclay, F-91191 Gif-sur-Yvette, France

W. Park, M. V. Purohit, A. W. Weidemann, and J. R. Wilson
University of South Carolina, Columbia, South Carolina 29208, USA

M. T. Allen, D. Aston, R. Bartoldus, P. Bechtle, N. Berger, A. M. Boyarski, R. Claus, J. P. Coleman,

M. R. Convery, M. Cristinziani, J. C. Dingfelder, D. Dong, J. Dorfan, G. P. Dubois-Felsmann, D. Dujmic, W. Dunwoodie, R. C. Field, T. Glanzman, S. J. Gowdy, M. T. Graham, V. Halyo, C. Hast, T. Hryn'ova, W. R. Innes, M. H. Kelsey, P. Kim, M. L. Kocian, D. W. G. S. Leith, S. Li, J. Libby, S. Luitz, V. Luth, H. L. Lynch, D. B. MacFarlane, H. Marsiske, R. Messner, D. R. Muller, C. P. O'Grady, V. E. Ozcan, A. Perazzo, M. Perl, B. N. Ratcliff, A. Roodman, A. A. Salnikov, R. H. Schindler, J. Schwiening, A. Snyder, J. Stelzer, D. Su, M. K. Sullivan, K. Suzuki, S. K. Swain, J. M. Thompson, J. Va'vra, N. van Bakel, M. Weaver, A. J. R. Weinstein, W. J. Wisniewski, M. Wittgen, D. H. Wright, A. K. Yarritu, K. Yi, and C. C. Young
Stanford Linear Accelerator Center, Stanford, California 94309, USA

P. R. Burchat, A. J. Edwards, S. A. Majewski, B. A. Petersen, C. Roat, and L. Wilden
Stanford University, Stanford, California 94305-4060, USA

S. Ahmed, M. S. Alam, R. Bula, J. A. Ernst, V. Jain, B. Pan, M. A. Saeed, F. R. Wappler, and S. B. Zain
State University of New York, Albany, New York 12222, USA

W. Bugg, M. Krishnamurthy, and S. M. Spanier
University of Tennessee, Knoxville, Tennessee 37996, USA

R. Eckmann, J. L. Ritchie, A. Satpathy, C. J. Schilling, and R. F. Schwitters
University of Texas at Austin, Austin, Texas 78712, USA

J. M. Izen, I. Kitayama, X. C. Lou, and S. Ye
University of Texas at Dallas, Richardson, Texas 75083, USA

F. Bianchi, F. Gallo, and D. Gamba
Università di Torino, Dipartimento di Fisica Sperimentale and INFN, I-10125 Torino, Italy

M. Bomben, L. Bosisio, C. Cartaro, F. Cossutti, G. Della Ricca, S. Dittongo, S. Grancagnolo, L. Lanceri, and L. Vitale
Università di Trieste, Dipartimento di Fisica and INFN, I-34127 Trieste, Italy

V. Azzolini and F. Martinez-Vidal
IFIC, Universitat de Valencia-CSIC, E-46071 Valencia, Spain

Sw. Banerjee, B. Bhuyan, C. M. Brown, D. Fortin, K. Hamano, R. Kowalewski, I. M. Nugent, J. M. Roney, and R. J. Sobie
University of Victoria, Victoria, British Columbia, Canada V8W 3P6

J. J. Back, P. F. Harrison, T. E. Latham, and G. B. Mohanty
Department of Physics, University of Warwick, Coventry CV4 7AL, United Kingdom

H. R. Band, X. Chen, B. Cheng, S. Dasu, M. Datta, A. M. Eichenbaum, K. T. Flood, J. J. Hollar, J. R. Johnson, P. E. Kutter, H. Li, R. Liu, B. Mellado, A. Mihalyi, A. K. Mohapatra, Y. Pan, M. Pierini, R. Prepost, P. Tan, S. L. Wu, and Z. Yu
University of Wisconsin, Madison, Wisconsin 53706, USA

H. Neal
Yale University, New Haven, Connecticut 06511, USA

(Dated: June 12, 2006)

We report on a study of inclusive B^- and $\overline{B}^0$ meson decays to D^0X, $\overline{D}^0X$, D^+X, D^-X, D_s^+X, D_s^-X, Λ_c^+X, $\overline{\Lambda}_c^-X$, based on a sample of 231 million $B\overline{B}$ events recorded with the *BABAR* detector at the $\Upsilon(4S)$ resonance. Events are selected by completely reconstructing one B and searching for a reconstructed charm particle in the rest of the event. From the measured branching fractions of these decays, we infer the number of charm and anti-charm particles per $\overline{B}$ decay, separately for charged and neutral parents. We derive the total charm yield per B^- decay, $n_c^- = 1.202 \pm 0.023 \pm 0.040^{+0.035}_{-0.029}$, and per $\overline{B}^0$ decay, $n_c^0 = 1.193 \pm 0.030 \pm 0.034^{+0.044}_{-0.035}$ where the first uncertainty is statistical, the second is systematic, and the third reflects the charm branching-fraction uncertainties. We also present the charm momentum distributions measured in the $\overline{B}$ rest frame.

PACS numbers: 13.25.Hw, 12.15.Hh, 11.30.Er

I. INTRODUCTION

The dominant process for the decay of a b quark is $b \to cW^{*-}$ [1], resulting in a (flavor) correlated c quark and a virtual W. In the decay of the W, the production of a $\overline{u}d$ or a $\overline{c}s$ pair are both Cabibbo-allowed and should be approximately equal, the latter being suppressed by a phase-space factor. The first process dominates hadronic b decays. The second can be easily distinguished as it produces a (flavor) anticorrelated $\overline{c}$ quark. Experimentally, we investigate correlated and anticorrelated charm production through the measurement of the inclusive B-decay rates to a limited number of charm hadron species, i.e. D^0, $\overline{D}^0$, D^+, D^-, D_s^+, D_s^-, Λ_c^+, $\overline{\Lambda}_c^-$, Ξ_c and charmonia, because all other charm particles decay into one of the previous hadrons.

The analysis presented here exploits a substantially larger data sample than the original *BABAR* result [2]. It also employs a more sophisticated fitting method to extract, in a correlated manner, the number of reconstructed B mesons and the charm hadron yields, which reduces the experimental systematic uncertainty. Other measurements [3–7] of these rates are more statistically limited and/or do not distinguish between the different parent B states. Besides the theoretical interest [8–11], the fact that anticorrelated charm particles are a background for many studies also motivates a more precise measurement of their production rates in B decays.

Most of the charged and neutral D mesons produced in $\overline{B}$ decays come from correlated production $\overline{B} \to DX$. However, a significant number of $\overline{B} \to \overline{D}X$ decays are expected through $b \to c\overline{c}s$ transitions, such as $\overline{B} \to D^{(*)}\overline{D}^{(*)}\overline{K}^{(*)}(n\pi)$. Although the branching fractions of the 3-body decays $\overline{B} \to D^{(*)}\overline{D}^{(*)}\overline{K}$ have been measured [12, 13], they do not saturate $\overline{B} \to \overline{D}X$ transitions [2]. It is therefore important to improve the precision on the $\overline{B} \to \overline{D}X$ branching fraction.

By contrast, anticorrelated D_s^- production, $\overline{B} \to D_s^- D(n\pi)$, is expected to dominate $\overline{B}$ decays to D_s mesons, since correlated production needs an extra $s\overline{s}$ pair created from the vacuum to give $\overline{B} \to D_s^+ K^-(n\pi)$. There is no prior published measurement for correlated D_s^+ production.

Correlated Λ_c^+ are produced in decays like $\overline{B} \to \Lambda_c^+ \overline{p}\pi^-(\pi)$, while anticorrelated $\overline{\Lambda}_c^-$ should originate predominantly from $\overline{B} \to \Xi_c \overline{\Lambda}_c^-(\pi)$. The decay $\overline{B} \to \Xi_c \overline{\Lambda}_c^-$ has recently been observed [14], confirming the hypothesis of associated $\Xi_c\ \overline{\Lambda}_c^-$ production. Another possibility for anticorrelated $\overline{\Lambda}_c^-$ production is $\overline{B} \to \Lambda_c^+ \overline{\Lambda}_c^- K$, the baryonic analogue of the $D\overline{D}K$ decay.

This analysis uses $\Upsilon(4S) \to B\overline{B}$ events in which either a B^+ or a B^0 meson (hereafter denoted $B_{\rm rec'd}$) decays into a hadronic final state and is fully reconstructed. We then reconstruct D, D_s and Λ_c^+ from the decay products of the recoiling B^- ($\overline{B}^0$) meson and compare the flavor of the charm hadron with that of the reconstructed B (taking into account B^0-$\overline{B}^0$ mixing). This allows separate measurements of the B^- ($\overline{B}^0$) $\to D^0\ X$, $D^+\ X$, $D_s^+\ X$, $\Lambda_c^+\ X$ and B^- ($\overline{B}^0$) $\to \overline{D}^0\ X$, $D^-\ X$, $D_s^-\ X$, $\overline{\Lambda}_c^-\ X$ branching fractions.

We then compute the average number of correlated (anticorrelated) charm particles per B^- decay, N_c^- ($N_{\overline{c}}^-$) :

$$N_c^- = \sum_C \mathcal{B}(B^- \to CX), \tag{1}$$

$$N_{\overline{c}}^- = \sum_{\overline{C}} \mathcal{B}(B^- \to \overline{C}X), \tag{2}$$

where the sum is performed over $C \equiv \{D^0,\ D^+,\ D_s^+,\ \Lambda_c^+,\ \Xi_c,\ (c\overline{c})\}$ or $\overline{C} \equiv \{\overline{D}^0,\ D^-,\ D_s^-,\ \overline{\Lambda}_c^-,\ (c\overline{c})\}$, where $(c\overline{c})$ refers to all charmonium states collectively. We neglect anticorrelated $\overline{\Xi}_c$ production, as it requires both a $\overline{c}s$ and an $s\overline{s}$ pair in the decay to give $\overline{\Xi}_c\Omega_c$. We then sum N_c^- and $N_{\overline{c}}^-$ to obtain the average number of charm plus anti-charm quarks per B^- decay, $n_c^- = N_c^- + N_{\overline{c}}^-$. We similarly define N_c^0, $N_{\overline{c}}^0$ and n_c^0 for $\overline{B}^0$ decays.

The above method also lends itself to a measurement of the momentum distribution of each charm species directly in the rest frame of the parent meson, because the four-momentum of each recoiling $\overline{B}$ is fully determined from those of the $\Upsilon(4S)$ and of the reconstructed B. The resulting charm spectra can then be compared to theoretical predictions in the same frame [15]. This avoids the significant smearing due to the Lorentz boost from the parent-$\overline{B}$ frame to the $\Upsilon(4S)$ frame affecting earlier measurements, such as those reported in [3]. These spectra might also show indications of four-quark states [16].

II. *BABAR* DETECTOR AND DATA SAMPLE

The measurements presented here are based on a sample of 231 million $B\overline{B}$ pairs (210 fb^{-1}) recorded at the $\Upsilon(4S)$ resonance with the *BABAR* detector at the PEP-II asymmetric-energy B factory at SLAC. The *BABAR* detector is described in detail elsewhere [17]. Charged-particle trajectories are measured by a 5-layer double-sided silicon vertex tracker and a 40-layer drift chamber, both operating in a 1.5-T solenoidal magnetic field.

*Also at Laboratoire de Physique Corpusculaire, Clermont-Ferrand, France
†Also with Università di Perugia, Dipartimento di Fisica, Perugia, Italy
‡Also with Università della Basilicata, Potenza, Italy

Charged-particle identification is provided by the average energy loss (dE/dx) in the tracking devices and by an internally reflecting ring-imaging Cherenkov detector. Photons are detected by a CsI(Tl) electromagnetic calorimeter. We use Monte Carlo simulations of the *BABAR* detector based on GEANT4 [18] to optimize selection criteria and determine selection efficiencies.

III. B MESON RECONSTRUCTION

We reconstruct B^+ and B^0 decays ($B_{\rm rec'd}$) in the modes $B^+ \to \overline{D}^{(*)0}\pi^+$, $\overline{D}^{(*)0}\rho^+$, $\overline{D}^{(*)0}a_1^+$ and $B^0 \to D^{(*)-}\pi^+$, $D^{(*)-}\rho^+$, $D^{(*)-}a_1^+$. $\overline{D}^0$ candidates are reconstructed in the $K^+\pi^-$, $K^+\pi^-\pi^0$, $K^+\pi^-\pi^+\pi^-$ and $K^0_S\pi^+\pi^-(K^0_S \to \pi^+\pi^-)$ decay channels, while D^- are reconstructed in the $K^+\pi^-\pi^-$ and $K^0_S\pi^-$ modes. D^* candidates are reconstructed in the $D^{*-} \to \overline{D}^0\pi^-$ and $\overline{D}^{*0} \to \overline{D}^0\pi^0$ decay modes.

The kinematic selection of fully reconstructed B decays relies on two variables. The first is $\Delta E = E^*_B - \sqrt{s}/2$, where E^*_B is the energy of the reconstructed B candidate in the e^+e^- center-of-mass frame and $\sqrt{s}$ is the invariant mass of the initial e^+e^- system. The second is the beam-energy substituted mass, defined by $m_{\rm ES} = \sqrt{(s/2 + \mathbf{p}_i\cdot\mathbf{p}_B)^2/E_i^2 - \mathbf{p}_B^2}$, where $\mathbf{p}_B$ is the $B_{\rm rec'd}$ momentum and $(E_i, \mathbf{p}_i)$ is the four-momentum of the initial e^+e^- system, both measured in the laboratory frame. We require $|\Delta E| < n\,\sigma_{\Delta E}$, using the resolution $\sigma_{\Delta E}$ measured for each decay mode, with $n = 2$ or 3 depending on the decay mode. If an event contains several B^+ (B^0) candidates, only the highest-purity B-decay mode is retained. The purity is defined, for each B-decay mode separately, as the fraction of signal B decays with $m_{\rm ES} > 5.27$ GeV/c^2, normalized to the total number of reconstructed B^+ (B^0) candidates in same interval.

The signal yield N_B of reconstructed B mesons is extracted from a fit to the $m_{\rm ES}$ spectra (Fig. 1). The B signal is modeled by a Crystal Ball signal function Γ_{CB} [19] which is a Gaussian peaking at the B meson mass modified by an exponential low-mass tail that accounts for photon energy loss. The B combinatorial background is modeled using the empirical ARGUS phase-space threshold function Γ_{ARG} [20]. All the signal and background parameters in these functions are extracted from the data. The signal yields of reconstructed B^+ and B^0 mesons are $N_{B^+} = 200359\pm705$ and $N_{B^0} = 110735\pm424$, where the errors reflect the statistical uncertainty in the number of combinatorial background events. These numbers provide the normalization for all the branching fractions reported below.

The contamination of misreconstructed B^0 events in the B^+ signal (and vice-versa) induces a background which peaks near the B mass. From the Monte Carlo simulation, the fraction of B^0 events in the reconstructed B^+ signal sample is found to be $c_0 = 0.038\pm0.009$(syst), and the fraction of B^+ events in the reconstructed B^0 signal sample $c_+ = 0.028 \pm 0.007$(syst). The systematic uncertainties take into account possible differences in reconstructing real or simulated events, as well as branching-fraction uncertainties for those B decay modes contributing to the wrong-charge contamination.

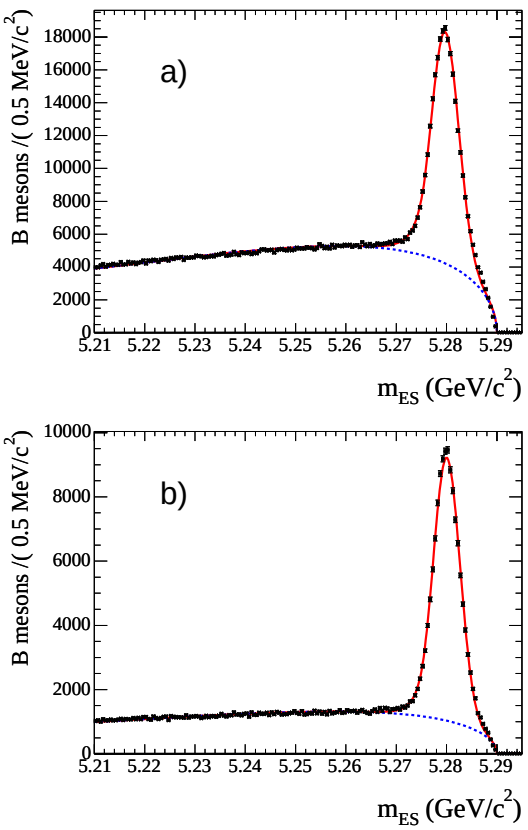

FIG. 1: $m_{\rm ES}$ spectra of reconstructed (a) B^+ and (b) B^0 candidates. The solid curve is the sum of the fitted signal and background whereas the dashed curve is the background component only.

IV. INCLUSIVE CHARM BRANCHING FRACTIONS

We now turn to the analysis of inclusive D, $\overline{D}$, D_s^-, D_s^+, Λ_c^+ and $\overline{\Lambda}_c^-$ production in the decays of the $\overline{B}$ mesons that recoil against the reconstructed B. Charm particles C are distinguished from anti-charm particles $\overline{C}$. They are reconstructed from charged tracks that do not belong to the reconstructed B. The decay modes considered are listed in Table I along with their branching fractions. Those are taken from Ref. [21] except in the case of the $D_s^+ \to \phi\pi^+$ channel [22] for which we use the more precise measurement reported in Ref. [23].

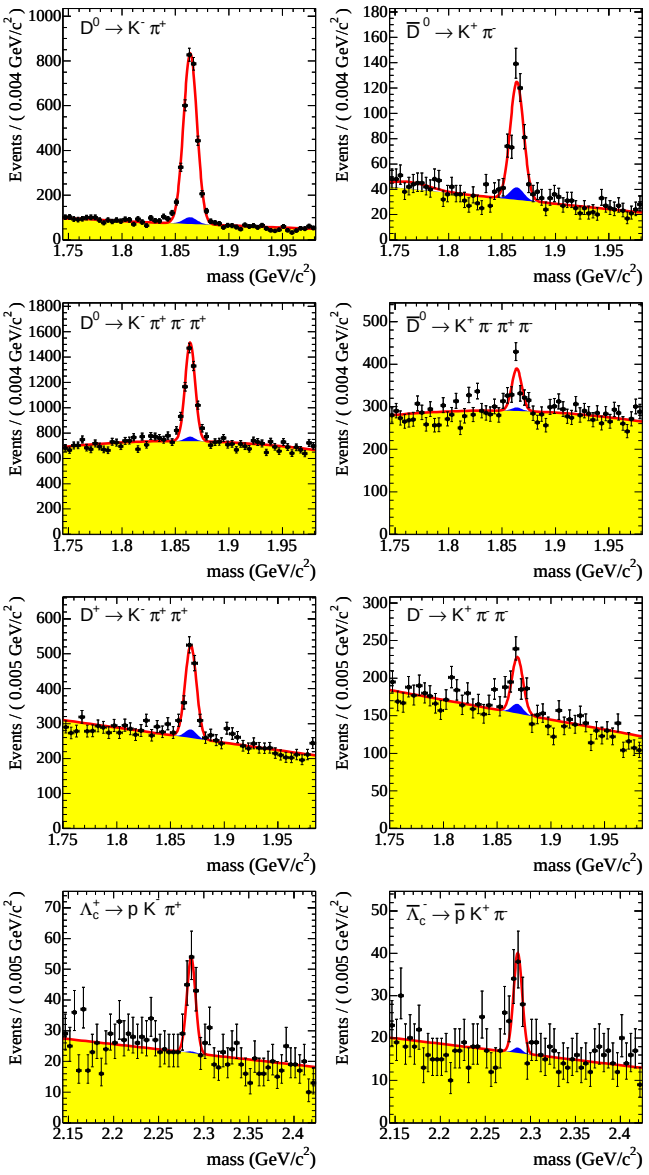

FIG. 2: Charm (left) and anti-charm (right) mass spectra in the recoil of B^+ candidates, for the subsample of events with $m_{\rm ES} > 5.270$ GeV/c^2 (B signal region). The solid curve shows the result of the two-dimensional fit. The dark shaded areas show the contribution of reconstructed D,$\overline{D}$, Λ_c^+ and $\overline{\Lambda}_c^-$ signal in the recoil of combinatorial $B^+_{\rm rec'd}$ background. The light shaded area corresponds to the fitted combinatorial (anti-) charm background.

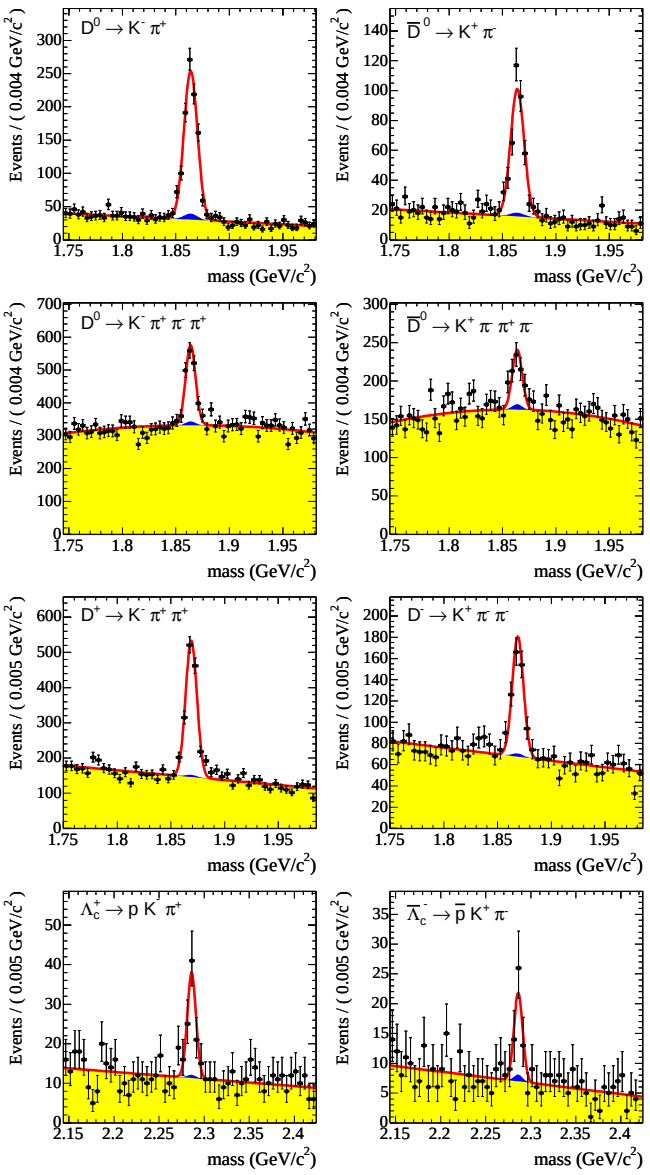

FIG. 3: Charm (left) and anti-charm (right) mass spectra as for Fig. 2 but in the recoil of $\overline{B}^0$ candidates.

A. Charm particle yields

The numbers of charm (anti-charm) particles are extracted from an unbinned maximum likelihood fit to the two-dimensional distribution $[m_{\rm ES}, m_{C\,(\overline{C})}]$, where $m_{\rm ES}$ is the beam-energy substituted mass of the reconstructed B and $m_{C\,(\overline{C})}$ is the mass of the charm (anti-charm) particle found among the recoil products. Figs. 2 to 5 show the results of these fits, projected onto the $m_{C\,(\overline{C})}$ axis, for events in the $m_{\rm ES}$ signal region ($m_{\rm ES} > 5.270$ GeV/c^2). The probability density function used to fit the $[m_{\rm ES}, m_{C\,(\overline{C})}]$ distributions is the sum of four components :

- P^{Csig}_{Bsig} : reconstructed charm (anti-charm) signal in the recoil of reconstructed B signal,
- P^{Csig}_{Bbkg} : reconstructed charm (anti-charm) signal in the recoil of combinatorial B background,
- P^{Cbkg}_{Bsig} : combinatorial charm (anti-charm) background in the recoil of reconstructed B signal,

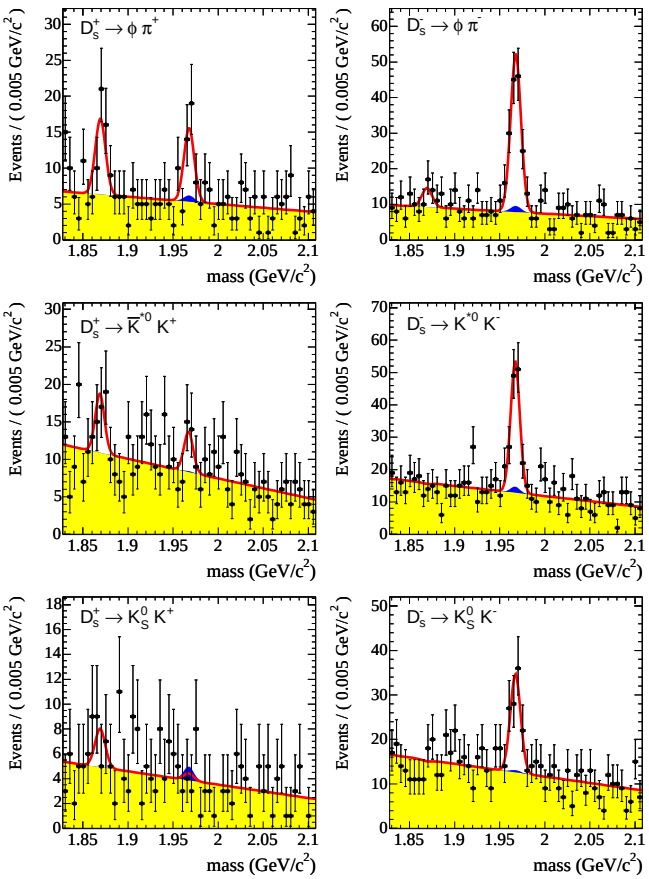

FIG. 4: D_s^+ (left) and D_s^- (right) mass spectra in the recoil of B^+ candidates, for the subsample of events with $m_{\rm ES} > 5.270$ GeV/c^2 (B signal region). The solid curve shows the result of the two-dimensional fit. The dark shaded areas show the contribution of reconstructed D_s^+, D_s^- signal in the recoil of combinatorial $B^+_{\rm rec'd}$ background. The light shaded area corresponds to the fitted combinatorial (anti-) charm background. The Gaussian peak at the D^+ mass accounts for reconstructed D^+ signal [24].

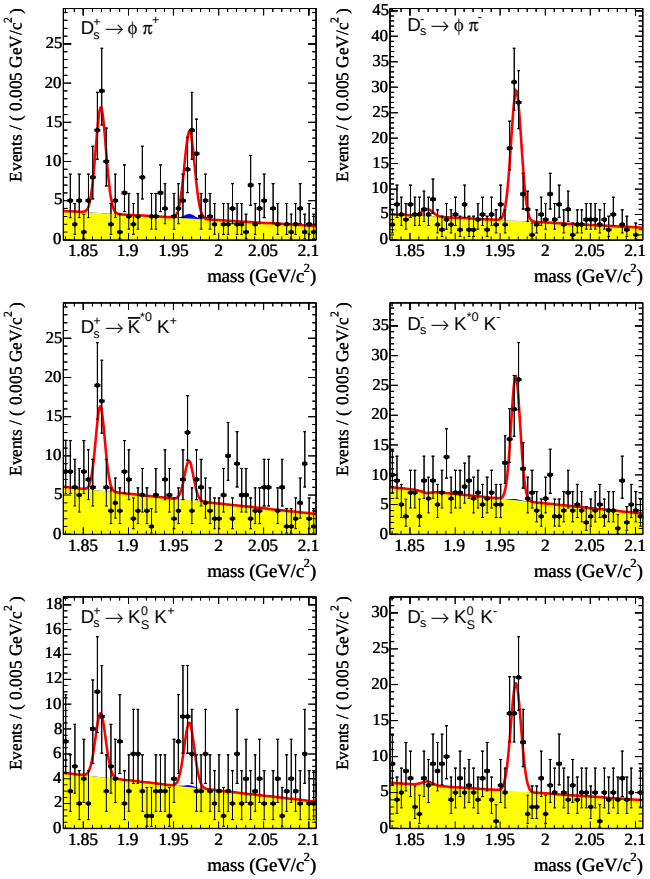

FIG. 5: D_s^+ and D_s^- mass spectra as for Fig. 4 but in the recoil of $\overline{B}^0$ candidates.

- P^{Cbkg}_{Bbkg} : combinatorial charm (anti-charm) background in the recoil of combinatorial B background,

These four components are modeled as follows :

$$\begin{aligned} P^{Csig}_{Bsig}(m_{\rm ES}, m_C) &\equiv \Gamma_{CB}(m_{\rm ES}) \times \rho_S(m_C)\,, \\ P^{Csig}_{Bbkg}(m_{\rm ES}, m_C) &\equiv \Gamma_{ARG}(m_{\rm ES} \times \rho_S(m_C)\,, \\ P^{Cbkg}_{Bsig}(m_{\rm ES}, m_C) &\equiv \Gamma_{CB}(m_{\rm ES}) \times \rho_{comb}(m_C)\,, \\ P^{Cbkg}_{Bbkg}(m_{\rm ES}, m_C) &\equiv \Gamma_{ARG}(m_{\rm ES}) \times \rho_{comb}(m_C)\,. \end{aligned} \quad (3)$$

The function Γ_{CB} with all its parameters fixed from the fit detailed in Sec. III is used to model the reconstructed B signal. The combinatorial B background is described as in Sec. III by an ARGUS function Γ_{ARG} whose shape parameter is floated in the fit to allow for a possible charm decay-mode dependence of this background. A Gaussian function $\rho_S(m_{C\,(\overline{C})})$ describes the mass shape of the reconstructed charm signal. Its mean is taken from the data. Its resolution, as measured in the data, is consistent with that in the simulation and is fixed. The combinatorial charm-background distribution is fitted with a linear function $\rho_{comb}(m_{C\,(\overline{C})})$ (except for the $D^0 \to K^-\,\pi^+\,\pi^-\,\pi^+$ for which a quadratic dependence is assumed) [24].

TABLE I: Charm particle decay modes and branching fractions.

$C \to f$	$\mathcal{B}(C \to f)$ (%)
$D^0 \to K^-\pi^+$	3.80 ± 0.09
$D^0 \to K^-\pi^+\pi^-\pi^+$	7.48 ± 0.31
$D^+ \to K^-\pi^+\pi^+$	9.1 ± 0.7
$D_s^+ \to \phi\pi^+(\phi \to K^+K^-)$	$4.81 \pm 0.64\,(49.3 \pm 1.0\%)$
$D_s^+ \to \overline{K}^{*0}K^+(\overline{K}^{*0} \to K^-\pi^+)$	$4.57 \pm 0.69\,(66.51 \pm 0.01\%)$
$D_s^+ \to K_S^0K^+(K_S^0 \to \pi^+\pi^-)$	$2.43 \pm 0.42\,(68.95 \pm 0.14\%)$
$\Lambda_c^+ \to pK^-\pi^+$	5.0 ± 1.3

TABLE II: p^*-averaged reconstruction efficiencies ϵ_C for each charm final state. The errors reflect the limited Monte Carlo statistics.

$C \to f$	ϵ_C (%)
$D^0 \to K^- \pi^+$	50.2 ± 0.3
$D^0 \to K^- \pi^+ \pi^- \pi^+$	20.1 ± 0.2
$D^+ \to K^- \pi^+ \pi^+$	33.7 ± 0.2
$D_s^+ \to \phi\pi^+$	33.0 ± 0.8
$D_s^+ \to \overline{K}^{*0} K^+$	18.0 ± 0.5
$D_s^+ \to K_S^0 K^+$	31.1 ± 0.8
$\Lambda_c^+ \to p K^- \pi^+$	26.7 ± 0.9

The reconstruction efficiencies for each charm final state $C \to f$ (Table II) are computed from the simulation as a function of p^*, the charm-particle momentum in the $\overline{B}$ rest frame, and applied event-by-event to obtain the efficiency-corrected charm and anti-charm signal yields. These are denoted respectively by $N^-(C \to f)$ ($N^0(C \to f)$) and $N^-(\overline{C} \to \overline{f})$ ($N^0(\overline{C} \to \overline{f})$) and are listed in Table III. We then determine the charm and anti-charm fractional production rates $\mathcal{B}_c^{-(0)}$ and $\overline{\mathcal{B}}_c^{-(0)}$, defined as :

$$\begin{aligned} \mathcal{B}_c^{-(0)} &= N^{-(0)}(C \to f)/[N_{B^+(B^0)} \times \mathcal{B}(C \to f)]\,, \\ \overline{\mathcal{B}}_c^{-(0)} &= N^{-(0)}(\overline{C} \to \overline{f})/[N_{B^+(B^0)} \times \mathcal{B}(C \to f)]\,, \end{aligned} \quad (4)$$

where N_{B^+} (N_{B^0}) is the number of reconstructed B^+ (B^0) mesons, and $\mathcal{B}(C \to f)$ is the $C \to f$ branching fraction reported in Table I. $\mathcal{B}_c^-$, $\overline{\mathcal{B}}_c^-$, $\mathcal{B}_c^0$ and $\overline{\mathcal{B}}_c^0$ are listed in Table III.

B. Correlated and anticorrelated charm branching fractions

For charged B, the branching fractions for correlated and anticorrelated C production are given by :

$$\begin{aligned} \mathcal{B}(B^- \to CX) &= \mathcal{B}_c^- - c_0\mathcal{B}_1^0\,, \\ \mathcal{B}(B^- \to \overline{C}X) &= \overline{\mathcal{B}}_c^- - c_0\mathcal{B}_2^0\,. \end{aligned} \quad (5)$$

The correlated (anticorrelated) $B^- \to CX$ branching fraction is equal to the charm (anti-charm) fractional production rate $\mathcal{B}_c^-$ ($\overline{\mathcal{B}}_c^-$) in the recoil of reconstructed B^+ mesons modified by a small correction term $c_0\mathcal{B}_1^0$ ($c_0\mathcal{B}_2^0$) that accounts for the B^0 contamination in the reconstructed B^+ sample. The factors $\mathcal{B}_1^0$ and $\mathcal{B}_2^0$ depend on the measured $\overline{B}^0 \to CX$ and $B^0 \to CX$ branching fractions, and on the $B^0\overline{B}^0$ mixing parameter χ_d [21]. Doubly Cabibbo-suppressed D^0 decays ($D^0 \to K^+\pi^-$ and $D^0 \to K^+\pi^+\pi^-\pi^-$) are also taken into account. We combine the results from the different D^0 and D_s decay modes to extract the final branching fractions listed in Table IV. The probability of the correlated D_s^+ production observed in B^- decays to be due to a background fluctuation is less than 5×10^{-4}.

For neutral B, charm and anti-charm production in the recoil of reconstructed B^0 mesons have to be corrected for $B^0\overline{B}^0$ mixing to obtain the correlated and anticorrelated charm branching fractions :

$$\begin{aligned} \mathcal{B}(\overline{B}^0 \to CX) &= \frac{\overline{\mathcal{B}}_c^0 - \chi_d\,(\mathcal{B}_c^0 + \overline{\mathcal{B}}_c^0)}{1 - 2\,\chi_d} - c_+\mathcal{B}_1^+\,, \\ \mathcal{B}(\overline{B}^0 \to \overline{C}X) &= \frac{\overline{\mathcal{B}}_c^0 - \chi_d\,(\overline{\mathcal{B}}_c^0 + \mathcal{B}_c^0)}{1 - 2\,\chi_d} - c_+\mathcal{B}_2^+\,. \end{aligned} \quad (6)$$

The correction factors $c_+\mathcal{B}_1^+$ and $c_+\mathcal{B}_2^+$ account for B^+ contamination in the B^0 sample and depend on the $B^- \to CX$ and $B^+ \to CX$ branching fractions. Combining the different D^0 and D_s modes, we obtain the final branching fractions listed in Table IV.

We also compute the fraction of anticorrelated charm production in $\overline{B}$ decays :

$$w(\overline{C}) = \frac{\mathcal{B}(\overline{B} \to \overline{C}X)}{\mathcal{B}(\overline{B} \to CX) + \mathcal{B}(\overline{B} \to \overline{C}X)}. \quad (7)$$

Here, many systematic uncertainties cancel out (tracking, K identification, D branching fractions, B counting). The results are given in Table V.

The main systematic uncertainties are associated with the track-finding efficiency, the models used to describe the $m_{\rm ES}$ and $m_{C\,(\overline{C})}$ distributions, and the particle identification efficiency. For example, the 2.7% absolute systematic uncertainty on $\mathcal{B}(B^- \to D^0X)$ reflects the quadratic sum of 1.3% attributed to the track-finding efficiency, 1.6% to the description of the $m_{\rm ES}$ distribution by the Γ_{ARG} and Γ_{CB} functions, 0.8% to the description of the $m_{C\,(\overline{C})}$ signal distribution by the ρ_S function, 1.4% to the particle identification, 0.5% to the Monte Carlo statistics, 0.3% to c_0, and 0.1% to $\mathcal{B}_1^0$.

The uncertainty affecting the track-finding efficiency is estimated with two different methods. The first uses a large inclusive sample of tracks with a minimum number of hits in the silicon vertex detector. The second relies on an $e^+e^- \to \tau^+\tau^-$ control sample. From these, we derive a relative systematic uncertainty of 0.8% per track.

The modeling of the $m_{\rm ES}$ distribution by the Γ_{CB} and the Γ_{ARG} functions affects both the charm signal yields and the numbers of reconstructed B mesons used in normalizing the branching fractions. The corresponding uncertainty is dominated by the dependence of the Γ_{ARG} shape parameter on the lower edge of the $m_{\rm ES}$ fit range. Varying the latter from 5.195 to 5.225 GeV/c^2 yields a variation in the branching fraction that is taken as systematic uncertainty. This range was chosen such that the branching fractions measured in the simulation change by ± 1 standard deviation.

The uncertainty associated with the description of the charm signal mass shape by the ρ_S function translates

TABLE III: Charm and anti-charm efficiency-corrected signal yields and fractional production rates. The uncertainties are statistical only.

C decay mode	C in recoil of $B^+_{\rm rec'd}$		$\overline{C}$ in recoil of $B^+_{\rm rec'd}$		C in recoil of $B^0_{\rm rec'd}$		$\overline{C}$ in recoil of $B^0_{\rm rec'd}$	
	$N^-(C\to f)$	$\mathcal{B}_c^-(\%)$	$N^-(\overline{C}\to \bar{f})$	$\overline{\mathcal{B}}_c^-(\%)$	$N^0(C\to f)$	$\mathcal{B}_c^0(\%)$	$N^0(\overline{C}\to \bar{f})$	$\overline{\mathcal{B}}_c^0(\%)$
$D^0\to K^-\pi^+$	5898±126	77.5±1.6	691±52	9.1±0.7	1731±70	41.1±1.7	669±44	15.9±1.0
$\to K^-\pi^+\pi^-\pi^+$	11010±383	73.4±2.6	1378±214	9.2±1.4	3418±239	41.2±2.9	1065±159	12.8±1.9
$D^+\to K^-\pi^+\pi^+$	1970±131	10.8±0.7	513±89	2.8±0.5	3044±122	30.2±1.2	869±74	8.6±0.7
$D_s^+\to\phi\pi^+$	85±24	1.8±0.5	385±42	8.1±0.9	97±21	3.7±0.8	227±30	8.7±1.2
$\to\overline{K}^{*0}K^+$	78±39	1.3±0.6	567±72	9.3±1.2	78±28	2.3±0.8	306±50	9.1±1.5
$\to K_S^0K^+$	0±16	0.0±0.5	212±39	6.6±1.2	48±19	2.7±1.1	148±29	8.3±1.6
$\Lambda_c^+\to pK^-\pi^+$	288±52	2.9±0.5	210±45	2.1±0.5	240±41	4.3±0.7	124±30	2.2±0.5

TABLE IV: $\overline{B}$ branching fractions. The first uncertainty is statistical, the second is systematic, and the third reflects charm branching-fraction uncertainties [21, 23].

	Correlated		Anticorrelated	
C	$\mathcal{B}(B^-\to CX)(\%)$	$\mathcal{B}(\overline{B}^0\to CX)(\%)$	$\mathcal{B}(B^-\to\overline{C}X)(\%)$	$\mathcal{B}(\overline{B}^0\to\overline{C}X)(\%)$
D^0	$78.6\pm1.6\pm2.7^{+2.0}_{-1.9}$	$47.4\pm2.0\pm1.5^{+1.3}_{-1.2}$	$8.6\pm0.6\pm0.3^{+0.2}_{-0.2}$	$8.1\pm1.4\pm0.5^{+0.2}_{-0.2}$
D^+	$9.9\pm0.8\pm0.5^{+0.8}_{-0.7}$	$36.9\pm1.6\pm1.4^{+2.6}_{-2.3}$	$2.5\pm0.5\pm0.1^{+0.2}_{-0.2}$	$2.3\pm1.1\pm0.3^{+0.2}_{-0.1}$
				<3.9 at 90% CL
D_s^+	$1.1^{+0.4}_{-0.3}\pm0.1^{+0.2}_{-0.1}$	$1.5\pm0.8\pm0.1^{+0.2}_{-0.2}$	$7.9\pm0.6\pm0.4^{+1.3}_{-1.0}$	$10.3\pm1.2\pm0.4^{+1.7}_{-1.3}$
		<2.6 at 90% CL		
Λ_c^+	$2.8\pm0.5\pm0.3^{+1.0}_{-0.6}$	$5.0\pm1.0\pm0.5^{+1.8}_{-1.0}$	$2.1\pm0.5\pm0.2^{+0.8}_{-0.4}$	$1.6\pm0.9\pm0.2^{+0.6}_{-0.3}$
				<3.1 at 90% CL

TABLE V: Fraction of anticorrelated charm as defined in Eq. (7).

Mode	B^- decays	$\overline{B}^0$ decays
$\overline{D}^0X$	$0.098\pm0.007\pm0.001$	$0.146\pm0.022\pm0.006$
D^-X	$0.204\pm0.035\pm0.001$	$0.058\pm0.028\pm0.006$
		<0.098 at 90% CL
D_s^-X	$0.884\pm0.038\pm0.002$	$0.879\pm0.066\pm0.005$
		>0.791 at 90% CL
$\overline{\Lambda}_c^-X$	$0.427\pm0.071\pm0.001$	$0.243^{+0.119}_{-0.121}\pm0.003$
		<0.403 at 90% CL

into an uncertainty on the charm reconstruction efficiency. It is estimated by fitting the simulated charm signal with a double instead of a single Gaussian.

The systematic uncertainties affecting the proton and charged kaon particle-identification efficiency are estimated using $D^0\to K^-\pi^+$ and $\Lambda^0\to p\pi^-$ samples recoiling against reconstructed B^+ and B^0 mesons. The D^0 or Λ^0 signal yields are extracted in a manner similar to that described in Sec. IV A, both with and without applying the proton or kaon particle-identification requirements. The ratio of these yields on real and simulated samples is proportional to the particle-identification efficiency in the data and the simulation, respectively. The difference between these two efficiencies is then taken as an estimate of the corresponding the systematic uncertainty (1.7% relative uncertainty per kaon and 1.3% per proton).

The statistical and systematic uncertainties in Table IV and Table V are computed separately for each charm decay mode; correlated errors are taken into account when averaging over D^0 and D_s final states.

C. Average charm production in $\overline{B}$ decays

To extract N_c from the results of Table IV, we still need to evaluate the $\overline{B}\to\Xi_cX$ and $\overline{B}\to(c\overline{c})X$ branching fractions. Because there exists no absolute measurement of the Ξ_c-decay branching fraction, the absolute rates for correlated Ξ_c production in B decays are unknown [14, 25]. Therefore, following the discussion in Sec. I, we assume that $\mathcal{B}(\overline{B}\to\Xi_cX)=\mathcal{B}(\overline{B}\to\overline{\Lambda}_c^-X)-\mathcal{B}(\overline{B}\to\Lambda_c^+\overline{\Lambda}_c^-\overline{K}(\pi))$ [26]. A recent measurement [27] indicates that $\overline{B}\to\Lambda_c^+\overline{\Lambda}_c^-\overline{K}$ decays have a branching fraction of the order of 7×10^{-4}, and thus can be neglected by comparison to $N_c^{-/0}$ (see also [2]). We take $\mathcal{B}(\overline{B}\to(c\overline{c})X)=(2.3\pm0.3)\%$ [28, 29] and, using Eqs. (1) and (2), we obtain for charm production in B^-

decays:

$$\begin{aligned} N_c^- &= 0.968 \pm 0.019 \pm 0.032^{+0.026}_{-0.022}, \\ N_{\overline{c}}^- &= 0.234 \pm 0.012 \pm 0.008^{+0.016}_{-0.012}, \\ n_c^- &= 1.202 \pm 0.023 \pm 0.040^{+0.035}_{-0.029}. \end{aligned}$$

and in $\overline{B}^0$ decays :

$$\begin{aligned} N_c^0 &= 0.947 \pm 0.030 \pm 0.028^{+0.035}_{-0.028}, \\ N_{\overline{c}}^0 &= 0.246 \pm 0.024 \pm 0.009^{+0.019}_{-0.014}, \\ n_c^0 &= 1.193 \pm 0.030 \pm 0.034^{+0.044}_{-0.035}. \end{aligned}$$

The results reported here are consistent [30] with, and supersede those of Ref. [2]. The three-fold increase in integrated luminosity accounts for the substantial reduction in statistical error. The experimental systematic uncertainties have been similarly reduced, primarily through the use of the two-dimensional $[m_{\rm ES}, m_{C\,(\overline{C})}]$ fit, which takes correctly into account the correlation between the fitted number of reconstructed B mesons and the corresponding charm yield.

D. Isospin analysis

The main source of anticorrelated $\overline{D}$ mesons produced in $\overline{B}$ decays is $b \to c\overline{c}s$ transitions. In these processes isospin should be conserved, leading to the expectation that : $\Gamma(B^- \to \overline{D}^0 X) = \Gamma(\overline{B}^0 \to D^- X)$ and $\Gamma(B^- \to D^- X) = \Gamma(\overline{B}^0 \to \overline{D}^0 X)$. However, $\overline{D}$ mesons can also arise from $\overline{D}^*$ mesons, whose decay does not conserve isospin since the $\overline{D}^{*0} \to D^-\pi^+$ channel is kinematically forbidden. Thus isospin invariance actually requires :

$$\begin{aligned} \Gamma_{dir}(B^- \to \overline{D}^0 X) &= \Gamma_{dir}(\overline{B}^0 \to D^- X) \\ \Gamma_{dir}(B^- \to D^- X) &= \Gamma_{dir}(\overline{B}^0 \to \overline{D}^0 X) \\ \Gamma(B^- \to \overline{D}^{*0} X) &= \Gamma(\overline{B}^0 \to D^{*-} X) \\ \Gamma(B^- \to D^{*-} X) &= \Gamma(\overline{B}^0 \to \overline{D}^{*0} X) \end{aligned} \tag{8}$$

where $\Gamma_{dir}(\overline{B} \to \overline{D} X)$ refers to the partial width of $\overline{B}$-meson decays to $\overline{D}$ mesons where the $\overline{D}$ state is *not* reached through a $\overline{D}^*$ cascade decay. Eqs. (8) lead to the following relations involving the measured anticorrelated $\overline{D}$ branching fractions in Table IV :

$$r\ x^* = \mathcal{B}(B^- \to \overline{D}^0 X) - \mathcal{B}(\overline{B}^0 \to D^- X)\frac{\tau_{B^+}}{\tau_{B^0}} \tag{9}$$

$$r\ x^* = \mathcal{B}(\overline{B}^0 \to \overline{D}^0 X)\frac{\tau_{B^+}}{\tau_{B^0}} - \mathcal{B}(B^- \to D^- X) \tag{10}$$

and :

$$\begin{aligned} x + x^* &= \tfrac{1}{2}\big[\mathcal{B}(B^- \to \overline{D}^0 X) + \mathcal{B}(B^- \to D^- X) \\ &+ \mathcal{B}(\overline{B}^0 \to \overline{D}^0 X)\tfrac{\tau_{B^+}}{\tau_{B^0}} + \mathcal{B}(\overline{B}^0 \to D^- X)\tfrac{\tau_{B^+}}{\tau_{B^0}}\big] \end{aligned} \tag{11}$$

where τ_B^+/τ_B^0 is the ratio of the B^+ to the B^0 lifetime, $r = \mathcal{B}(D^{*-} \to \overline{D}^0\pi^-)$, $x = \mathcal{B}_{dir}(B^- \to \overline{D}^0 + D^- X)$ and $x^* = \mathcal{B}(B^- \to \overline{D}^{*0} + D^{*-} X)$ [31]. That both Eqs. (9) and (10) must be satisfied is a consequence of isospin invariance. From these two equations, we extract x^* with a chi-squared method, and using in addition Eq. (11) we calculate :

$$\begin{aligned} \mathcal{B}(B^- \to \overline{D}^{*0} + D^{*-} X) &= 9.1 \pm 1.5 \pm 0.6\% \\ \mathcal{B}_{dir}(B^- \to \overline{D}^0 + D^- X) &= 2.1 \pm 1.7 \pm 0.7\% \\ &< 4.5\% \text{ at } 90\% \text{ CL} \\ \frac{\mathcal{B}_{dir}(\overline{B} \to \overline{D}^0 + D^- X)}{\mathcal{B}(\overline{B} \to \overline{D}^{*0} + D^{*-} X)} &= 0.23^{+0.25}_{-0.19} \pm 0.09 \\ &< 0.60 \text{ at } 90\% \text{ CL} \end{aligned}$$

Here the first uncertainty is statistical, the second is systematic and includes charm branching-fraction uncertainties, as well as those affecting the values of τ_B^+/τ_B^0 and $\mathcal{B}(D^{*-} \to \overline{D}^0\pi^-)$ taken from Ref. [21]. The χ^2 of the fit to Eqs. (9) and (10) is 0.01 for 1 degree of freedom.

V. CHARM MOMENTUM DISTRIBUTIONS IN THE $\overline{B}$ REST FRAME

As the four-momentum of the recoiling $\overline{B}$ is fully determined, each reconstructed charm hadron can be boosted into the rest frame of its parent $\overline{B}$, yielding the p^* distribution of the corresponding (anti-charm) charm species in the $\overline{B}$ frame. The number of $C\,(\overline{C})$ candidates, their fractional production rates and the $\overline{B} \to C\,(\overline{C})X$ branching fractions are then determined in each p^* bin by the same methods as in Sec. IV, separately for B^- and $\overline{B}^0$ decays. The systematic uncertainties are assumed to be independent of p^*, except for the error associated with the B^0 (B^+) contamination in the B^+ (B^0) sample : the latter is computed bin-by-bin with a relative uncertainty on c_+ and c_0 increased to 100%.

Figs. 6 and 7 show the result for correlated and anticorrelated D^0, D^+, D_s and Λ_c^+ production in B^- and $\overline{B}^0$ decays, respectively. The numerical values are tabulated in the Appendix.

Correlated D^0 and D^+ (Figs. 6a, c and 7a, c) are produced in several types of transitions : $b \to c\ell^-\nu$, $b \to c\overline{u}d$ and $b \to c\overline{c}s$ which explains the fairly large spread of their momentum. High-p^* correlated D's are produced in two-body decays such as $B^- \to D^0\pi^-$ while low momentum D's might come from higher multiplicity final states such as $\overline{B} \to D\overline{D}K(X_{light})$ where X_{light} is any number of pions and/or photons. The latter processes are also the main source of anticorrelated $\overline{D}^0$ and D^- production (Figs. 6b, d and 7b, d) which explains why anticorrelated $\overline{D}$ spectra are softer than their correlated counterparts.

Anticorrelated D_s^- spectra (Figs. 6f and 7f) have a very different shape compared to anticorrelated $\overline{D}$ spectra. They are peaked at high p^* values which is suggestive of the two-body decays $\overline{B} \to D^{(*)}D_s^-$ and $\overline{B} \to D^{(*)}D_s^{*-}$.

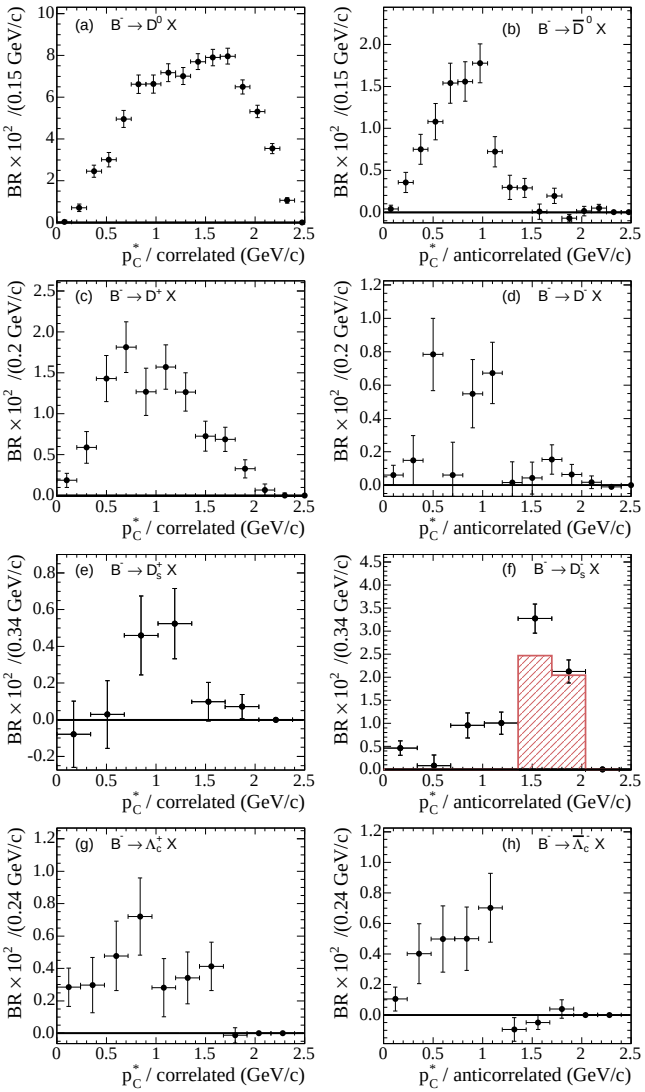

FIG. 6: Momentum spectra, in the B^- rest frame, of correlated (left) and anticorrelated (right) charm particles : $D^0/\overline{D}^0$ (a)(b), $D^\pm$ (c)(d), $D_s^\pm$ (e)(f), $\Lambda_c^\pm$ (g)(h). The error bars are statistical only. The histogram in frame (f) represents the contribution of $B^- \to D^{(*)0} D_s^{(*)-}$ two-body decays assuming the branching fractions of Ref. [21] and [23].

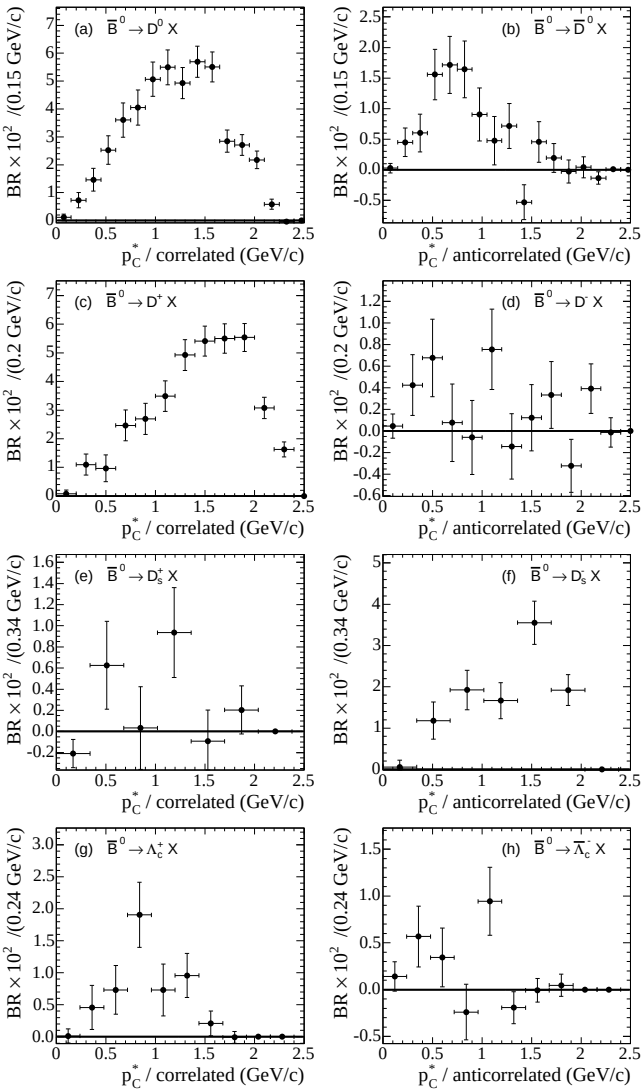

FIG. 7: Momentum spectra, in the $\overline{B}^0$ rest frame, of correlated (left) and anticorrelated (right) charm particles : $D^0/\overline{D}^0$ (a)(b), $D^\pm$ (c)(d), $D_s^\pm$ (e)(f), $\Lambda_c^\pm$ (g)(h). The error bars are statistical only.

These decays represent a large fraction of the total anticorrelated D_s^- production as shown in Fig. 6. In contrast, the corresponding two-body processes $\overline{B} \to D^{(*)} D^-$ and $\overline{B} \to D^{(*)} D^{*-}$ are Cabibbo-suppressed.

In the case of anticorrelated $\overline{\Lambda}_c^-$ production associated with Ξ_c production, for decays such as $\overline{B} \to \Xi_c \overline{\Lambda}_c^- (X_{light})$, the anticorrelated $\overline{\Lambda}_c^-$ spectra should have a cut-off at $p^* < 1.15$ GeV/c. This is actually observed in the data, both in B^- (Fig. 6h) and in $\overline{B}^0$ (Fig. 7h) decays.

VI. CONCLUSIONS

We have measured the branching fractions for inclusive decays of B mesons to flavor-tagged D, D_s and Λ_c^+, separately for B^- and $\overline{B}^0$. We observe a significant production of anticorrelated D^0 and D^+ mesons in B decays, with the branching fractions reported in Table IV. These results are consistent with and supersede our previous measurement [2]. We find evidence for correlated D_s^+ production in B^- decays, a process which has not been previously reported.

The sum of all correlated charm branching fractions, N_c, is compatible with 1, for charged as well as for neutral B mesons. The numbers of charm particles per B^- decay ($n_c^- = 1.202 \pm 0.023 \pm 0.040^{+0.035}_{-0.029}$) and per $\overline{B}^0$ decay

($n_c^0 = 1.193 \pm 0.030 \pm 0.034^{+0.044}_{-0.035}$) are consistent with previous measurements [2, 4, 28] and with theoretical expectations [8–11].

Assuming isospin conservation in the $b \to c\bar{c}s$ transition, we show that anticorrelated $\overline{D}$ mesons are mainly produced by cascade decays $\overline{B} \to \overline{D}^* X \to \overline{D} X$.

Finally, the technique developed for this analysis allows us to measure the inclusive momentum spectra of flavor-tagged D, D_s and Λ_c^+ in the rest frame of the $\overline{B}$ parent, separately in B^- and $\overline{B}^0$ decays, eventually providing insight into B-decay mechanisms.

Acknowledgments

We are grateful for the excellent luminosity and machine conditions provided by our PEP-II colleagues, and for the substantial dedicated effort from the computing organizations that support *BABAR*. The collaborating institutions wish to thank SLAC for its support and kind hospitality. This work is supported by DOE and NSF (USA), NSERC (Canada), IHEP (China), CEA and CNRS-IN2P3 (France), BMBF and DFG (Germany), INFN (Italy), FOM (The Netherlands), NFR (Norway), MIST (Russia), and PPARC (United Kingdom). Individuals have received support from CONACyT (Mexico), Marie Curie EIF (European Union), the A. P. Sloan Foundation, the Research Corporation, and the Alexander von Humboldt Foundation.

[1] Charge conjugation is implied for all decay processes mentioned in this paper.
[2] *BABAR* Collaboration, B. Aubert *et al.*, Phys. Rev. D **70**, 091106(R) (2004).
[3] CLEO collaboration, L. Gibbons *et al.*,Phys. Rev. D **56**, 3783 (1997).
[4] CLEO collaboration, T.E. Coan *et al.*, Phys. Rev. Lett. **80**, 1150 (1998).
[5] DELPHI collaboration, J. Abdallah *et al.*, Phys. Lett. B **561**, 26 (2003).
[6] CLEO collaboration, R. Ammar *et al.*, Phys. Rev. D **55**, 13 (1997).
[7] BELLE collaboration, R. Seuster *et al.*, Phys. Rev. D **73**, 032002 (2006).
[8] E. Bagan *et al.*, Phys. Lett. B **351**, 546 (1995).
[9] G. Buchalla *et al.*, Phys. Lett. B **364**, 188 (1995).
[10] M. Neubert, 17th Int. Symposium on Lepton-Photon Interactions, 10-15 Aug 95, Beijing, China, p. 298 (World Scientific).
[11] A. Lenz, hep-ph/0011258 and references therein.
[12] ALEPH collaboration, R. Barate *et al.*, Eur. Phys. Jour. C **4**, 387 (1998).
[13] *BABAR* collaboration, B. Aubert *et al.*, Phys. Rev. D **68**, 092001 (2003).
[14] BELLE collaboration, R. Chistov *et al.*, hep-ex/0510074.
[15] C.W. Bauer, B. Grinstein, D. Pirjol, I.W. Stewart, Phys. Rev. D **67**, 014010 (2003).
[16] I. Bigi, L. Maiani, F. Piccinini, A.D. Polosa, V. Riquer, Phys. Rev. D **72**, 114016 (2005).
[17] *BABAR* Collaboration, B. Aubert *et al.*, Nucl. Instr. Methods Phys. Res., Sect. A **479**,1 (2002).
[18] GEANT4 Collaboration, S. Agostinelli *et al.* Nucl. Instr. Methods Phys. Res., Sect. A **506**, 250 (2003).
[19] CRYSTAL BALL collaboration, T. Skwarnicki *et al.*, DESY F31-86-02.
[20] ARGUS collaboration, H. Albrecht *et al.*, Z. Phys. C **48**, 543 (1990).
[21] Particle Data Group, S. Eidelman *et al.*, Phys. Lett. B **592**, 1 (2004).
[22] We consider any K^+K^- combination with an invariant mass in the range $1010.6 < m_{K^+K^-} < 1028.6$ MeV/c^2 to be a ϕ meson when reconstructing the $D_s^+ \to \phi(\to K^+K^-)\pi^+$ decay.
[23] *BABAR* collaboration, B. Aubert *et al.*, Phys. Rev. D **71**, 091104 (2005).
[24] In some cases, a satellite contribution needs to be added. It includes a reflection from $D^0 \to K^-K^+$ in the $D^0 \to K^-\pi^+$ mass spectra and a signal at the D^+ mass (from $D^+ \to \phi\pi^+$, $\overline{K}^{*0}K^+$, $K_S^0K^+$ Cabibbo-suppressed decays) in the D_s mass spectra.
[25] CLEO collaboration, B. Barish *et al.*, Phys. Rev. Lett. **79**, 3599 (1997).
[26] We also neglect the contribution of the $\overline{B} \to D\Lambda^0\overline{\Lambda}_c^-$ decays because of the very small phase space available.
[27] BELLE collaboration, N. Gabyshev *et al.*, hep-ex/0508015.
[28] ALEPH, CDF, DELPHI, L3, OPAL, SLD combined results, hep-ex/0112028, CERN-EP/2001-050.
[29] M. Beneke *et al.*, Phys. Rev. D **59**, 054003 (1999).
[30] Provided one takes into account the 25% change in the D_s^+ branching fraction [21, 23] assumed in interpreting the $D_s^+ \to \phi\pi^+$ yield.
[31] Assuming isospin conservation, we have also : $x = \mathcal{B}_{dir}(\overline{B}^0 \to \overline{D}^0 + D^-X) \times \frac{\tau_{B^+}}{\tau_{B^0}}$ and $x^* = \mathcal{B}(\overline{B}^0 \to \overline{D}^{*0} + D^{*-}X) \times \frac{\tau_{B^+}}{\tau_{B^0}}$

APPENDIX : CHARM p^* SPECTRA

This appendix tabulates the measured p^* dependence of the branching fractions displayed in Figs. 6 and 7. In Tables VI to XIII, the first uncertainty is statistical, the second is systematic and includes charm branching-fraction uncertainties. Within each table, the statistical uncertainties are uncorrelated whereas the systematic errors are fully correlated.

TABLE VI: Correlated and anticorrelated D^0 production in B^- decays.

p^* range (GeV/c)	correlated prod. $\mathcal{B}(B^- \to X_c X)$ (%)	anticorrelated prod. $\mathcal{B}(B^- \to X_{\overline{c}} X)$ (%)
0.00 - 0.15	0.03±0.06±0.01	0.04±0.04±0.01
0.15 - 0.30	0.70±0.18±0.03	0.36±0.12±0.02
0.30 - 0.45	2.45±0.29±0.11	0.75±0.18±0.03
0.45 - 0.60	3.01±0.34±0.13	1.08±0.22±0.05
0.60 - 0.75	4.96±0.40±0.22	1.54±0.24±0.07
0.75 - 0.90	6.62±0.44±0.30	1.56±0.23±0.07
0.90 - 1.05	6.63±0.43±0.30	1.78±0.23±0.07
1.05 - 1.20	7.18±0.43±0.32	0.72±0.18±0.04
1.20 - 1.35	7.01±0.41±0.32	0.30±0.14±0.05
1.35 - 1.50	7.70±0.38±0.35	0.29±0.11±0.02
1.50 - 1.65	7.90±0.39±0.36	0.01±0.09±0.05
1.65 - 1.80	7.96±0.38±0.40	0.20±0.09±0.02
1.80 - 1.95	6.49±0.33±0.32	-0.07±0.04±0.02
1.95 - 2.10	5.32±0.29±0.26	0.02±0.06±0.02
2.10 - 2.25	3.54±0.24±0.19	0.05±0.04±0.00
2.25 - 2.40	1.06±0.13±0.06	-

TABLE VII: Correlated and anticorrelated D^+ production in B^- decays.

p^* range (GeV/c)	correlated prod. $\mathcal{B}(B^- \to X_c X)$ (%)	anticorrelated prod. $\mathcal{B}(B^- \to X_{\overline{c}} X)$ (%)
0.00 - 0.20	0.19±0.09±0.02	0.06±0.06±0.01
0.20 - 0.40	0.59±0.19±0.06	0.15±0.15±0.02
0.40 - 0.60	1.43±0.28±0.14	0.78±0.22±0.07
0.60 - 0.80	1.81±0.31±0.17	0.06±0.20±0.02
0.80 - 1.00	1.27±0.29±0.13	0.55±0.21±0.05
1.00 - 1.20	1.57±0.27±0.16	0.67±0.18±0.06
1.20 - 1.40	1.27±0.23±0.16	0.02±0.12±0.03
1.40 - 1.60	0.72±0.18±0.15	0.04±0.10±0.04
1.60 - 1.80	0.69±0.15±0.16	0.15±0.09±0.04
1.80 - 2.00	0.33±0.11±0.16	0.06±0.06±0.03
2.00 - 2.20	0.07±0.07±0.09	0.02±0.04±0.03

TABLE VIII: Correlated and anticorrelated D_s production in B^- decays.

p^* range (GeV/c)	correlated prod. $\mathcal{B}(B^- \to X_c X)$ (%)	anticorrelated prod. $\mathcal{B}(B^- \to X_{\overline{c}} X)$ (%)
0.00 - 0.34	-0.08±0.18±0.02	0.46±0.16±0.07
0.34 - 0.68	0.03±0.18±0.03	0.08±0.23±0.04
0.68 - 1.02	0.46±0.22±0.09	0.95±0.27±0.14
1.02 - 1.36	0.52±0.19±0.11	1.00±0.24±0.15
1.36 - 1.70	0.10±0.11±0.03	3.27±0.32±0.49
1.70 - 2.04	0.07±0.07±0.02	2.13±0.25±0.32

TABLE IX: Correlated and anticorrelated Λ_c^+ production in B^- decays.

p^* range (GeV/c)	correlated prod. $\mathcal{B}(B^- \to X_c X)$ (%)	anticorrelated prod. $\mathcal{B}(B^- \to X_{\overline{c}} X)$ (%)
0.00 - 0.24	0.28±0.12±0.09	0.10±0.08±0.03
0.24 - 0.48	0.30±0.17±0.09	0.40±0.20±0.12
0.48 - 0.72	0.48±0.21±0.15	0.50±0.22±0.15
0.72 - 0.96	0.72±0.24±0.22	0.50±0.21±0.15
0.96 - 1.20	0.28±0.18±0.09	0.70±0.23±0.21
1.20 - 1.44	0.34±0.16±0.11	-0.10±0.08±0.03
1.44 - 1.68	0.41±0.15±0.13	-0.05±0.05±0.01

TABLE X: Correlated and anticorrelated D^0 production in $\overline{B}^0$ decays.

p^* range (GeV/c)	correlated prod. $\mathcal{B}(B^- \to X_c X)$ (%)	anticorrelated prod. $\mathcal{B}(B^- \to X_{\overline{c}} X)$ (%)
0.00 - 0.15	0.11±0.12±0.01	0.03±0.08±0.01
0.15 - 0.30	0.73±0.28±0.03	0.45±0.23±0.03
0.30 - 0.45	1.46±0.41±0.07	0.60±0.31±0.04
0.45 - 0.60	2.53±0.51±0.11	1.56±0.41±0.11
0.60 - 0.75	3.60±0.62±0.16	1.71±0.47±0.12
0.75 - 0.90	4.05±0.63±0.20	1.64±0.46±0.12
0.90 - 1.05	5.07±0.61±0.23	0.90±0.43±0.07
1.05 - 1.20	5.50±0.62±0.25	0.48±0.40±0.06
1.20 - 1.35	4.93±0.56±0.24	0.72±0.37±0.08
1.35 - 1.50	5.70±0.56±0.27	-0.53±0.29±0.07
1.50 - 1.65	5.51±0.53±0.27	0.45±0.33±0.09
1.65 - 1.80	2.85±0.40±0.23	0.19±0.24±0.07
1.80 - 1.95	2.71±0.37±0.19	-0.03±0.19±0.06
1.95 - 2.10	2.17±0.32±0.16	0.04±0.17±0.05
2.10 - 2.25	0.58±0.18±0.11	-0.14±0.10±0.02

TABLE XI: Correlated and anticorrelated D^+ production in $\overline{B}^0$ decays.

p^* range (GeV/c)	correlated prod. $\mathcal{B}(B^- \to X_c X)$ (%)	anticorrelated prod. $\mathcal{B}(B^- \to X_{\overline{c}} X)$ (%)
0.00 - 0.20	0.08±0.12±0.01	0.05±0.11±0.01
0.20 - 0.40	1.10±0.37±0.09	0.42±0.28±0.07
0.40 - 0.60	0.97±0.47±0.08	0.68±0.36±0.11
0.60 - 0.80	2.47±0.54±0.19	0.08±0.36±0.02
0.80 - 1.00	2.70±0.54±0.21	-0.06±0.34±0.02
1.00 - 1.20	3.49±0.53±0.28	0.76±0.37±0.12
1.20 - 1.40	4.92±0.54±0.39	-0.14±0.30±0.04
1.40 - 1.60	5.41±0.52±0.44	0.12±0.31±0.04
1.60 - 1.80	5.50±0.51±0.45	0.33±0.31±0.06
1.80 - 2.00	5.54±0.49±0.45	-0.32±0.25±0.06
2.00 - 2.20	3.08±0.37±0.25	0.39±0.23±0.06
2.20 - 2.40	1.63±0.26±0.13	-0.01±0.14±0.01

TABLE XII: Correlated and anticorrelated D_s production in $\overline{B}^0$ decays.

p^* range (GeV/c)	correlated prod. $\mathcal{B}(B^- \to X_c X)$ (%)	anticorrelated prod. $\mathcal{B}(B^- \to X_{\overline{c}} X)$ (%)
0.00 - 0.34	-0.21±0.13±0.03	0.06±0.16±0.02
0.34 - 0.68	0.63±0.42±0.09	1.18±0.45±0.18
0.68 - 1.02	0.03±0.39±0.01	1.92±0.48±0.29
1.02 - 1.36	0.94±0.43±0.14	1.66±0.43±0.25
1.36 - 1.70	-0.09±0.29±0.03	3.55±0.52±0.54
1.70 - 2.04	0.20±0.23±0.04	1.92±0.37±0.29

TABLE XIII: Correlated and anticorrelated Λ_c^+ production in $\overline{B}^0$ decays.

p^* range (GeV/c)	correlated prod. $\mathcal{B}(B^- \to X_c X)$ (%)	anticorrelated prod. $\mathcal{B}(B^- \to X_{\overline{c}} X)$ (%)
0.00 - 0.24	0.01±0.11±0.01	0.14±0.16±0.05
0.24 - 0.48	0.46±0.34±0.15	0.57±0.33±0.19
0.48 - 0.72	0.73±0.38±0.23	0.34±0.31±0.12
0.72 - 0.96	1.90±0.51±0.60	-0.24±0.30±0.08
0.96 - 1.20	0.73±0.40±0.23	0.94±0.36±0.32
1.20 - 1.44	0.96±0.35±0.30	-0.19±0.17±0.07
1.44 - 1.68	0.21±0.19±0.07	-0.01±0.13±0.01

HADRONIC B DECAYS AT *BABAR*

A. Zghiche for the *BABAR* collaboration[a]

[a]Laboratoire d'Annecy-Le-Vieux de Physique des Particules
9 Chemin de Bellevue, BP 110, F-74941 Annecy-le-Vieux CEDEX - France

By means of hadronic B decays, the *BABAR* experiment aims to constrain the CKM matrix performing *CP* parameter measurements. It also seeks to test QCD factorization predictions and other models for B structure and decay mechanisms. We will present some of the on-going *CP* related analyses in the first section, while the second section will be dedicated to report on the conducted investigations on subjects as diverse as probing the gluon component in the B meson wave function, new physics and final state interactions in annihilation processes, intrinsic charm searches and first observation of strange charmed baryon production in B decays.

1. *CP* related analyses

In this section we report on on-going hadronic B decays measurements of branching fractions and *CP* asymmetries which are defined, for the $B \to f$ decay, as :

$$\mathcal{A}_{CP} = \frac{\mathcal{B}(B \to f) - \mathcal{B}(\overline{B} \to \overline{f})}{\mathcal{B}(B \to f) + \mathcal{B}(\overline{B} \to \overline{f})}$$

These are the first steps in analyses that could be used, in the future, to measure CKM matrix parameters like $\gamma \equiv \arg\left[-\frac{V_{ud}V_{ub}^*}{V_{cd}V_{cb}^*}\right]$ or a combination of γ and $\beta \equiv \arg\left[-\frac{V_{cd}V_{cb}^*}{V_{td}V_{tb}^*}\right]$.

1.1. Measurement of the branching fraction and decay rate asymmetry of $B^- \to D_{\pi^+\pi^-\pi^0}K^-$

The decays $B \to D^{(*)0}K^{(*)}$ can be used to measure the angle γ taking advantage of the interference between $b \to u\bar{c}s$ and $b \to c\bar{u}s$ decay amplitudes. Different approaches have been developed, among which γ measurements involving D decays to multi-body, using a Dalitz plot analysis technique as described in reference [1]. In this analysis, we measure the branching fraction of the decay modes $B^- \to D^0(\overline{D}^0)K^-$ with the D^0 ($\overline{D}^0$)-decay : $D^0(\overline{D}^0) \to \pi^+\pi^-\pi^0$, which is Cabibbo suppressed. They yield a much smaller event sample compared to Cabibbo allowed D decays but the interfering D^0 and $\overline{D}^0$ amplitudes have similar magnitudes. Therefore, the sensitivity to γ of this D decay channel is expected to be relevant. In addition, due to interference, the production rate may differ from the product $\mathcal{B}_{prod} \equiv \mathcal{B}(B^- \to D^0K^-) \times \mathcal{B}(D^0 \to \pi^+\pi^-\pi^0) = (4.1 \pm 1.6) \times 10^{-6}$ by up to about $0.2\mathcal{B}_{prod}$ [2]. From a sample of 229 million of $B\overline{B}$ pairs, we found 133 ± 23 signal events which correspond to a branching ratio of $\mathcal{B}(B^- \to D_{\pi^+\pi^-\pi^0}K^-) = (5.5 \pm 1.0 \pm 0.7) \times 10^{-6}$. We determine the raw asymmetry and do not find any significant deviation from zero : $\mathcal{A}_{CP}^{raw} = 0.02 \pm 0.16 \pm 0.03$. The γ extraction is underway using the full Dalitz analysis of the D-decay [3].

1.2. Measurement of the branching fraction $B^0 \to \overline{D}^0(D^0)K^+\pi^-$

To determine the feasibility of measuring γ with the method proposed by R. Aleksan et al. [4], that uses three-body $B \to DK\pi$ decays, we have studied $\overline{D}^0(D^0)K^+\pi^-$ final states with $205fb^{-1}$ data sample. In these modes, the CKM suppressed $b \to u\bar{c}s$ processes contain color allowed diagrams, resulting in larger rates and more significant *CP* violation effects than the two-body $B \to DK$ decays. We measured $\mathcal{B}(B^0 \to \overline{D}^0K^+\pi^-) = (8.6 \pm 1.5 \pm 1.0) \times 10^{-5}$ combining D modes ($D^0 \to K\pi$, $D^0 \to K\pi\pi^0$, $D^0 \to K\pi\pi\pi$) and excluding $B^0 \to D^{*-}(2010)K^+$ contribution. Using Dalitz analysis we identified two resonant contributions: $\mathcal{B}(B^0 \to \overline{D}^0K^{*0}) \times \mathcal{B}(K^{*0} \to K^+\pi^-) = (3.9 \pm 0.6 \pm 0.4) \times 10^{-5}$ and $\mathcal{B}(B^0 \to D_2^{*-}(2460)K^+) \times \mathcal{B}(D_2^{*-}(2460) \to \overline{D}^0\pi^-) = (1.9 \pm 0.4 \pm 0.3) \times 10^{-5}$. We also set an

upper limit at 90% CL on the CKM suppressed channel : $\mathcal{B}(B^0 \to D^0 K^+\pi^-) < 1.9\times10^{-5}$. However, we come to the conclusion that measuring γ is very difficult with this mode and that approximately $2000 fb^{-1}$ are necessary to constrain γ within $\pm$ 50° at 3σ level.

1.3. Search for $B \to D_s^+ X_{light}$ with $X_{light} \equiv \pi^0$, a_0^-, a_1^-

The value of $\sin(2\beta+\gamma)$ can be extracted from the measurement of the time dependent *CP* asymmetry in $B^0 \to D^- X^+_{light}$ decays where $X^+_{light} \equiv \pi^+$, a_0^+, a_2^+. In this case, the asymmetry is given by : $\mathcal{A}_{CP}(\Delta t) = r \times \sin(2\beta+\gamma) \times sin(\Delta m_d \Delta t)$ where $r = \mathcal{B}(B^0 \to D^+ X^-_{light})/\mathcal{B}(B^0 \to D^- X^+_{light})$. The decay $B^0 \to D^+ X^-_{light}$ is doubly Cabibbo suppressed and difficult to measure directly. Using $SU(3)$ flavor symmetry, it is possible to infer the value of $\mathcal{B}(B^0 \to D^+ X^-_{light})$ from the value of $\mathcal{B}(B \to D_s^+ X_{light})$, the latter being less suppressed.
If $X^+_{light} \equiv \pi^+$, then r is expected to be very small ($r \approx 0.02$) which implies a small asymmetry. In this case r may be deduced from the rate $\mathcal{B}(B^+ \to D_s^+\pi^0)$. We measure this branching ratio from a sample of 124 millions of $B\overline{B}$ pairs, we do not see any significant signal and quote an upper limit at 90% CL of : $\mathcal{B}(B^+ \to D_s^+\pi^0) < 2.8 \times 10^{-5}$ in agreement with a previous measurement by CLEO ($< 2.4 \times 10^{-4}$ from ref. [2]) and with the value of 0.9×10^{-5} expected from the rate of $\mathcal{B}(B^0 \to D_s^+\pi^-)$ measured by Belle and *BABAR* experiments. If $X^+_{light} \equiv a_0^+ (a_2^+)$, r might be quite large. This is due to the coupling constant of the W to the a_0 scalar meson (a_2 tensor meson) which is small and decreases the production rate of the Cabibbo allowed decay $B^0 \to D^- a_0^+(a_2^+)$. The factorization hypothesis predicts a similar rate for Cabibbo allowed and Cabibbo suppressed decays [5] which results in $r \approx 1$. These decays are not yet within the experiment reach (branching ratios around 10^{-6}), nevertheless, the theoretical predictions can be tested with the measurement of the branching ratio of the decay $B^0 \to D_s^+ a_0^- (a_2^-)$ expected at larger values : $\mathcal{B}(B^0 \to D_s^+ a_0^- (a_2^-) \approx 7.5(1.5) \times 10^{-5}$ (ref. [5,6]). From a sample of 230 million of $B\overline{B}$ pairs, we measure these two branching ratios. The a_0^- (a_2^-) is reconstructed in $a^-_{0(2)} \to \eta(\to \gamma\gamma)\pi^+$ which has a branching ratio of the order of 100 % (only 15 % for the a_2^-). We do not find any significant signal and quote the upper limits at 90% CL : $\mathcal{B}(B^0 \to D_s^+ a^-_{0(2)}) < 4.0\,(25) \times 10^{-5}$ which shows a discrepancy of at least a factor two with the theoretical prediction for a_0.

1.4. Charmless decays

The decay $B^+ \to K^{*+}(\to K^+\pi^0)\pi^0$ and its *CP* asymmetry are particularly interesting in light of the recent measurement of direct *CP* violation in the decay $B^0 \to K^+\pi^-$ [7]. It may provide valuable test of theoretical models such as those based on QCD factorization or SU(3) flavor symmetry. It has been argued that the influence of final state interactions like charming penguins and similar long distance rescattering effects on both the branching fraction and *CP* asymmetry of $B \to K\pi$ decays may be significant. From a sample of 232 million of $B\overline{B}$ pairs we find 88.5 ± 25.7 signal events which correspond to the branching ratio : $\mathcal{B}(B^+ \to K^{*+}\pi^0) = (6.9 \pm 2.0 \pm 1.3) \times 10^{-6}$ and we do not find any hint of direct *CP* violation : $\mathcal{A}_{CP} = 0.04 \pm 0.29 \pm 0.05$ [8]. These results do not rule out the charming penguins hypothesis considering the large values of the uncertainties for both the branching ratio and the *CP* asymmetry.

2. Selection of other recent analyses

2.1. Measurement of the $B^0 \to D^{*-} D_s^{*+}$ and $D_s^+ \to \phi\pi^+$ branching ratios

We present two measurements of the branching ratio $\mathcal{B}(B^0 \to D^{*-} D_s^{*+})$ which lead to a precise determination of the reference $\mathcal{B}(D_s^+ \to \phi\pi^+)$. They have been performed on a sample of 123 million of $B\overline{B}$ pairs. The $B^0 \to D^{*-} D_s^{*+} \to (\overline{D}^0\pi^-)(D_s^+\gamma)$ decay is reconstructed using two different methods. The first one combines the fully reconstructed D^{*-} with the photon from the $D_s^{*+} \to D_s^+\gamma$ decay, without explicit reconstruction of the D_s^+. To extract the num-

ber of partially reconstructed events, we compute the "missing mass" m_{miss} recoiling against the $D^{*-}\gamma$ system assuming that a $B^0 \to D^{*-}D_s^{*+} \to (\overline{D}^0\pi^-)(D_s^+\gamma)$ decay took place. For signal events, m_{miss} peaks at the D_s mass. We find, with this method, the following branching ratio : $\mathcal{B}_1 \equiv \mathcal{B}(B^0 \to D^{*-}D_s^{*+}) = (1.88 \pm 0.09 \pm 0.17)$ % which is in agreement with the factorization model prediction : $\mathcal{B}(B^0 \to D^{*-}D_s^{*+})_{theo} = (2.4 \pm 0.7)$ %. The second method uses a full reconstruction technique of the decay chain $B^0 \to D^{*-}D_s^{*+}$ where the D_s candidate is reconstructed in the mode : $D_s^+ \to \phi\pi^+ \to (K^+K^-)\pi^+$. We measure the branching ratio $\mathcal{B}_2 \equiv \mathcal{B}(B^0 \to D^{*-}D_s^{*+}) \times \mathcal{B}(D_s^+ \to \phi\pi^+) = (8.81 \pm 0.86_{stat}) \times 10^{-4}$.
From the ratio $\mathcal{B}_2/\mathcal{B}_1$, where many systematics cancel out, we get a precise measurement of : $\mathcal{B}(D_s^+ \to \phi\pi^+) = (4.81 \pm 0.52 \pm 0.38)$ %. [9]. which shows a different central value and an improvement on the uncertainty by about a factor of two compared to previous measurements [2].

2.2. Search for the rare decays $\overline{B}^0 \to D^{(*)0}\gamma$

Within the standard model, the rare decay $\overline{B}^0 \to D^{(*)0}\gamma$ is dominated by the W-boson exchange process. Its branching fraction is estimated to be of the order of 10^{-6} but the presence of a large $q\overline{q}$ g (color octet) component in the wave function of the B meson may reduce the color suppression enough to enhance the branching fraction by a factor of 10. A limit of $\mathcal{B}(\overline{B}^0 \to D^{(*)0}\gamma) < 5.0 \times 10^{-5}$ at 90% CL has been published by the CLEO collaboration. With 87.8 million of $B\overline{B}$ pairs, we set an upper limit of $\mathcal{B}(\overline{B}^0 \to D^{(*)0}\gamma) < 2.5 \times 10^{-5}$ at 90% CL [10]in agreement with the theoretical expectations.

2.3. Search for the rare decays $B^+ \to D^{(*)+}K^0$

This decay is expected to occur via a pure annihilation diagram. Such processes provide interesting insights into the internal dynamics of B mesons. This kind of diagram cannot be calculated in QCD factorization since both quarks play a role. The amplitudes are expected to be suppressed, with respect to the amplitudes of spectator quark trees, by a factor $f_B/m_B \approx 0.04$. The branching fractions are expected to be of the order of 10^{-8} and have never been observed. Some studies [11] indicate , though, that processes with a spectator quark can contribute to annihilation-mediated decays by *rescattering* and the branching ratio is expected to raise up to 10^{-5} if large rescattering occurs [11]. We reconstruct the two decay modes $B^+ \to D^{*+}K_S^0$ and $B^+ \to D^+K_S^0$ within a sample of 226 million of $B\overline{B}$ pairs. We do not see any significant excess of signal, we therefore set the upper limits at 90 % CL : $\mathcal{B}(B^+ \to D^+K_S^0) < 0.5 \times 10^{-5}$ and $\mathcal{B}(B^+ \to D^{*+}K_S^0) < 0.9 \times 10^{-5}$ thus beginning to constrain the rescattering effects.

2.4. Search for the rare decays $B^- \to D_s^{(*)-}\phi$

In this other annihilation process $B^- \to D_s^{(*)-}\phi$, the branching fraction is expected to be suppressed in the standard model down to 10^{-6}-10^{-7}. Searches of $B^- \to D_s^{(*)-}\phi$ decays could be sensitive to the new physics (NP) contributions such as Higgs doublet model which predicts a branching fraction of the order of 10^{-5} or the minimal supersymmetric model with R-parity violation which predicts 10^{-4}. Upper limits from CLEO are respectively 3.2 and 4.0×10^{-4} at 90% CL. Based on 234 million of $B\overline{B}$ pairs, and reconstructing D_s^- into $\phi\pi^-$ we have found no evidence for $B^- \to D_s^{(*)-}\phi$ decays. We set upper limits at 90% CL for: $\mathcal{B}(B^- \to D_s^-\phi) < 1.8 \times 10^{-6}$ and for $\mathcal{B}(B^- \to D_s^{*-}\phi) < 1.1 \times 10^{-5}$ [12] using the new *BABAR* $\mathcal{B}(D_s^- \to \phi\pi^-)$ value [section 2.1]. Our limits are more than two orders of magnitude lower than those of CLEO ruling out the two mentioned NP models.

2.5. Search for $B \to J/\psi\, D$ Decays

The spectra of the momentum of inclusive J/ψ mesons in the $\Upsilon(4S)$ rest frame observed by CLEO and by *BABAR*, compared with calculations using non-relativistic QCD (NRQCD), show an excess at low momentum, corresponding to a branching fraction of approximately 6×10^{-4}. Many hypotheses have been proposed to explain this result but no experimental evidence has been found to support them. The presence of $b\overline{u}c\overline{c}$ components (intrinsic charm) in

the B-meson wave function has also been suggested to enhance the branching ratio of decays such as $B \to J/\psi\,\overline{D}(\pi)$ to the order of 10^{-4} while pertubative QCD predicts a branching ratio for $B \to J/\psi\,\overline{D}$ of 10^{-8}-10^{-9}. We test the decay channels $B \to J/\psi\,D$ within a sample of 124 million of $B\overline{B}$ pairs. We do not find any evidence of signal and obtain upper limits of 1.3×10^{-5} for $B^0 \to J/\psi\,\overline{D}^0$ and 1.2×10^{-4} for $B^+ \to J/\psi\,D^+$ at 90 % CL. Therefore, intrinsic charm is ruled out as the explanation of low momentum J/ψ excess in B decays. More details on this analysis can be found in reference [13].

2.6. Production and decay of the Ξ_c^0 and Ω_c^0 at *BABAR*

We present a study of the Ξ_c^0 (csd) [14], and Ω_c^0 (ssc) [15] charmed baryons using for the former a luminosity of 116.1 fb^{-1} through two decay modes : $\Xi_c^0 \to \Omega^- K^+$ and $\Xi_c^0 \to \Xi^- \pi^+$. We measure, the ratio of the two decay rates to be $0.294 \pm 0.018 \pm 0.016$ which is compatible with the prediction, in a spectator quark model calculation, of 0.32. For Ω_c^0, we use 230 fb^{-1} and we reconstruct the baryon through three decay modes to compare the branching fractions $[\mathcal{B}1]$: $\Omega_c^0 \to \Omega^-\pi^+$, $[\mathcal{B}2]$: $\Omega_c^0 \to \Omega^-\pi^+\pi^-\pi^+$ and $[\mathcal{B}3]$: $\Omega_c^0 \to \Xi^- K^-\pi^+\pi^+$. We find the branching fraction ratios $[\mathcal{B}3]/[\mathcal{B}1] = 0.31 \pm 0.015 \pm 0.040$ and $[\mathcal{B}2]/[\mathcal{B}1] < 0.30$ at 90% CL. We also measure the p^* distribution of both charmed baryons, in the $\Upsilon(4S)$ frame, in order to study the production mechanisms in both $c\overline{c}$ and $B\overline{B}$ events. We find a double-peak structure in the p^* spectrum of either baryon. This is due to two production mechanisms: the peak at lower p^* is due to charmed baryon production in B meson decays (first observation in the case of Ω_c^0) and the peak at higher p^* is due to charmed baryon production from the $c\overline{c}$ continuum. From these spectra we compute the cross-section of the production of Ξ_c^0 in continuum : $\sigma(e^+e^- \to c\overline{c} \to \Xi_c^0 X) \times \mathcal{B}(\Xi_c^0 \to \Xi^-\pi^+) = (388 \pm 39 \pm 41)$ fb and the rate of Ξ_c^0 production in B decay : $\mathcal{B}(B \to \Xi_c^0 X) \times \mathcal{B}(\Xi_c^0 \to \Xi^-\pi^+) = (2.11 \pm 0.19 \pm 0.25) \times 10^{-4}$.

The high rate of Ξ_c^0 production at low p^* in B decays (below 1.2 GeV/c) implies that the invariant mass of the recoiling antibaryon system is typically above 2.0 GeV/c^2. This can be explained naturally by a substantial rate of charmed baryon pair production through the $b \to c\overline{c}s$ weak decay process which was observed indirectly in a previous *BABAR* analysis [16].

References

REFERENCES

1. A. Giri, Y. Grossman, A. Soffer and J. Zupan, *Phys. Rev.* D **68**, 054018 (2003).
2. S. Eidelman *et al.* [Particle Data Group], *Phys. Lett.* B **592**, 1 (2004).
3. B. Aubert *et al.* [*BABAR* collaboration], `hep-ex`/0505084 and references therein.
4. R. Aleksan *et al. Phys. Rev.* D **67**, 096002 (2003)
5. M. Diehl, G. Hiller, `hep-ph`/0105194
6. C.S. Kim, J.P. Lee, and M. Bauer, Z. Phys. **C 29**, 637 (1985).
7. B. Aubert *et al.* [*BABAR* collaboration], *Phys. Rev. Lett.* **93**, 131801 (2004); Y. Chao *et al.* [Belle collaboration], *Phys. Rev. Lett.* **93**, 191802 (2004).
8. B. Aubert *et al.* [*BABAR* collaboration], *Phys. Rev.* D **71**, 111101(R) (2005)
9. B. Aubert *et al.* [*BABAR* collaboration], *Phys. Rev.* D **71**, 091104 (2005) and references therein.
10. B. Aubert *et al.* [*BABAR* collaboration], `hep-ex`/0506070 and references therein. .
11. M. Blok, M. Gronau and J.L. Rosner, *Phys. Rev. Lett.* **78**, 3999 (1997).
12. B. Aubert *et al.* [*BABAR* collaboration], `hep-ex`/0506073 and references therein.
13. B. Aubert *et al.* [*BABAR* collaboration], *Phys. Rev.* D **71**, 091103 (2005) and references therein.
14. B. Aubert *et al* [*BABAR* collaboration],*Phys. Rev. Lett.* **95**, 142003 (2005) and references therein.
15. B. Aubert *et al* [*BABAR* collaboration], `hep-ex`/0507011 and references therein.
16. B. Aubert *et al.* [*BABAR* collaboration],*Phys. Rev.* D **70**, 091106 (2004).

BABAR-PUB-04/33
SLAC-PUB-10629

Measurement of the Branching Fractions for Inclusive B^- and $\overline{B}^0$ Decays to Flavor-tagged D, D_s and Λ_c

B. Aubert,[1] R. Barate,[1] D. Boutigny,[1] F. Couderc,[1] J.-M. Gaillard,[1] A. Hicheur,[1] Y. Karyotakis,[1] J. P. Lees,[1] V. Tisserand,[1] A. Zghiche,[1] A. Palano,[2] A. Pompili,[2] J. C. Chen,[3] N. D. Qi,[3] G. Rong,[3] P. Wang,[3] Y. S. Zhu,[3] G. Eigen,[4] I. Ofte,[4] B. Stugu,[4] G. S. Abrams,[5] A. W. Borgland,[5] A. B. Breon,[5] D. N. Brown,[5] J. Button-Shafer,[5] R. N. Cahn,[5] E. Charles,[5] C. T. Day,[5] M. S. Gill,[5] A. V. Gritsan,[5] Y. Groysman,[5] R. G. Jacobsen,[5] R. W. Kadel,[5] J. Kadyk,[5] L. T. Kerth,[5] Yu. G. Kolomensky,[5] G. Kukartsev,[5] G. Lynch,[5] L. M. Mir,[5] P. J. Oddone,[5] T. J. Orimoto,[5] M. Pripstein,[5] N. A. Roe,[5] M. T. Ronan,[5] V. G. Shelkov,[5] W. A. Wenzel,[5] M. Barrett,[6] K. E. Ford,[6] T. J. Harrison,[6] A. J. Hart,[6] C. M. Hawkes,[6] S. E. Morgan,[6] A. T. Watson,[6] M. Fritsch,[7] K. Goetzen,[7] T. Held,[7] H. Koch,[7] B. Lewandowski,[7] M. Pelizaeus,[7] M. Steinke,[7] J. T. Boyd,[8] N. Chevalier,[8] W. N. Cottingham,[8] M. P. Kelly,[8] T. E. Latham,[8] F. F. Wilson,[8] T. Cuhadar-Donszelmann,[9] C. Hearty,[9] N. S. Knecht,[9] T. S. Mattison,[9] J. A. McKenna,[9] D. Thiessen,[9] A. Khan,[10] P. Kyberd,[10] L. Teodorescu,[10] A. E. Blinov,[11] V. E. Blinov,[11] V. P. Druzhinin,[11] V. B. Golubev,[11] V. N. Ivanchenko,[11] E. A. Kravchenko,[11] A. P. Onuchin,[11] S. I. Serednyakov,[11] Yu. I. Skovpen,[11] E. P. Solodov,[11] A. N. Yushkov,[11] D. Best,[12] M. Bruinsma,[12] M. Chao,[12] I. Eschrich,[12] D. Kirkby,[12] A. J. Lankford,[12] M. Mandelkern,[12] R. K. Mommsen,[12] W. Roethel,[12] D. P. Stoker,[12] C. Buchanan,[13] B. L. Hartfiel,[13] S. D. Foulkes,[14] J. W. Gary,[14] B. C. Shen,[14] K. Wang,[14] D. del Re,[15] H. K. Hadavand,[15] E. J. Hill,[15] D. B. MacFarlane,[15] H. P. Paar,[15] Sh. Rahatlou,[15] V. Sharma,[15] J. W. Berryhill,[16] C. Campagnari,[16] B. Dahmes,[16] O. Long,[16] A. Lu,[16] M. A. Mazur,[16] J. D. Richman,[16] W. Verkerke,[16] T. W. Beck,[17] A. M. Eisner,[17] C. A. Heusch,[17] J. Kroseberg,[17] W. S. Lockman,[17] G. Nesom,[17] T. Schalk,[17] B. A. Schumm,[17] A. Seiden,[17] P. Spradlin,[17] D. C. Williams,[17] M. G. Wilson,[17] J. Albert,[18] E. Chen,[18] G. P. Dubois-Felsmann,[18] A. Dvoretskii,[18] D. G. Hitlin,[18] I. Narsky,[18] T. Piatenko,[18] F. C. Porter,[18] A. Ryd,[18] A. Samuel,[18] S. Yang,[18] S. Jayatilleke,[19] G. Mancinelli,[19] B. T. Meadows,[19] M. D. Sokoloff,[19] T. Abe,[20] F. Blanc,[20] P. Bloom,[20] S. Chen,[20] W. T. Ford,[20] U. Nauenberg,[20] A. Olivas,[20] P. Rankin,[20] J. G. Smith,[20] J. Zhang,[20] L. Zhang,[20] A. Chen,[21] J. L. Harton,[21] A. Soffer,[21] W. H. Toki,[21] R. J. Wilson,[21] Q. L. Zeng,[21] D. Altenburg,[22] T. Brandt,[22] J. Brose,[22] M. Dickopp,[22] E. Feltresi,[22] A. Hauke,[22] H. M. Lacker,[22] R. Müller-Pfefferkorn,[22] R. Nogowski,[22] S. Otto,[22] A. Petzold,[22] J. Schubert,[22] K. R. Schubert,[22] R. Schwierz,[22] B. Spaan,[22] J. E. Sundermann,[22] D. Bernard,[23] G. R. Bonneaud,[23] F. Brochard,[23] P. Grenier,[23] S. Schrenk,[23] Ch. Thiebaux,[23] G. Vasileiadis,[23] M. Verderi,[23] D. J. Bard,[24] P. J. Clark,[24] D. Lavin,[24] F. Muheim,[24] S. Playfer,[24] Y. Xie,[24] M. Andreotti,[25] V. Azzolini,[25] D. Bettoni,[25] C. Bozzi,[25] R. Calabrese,[25] G. Cibinetto,[25] E. Luppi,[25] M. Negrini,[25] L. Piemontese,[25] A. Sarti,[25] E. Treadwell,[26] F. Anulli,[27] R. Baldini-Ferroli,[27] A. Calcaterra,[27] R. de Sangro,[27] G. Finocchiaro,[27] P. Patteri,[27] I. M. Peruzzi,[27] M. Piccolo,[27] A. Zallo,[27] A. Buzzo,[28] R. Capra,[28] R. Contri,[28] G. Crosetti,[28] M. Lo Vetere,[28] M. Macri,[28] M. R. Monge,[28] S. Passaggio,[28] C. Patrignani,[28] E. Robutti,[28] A. Santroni,[28] S. Tosi,[28] S. Bailey,[29] G. Brandenburg,[29] K. S. Chaisanguanthum,[29] M. Morii,[29] E. Won,[29] R. S. Dubitzky,[30] U. Langenegger,[30] W. Bhimji,[31] D. A. Bowerman,[31] P. D. Dauncey,[31] U. Egede,[31] J. R. Gaillard,[31] G. W. Morton,[31] J. A. Nash,[31] M. B. Nikolich,[31] G. P. Taylor,[31] M. J. Charles,[32] G. J. Grenier,[32] U. Mallik,[32] J. Cochran,[33] H. B. Crawley,[33] J. Lamsa,[33] W. T. Meyer,[33] S. Prell,[33] E. I. Rosenberg,[33] A. E. Rubin,[33] J. Yi,[33] M. Biasini,[34] R. Covarelli,[34] M. Pioppi,[34] M. Davier,[35] X. Giroux,[35] G. Grosdidier,[35] A. Höcker,[35] S. Laplace,[35] F. Le Diberder,[35] V. Lepeltier,[35] A. M. Lutz,[35] T. C. Petersen,[35] S. Plaszczynski,[35] M. H. Schune,[35] L. Tantot,[35] G. Wormser,[35] C. H. Cheng,[36] D. J. Lange,[36] M. C. Simani,[36] D. M. Wright,[36] A. J. Bevan,[37] C. A. Chavez,[37] J. P. Coleman,[37] I. J. Forster,[37] J. R. Fry,[37] E. Gabathuler,[37] R. Gamet,[37] D. E. Hutchcroft,[37] R. J. Parry,[37] D. J. Payne,[37] R. J. Sloane,[37] C. Touramanis,[37] J. J. Back,[38,*] C. M. Cormack,[38] P. F. Harrison,[38,*] F. Di Lodovico,[38] G. B. Mohanty,[38,*] C. L. Brown,[39] G. Cowan,[39] R. L. Flack,[39] H. U. Flaecher,[39] M. G. Green,[39] P. S. Jackson,[39] T. R. McMahon,[39] S. Ricciardi,[39] F. Salvatore,[39] M. A. Winter,[39] D. Brown,[40] C. L. Davis,[40] J. Allison,[41] N. R. Barlow,[41] R. J. Barlow,[41] P. A. Hart,[41] M. C. Hodgkinson,[41] G. D. Lafferty,[41] A. J. Lyon,[41] J. C. Williams,[41] A. Farbin,[42] W. D. Hulsbergen,[42] A. Jawahery,[42] D. Kovalskyi,[42] C. K. Lae,[42] V. Lillard,[42] D. A. Roberts,[42] G. Blaylock,[43] C. Dallapiccola,[43] K. T. Flood,[43] S. S. Hertzbach,[43] R. Kofler,[43] V. B. Koptchev,[43] T. B. Moore,[43] S. Saremi,[43] H. Staengle,[43] S. Willocq,[43] R. Cowan,[44] G. Sciolla,[44] S. J. Sekula,[44] F. Taylor,[44] R. K. Yamamoto,[44]

D. J. J. Mangeol,[45] P. M. Patel,[45] S. H. Robertson,[45] A. Lazzaro,[46] V. Lombardo,[46] F. Palombo,[46] J. M. Bauer,[47] L. Cremaldi,[47] V. Eschenburg,[47] R. Godang,[47] R. Kroeger,[47] J. Reidy,[47] D. A. Sanders,[47] D. J. Summers,[47] H. W. Zhao,[47] S. Brunet,[48] D. Côté,[48] P. Taras,[48] H. Nicholson,[49] N. Cavallo,[50,†] F. Fabozzi,[50,†] C. Gatto,[50] L. Lista,[50] D. Monorchio,[50] P. Paolucci,[50] D. Piccolo,[50] C. Sciacca,[50] M. Baak,[51] H. Bulten,[51] G. Raven,[51] H. L. Snoek,[51] L. Wilden,[51] C. P. Jessop,[52] J. M. LoSecco,[52] T. Allmendinger,[53] K. K. Gan,[53] K. Honscheid,[53] D. Hufnagel,[53] H. Kagan,[53] R. Kass,[53] T. Pulliam,[53] A. M. Rahimi,[53] R. Ter-Antonyan,[53] Q. K. Wong,[53] J. Brau,[54] R. Frey,[54] O. Igonkina,[54] C. T. Potter,[54] N. B. Sinev,[54] D. Strom,[54] E. Torrence,[54] F. Colecchia,[55] A. Dorigo,[55] F. Galeazzi,[55] M. Margoni,[55] M. Morandin,[55] M. Posocco,[55] M. Rotondo,[55] F. Simonetto,[55] R. Stroili,[55] G. Tiozzo,[55] C. Voci,[55] M. Benayoun,[56] H. Briand,[56] J. Chauveau,[56] P. David,[56] Ch. de la Vaissière,[56] L. Del Buono,[56] O. Hamon,[56] M. J. J. John,[56] Ph. Leruste,[56] J. Malcles,[56] J. Ocariz,[56] M. Pivk,[56] L. Roos,[56] S. T'Jampens,[56] G. Therin,[56] P. F. Manfredi,[57] V. Re,[57] P. K. Behera,[58] L. Gladney,[58] Q. H. Guo,[58] J. Panetta,[58] C. Angelini,[59] G. Batignani,[59] S. Bettarini,[59] M. Bondioli,[59] F. Bucci,[59] G. Calderini,[59] M. Carpinelli,[59] F. Forti,[59] M. A. Giorgi,[59] A. Lusiani,[59] G. Marchiori,[59] F. Martinez-Vidal,[59,‡] M. Morganti,[59] N. Neri,[59] E. Paoloni,[59] M. Rama,[59] G. Rizzo,[59] F. Sandrelli,[59] J. Walsh,[59] M. Haire,[60] D. Judd,[60] K. Paick,[60] D. E. Wagoner,[60] N. Danielson,[61] P. Elmer,[61] Y. P. Lau,[61] C. Lu,[61] V. Miftakov,[61] J. Olsen,[61] A. J. S. Smith,[61] A. V. Telnov,[61] F. Bellini,[62] G. Cavoto,[61,62] R. Faccini,[62] F. Ferrarotto,[62] F. Ferroni,[62] M. Gaspero,[62] L. Li Gioi,[62] M. A. Mazzoni,[62] S. Morganti,[62] M. Pierini,[62] G. Piredda,[62] F. Safai Tehrani,[62] C. Voena,[62] S. Christ,[63] G. Wagner,[63] R. Waldi,[63] T. Adye,[64] N. De Groot,[64] B. Franek,[64] N. I. Geddes,[64] G. P. Gopal,[64] E. O. Olaiya,[64] R. Aleksan,[65] S. Emery,[65] A. Gaidot,[65] S. F. Ganzhur,[65] P.-F. Giraud,[65] G. Hamel de Monchenault,[65] W. Kozanecki,[65] M. Legendre,[65] G. W. London,[65] B. Mayer,[65] G. Schott,[65] G. Vasseur,[65] Ch. Yèche,[65] M. Zito,[65] M. V. Purohit,[66] A. W. Weidemann,[66] J. R. Wilson,[66] F. X. Yumiceva,[66] D. Aston,[67] R. Bartoldus,[67] N. Berger,[67] A. M. Boyarski,[67] O. L. Buchmueller,[67] R. Claus,[67] M. R. Convery,[67] M. Cristinziani,[67] G. De Nardo,[67] D. Dong,[67] J. Dorfan,[67] D. Dujmic,[67] W. Dunwoodie,[67] E. E. Elsen,[67] S. Fan,[67] R. C. Field,[67] T. Glanzman,[67] S. J. Gowdy,[67] T. Hadig,[67] V. Halyo,[67] C. Hast,[67] T. Hryn'ova,[67] W. R. Innes,[67] M. H. Kelsey,[67] P. Kim,[67] M. L. Kocian,[67] D. W. G. S. Leith,[67] J. Libby,[67] S. Luitz,[67] V. Luth,[67] H. L. Lynch,[67] H. Marsiske,[67] R. Messner,[67] D. R. Muller,[67] C. P. O'Grady,[67] V. E. Ozcan,[67] A. Perazzo,[67] M. Perl,[67] S. Petrak,[67] B. N. Ratcliff,[67] A. Roodman,[67] A. A. Salnikov,[67] R. H. Schindler,[67] J. Schwiening,[67] G. Simi,[67] A. Snyder,[67] A. Soha,[67] J. Stelzer,[67] D. Su,[67] M. K. Sullivan,[67] J. Va'vra,[67] S. R. Wagner,[67] M. Weaver,[67] A. J. R. Weinstein,[67] W. J. Wisniewski,[67] M. Wittgen,[67] D. H. Wright,[67] A. K. Yarritu,[67] C. C. Young,[67] P. R. Burchat,[68] A. J. Edwards,[68] T. I. Meyer,[68] B. A. Petersen,[68] C. Roat,[68] S. Ahmed,[69] M. S. Alam,[69] J. A. Ernst,[69] M. A. Saeed,[69] M. Saleem,[69] F. R. Wappler,[69] W. Bugg,[70] M. Krishnamurthy,[70] S. M. Spanier,[70] R. Eckmann,[71] H. Kim,[71] J. L. Ritchie,[71] A. Satpathy,[71] R. F. Schwitters,[71] J. M. Izen,[72] I. Kitayama,[72] X. C. Lou,[72] S. Ye,[72] F. Bianchi,[73] M. Bona,[73] F. Gallo,[73] D. Gamba,[73] L. Bosisio,[74] C. Cartaro,[74] F. Cossutti,[74] G. Della Ricca,[74] S. Dittongo,[74] S. Grancagnolo,[74] L. Lanceri,[74] P. Poropat,[74,§] L. Vitale,[74] G. Vuagnin,[74] R. S. Panvini,[75] Sw. Banerjee,[76] C. M. Brown,[76] D. Fortin,[76] P. D. Jackson,[76] R. Kowalewski,[76] J. M. Roney,[76] R. J. Sobie,[76] H. R. Band,[77] B. Cheng,[77] S. Dasu,[77] M. Datta,[77] A. M. Eichenbaum,[77] M. Graham,[77] J. J. Hollar,[77] J. R. Johnson,[77] P. E. Kutter,[77] H. Li,[77] R. Liu,[77] A. Mihalyi,[77] A. K. Mohapatra,[77] Y. Pan,[77] R. Prepost,[77] P. Tan,[77] J. H. von Wimmersperg-Toeller,[77] J. Wu,[77] S. L. Wu,[77] Z. Yu,[77] M. G. Greene,[78] and H. Neal[78]

(The *BABAR* Collaboration)

[1]*Laboratoire de Physique des Particules, F-74941 Annecy-le-Vieux, France*
[2]*Università di Bari, Dipartimento di Fisica and INFN, I-70126 Bari, Italy*
[3]*Institute of High Energy Physics, Beijing 100039, China*
[4]*University of Bergen, Inst. of Physics, N-5007 Bergen, Norway*
[5]*Lawrence Berkeley National Laboratory and University of California, Berkeley, CA 94720, USA*
[6]*University of Birmingham, Birmingham, B15 2TT, United Kingdom*
[7]*Ruhr Universität Bochum, Institut für Experimentalphysik 1, D-44780 Bochum, Germany*
[8]*University of Bristol, Bristol BS8 1TL, United Kingdom*
[9]*University of British Columbia, Vancouver, BC, Canada V6T 1Z1*
[10]*Brunel University, Uxbridge, Middlesex UB8 3PH, United Kingdom*
[11]*Budker Institute of Nuclear Physics, Novosibirsk 630090, Russia*
[12]*University of California at Irvine, Irvine, CA 92697, USA*
[13]*University of California at Los Angeles, Los Angeles, CA 90024, USA*
[14]*University of California at Riverside, Riverside, CA 92521, USA*
[15]*University of California at San Diego, La Jolla, CA 92093, USA*

[16] University of California at Santa Barbara, Santa Barbara, CA 93106, USA
[17] University of California at Santa Cruz, Institute for Particle Physics, Santa Cruz, CA 95064, USA
[18] California Institute of Technology, Pasadena, CA 91125, USA
[19] University of Cincinnati, Cincinnati, OH 45221, USA
[20] University of Colorado, Boulder, CO 80309, USA
[21] Colorado State University, Fort Collins, CO 80523, USA
[22] Technische Universität Dresden, Institut für Kern- und Teilchenphysik, D-01062 Dresden, Germany
[23] Ecole Polytechnique, LLR, F-91128 Palaiseau, France
[24] University of Edinburgh, Edinburgh EH9 3JZ, United Kingdom
[25] Università di Ferrara, Dipartimento di Fisica and INFN, I-44100 Ferrara, Italy
[26] Florida A&M University, Tallahassee, FL 32307, USA
[27] Laboratori Nazionali di Frascati dell'INFN, I-00044 Frascati, Italy
[28] Università di Genova, Dipartimento di Fisica and INFN, I-16146 Genova, Italy
[29] Harvard University, Cambridge, MA 02138, USA
[30] Universität Heidelberg, Physikalisches Institut, Philosophenweg 12, D-69120 Heidelberg, Germany
[31] Imperial College London, London, SW7 2AZ, United Kingdom
[32] University of Iowa, Iowa City, IA 52242, USA
[33] Iowa State University, Ames, IA 50011-3160, USA
[34] Università di Perugia, Dipartimento di Fisica and INFN, I-06100 Perugia, Italy
[35] Laboratoire de l'Accélérateur Linéaire, F-91898 Orsay, France
[36] Lawrence Livermore National Laboratory, Livermore, CA 94550, USA
[37] University of Liverpool, Liverpool L69 72E, United Kingdom
[38] Queen Mary, University of London, E1 4NS, United Kingdom
[39] University of London, Royal Holloway and Bedford New College, Egham, Surrey TW20 0EX, United Kingdom
[40] University of Louisville, Louisville, KY 40292, USA
[41] University of Manchester, Manchester M13 9PL, United Kingdom
[42] University of Maryland, College Park, MD 20742, USA
[43] University of Massachusetts, Amherst, MA 01003, USA
[44] Massachusetts Institute of Technology, Laboratory for Nuclear Science, Cambridge, MA 02139, USA
[45] McGill University, Montréal, QC, Canada H3A 2T8
[46] Università di Milano, Dipartimento di Fisica and INFN, I-20133 Milano, Italy
[47] University of Mississippi, University, MS 38677, USA
[48] Université de Montréal, Laboratoire René J. A. Lévesque, Montréal, QC, Canada H3C 3J7
[49] Mount Holyoke College, South Hadley, MA 01075, USA
[50] Università di Napoli Federico II, Dipartimento di Scienze Fisiche and INFN, I-80126, Napoli, Italy
[51] NIKHEF, National Institute for Nuclear Physics and High Energy Physics, NL-1009 DB Amsterdam, The Netherlands
[52] University of Notre Dame, Notre Dame, IN 46556, USA
[53] Ohio State University, Columbus, OH 43210, USA
[54] University of Oregon, Eugene, OR 97403, USA
[55] Università di Padova, Dipartimento di Fisica and INFN, I-35131 Padova, Italy
[56] Universités Paris VI et VII, Laboratoire de Physique Nucléaire et de Hautes Energies, F-75252 Paris, France
[57] Università di Pavia, Dipartimento di Elettronica and INFN, I-27100 Pavia, Italy
[58] University of Pennsylvania, Philadelphia, PA 19104, USA
[59] Università di Pisa, Dipartimento di Fisica, Scuola Normale Superiore and INFN, I-56127 Pisa, Italy
[60] Prairie View A&M University, Prairie View, TX 77446, USA
[61] Princeton University, Princeton, NJ 08544, USA
[62] Università di Roma La Sapienza, Dipartimento di Fisica and INFN, I-00185 Roma, Italy
[63] Universität Rostock, D-18051 Rostock, Germany
[64] Rutherford Appleton Laboratory, Chilton, Didcot, Oxon, OX11 0QX, United Kingdom
[65] DSM/Dapnia, CEA/Saclay, F-91191 Gif-sur-Yvette, France
[66] University of South Carolina, Columbia, SC 29208, USA
[67] Stanford Linear Accelerator Center, Stanford, CA 94309, USA
[68] Stanford University, Stanford, CA 94305-4060, USA
[69] State University of New York, Albany, NY 12222, USA
[70] University of Tennessee, Knoxville, TN 37996, USA
[71] University of Texas at Austin, Austin, TX 78712, USA
[72] University of Texas at Dallas, Richardson, TX 75083, USA
[73] Università di Torino, Dipartimento di Fisica Sperimentale and INFN, I-10125 Torino, Italy
[74] Università di Trieste, Dipartimento di Fisica and INFN, I-34127 Trieste, Italy
[75] Vanderbilt University, Nashville, TN 37235, USA
[76] University of Victoria, Victoria, BC, Canada V8W 3P6
[77] University of Wisconsin, Madison, WI 53706, USA
[78] Yale University, New Haven, CT 06511, USA

(Dated: February 19, 2007)

We report on the inclusive branching fractions of B^- and of $\overline{B}^0$ mesons decaying to D^0X, $\overline{D}^0X$, D^+X, D^-X, D_s^+X, D_s^-X, Λ_c^+X, $\overline{\Lambda}_c^-X$, based on a sample of 88.9 million $B\overline{B}$ events recorded with the *BABAR* detector at the $\Upsilon(4S)$ resonance. Events are selected by completely reconstructing one B and searching for a reconstructed charmed particle in the rest of the event. We measure the number of charmed and of anti-charmed particles per B decay and derive the total charm yield per B^- decay, $n_c^- = 1.313 \pm 0.037 \pm 0.062^{+0.063}_{-0.042}$, and per $\overline{B}^0$ decay, $n_c^0 = 1.276 \pm 0.062 \pm 0.058^{+0.066}_{-0.046}$ where the first uncertainty is statistical, the second is systematic, and the third reflects the charm branching-fraction uncertainties.

PACS numbers: 13.25.Hw, 12.15.Hh, 11.30.Er

The dominant process for the decay of a b quark is $b \to cW^{*-}$ [1], resulting in a (flavor) correlated c quark and a virtual W. In the decay of the W, the production of a $\overline{u}d$ or a $\overline{c}s$ pair are both Cabibbo-allowed and should be equal, the latter being only suppressed by a phase-space factor. The first process dominates hadronic b decays, while the second can be easily distinguished as it will produce a (flavor) anti-correlated $\overline{c}$ quark. Experimentally, correlated and anti-correlated charm production can be investigated through the measurement of the inclusive B-decay rates to flavor-tagged charmed mesons or baryons. Current measurements [2–4] of these rates have statistically limited precision and do not distinguish among the different B parent states.

Most of the charged and neutral D mesons produced in $\overline{B}$ decays come from correlated production $\overline{B} \to DX$. However, a significant number of $\overline{B} \to \overline{D}X$ decays are expected through $b \to c\overline{c}s$ transitions, such as $\overline{B} \to D^{(*)}\overline{D}^{(*)}\overline{K}^{(*)}(n\pi)$. Although the branching fractions of the 3-body decays $\overline{B} \to D^{(*)}\overline{D}^{(*)}\overline{K}$ have been measured [5, 6], it is not clear whether they saturate $\overline{B} \to \overline{D}X$ transitions. It is therefore important to improve the precision on the branching fraction $\mathcal{B}(\overline{B} \to \overline{D}X)$.

By contrast, the anti-correlated D_s^- production $\overline{B} \to D_s^- D(n\pi)$ is expected to dominate $\overline{B}$ decays to D_s mesons, since correlated production needs an extra $s\overline{s}$ pair created from the vacuum to give $\overline{B} \to D_s^+ K^-(n\pi)$. There is no prior published measurement of $\mathcal{B}(\overline{B} \to D_s^+X)$.

All strangeless charmed baryons decay to Λ_c. Correlated Λ_c are produced in decays like $B^- \to \Lambda_c^+ \overline{p}\pi^-(\pi)$, while anti-correlated $\overline{\Lambda}_c^-$ should originate from $B^- \to \Xi_c\overline{\Lambda}_c^-(\pi)$. Another possibility is $B^- \to \Lambda_c^+\overline{\Lambda}_c^- K^-$, the baryonic analogue of the $D\overline{D}K$ decay. The rates for Ξ_c production in B decays [7] are unknown, because there is no absolute measurement of Ξ_c decay branching fractions.

This analysis uses $\Upsilon(4S) \to B\overline{B}$ events in which either a B^+ or a B^0 meson (hereafter denoted B_{reco}) decays into a hadronic final state and is fully reconstructed. We then reconstruct D, D_s and Λ_c from the recoiling B^- ($\overline{B}^0$) meson and compare the flavor of the charm hadron with that of the B_{reco}, thus allowing separate measurements of the B^- ($\overline{B}^0$) $\to D^0\ X$, $D^+\ X$, $D_s^+\ X$, $\Lambda_c^+\ X$ and B^- ($\overline{B}^0$) $\to \overline{D}^0\ X$, $D^-\ X$, $D_s^-\ X$, $\overline{\Lambda}_c^-\ X$ branching fractions. We extract $\mathcal{B}(B^- \to \Lambda_c^+\overline{\Lambda}_c^- K^-)$ from the missing-mass spectra of the $\Lambda_c^+K^-$ or $\overline{\Lambda}_c^-K^-$ systems recoiling against the B_{reco}. We can then evaluate indirectly $\mathcal{B}(B^- \to \Xi_c X) = \mathcal{B}(B^- \to \overline{\Lambda}_c^- X) - \mathcal{B}(B^- \to \Lambda_c^+\overline{\Lambda}_c^- K^-)$ and compute the average number of charm (anti-charm) particles per B^- decay, N_c^- ($N_{\overline{c}}^-$):

$$N_c^- = \sum_{X_c} \mathcal{B}(B^- \to X_c X), \quad (1)$$

$$N_{\overline{c}}^- = \sum_{\overline{X}_c} \mathcal{B}(B^- \to \overline{X}_c X), \quad (2)$$

where the sum is performed over $X_c = D^+$, D^0, D_s^+, Λ_c^+, Ξ_c, $(c\overline{c})$ or $\overline{X}_c = D^-$, $\overline{D}^0$, D_s^-, $\overline{\Lambda}_c^-$, $(c\overline{c})$, and $(c\overline{c})$ refers to all charmonium states collectively. We neglect $\overline{\Xi}_c$ production, as it requires both a $\overline{c}s$ and an $s\overline{s}$ pair in the decay to give $\overline{\Xi}_c\Omega_c$. We can sum N_c^- and $N_{\overline{c}}^-$ to obtain the average number of charm plus anti-charm quarks per B^- decay, $n_c^- = N_c^- + N_{\overline{c}}^-$ (and similarly for $\overline{B}^0$ decays). In addition to the theoretical interest [8–10], the fact that anti-correlated charmed particles are a background for many studies also motivates a more precise measurement of their production rates in B decays.

The measurements presented here are based on a sample of 88.9 million $B\overline{B}$ pairs (81.9 fb^{-1}) recorded at the $\Upsilon(4S)$ resonance with the *BABAR* detector at the PEP-II asymmetric-energy B-meson factory at SLAC. The *BABAR* detector is described in detail elsewhere [11]. Charged-particle trajectories are measured by a 5-layer double-sided silicon vertex tracker and a 40-layer drift chamber, both operating in a 1.5-T solenoidal magnetic field. Charged-particle identification is provided by the average energy loss (dE/dx) in the tracking devices and by an internally reflecting ring-imaging Cherenkov detector. Photons are detected by a CsI(Tl) electromagnetic calorimeter. We use Monte Carlo simulations of the *BABAR* detector based on GEANT4 [12] to optimize selection criteria and determine selection efficiencies.

We reconstruct B^+ and B^0 decays (B_{reco}) in the modes $B^+ \to \overline{D}^{(*)0}\pi^+$, $\overline{D}^{(*)0}\rho^+$, $\overline{D}^{(*)0}a_1^+$ and $B^0 \to D^{(*)-}\pi^+$, $D^{(*)-}\rho^+$, $D^{(*)-}a_1^+$. $\overline{D}^0$ candidates are reconstructed in the $K^+\pi^-$, $K^+\pi^-\pi^0$, $K^+\pi^-\pi^+\pi^-$ and $K_S^0\pi^+\pi^-(K_S^0 \to \pi^+\pi^-)$ decay channels, while D^- are reconstructed in the $K^+\pi^-\pi^-$ and $K_S^0\pi^-$ modes. D^* candidates are reconstructed in the $D^{*-} \to \overline{D}^0\pi^-$ and $\overline{D}^{*0} \to \overline{D}^0\pi^0$, $\overline{D}^0\gamma$ decay modes. The first kinematic variable used to

identify fully reconstructed B decays is the beam-energy substituted mass, $m_{\rm ES} = \sqrt{(s/2 + \mathbf{p}_i \cdot \mathbf{p}_B)^2/E_i^2 - \mathbf{p}_B^2}$, where $\mathbf{p}_B$ is the B_{reco} momentum and $(E_i, \mathbf{p}_i)$ is the four-momentum of the initial e^+e^- system, both measured in the laboratory frame. The invariant mass of the initial e^+e^- system is $\sqrt{s}$. The second variable is $\Delta E = E_B^* - \sqrt{s}/2$, where E_B^* is the $B_{\rm reco}$ candidate energy in the center-of-mass frame. We require $|\Delta E| < n\,\sigma_{\Delta E}$ with $n = 2$ or 3, depending on the decay mode, and using the measured resolution $\sigma_{\Delta E}$ for each decay mode.

In the $m_{\rm ES}$ spectra (Fig. 1), we define a signal region with $5.274 < m_{\rm ES} < 5.290$ GeV/c^2 and a background control region with $5.220 < m_{\rm ES} < 5.260$ GeV/c^2. For each of the B-decay modes, the combinatorial background in the signal region is derived from a fit to the $m_{\rm ES}$ distribution that uses an empirical phase-space threshold function [13] for the background, together with a signal function [14] peaked at the B meson mass. The numbers of reconstructed B^+ and B^0 candidates, $N_{B^+} = 85840 \pm 1910$ (syst.) and $N_{B^0} = 48322 \pm 590$ (syst.), are then obtained by subtracting this background from the total number of events found in the signal region. These measured B meson yields provide the normalization of all branching fraction measurements reported below. The systematic uncertainties quoted above are computed by varying the boundaries of the signal and background regions, and by comparing the shapes of the threshold function [13] in the data and in the simulation.

The contamination of B^0 events in the B^+ signal induces a background which peaks near the B mass. From the Monte Carlo simulation, the fraction of B^0 events in the reconstructed B^+ signal sample is found to be $c_0 = 0.034$, and the fraction of B^+ events in the reconstructed B^0 signal sample to be $c_+ = 0.019$. A 100 % systematic uncertainty is conservatively assigned to these numbers but they will have a small effect on the final results.

We now turn to the analysis of inclusive D, D_s and Λ_c production in the decays of the $\overline{B}$'s that recoil against the reconstructed B. Charmed particles X_c (correlated production) are distinguished from anti-charmed particles $\overline{X}_c$ (anti-correlated production). They are reconstructed from charged tracks that do not belong to the B_{reco}. The decay modes considered are listed in Table I.

For charged B decays, Fig. 2 shows the D, D_s, and Λ_c mass spectra of correlated and anti-correlated candidates recoiling against B's reconstructed in the $m_{\rm ES}$ signal region, for some selected decay modes. These spectra are fitted with the sum of a Gaussian signal and a linear background (including a satellite peak for some channels [15]). The shaded areas correspond to well reconstructed D, D_s or Λ_c from the combinatorial $B_{\rm reco}$ background. They are obtained from data in the $m_{\rm ES}$ background control region, normalized to the number of combinatorial background events expected under the

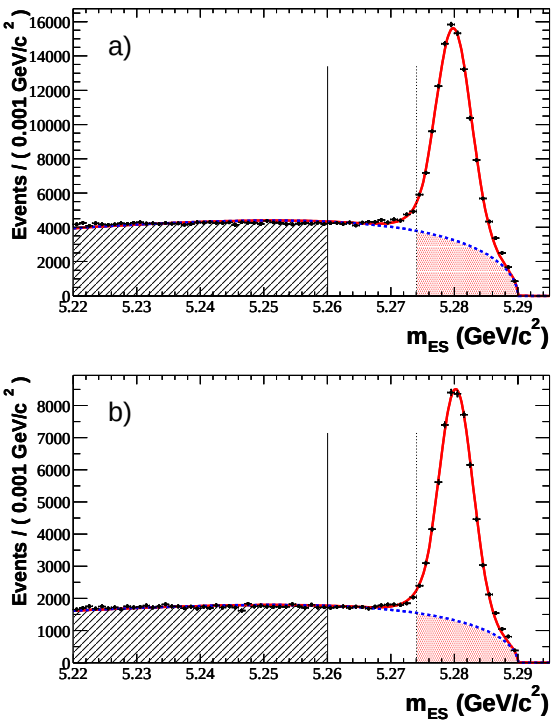

FIG. 1: $m_{\rm ES}$ spectra of reconstructed (a) B^+ and (b) B^0 candidates. The full vertical line shows the upper limit of the background control region (hatched), the dotted vertical line the lower limit of the B signal region. The crossed area shows the background under the B signal. The solid curve is the sum of the fitted signal and background, the dashed curve is the background component only.

B_{reco} peak. The background-subtracted reconstructed signal yields are listed in Table I. The reconstruction efficiencies for each charmed (anti-charmed) final state $X_c \to f$ ($\overline{X}_c \to \overline{f}$) are computed from the simulation as a function of the charmed-particle momentum in the B^- center-of-mass frame, and are applied event-by-event to obtain the efficiency-corrected charm signal yields $N(X_c \to f)$ ($N(\overline{X}_c \to \overline{f})$). The final branching fractions are computed from these yields, the number of B_{reco}, and the intermediate branching fractions $\mathcal{B}(X_c \to f)$ taken from [16]. They are given by

$$\mathcal{B}(B^- \to X_c X) = \frac{N(X_c \to f)}{N_{B^+} \times \mathcal{B}(X_c \to f)} - c_0 \mathcal{B}_0. \qquad (3)$$

Here the raw branching fraction for $B^- \to X_c X$ is modified by a small corrective term, $c_0\mathcal{B}_0$, that accounts for the B^0 contamination in the reconstructed B^+ sample. The factor $\mathcal{B}_0$ depends on the measured $\overline{B}^0 \to X_c X$ and $B^0 \to X_c X$ branching fractions, and on the $B^0 - \overline{B}^0$ mixing parameter χ_d [16]. It ranges from less than 3% for Λ_c to as much as 50% for correlated D^0 and D^+. Doubly Cabibbo-suppressed D^0 decays are also taken into account. The branching fractions and their errors are

TABLE I: Charmed-particle signal yields and B branching fractions per decay mode. The first uncertainty is statistical, the second is systematic (but does not include the charm branching fraction uncertainties).

X_c decay mode	$B^- \to X_c X$		$B^- \to \overline{X}_c X$		$\overline{B}^0 \to X_c X$		$\overline{B}^0 \to \overline{X}_c X$	
	yield	$\mathcal{B}(\%)$	yield	$\mathcal{B}(\%)$	yield	$\mathcal{B}(\%)$	yield	$\mathcal{B}(\%)$
$D^0 \to K^-\pi^+$	1273±42	79.2±2.6±3.9	160±16	9.3±1.0±0.5	397±24	50.3±3.4±2.4	139±14	7.3±2.2±0.5
$\to K^-\pi^+\pi^-\pi^+$	998±65	80.6±5.3±7.5	173±30	13.4±2.4±1.3	332±36	56.2±6.8±5.4	83±23	1.8±4.4±0.5
$D^+ \to K^-\pi^+\pi^+$	262±29	9.8±1.2±1.2	98±20	3.8±0.9±0.4	452±31	39.7±3.0±2.8	125±18	2.3±1.8±0.3
$D_s^+ \to \phi\pi^+$	11±5	2.2±1.1±0.3	82±11	16.5±2.3±1.7	24±6	8.3±2.8±0.8	28±6	9.9±2.9±1.0
$\to \overline{K}^{*0}K^+$	0±3	0.0±1.1±0.2	55±11	18.0±3.5±1.7	3±4	0.0±2.8±0.1	14±5	9.9±4.1±1.2
$\to K_S^0 K^+$	0±3	0.0±0.9±0.2	31±9	9.2±2.7±0.8	12±5	5.0±3.4±0.4	23±6	13.3±4.3±1.0
$\Lambda_c^+ \to pK^-\pi^+$	41±9	3.5±0.8±0.3	33±9	2.9±0.8±0.3	28±8	4.9±1.7±0.4	16±6	2.0±1.2±0.2

given in Table I. The statistical and systematic uncertainties are computed separately for each channel. For example, the 3.9% absolute systematic uncertainty on $\mathcal{B}(B^- \to D^0(K^-\pi^+)X)$ reflects the quadratic sum of 1.8% attributed to N_{B^+}, 1.3% to the error on the rate of true D's in the B combinatorial background, 0.8% to the Monte Carlo statistics, 1.2% to the track-finding efficiency, 2.5% to the particle identification, 1.2% to c_0, and 0.1% to $\mathcal{B}_0$. We combine the results from the different D^0 and D_s decay modes to extract the final branching fractions listed in Table II.

TABLE II: Combined B^- branching fractions. The first uncertainty is statistical, the second is systematic, and the third reflects charm branching-fraction uncertainties [16].

	correlated	anti-correlated
X_c	$\mathcal{B}(B^- \to X_c X)(\%)$	$\mathcal{B}(B^- \to \overline{X}_c X)(\%)$
D^0	$79.3 \pm 2.5 \pm 4.0^{+2.0}_{-1.9}$	$9.8 \pm 0.9 \pm 0.5^{+0.3}_{-0.3}$
D^+	$9.8 \pm 1.2 \pm 1.2^{+0.8}_{-0.7}$	$3.8 \pm 0.9 \pm 0.4^{+0.3}_{-0.3}$
D_s^+	$0.5 \pm 0.6 \pm 0.2^{+0.2}_{-0.1}$	$14.3 \pm 1.6 \pm 1.5^{+4.9}_{-3.0}$
	< 2.2 at 90% CL	
Λ_c^+	$3.5 \pm 0.8 \pm 0.3^{+1.3}_{-0.8}$	$2.9 \pm 0.8 \pm 0.3^{+1.1}_{-0.6}$

To extract N_c from these numbers, we need to evaluate the contribution of $B^- \to \Lambda_c^+ \overline{\Lambda}_c^- K^-$. Combining the four-momenta of the recoiling B^-, of a K^- and of the reconstructed Λ_c^+ or $\overline{\Lambda}_c^-$ candidate, we compute the missing mass: the absence of signal at the Λ_c mass excludes a significant contribution of this process. We therefore take $\mathcal{B}(B^- \to \Xi_c X) = \mathcal{B}(B^- \to \overline{\Lambda}_c^- X)$ in the computation of N_c. Using Eqs. 1 and 2 and taking $\mathcal{B}(B^- \to (c\overline{c})X) = (2.3 \pm 0.3)\%$ [17] [18], one obtains:

$$\begin{aligned} N_c^- &= 0.983 \pm 0.030 \pm 0.046^{+0.028}_{-0.023}, \\ N_{\overline{c}}^- &= 0.330 \pm 0.022 \pm 0.020^{+0.051}_{-0.031}, \\ n_c^- &= 1.313 \pm 0.037 \pm 0.062^{+0.063}_{-0.042}. \end{aligned}$$

The reconstruction of D, D_s and Λ_c from $\overline{B}^0$ decays is performed in the same way as that in the B^- analysis. The corresponding yields are listed in Table I. We then compute for each decay channel $X_c \to f$ the efficiency-corrected signal yields $N(X_c \to f)$ ($N(\overline{X}_c \to \bar{f})$) and define the raw branching fractions $\mathcal{B}_c$ and $\overline{\mathcal{B}}_c$ as

$$\mathcal{B}_c = N(X_c \to f)/[N_{B^0} \times \mathcal{B}(X_c \to f)] \quad (4)$$

$$\overline{\mathcal{B}}_c = N(\overline{X}_c \to \bar{f})/[N_{B^0} \times \mathcal{B}(X_c \to f)]. \quad (5)$$

After correcting these numbers for $B^0\overline{B}^0$ mixing, we obtain the final branching fraction for $\overline{B}^0 \to X_c X$:

$$\mathcal{B}(\overline{B}^0 \to X_c X) = \frac{\mathcal{B}_c - \chi_d(\mathcal{B}_c + \overline{\mathcal{B}}_c) - c_+\mathcal{B}_+}{1 - 2\chi_d}, \quad (6)$$

where $\chi_d = 0.181 \pm 0.004$ is the $B^0 - \overline{B}^0$ mixing parameter [16]. The correcting factor $\mathcal{B}_+$ accounts for B^+ contamination in the B^0 sample and depends on $\mathcal{B}(B^- \to X_c X)$ and $\mathcal{B}(B^+ \to X_c X)$. The results are given in Table I. Combining the different D^0 or D_s modes, we obtain the final branching fractions listed in Table III.

TABLE III: Combined $\overline{B}^0$ branching fractions. The first uncertainty is statistical, the second is systematic, and the third reflects charm branching-fraction uncertainties [16].

	correlated	anti-correlated
X_c	$\mathcal{B}(\overline{B}^0 \to X_c X)(\%)$	$\mathcal{B}(\overline{B}^0 \to \overline{X}_c X)(\%)$
D^0	$51.1 \pm 3.1 \pm 2.5^{+1.3}_{-1.3}$	$6.3 \pm 1.9 \pm 0.5^{+0.2}_{-0.2}$
D^+	$39.7 \pm 3.0 \pm 2.8^{+2.8}_{-2.5}$	$2.3 \pm 1.8 \pm 0.3^{+0.2}_{-0.2}$
		< 5.1 at 90% CL
D_s^+	$3.9 \pm 1.7 \pm 0.4^{+1.3}_{-0.8}$	$10.9 \pm 2.1 \pm 0.8^{+3.8}_{-2.3}$
	< 8.7 at 90% CL	
Λ_c^+	$4.9 \pm 1.7 \pm 0.4^{+1.8}_{-1.0}$	$2.0 \pm 1.2 \pm 0.2^{+0.7}_{-0.4}$
		< 3.8 at 90% CL

To compute N_c, we neglect $\overline{B}^0 \to \Lambda_c^+ \overline{\Lambda}_c^- K^0$ production and assume that $\mathcal{B}(\overline{B}^0 \to \Xi_c X) = \mathcal{B}(\overline{B}^0 \to \overline{\Lambda}_c^- X)$. Substituting $\overline{B}^0$ for B^- in Eqs. 1 and 2 and taking

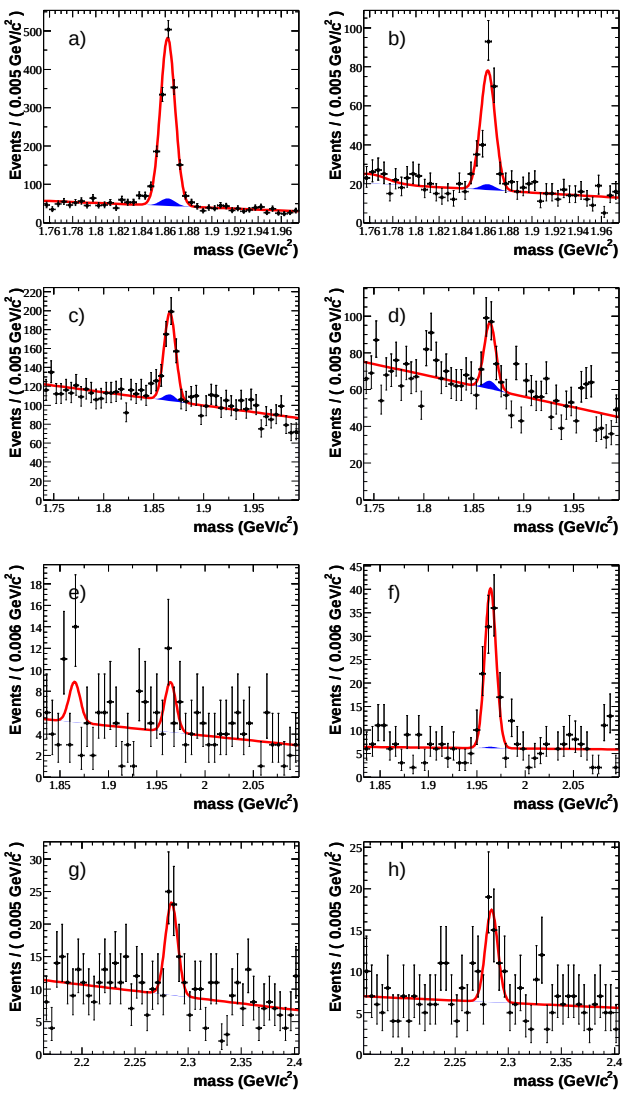

FIG. 2: Correlated (left) and anti-correlated (right) charmed particle mass spectra in the recoil of B^+ events, for (a),(b) $D^0 \to K^-\pi^+$; (c),(d) $D^+ \to K^-\pi^+\pi^+$; (e),(f) $D_s^+ \to \phi\pi^+$; and (g),(h) $\Lambda_c^+ \to pK^-\pi^+$. The solid curve is the sum of a Gaussian signal and of a linear background plus mode-dependent satellite contributions [15]. The shaded areas show the contribution of well reconstructed D, D_s or Λ_c in the B^+ combinatorial background.

$\mathcal{B}(B^0 \to (c\overline{c})X) = (2.3 \pm 0.3)\%$ [17] [18], we obtain:

$$\begin{aligned} N_c^0 &= 1.039 \pm 0.051 \pm 0.049^{+0.039}_{-0.031}, \\ N_{\overline{c}}^0 &= 0.237 \pm 0.036 \pm 0.012^{+0.039}_{-0.024}, \\ n_c^0 &= 1.276 \pm 0.062 \pm 0.058^{+0.066}_{-0.046}. \end{aligned}$$

We also compute the fraction of anti-correlated charm production in B decays, $w(\overline{X}_c) = \mathcal{B}(\overline{B} \to \overline{X}_c X)/(\mathcal{B}(\overline{B} \to X_c X) + \mathcal{B}(\overline{B} \to \overline{X}_c X))$. Here, many systematic uncertainties cancel (tracking, K identification, D branching fractions, B counting). The results are given in Table IV. We obtain an upper limit on the correlated D_s^+ fraction in B^- decays : $\mathcal{B}(B^- \to D_s^+ X)/\mathcal{B}(B^- \to D_s^\pm X) < 0.126$ at 90% CL.

TABLE IV: Fraction w of anti-correlated charm.

Mode	B^- decays	$\overline{B}^0$ decays
$\overline{D}^0 X$	$0.110 \pm 0.010 \pm 0.003$	$0.110 \pm 0.031 \pm 0.008$
$D^- X$	$0.278 \pm 0.052 \pm 0.009$	$0.055 \pm 0.040 \pm 0.006$
$D_s^- X$	$0.966 \pm 0.039 \pm 0.012$	$0.733 \pm 0.092 \pm 0.010$
$\overline{\Lambda}_c^- X$	$0.452 \pm 0.090 \pm 0.003$	$0.286 \pm 0.142 \pm 0.007$

In conclusion, we have measured for the first time the branching fractions for inclusive decays of B mesons to flavor-tagged D, D_s and Λ_c, separately for B^- and $\overline{B}^0$. We observe significant production of anti-correlated D^0 and D^+ mesons in B decays (Table IV), with the branching fractions detailed in Tables II and III. The correlated D_s production in B^- decays is measured to be small.

As expected, the sum of all correlated charm branching fractions, N_c, is compatible with 1, for charged as well as for neutral B's. The numbers of charmed particles per B^- decay ($n_c^- = 1.313 \pm 0.037 \pm 0.062^{+0.063}_{-0.042}$) and per $\overline{B}^0$ decay ($n_c^0 = 1.276 \pm 0.062 \pm 0.058^{+0.066}_{-0.046}$) are consistent with previous measurements [2, 17, 19] and with theoretical expectations [8–10].

We are grateful for the excellent luminosity and machine conditions provided by our PEP-II colleagues, and for the substantial dedicated effort from the computing organizations that support *BABAR*. The collaborating institutions wish to thank SLAC for its support and kind hospitality. This work is supported by DOE and NSF (USA), NSERC (Canada), IHEP (China), CEA and CNRS-IN2P3 (France), BMBF and DFG (Germany), INFN (Italy), FOM (The Netherlands), NFR (Norway), MIST (Russia), and PPARC (United Kingdom). Individuals have received support from CONACyT (Mexico), A. P. Sloan Foundation, Research Corporation, and Alexander von Humboldt Foundation.

* Now at Department of Physics, University of Warwick, Coventry, United Kingdom
† Also with Università della Basilicata, Potenza, Italy
‡ Also with IFIC, Instituto de Física Corpuscular, CSIC-Universidad de Valencia, Valencia, Spain
§ Deceased

[1] Throughout this paper, the named reaction refers also to its complex conjugate.
[2] CLEO collaboration, T.E.Coan *et al.*, Phys. Rev. Lett. **80**, 1150 (1998).
[3] DELPHI collaboration, J.Abdallah *et al.*, Phys. Lett. B **561**, 26 (2003).
[4] CLEO collaboration, R.Ammar *et al.*, Phys. Rev. D **55**, 13 (1997).

[5] ALEPH collaboration, R. Barate *et al.*, Eur. Phys. Jour. C **4**, 387 (1998).

[6] *BABAR* Collaboration, B. Aubert *et al.*, Phys. Rev. D **68**, 092001 (2003).

[7] CLEO collaboration, B. Barish *et al.*, Phys. Rev. Lett. **79**, 3599 (1997).

[8] E. Bagan *et al.*, Phys. Lett. B **351**, 546 (1995).

[9] G. Buchalla *et al.*, Phys. Lett. B **364**, 188 (1995).

[10] M. Neubert, 17th Int. Symposium on Lepton-Photon Interactions, 10-15 Aug 95, Beijing, China, p. 298 (World Scientific).

[11] *BABAR* Collaboration, B. Aubert *et al.*, Nucl. Instr. Meth. A **479**,1 (2002).

[12] GEANT4 Collaboration, S. Agostinelli *et al.* Nucl. Instrum. Methods Phys Res. Sect. A 506, 250 (2003).

[13] ARGUS collaboration, H. Albrecht *et al.*, Z. Phys. C **48**, 543 (1990).

[14] CRYSTAL BALL collaboration, T. Skwarnicki, DESY F31-86-02.

[15] Satellite contributions include a reflection from $D^0 \to K^-K^+$ in the $D^0 \to K^-\pi^+$ mass spectrum and a signal at the D^+ mass (from $D^+ \to \phi\pi^+$ decays) in the $D_s^+ \to \phi\pi^+$ mass spectrum.

[16] S. Eidelman *et al.* (Particle Data Group Collaboration), Phys. Lett. B **592**, 1 (2004).

[17] ALEPH, CDF, DELPHI, L3, OPAL, SLD combined results, hep-ex/0112028.

[18] M. Beneke *et al.*, Phys. Rev. D **59**, 054003 (1999).

[19] CLEO collaboration, L. Gibbons *et al.*, Phys. Rev. D **56**, 3783 (1997).

Publications de Amina Zghiche

1. **"Measurement of the absolute branching fractions B –¿ D pi, D* pi, D** pi with a missing mass method"**
   B. Aubert *et al.* [BABAR Collaboration]
   Phys. Rev. D **74**, 111102 (2006) [arXiv:hep-ex/0609033]

2. **"Observation of B+ –¿ anti-K0 K+ and B0 –¿ K0 anti-K0"**
   B. Aubert *et al.* [BABAR Collaboration]
   Phys. Rev. Lett. **97**, 171805 (2006) [arXiv:hep-ex/0608036]

3. **"Measurement of the branching fraction and time-dependent CP asymmetry in the decay B0 –¿ D*+ D*- K0(S)"**
   B. Aubert *et al.* [BABAR Collaboration]
   Phys. Rev. D **74**, 091101 (2006) [arXiv:hep-ex/0608016]

4. **"Precise branching ratio measurements of the decays D0 –¿ pi- pi+ pi0 and D0 –¿ K- K+ pi0"**
   B. Aubert *et al.* [BABAR Collaboration]
   Phys. Rev. D **74**, 091102 (2006) [arXiv:hep-ex/0608009]

5. **"Measurement of branching fractions and charge asymmetries in B decays to an eta meson and a K* meson"**
   B. Aubert *et al.* [BABAR Collaboration]
   Phys. Rev. Lett. **97**, 201802 (2006) [arXiv:hep-ex/0608005]

6. **"Branching fraction measurements of charged B decays to K*+ K+ K-, K*+ pi+ K-, K*+ K+ pi- and K*+ pi+ pi- final states"**
   B. Aubert *et al.* [BABAR Collaboration]
   Phys. Rev. D **74**, 051104 (2006) [arXiv:hep-ex/0607113]

7. **"Measurement of the ratio B(B+ –¿ X e nu)/B(B0 –¿ X e nu)"**
   B. Aubert *et al.* [BABAR Collaboration]
   Phys. Rev. D **74**, 091105 (2006) [arXiv:hep-ex/0607111]

8. **"Measurement of the B –¿ pi l nu branching fraction and determination of —V(ub)— with tagged B mesons"**
   B. Aubert *et al.* [BABAR Collaboration]
   Phys. Rev. Lett. **97**, 211801 (2006) [arXiv:hep-ex/0607089]

9. **"Measurement of the branching fraction and photon energy moments of B –¿ X/s gamma and A(CP)(B –¿ X(s+d) gamma)"**
   B. Aubert *et al.* [BaBar Collaboration]
   Phys. Rev. Lett. **97**, 171803 (2006) [arXiv:hep-ex/0607071]

10. **"Searches for B0 decays to eta K0, eta eta, eta' eta', eta Phi, and eta' Phi"**
    B. Aubert *et al.* [BaBar Collaboration]
    Phys. Rev. D **74**, 051106 (2006) [arXiv:hep-ex/0607063]

11. **"Measurements of branching fractions, polarizations, and direct CP-violation asymmetries in B –¿ rho K* and B –¿ f0(980) K* decays"**
    B. Aubert *et al.* [BABAR Collaboration]
    Phys. Rev. Lett. **97**, 201801 (2006) [arXiv:hep-ex/0607057]

12. **"Search for B+ −¿ X(3872) K+, X(3872) −¿ J/psi gamma"**
B. Aubert *et al.* [BABAR Collaboration]
Phys. Rev. D **74**, 071101 (2006) [arXiv:hep-ex/0607050]

13. **"Measurements of the decays B0 −¿ anti-D0 p anti-p, B0 −¿ anti-D*0 p anti-p, B0 −¿ D-p anti-p pi+, and B0 −¿ D*- p anti-p pi+"**
B. Aubert *et al.* [BABAR Collaboration]
Phys. Rev. D **74**, 051101 (2006) [arXiv:hep-ex/0607039]

14. **"Observation of e+ e- annihilations into the C = +1 hadronic final states rho0 rho0 and Phi rho0"**
B. Aubert *et al.* [BABAR Collaboration]
Phys. Rev. Lett. **97**, 112002 (2006) [arXiv:hep-ex/0606054]

15. **"Search for the decay of a B0 or anti-B0 meson to anti-K*0 K0 or K*0 anti-K0"**
B. Aubert *et al.* [BABAR Collaboration]
Phys. Rev. D **74**, 072008 (2006) [arXiv:hep-ex/0606050]

16. **"Measurement of the spin of the Omega- hyperon at BABAR"**
B. Aubert *et al.* [BABAR Collaboration]
Phys. Rev. Lett. **97**, 112001 (2006) [arXiv:hep-ex/0606039]

17. **"Search for the decay B0 −¿ K0(S) K0(S) K0(L)"**
B. Aubert *et al.* [BABAR Collaboration]
Phys. Rev. D **74**, 032005 (2006) [arXiv:hep-ex/0606031]

18. **"Search for doubly charmed baryons Xi/cc+ and Xi/cc++ in BABAR"**
B. Aubert *et al.* [BABAR Collaboration]
Phys. Rev. D **74**, 011103 (2006) [arXiv:hep-ex/0605075]

19. **"Measurement of the D+ −¿ pi+ pi0 and D+ −¿ K+ pi0 branching fractions"**
B. Aubert *et al.* [BABAR Collaboration]
Phys. Rev. D **74**, 011107 (2006) [arXiv:hep-ex/0605044]

20. **"Search for B+ −¿ Phi pi+ and B0 −¿ Phi pi0 decays"**
B. Aubert *et al.* [BABAR Collaboration]
Phys. Rev. D **74**, 011102 (2006) [arXiv:hep-ex/0605037]

21. **"Study of B −¿ D(*) D/s(J)(*) decays and measurement of D/s- and D/sJ(2460)- branching fractions"**
B. Aubert *et al.* [BABAR Collaboration]
Phys. Rev. D **74**, 031103 (2006) [arXiv:hep-ex/0605036]

22. **"Search for the decay B0 −¿ a1+- rho-+"**
B. Aubert *et al.* [BaBar Collaboration]
Phys. Rev. D **74**, 031104 (2006) [arXiv:hep-ex/0605024]

23. **"Measurement of the eta and eta' transition form factors at q**2 = 112-GeV**2"**
B. Aubert *et al.* [BABAR Collaboration]
Phys. Rev. D **74**, 012002 (2006) [arXiv:hep-ex/0605018]

24. **"B meson decays to omega K*, omega rho, omega omega, omega Phi, and omega f0"**
B. Aubert *et al.* [BABAR Collaboration]
Phys. Rev. D **74**, 051102 (2006) [arXiv:hep-ex/0605017]

25. **"Search for B meson decays to eta' eta' K"**
B. Aubert *et al.* [BaBar Collaboration]
Phys. Rev. D **74**, 031105 (2006) [arXiv:hep-ex/0605008]

26. **"Dalitz plot analysis of the decay B+- −¿ K+- K+- K-+"**
B. Aubert *et al.* [BABAR Collaboration]
Phys. Rev. D **74**, 032003 (2006) [arXiv:hep-ex/0605003]

27. **"Measurement of branching fractions and CP-violating charge asymmetries for B meson decays to D(*) anti-D(*), and implications for the CKM angle gamma"**
B. Aubert *et al.* [BABAR Collaboration]
Phys. Rev. D **73**, 112004 (2006) [arXiv:hep-ex/0604037]

28. **"Observation of Upsilon(4S) decays to pi+ pi- Upsilon(1S) and pi+ pi- Upsilon(2S)"**
B. Aubert *et al.* [BABAR Collaboration]
Phys. Rev. Lett. **96**, 232001 (2006) [arXiv:hep-ex/0604031]

29. **"A study of the D/sJ*(2317)+ and D/sJ(2460)+ mesons in inclusive c anti-c production near s**(1/2) = 10.6-GeV"**
B. Aubert *et al.* [BABAR Collaboration]
Phys. Rev. D **74**, 032007 (2006) [arXiv:hep-ex/0604030]

30. **"Measurement of the B- −¿ D0 K*- branching fraction"**
B. Aubert *et al.* [BaBar Collaboration]
Phys. Rev. D **73**, 111104 (2006) [arXiv:hep-ex/0604017]

31. **"Measurement of anti-B0 −¿ D(*)0 anti-K(*)0 branching fractions"**
B. Aubert *et al.* [BABAR Collaboration]
Phys. Rev. D **74**, 031101 (2006) [arXiv:hep-ex/0604016]

32. **"Search for the decay tau- −¿ 3pi- 2pi+ 2pi0 nu/tau"**
B. Aubert *et al.* [BABAR Collaboration]
Phys. Rev. D **73**, 112003 (2006) [arXiv:hep-ex/0604014]

33. **"Study of the decay anti-B0 −¿ D*+ omega pi-"**
B. Aubert *et al.* [BABAR Collaboration]
Phys. Rev. D **74**, 012001 (2006) [arXiv:hep-ex/0604009]

34. **"Measurements of branching fractions, rate asymmetries, and angular distributions in the rare decays B −¿ K l+ l- and B −¿ K* l+ l-"**
B. Aubert *et al.* [BABAR Collaboration]
Phys. Rev. D **73**, 092001 (2006) [arXiv:hep-ex/0604007]

35. **"Search for the charmed pentaquark candidate Theta/c(3100)0 in e+ e- annihilations at s**(1/2) = 10.58-GeV"**
B. Aubert *et al.* [BABAR Collaboration]
Phys. Rev. D **73**, 091101 (2006) [arXiv:hep-ex/0604006]

36. **"Measurement of branching fractions in radiative B decays to eta K gamma and search for B decays to eta' K gamma"**
B. Aubert *et al.* [BABAR Collaboration]
Phys. Rev. D **74**, 031102 (2006) [arXiv:hep-ex/0603054]

37. **"Search for T, CP and CPT violation in B0 anti-B0 mixing with inclusive dilepton events"**
B. Aubert *et al.* [BABAR Collaboration]
Phys. Rev. Lett. **96**, 251802 (2006) [arXiv:hep-ex/0603053]

38. **"Observation of B0 meson decay to a1(1260)+- pi-+"**
B. Aubert *et al.* [BABAR Collaboration]
Phys. Rev. Lett. **97**, 051802 (2006) [arXiv:hep-ex/0603050]

39. **"Measurements of CP-violating asymmetries and branching fractions in B decays to omega K and omega pi"**
B. Aubert *et al.* [BABAR Collaboration]
Phys. Rev. D **74**, 011106 (2006) [arXiv:hep-ex/0603040]

40. **"Branching fraction limits for B0 decays to eta' eta, eta' pi0 and eta pi0"**
B. Aubert *et al.* [BABAR Collaboration]
Phys. Rev. D **73**, 071102 (2006) [arXiv:hep-ex/0603013]

41. **"Measurements of the branching fraction and time-dependent CP asymmetries of B0 −¿ J/psi pi0 decays"**
B. Aubert *et al.* [BaBar Collaboration]
Phys. Rev. D **74**, 011101 (2006) [arXiv:hep-ex/0603012]

42. **"Measurement of time-dependent CP asymmetries in B0 −¿ D(*)+- pi-+ and B0 −¿ D+- rho-+ decays"**
B. Aubert *et al.* [BABAR Collaboration]
Phys. Rev. D **73**, 111101 (2006) [arXiv:hep-ex/0602049]

43. **"Measurements of the B −¿ D* form factors using the decay anti-B0 −¿ D*+ e- anti-nu/e"**
B. Aubert *et al.* [BABAR Collaboration]
Phys. Rev. D **74**, 092004 (2006) [arXiv:hep-ex/0602023]

44. **"The $e^+e^- \to 3(\pi^+\pi^-), 2(\pi^+\pi^-\pi^0)$ and $K^+K^-2(\pi^+\pi^-)$ cross sections at center-of-mass energies from production threshold to 4.5-GeV measured with initial-state radiation"**
B. Aubert *et al.* [BABAR Collaboration]
Phys. Rev. D **73**, 052003 (2006) [arXiv:hep-ex/0602006]

45. **"Determinations of —V(ub)— from inclusive semileptonic B decays with reduced model dependence"**
B. Aubert *et al.* [BABAR Collaboration]
Phys. Rev. Lett. **96**, 221801 (2006) [arXiv:hep-ex/0601046]

46. **"Measurements of the branching fractions and CP-asymmetries of B- −¿ D0(CP) K- decays"**
B. Aubert *et al.* [BABAR Collaboration]
Phys. Rev. D **73**, 051105 (2006) [arXiv:hep-ex/0512067]

47. **"Search for the rare decays B0 −¿ D/s(*)+ a0(2)-"**
B. Aubert *et al.* [BABAR Collaboration]
Phys. Rev. D **73**, 071103 (2006) [arXiv:hep-ex/0512031]

48. **"Search for rare quark-annihilation decays, B- −¿ D/s(*)- Phi"**
B. Aubert *et al.* [BABAR Collaboration]
Phys. Rev. D **73**, 011103 (2006) [arXiv:hep-ex/0512028]

49. **"A study of e+ e- −¿ p anti-p using initial state radiation with BABAR"**
B. Aubert *et al.* [BABAR Collaboration]
Phys. Rev. D **73**, 012005 (2006) [arXiv:hep-ex/0512023]

50. **"A search for the rare decay $B^0 \to \tau^+\tau^-$ at BABAR"**
B. Aubert *et al.* [BABAR Collaboration]
Phys. Rev. Lett. **96**, 241802 (2006) [arXiv:hep-ex/0511015]

51. **"Measurements of the absolute branching fractions of B+- −¿ K+- X/(c anti-c)"**
B. Aubert *et al.* [BABAR Collaboration]
Phys. Rev. Lett. **96**, 052002 (2006) [arXiv:hep-ex/0510070]

52. **"Search for the W-exchange decays B0 −¿ D/s(*)- D/s(*)+"**
B. Aubert *et al.* [BABAR Collaboration]
Phys. Rev. D **72**, 111101 (2005) [arXiv:hep-ex/0510051]

53. **"Measurement of the inclusive electron spectrum in charmless semileptonic B decays near the kinematic endpoint and determination of —V(ub)—"**
B. Aubert *et al.* [BABAR Collaboration]
Phys. Rev. D **73**, 012006 (2006) [arXiv:hep-ex/0509040]

54. **"Measurement of branching fractions and resonance contributions for B0 −¿ anti-D0 K+ pi- and search for B0 −¿ D0 K+ pi- decays"**
B. Aubert *et al.* [BABAR Collaboration]
Phys. Rev. Lett. **96**, 011803 (2006) [arXiv:hep-ex/0509036]

55. **"Measurement of the branching ratios $\Gamma(D_s^{*+} \to D_s^+\pi^0)/\Gamma(D_s^{*+} \to D_s^+\gamma)$ and $\Gamma(D^{*0} \to D^0\pi^0)/\Gamma(D^{*0} \to D^0\gamma)$"**
B. Aubert *et al.* [BABAR Collaboration]
Phys. Rev. D **72**, 091101 (2005) [arXiv:hep-ex/0508039]

56. **"Measurements of neutral B decay branching fractions to $K^0_S\pi^+\pi^-$ final states and the charge asymmetry of $B^0 \to K^{*+}\pi^-$"**
B. Aubert *et al.* [BABAR Collaboration]
Phys. Rev. D **73**, 031101 (2006) [arXiv:hep-ex/0508013]

57. **"Search for lepton flavor violation in the decay $\tau^\pm \to e^\pm\gamma$"**
B. Aubert *et al.* [BABAR Collaboration]
Phys. Rev. Lett. **96**, 041801 (2006) [arXiv:hep-ex/0508012]

58. **"Measurements of the $B \to X_s\gamma$ branching fraction and photon spectrum from a sum of exclusive final states"**
B. Aubert *et al.* [BABAR Collaboration]
Phys. Rev. D **72**, 052004 (2005) [arXiv:hep-ex/0508004]

59. **"A study of $b \to c$ and $b \to u$ interference in the decay $B^- \to (K^+\pi^-)DK^{*-}$"**
B. Aubert *et al.* [BABAR Collaboration]
Phys. Rev. D **72**, 071104 (2005) [arXiv:hep-ex/0508001]

60. **"Study of $J/\psi\pi^+\pi^-$ states produced in $B^0 \to J/\psi\pi^+\pi^-K^0$ and $B^- \to J/\psi\pi^+\pi^-K^-$"**
B. Aubert *et al.* [BABAR Collaboration]
Phys. Rev. D **73**, 011101 (2006) [arXiv:hep-ex/0507090]

61. **"A search for the decay $B^+ \to \tau^+\nu_\tau$"**
B. Aubert *et al.* [BABAR Collaboration]
Phys. Rev. D **73**, 057101 (2006) [arXiv:hep-ex/0507069]

62. **"Measurement of the $\overline{B}^0$ lifetime and the $B^0\overline{B}^0$ oscillation frequency using partially reconstructed $\overline{B}^0 \to D^{*+}\ell^-\bar{\nu}_\ell$ decays"**
B. Aubert *et al.* [BABAR Collaboration]
Phys. Rev. D **73**, 012004 (2006) [arXiv:hep-ex/0507054]

63. **"Measurement of the time-dependent CP-violating asymmetry in $B^0 \to K^0_S\pi^0\gamma$ decays"**
B. Aubert *et al.* [BaBar Collaboration]
Phys. Rev. D **72**, 051103 (2005) [arXiv:hep-ex/0507038]

64. **"Dalitz plot analysis of $D^0 \to \bar{K}^0K^+K^-$"**
B. Aubert *et al.* [BABAR Collaboration]
Phys. Rev. D **72**, 052008 (2005) [arXiv:hep-ex/0507026]

65. **"An amplitude analysis of the decay $B^\pm \to \pi^\pm\pi^\pm\pi^\mp$"**
B. Aubert *et al.* [BABAR Collaboration]
Phys. Rev. D **72**, 052002 (2005) [arXiv:hep-ex/0507025]

66. **"Evidence for $B^+ \to \bar{K}^0K^+$ and $B^0 \to K^0\bar{K}^0$, and measurement of the branching fraction and search for direct CP violation in $B^+ \to K^0\pi^+$"**
B. Aubert *et al.* [BaBar Collaboration]
Phys. Rev. Lett. **95**, 221801 (2005) [arXiv:hep-ex/0507023]

67. **"Measurement of the $B^+ \to p\bar{p}K^+$ branching fraction and study of the decay dynamics"**
B. Aubert *et al.* [BABAR Collaboration]
Phys. Rev. D **72**, 051101 (2005) [arXiv:hep-ex/0507012]

68. **"A precision measurement of the Λ_c^+ baryon mass"**
B. Aubert *et al.* [BABAR Collaboration]
Phys. Rev. D **72**, 052006 (2005) [arXiv:hep-ex/0507009]

69. **"Dalitz-plot analysis of the decays $B^{\pm} \to K^{\pm}\pi^{\mp}\pi^{\pm}$"**
B. Aubert *et al.* [BABAR Collaboration]
Phys. Rev. D **72**, 072003 (2005) [Erratum-ibid. D **74**, 099903 (2006)] [arXiv:hep-ex/0507004]

70. **"Study of $B \to \pi\ell\nu$ and $B \to \rho\ell\nu$ decays and determination of $|V_{ub}|$"**
B. Aubert *et al.* [BABAR Collaboration]
Phys. Rev. D **72**, 051102 (2005) [arXiv:hep-ex/0507003]

71. **"Measurement of CP asymmetries for the decays $B^{\pm} \to D^0_{CP}K^{*\pm}$"**
B. Aubert *et al.* [BABAR Collaboration]
Phys. Rev. D **72**, 071103 (2005) [arXiv:hep-ex/0507002]

72. **"Measurement of time-dependent CP asymmetries and the CP-odd fraction in the decay $B^0 \to D^{*+}D^{*-}$"**
B. Aubert *et al.* [BaBar Collaboration]
Phys. Rev. Lett. **95**, 151804 (2005) [arXiv:hep-ex/0506082]

73. **"Observation of a broad structure in the $\pi^+\pi^- J/\psi$ mass spectrum around 4.26-GeV/c^2"**
B. Aubert *et al.* [BABAR Collaboration]
Phys. Rev. Lett. **95**, 142001 (2005) [arXiv:hep-ex/0506081]

74. **"Search for the rare decay $\overline{B}^0 \to D^{*0}\gamma$"**
B. Aubert *et al.* [BABAR Collaboration]
Phys. Rev. D **72**, 051106 (2005) [arXiv:hep-ex/0506070]

75. **"Search for lepton-flavor and lepton-number violation in the decay $\tau^- \to \ell^{\mp}h^{\pm}h'^-$"**
B. Aubert *et al.* [BaBar Collaboration]
Phys. Rev. Lett. **95**, 191801 (2005) [arXiv:hep-ex/0506066]

76. **"Measurement of double charmonium production in e^+e^- annihilations at $\sqrt{s} = 10.6$ GeV"**
B. Aubert *et al.* [BABAR Collaboration]
Phys. Rev. D **72**, 031101 (2005) [arXiv:hep-ex/0506062]

77. **"Determination of $|V_{ub}|$ from measurements of the electron and neutrino momenta in inclusive semileptonic B decays"**
B. Aubert *et al.* [BABAR Collaboration]
Phys. Rev. Lett. **95**, 111801 (2005) [Erratum-ibid. **97**, 019903 (2006)] [arXiv:hep-ex/0506036]

78. **"Search for the decay $\tau^- \to 4\pi^- 3\pi^+(\pi^0)\nu_\tau$"**
B. Aubert *et al.* [BABAR Collaboration]
Phys. Rev. D **72**, 012003 (2005) [arXiv:hep-ex/0506007]

79. **"Search for the rare decays $B^+ \to D^{(*)+}K^0_S$"**
B. Aubert *et al.* [BABAR Collaboration]
Phys. Rev. D **72**, 011102 (2005) [arXiv:hep-ex/0505099]

80. **"Measurement of time-dependent CP asymmetries in $B^0 \to D^{(*)\pm}D^{\mp}$ decays"**
B. Aubert *et al.* [BABAR Collaboration]
Phys. Rev. Lett. **95**, 131802 (2005) [arXiv:hep-ex/0505092]

81. **"Measurement of the branching fraction and decay rate asymmetry of $B^- \to D(\pi^+\pi^-\pi^0)K^-$"**
B. Aubert *et al.* [BABAR Collaboration]
Phys. Rev. D **72**, 071102 (2005) [arXiv:hep-ex/0505084]

82. **"Study of the $\tau^- \to 3h^- 2h^+\nu_\tau$ decay"**
B. Aubert *et al.* [the BABAR Collaborations]
Phys. Rev. D **72**, 072001 (2005) [arXiv:hep-ex/0505004]

83. **"Search for $b \to u$ transitions in $B^- \to D^0K^-$ and $B^- \to D^{*0}K^-$"**
B. Aubert *et al.* [BABAR Collaboration]
Phys. Rev. D **72**, 032004 (2005) [arXiv:hep-ex/0504047]

84. **"Measurement of γ in $B^{\mp} \to D^{(*)}K^{\mp}$ decays with a Dalitz analysis of $D \to K^0_S\pi^-\pi^+$"**
B. Aubert *et al.* [BABAR Collaboration]
Phys. Rev. Lett. **95**, 121802 (2005) [arXiv:hep-ex/0504039]

85. **"Measurement of time-dependent CP-violating asymmetries and constraints on $\sin(2\beta+\gamma)$ with partial reconstruction of $B \to D^{*\mp}\pi^{\pm}$ decays"**
B. Aubert *et al.* [BABAR Collaboration]
Phys. Rev. D **71**, 112003 (2005) [arXiv:hep-ex/0504035]

86. **"Production and decay of Ξ_c^0 at BABAR"**
B. Aubert *et al.* [BABAR Collaboration]
Phys. Rev. Lett. **95**, 142003 (2005) [arXiv:hep-ex/0504014]

87. **"Evidence for the decay $B^{\pm} \to K^{*\pm}\pi^0$"**
B. Aubert *et al.* [BABAR Collaboration]
Phys. Rev. D **71**, 111101 (2005) [arXiv:hep-ex/0504009]

88. **"Measurement of the branching fraction of $\Upsilon(4S) \to B^0\overline{B}^0$"**
B. Aubert *et al.* [BABAR Collaboration]
Phys. Rev. Lett. **95**, 042001 (2005) [arXiv:hep-ex/0504001]

89. **"Improved measurement of the CKM angle alpha using $B^0 \to \rho^+\rho^-$ decays"**
B. Aubert *et al.* [BABAR Collaboration]
Phys. Rev. Lett. **95**, 041805 (2005) [arXiv:hep-ex/0503049]

90. **"Measurement of branching fractions and charge asymmetries in B^+ decays to $\eta\pi^+, \eta K^+, \eta\rho^+$ and $\eta'\pi^+$, and search for B^0 decays to ηK^0 and $\eta\omega$"**
B. Aubert *et al.* [BABAR Collaboration]
Phys. Rev. Lett. **95**, 131803 (2005) [arXiv:hep-ex/0503035]

91. **"Search for $B \to J/\psi D$ decays"**
B. Aubert *et al.* [BABAR Collaboration]
Phys. Rev. D **71**, 091103 (2005) [arXiv:hep-ex/0503021]

92. **"Measurement of the branching fraction and the CP-violating asymmetry for the decay $B^0 \to K^0_S\pi^0$"**
B. Aubert *et al.* [BABAR Collaboration]
Phys. Rev. D **71**, 111102 (2005) [arXiv:hep-ex/0503011]

93. **"Measurement of the $B^0 \to D^{*-}D_s^{*+}$ and $D_s^+ \to \phi\pi^+$ branching fractions"**
B. Aubert *et al.* [BaBar Collaboration]
Phys. Rev. D **71**, 091104 (2005) [arXiv:hep-ex/0502041]

94. **"Search for lepton flavor violation in the decay $\tau \to \mu\gamma$"**
B. Aubert *et al.* [BABAR Collaboration]
Phys. Rev. Lett. **95**, 041802 (2005) [arXiv:hep-ex/0502032]

95. **"The $e^+e^- \to \pi^+\pi^-\pi^+\pi^-$, $K^+K^-\pi^+\pi^-$, and $K^+K^-K^+K^-$ cross sections at center-of-mass energies 0.5-GeV - 4.5-GeV measured with initial-state radiation"**
B. Aubert *et al.* [BABAR Collaboration]
Phys. Rev. D **71**, 052001 (2005) [arXiv:hep-ex/0502025]

96. **"Measurement of CP asymmetries in $B^0 \to \phi K^0$ and $B0 \to K^+K^-K^0_S$ decays"**
B. Aubert *et al.* [BABAR Collaboration]
Phys. Rev. D **71**, 091102 (2005) [arXiv:hep-ex/0502019]

97. **"Measurements of branching fractions and time-dependent CP-violating asymmetries in $B \to \eta' K$ decays"**
B. Aubert *et al.* [BaBar Collaboration]
Phys. Rev. Lett. **94**, 191802 (2005) [arXiv:hep-ex/0502017]

98. **"Branching fraction and CP asymmetries of $B^0 \to K^0_S K^0_S K^0_S$"**
B. Aubert *et al.* [BABAR Collaboration]
Phys. Rev. Lett. **95**, 011801 (2005) [arXiv:hep-ex/0502013]

99. **"Search for strange-pentaquark production in e^+e^- annihilation at $\sqrt{s} = 10.58$ GeV"**
B. Aubert *et al.* [BABAR Collaboration]
Phys. Rev. Lett. **95**, 042002 (2005) [arXiv:hep-ex/0502004]

100. **"A search for CP violation and a measurement of the relative branching fraction in $D^+ \to K^-K^+\pi^+$ decays"**
B. Aubert *et al.* [BABAR Collaboration]
Phys. Rev. D **71**, 091101 (2005) [arXiv:hep-ex/0501075]

101. **"Improved measurements of CP-violating asymmetry amplitudes in $B^0 \to \pi + \pi^-$ decays"**
B. Aubert *et al.* [BaBar Collaboration]
Phys. Rev. Lett. **95**, 151803 (2005) [arXiv:hep-ex/0501071]

102. **"Search for factorization-suppressed $B \to \chi_c K^{(*)}$ decays"**
B. Aubert *et al.* [BABAR Collaboration]
Phys. Rev. Lett. **94**, 171801 (2005) [arXiv:hep-ex/0501061]

103. **"Search for the radiative decay $B \to \phi\gamma$"**
B. Aubert *et al.* [BABAR Collaboration]
Phys. Rev. D **72**, 091103 (2005) [arXiv:hep-ex/0501038]

104. **"Limit on the $B^0 \to \rho^0\rho^0$ branching fraction and implications for the CKM angle alpha"**
B. Aubert *et al.* [BABAR Collaboration]
Phys. Rev. Lett. **94**, 131801 (2005) [arXiv:hep-ex/0412067]

105. **"Measurement of branching fractions and charge asymmetries for exclusive B decays to charmonium"**
B. Aubert *et al.* [BABAR Collaboration]
Phys. Rev. Lett. **94**, 141801 (2005) [arXiv:hep-ex/0412062]

106. **"Search for a charged partner of the X(3872) in the B meson decay $B \to X^-K$, $X^- \to J/\psi\pi^-\pi^0$"**
B. Aubert *et al.* [BaBar Collaboration]
Phys. Rev. D **71**, 031501 (2005) [arXiv:hep-ex/0412051]

107. **"Measurement of branching fraction and Dalitz distribution for $B^0 \to D^{(*)\pm}K^0\pi^\mp$ decays"**
B. Aubert *et al.* [BABAR Collaboration]
Phys. Rev. Lett. **95**, 171802 (2005) [arXiv:hep-ex/0412040]

108. **"Branching fractions and CP asymmetries in $B^0 \to \pi^0\pi^0$, $B^+ \to \pi^+\pi^0$ and $B^+ \to K^+\pi^0$ decays and isospin analysis of the $B \to \pi\pi$ system"**
B. Aubert *et al.* [BABAR Collaboration]
Phys. Rev. Lett. **94**, 181802 (2005) [arXiv:hep-ex/0412037]

109. **"Measurement of the ratio $B(B^- \to D^{*0}K^-)/B(B^- \to D^{*0}\pi^-)$ and of the CP asymmetry of $B^- \to D^{*0}_{CP+}K^-$ decays"**
B. Aubert *et al.* [BABAR Collaboration]
Phys. Rev. D **71**, 031102 (2005) [arXiv:hep-ex/0411091]

110. **"A search for the decay $B^+ \to K^+\nu\bar{\nu}$"**
B. Aubert *et al.* [BABAR Collaboration]
Phys. Rev. Lett. **94**, 101801 (2005) [arXiv:hep-ex/0411061]

111. **"Measurements of B meson decays to ωK^* and $\omega\rho$"**
B. Aubert *et al.* [BABAR Collaboration]
Phys. Rev. D **71**, 031103 (2005) [arXiv:hep-ex/0411054]

112. **"Ambiguity-free measurement of $\cos(2\beta)$: Time-integrated and time-dependent angular analyses of $B \to J/\psi K\pi$"**
B. Aubert *et al.* [BABAR Collaboration]
Phys. Rev. D **71**, 032005 (2005) [arXiv:hep-ex/0411016]

113. **"Improved measurement of CP asymmetries in $B^0 \to (c\bar{c})K^{(*)0}$ decays"**
B. Aubert *et al.* [BABAR Collaboration]
Phys. Rev. Lett. **94**, 161803 (2005) [arXiv:hep-ex/0408127]

114. **"Measurement of the branching fractions for inclusive B^- and $\overline{B}^0$ decays to flavor-tagged D, D_s and Λ_c"**
B. Aubert *et al.* [BABAR Collaboration]
Phys. Rev. D **70**, 091106 (2004) [arXiv:hep-ex/0408113]

115. **"Search for decays of B^0 mesons into pairs of charged leptons: $B0 \to e^+e^-$, $B^0 \to \mu^+\mu^-$, $B^0 \to e^\pm\mu^\mp$"**
B. Aubert *et al.* [BABAR Collaboration]
Phys. Rev. Lett. **94**, 221803 (2005) [arXiv:hep-ex/0408096]

116. **"Search for $D^0 - \bar{D}^0$ mixing using semileptonic decay modes"**
B. Aubert *et al.* [BABAR Collaboration]
Phys. Rev. D **70**, 091102 (2004) [arXiv:hep-ex/0408066]

117. **"Study of $e^+e^- \to \pi^+\pi^-\pi^0$ process using initial state radiation with BaBar"**
B. Aubert *et al.* [BABAR Collaboration]
Phys. Rev. D **70**, 072004 (2004) [arXiv:hep-ex/0408078]

118. **"Measurement of neutral B decay branching fractions to $K^0_S\pi^+\pi^-$ final states"**
B. Aubert *et al.* [BABAR Collaboration]
Phys. Rev. D **70**, 091103 (2004) [arXiv:hep-ex/0408054]

119. **"Study of $B \to D^{(*)+}_{sJ}\bar{D}^{(*)}$ decays"**
B. Aubert *et al.* [BABAR Collaboration]
Phys. Rev. Lett. **93**, 181801 (2004) [arXiv:hep-ex/0408041]

120. **"Search for the radiative penguin decays $B^+ \to \rho^+\gamma$, $B^0 \to \rho^0\gamma$, and $B^0 \to \omega\gamma$"**
B. Aubert *et al.* [BABAR Collaboration]
Phys. Rev. Lett. **94**, 011801 (2005) [arXiv:hep-ex/0408034]

121. **"Measurement of the $\overline{B}^0 \to D^{*+}\ell^-\bar{\nu}_\ell$ decay rate and $|V_{cb}|$"**
B. Aubert *et al.* [BABAR Collaboration]
Phys. Rev. D **71**, 051502 (2005) [arXiv:hep-ex/0408027]

122. **"Search for flavor-changing neutral current and lepton flavor violating decays of $D^0 \to \ell^+\ell^-$"**
B. Aubert *et al.* [BABAR Collaboration]
Phys. Rev. Lett. **93**, 191801 (2004) [arXiv:hep-ex/0408023]

123. **"Search for the decay $B^0 \to J/\psi\gamma$"**
B. Aubert *et al.* [BABAR Collaboration]
Phys. Rev. D **70**, 091104 (2004) [arXiv:hep-ex/0408018]

124. **"Measurement of the $B^0 \to \phi K^0$ decay amplitudes"**
B. Aubert *et al.* [BABAR Collaboration]
Phys. Rev. Lett. **93**, 231804 (2004) [arXiv:hep-ex/0408017]

125. **"Observation of direct CP violation in $B^0 \to K^+\pi^-$ decays"**
B. Aubert *et al.* [BaBar Collaboration]
Phys. Rev. Lett. **93**, 131801 (2004) [arXiv:hep-ex/0407057]

126. **"Search for the rare leptonic decay $B^- \to \tau^- \bar{\nu}_\tau$"**
B. Aubert *et al.* [BABAR Collaboration]
Phys. Rev. Lett. **95**, 041804 (2005) [arXiv:hep-ex/0407038]

127. **"Search for B-meson decays to two-body final states with $a0(980)$ mesons"**
B. Aubert *et al.* [BABAR Collaboration]
Phys. Rev. D **70**, 111102 (2004) [arXiv:hep-ex/0407013]

128. **"Measurement of branching fractions, and CP and isospin asymmetries, for $B \to K^* \gamma$"**
B. Aubert *et al.* [BABAR Collaboration]
Phys. Rev. D **70**, 112006 (2004) [arXiv:hep-ex/0407003]

129. **"Measurements of the branching fraction and CP-violation asymmetries in $B^0 \to f0(980)K^0_S$"**
B. Aubert *et al.* [BABAR Collaboration]
Phys. Rev. Lett. **94**, 041802 (2005) [arXiv:hep-ex/0406040]

130. **"Study of the $B \to J/\psi K^- \pi^+ \pi^-$ decay and measurement of the $B \to X(3872)K^-$ branching fraction"**
B. Aubert *et al.* [BABAR Collaboration]
Phys. Rev. D **71**, 071103 (2005) [arXiv:hep-ex/0406022]

131. **"Branching fractions and CP asymmetries in $B^0 \to K^+ K^- K^0_S$ and $B^+ \to K^+ K^0_S K^0_S$"**
B. Aubert *et al.* [BABAR Collaboration]
Phys. Rev. Lett. **93**, 181805 (2004) [arXiv:hep-ex/0406005]

132. **"Measurement of time-dependent CP-violating asymmetries in $B^0 \to K^{*0}\gamma(K^{*0} \to K^0_S \pi^0)$ decays"**
B. Aubert *et al.* [BABAR Collaboration]
Phys. Rev. Lett. **93**, 201801 (2004) [arXiv:hep-ex/0405082]

133. **"Search for B^0 decays to invisible final states and to $\nu\bar{\nu}\gamma$"**
B. Aubert *et al.* [BABAR Collaboration]
Phys. Rev. Lett. **93**, 091802 (2004) [arXiv:hep-ex/0405071]

134. **"A measurement of the total width, the electronic width, and the mass of the $\Upsilon(10580)$ resonance"**
B. Aubert *et al.* [BABAR Collaboration]
Phys. Rev. D **72**, 032005 (2005) [arXiv:hep-ex/0405025]

135. **"Study of the decay $B^0(\overline{B}^0) \to \rho^+ \rho^-$, and constraints on the CKM angle α"**
B. Aubert *et al.* [BABAR Collaboration]
Phys. Rev. Lett. **93**, 231801 (2004) [arXiv:hep-ex/0404029]

136. **"Determination of the branching fraction for $B \to X_c \ell \nu$ decays and of $|V_{cb}|$ from hadronic mass and lepton energy moments"**
B. Aubert *et al.* [BABAR Collaboration]
Phys. Rev. Lett. **93**, 011803 (2004) [arXiv:hep-ex/0404017]

137. **"Measurement of the $B \to X_s \ell^+ \ell^-$ branching fraction with a sum over exclusive modes"**
B. Aubert *et al.* [BABAR Collaboration]
Phys. Rev. Lett. **93**, 081802 (2004) [arXiv:hep-ex/0404006]

138. **"Measurement of the ratio of decay amplitudes for $\overline{B}^0 \to J/\psi K^{*0}$ and $B^0 \to J/\psi K^{*0}$"**
B. Aubert *et al.* [BABAR Collaboration]
Phys. Rev. Lett. **93**, 081801 (2004) [arXiv:hep-ex/0404005]

139. **"Searches for B^0 decays to combinations of charmless isoscalar mesons"**
B. Aubert *et al.* [BABAR Collaboration]
Phys. Rev. Lett. **93**, 181806 (2004) [arXiv:hep-ex/0403046]

140. **"Measurement of the direct CP asymmetry in $b \to s\gamma$ decays"**
B. Aubert *et al.* [BABAR Collaboration]
Phys. Rev. Lett. **93**, 021804 (2004) [arXiv:hep-ex/0403035]

141. **"Measurements of moments of the hadronic mass distribution in semileptonic B decays"**
B. Aubert *et al.* [BABAR Collaboration]
Phys. Rev. D **69**, 111103 (2004) [arXiv:hep-ex/0403031]

142. **"Measurement of the electron energy spectrum and its moments in inclusive $B \to Xe\nu$ decays"**
B. Aubert *et al.* [BABAR Collaboration]
Phys. Rev. D **69**, 111104 (2004) [arXiv:hep-ex/0403030]

143. **"Measurement of the time-dependent CP asymmetry in the $B^0 \to \phi K^0$ decay"**
B. Aubert *et al.* [BABAR Collaboration]
Phys. Rev. Lett. **93**, 071801 (2004) [arXiv:hep-ex/0403026]

144. **"B meson decays to $\eta^{(\prime)}K^*$, $\eta^{(\prime)}\rho$, $\eta^{(\prime)}\pi^0$, $\omega\pi^0$, and $\phi\pi^0$"**
B. Aubert *et al.* [BABAR Collaboration]
Phys. Rev. D **70**, 032006 (2004) [arXiv:hep-ex/0403025]

145. **"Branching fraction measurements of $B \to \eta_c K$ decays"**
B. Aubert *et al.* [BABAR Collaboration]
Phys. Rev. D **70**, 011101 (2004) [arXiv:hep-ex/0403007]

146. **"Search for the decay $B^0 \to p\bar{p}$"**
B. Aubert *et al.* [BaBar Collaboration]
Phys. Rev. D **69**, 091503 (2004) [arXiv:hep-ex/0403003]

147. **"Limits on the decay rate difference of neutral$-B$ mesons and on CP, T, and CPT violation in $B^0\overline{B}^0$ oscillations"**
B. Aubert *et al.* [BABAR Collaboration]
Phys. Rev. D **70**, 012007 (2004) [arXiv:hep-ex/0403002]

148. **"Measurements of CP violating asymmetries in $B^0 \to K^0_S\pi^0$ decays"**
B. Aubert *et al.* [BABAR Collaboration]
Phys. Rev. Lett. **93**, 131805 (2004) [arXiv:hep-ex/0403001]

149. **"Observation of the decay $B \to J/\psi\eta K$ and search for $X(3872) \to J/\psi\eta$"**
B. Aubert *et al.* [BABAR Collaboration]
Phys. Rev. Lett. **93**, 041801 (2004) [arXiv:hep-ex/0402025]

150. **"Search for $B^\pm \to (K^\mp\pi^\pm)(D)K^\pm$ and upper limit on the $b \to u$ amplitude in $B^\pm \to DK^\pm$"**
B. Aubert *et al.* [BABAR Collaboration]
Phys. Rev. Lett. **93**, 131804 (2004) [arXiv:hep-ex/0402024]

151. **"Study of $B^\pm \to J/\psi\pi^\pm$ and $B^\pm \to J/\psi K^\pm$ decays: Measurement of the ratio of branching fractions and search for direct CP violation"**
B. Aubert *et al.* [BABAR Collaboration]
Phys. Rev. Lett. **92**, 241802 (2004) [arXiv:hep-ex/0401035]

152. **"Measurement of the B^+/B^0 production ratio from the $\Upsilon(4S)$ meson using $B^+ \to J/\psi K^+$ and $B^0 \to J/\psi K^0_S$ decays"**
B. Aubert *et al.* [BABAR Collaboration]
Phys. Rev. D **69**, 071101 (2004) [arXiv:hep-ex/0401028]

153. **"Study of high momentum η' production in $B \to \eta' X_s$"**
B. Aubert *et al.* [BABAR Collaboration]
Phys. Rev. Lett. **93**, 061801 (2004) [arXiv:hep-ex/0401006]

154. **"Search for the rare leptonic decay $B^+ \to \mu^+\nu_\mu$"**
B. Aubert *et al.* [BABAR Collaboration]
Phys. Rev. Lett. **92**, 221803 (2004) [arXiv:hep-ex/0401002]

155. **"Measurements of branching fractions and CP-violating asymmetries in B meson decays to charmless two-body states containing a K^0"**
B. Aubert *et al.* [BABAR Collaboration]
Phys. Rev. Lett. **92**, 201802 (2004) [arXiv:hep-ex/0312055]

156. **"Measurement of the branching fraction for $B^- \to D^0 K^{*-}$"**
B. Aubert *et al.* [BABAR Collaboration]
Phys. Rev. D **69**, 051101 (2004) [arXiv:hep-ex/0312051]

157. **"Search for lepton flavor violation in the decay $\tau^- \to \ell^- \ell^+ \ell^-$"**
B. Aubert *et al.* [BABAR Collaboration]
Phys. Rev. Lett. **92**, 121801 (2004) [arXiv:hep-ex/0312027]

158. **"Measurement of branching fractions and charge asymmetries in $B^\pm \to \rho^\pm \pi^0$ and $B^\pm \to \rho^0 \pi^\pm$ decays, and search for $B^0 \to \rho^0 \pi^0$"**
B. Aubert *et al.* [BABAR Collaboration]
Phys. Rev. Lett. **93**, 051802 (2004) [arXiv:hep-ex/0311049]

159. **"Measurements of the mass and width of the η_c meson and of an $\eta_c(2S)$ candidate"**
B. Aubert *et al.* [BABAR Collaboration]
Phys. Rev. Lett. **92**, 142002 (2004) [arXiv:hep-ex/0311038]

160. **"Limits on the decay-rate difference of neutral B mesons and on CP, T, and CPT violation in $B^0 \overline{B}^0$ oscillations"**
B. Aubert *et al.* [BABAR Collaboration]
Phys. Rev. Lett. **92**, 181801 (2004) [arXiv:hep-ex/0311037]

161. **"Measurement of the branching fractions and CP-asymmetry of $B^- \to D^0(CP)K^-$ decays with the BaBar detector"**
B. Aubert *et al.* [BABAR Collaboration]
Phys. Rev. Lett. **92**, 202002 (2004) [arXiv:hep-ex/0311032]

162. **"Observation of the decay $B^0 \to \rho^+ \rho^-$ and measurement of the branching fraction and polarization"**
B. Aubert *et al.* [BABAR Collaboration]
Phys. Rev. D **69**, 031102 (2004) [arXiv:hep-ex/0311017]

163. **"Observation of $B^0 \to \omega K^0$, $B^+ \to \eta \pi^+$, and $B^+ \to \eta K^+$ and study of related decays"**
B. Aubert *et al.* [BABAR Collaboration]
Phys. Rev. Lett. **92**, 061801 (2004) [arXiv:hep-ex/0311016]

164. **"Measurement of the average ϕ multiplicity in B meson decay"**
B. Aubert *et al.* [BABAR Collaboration]
Phys. Rev. D **69**, 052005 (2004) [arXiv:hep-ex/0311008]

165. **"Observation of a narrow meson decaying to $D_s^+ \pi^0 \gamma$ at a mass of 2.458-GeV/c^2"**
B. Aubert *et al.* [BABAR Collaboration]
Phys. Rev. D **69**, 031101 (2004) [arXiv:hep-ex/0310050]

166. **"Measurement of time-dependent CP asymmetries and constraints on $\sin(2\beta + \gamma)$ with partial reconstruction of $B^0 \to D^{*\mp} \pi^\pm$ decays"**
B. Aubert *et al.* [BABAR Collaboration]
Phys. Rev. Lett. **92**, 251802 (2004) [arXiv:hep-ex/0310037]

167. **"Measurement of branching fractions of color-suppressed decays of the $\overline{B}^0$ meson to $D^{(*)0}\pi^0$, $D^{(*)0}\eta$, $D^{(*)0}\omega$, and $D^0\eta'$"**
B. Aubert *et al.* [BABAR Collaboration]
Phys. Rev. D **69**, 032004 (2004) [arXiv:hep-ex/0310028]

168. **"J/ψ production via initial state radiation in $e^+e^- \to \mu^+\mu^-\gamma$ at an e^+e^- center-of-mass energy near 10.6-GeV"**
B. Aubert *et al.* [BABAR Collaboration]
Phys. Rev. D **69**, 011103 (2004) [arXiv:hep-ex/0310027]

169. **"Measurement of the branching fraction for $B^{\pm} \to \chi_c^0 K^{\pm}$"**
B. Aubert *et al.* [BABAR Collaboration]
Phys. Rev. D **69**, 071103 (2004) [arXiv:hep-ex/0310015]

170. **"Measurement of $\sin(2\beta)$ using hadronic J/ψ decays"**
B. Aubert *et al.* [BABAR Collaboration]
Phys. Rev. D **69**, 052001 (2004) [arXiv:hep-ex/0309039]

171. **"Measurements of branching fractions in $B \to \phi K$ and $B \to \phi\pi$ and search for direct CP violation in $B^{\pm} \to \phi K^{\pm}$"**
B. Aubert *et al.* [BABAR Collaboration]
Phys. Rev. D **69**, 011102 (2004) [arXiv:hep-ex/0309025]

172. **"Measurements of the branching fractions of charged B decays to $K^{\pm}\pi^{\mp}\pi^{\pm}$ final states"**
B. Aubert *et al.* [BABAR Collaboration]
Phys. Rev. D **70**, 092001 (2004) [arXiv:hep-ex/0308065]

173. **"Measurement of the branching fraction and polarization for the decay $B^- \to D^{0*}K^{*-}$"**
B. Aubert *et al.* [BABAR Collaboration]
Phys. Rev. Lett. **92**, 141801 (2004) [arXiv:hep-ex/0308057]

174. **"Evidence for the rare decay $B \to K^*\ell^+\ell^-$ and measurement of the $B \to K\ell^+\ell^-$ branching fraction"**
B. Aubert *et al.* [BABAR Collaboration]
Phys. Rev. Lett. **91**, 221802 (2003) [arXiv:hep-ex/0308042]

175. **"Measurement of the $B^0 \to K_2^*(1430)^0\gamma$ and $B^+ \to K_2^*(1430)^+\gamma$ branching fractions"**
B. Aubert *et al.* [BABAR Collaboration]
Phys. Rev. D **70**, 091105 (2004) [arXiv:hep-ex/0409035]

176. **"Measurement of time dependent CP asymmetry in $B^0 \to D^{(*)\pm}\pi^{\mp}$ decays and constraints on $|\sin(2\beta+\gamma)|$"**
B. Aubert *et al.* [BABAR Collaboration]
Phys. Rev. Lett. **92**, 251801 (2004) [arXiv:hep-ex/0308018]

177. **"Observation of the decay $B^0 \to \pi^0\pi^0$"**
B. Aubert *et al.* [BABAR Collaboration]
Phys. Rev. Lett. **91**, 241801 (2003) [arXiv:hep-ex/0308012]

178. **"Measurement of the inclusive charmless semileptonic branching ratio of B mesons and determination of $|V_{ub}|$"**
B. Aubert *et al.* [BABAR Collaboration]
Phys. Rev. Lett. **92**, 071802 (2004) [arXiv:hep-ex/0307062]

179. **"Rates, polarizations, and asymmetries in charmless vector-vector B meson decays"**
B. Aubert *et al.* [BABAR Collaboration]
Phys. Rev. Lett. **91**, 171802 (2003) [arXiv:hep-ex/0307026]

180. **"Measurement of time-dependent CP asymmetries and the CP-odd fraction in the decay $B^0 \to D^{*+}D^{*-}$"**
B. Aubert *et al.* [BABAR Collaboration]
Phys. Rev. Lett. **91**, 131801 (2003) [arXiv:hep-ex/0306052]

181. **"Search for the radiative decays $B \to \rho\gamma$ and $B^0 \to \omega\gamma$"**
B. Aubert *et al.* [BABAR Collaboration]
Phys. Rev. Lett. **92**, 111801 (2004) [arXiv:hep-ex/0306038]

182. **"Measurements of branching fractions and CP-violating asymmetries in $B^0 \to \rho^{\pm}h^{\mp}$ decays"**
B. Aubert *et al.* [BABAR Collaboration]
Phys. Rev. Lett. **91**, 201802 (2003) [arXiv:hep-ex/0306030]

183. **"Limits on $D^0\bar{D}^0$ mixing and CP violation from the ratio of lifetimes for decay to $K^-\pi^+$, K^-K^+ and $\pi^-\pi^+$"**
B. Aubert *et al.* [BABAR Collaboration]
Phys. Rev. Lett. **91**, 121801 (2003) [arXiv:hep-ex/0306003]

184. **"Measurement of the branching fractions for the exclusive decays of B^0 and B^+ to $\bar{D}^{(*)}D^{(*)}K$"**
B. Aubert *et al.* [BABAR Collaboration]
Phys. Rev. D **68**, 092001 (2003) [arXiv:hep-ex/0305003]

185. **"Observation of a narrow meson decaying to $D_s^+\pi^0$ at a mass of 2.32-GeV/c^2"**
B. Aubert *et al.* [BABAR Collaboration]
Phys. Rev. Lett. **90**, 242001 (2003) [arXiv:hep-ex/0304021]

186. **"Rare B decays into states containing a J/ψ meson and a meson with $s\bar{s}$ quark content"**
B. Aubert *et al.* [BABAR Collaboration]
Phys. Rev. Lett. **91**, 071801 (2003) [arXiv:hep-ex/0304014]

187. **"Search for $D^0 - \bar{D}^0$ mixing and a measurement of the doubly Cabibbo-suppressed decay rate in $D^0 \to K\pi$ decays"**
B. Aubert *et al.* [BABAR Collaboration]
Phys. Rev. Lett. **91**, 171801 (2003) [arXiv:hep-ex/0304007]

188. **"Measurements of the branching fractions and charge asymmetries of charmless three-body charged B decays"**
B. Aubert *et al.* [BABAR Collaboration]
Phys. Rev. Lett. **91**, 051801 (2003) [arXiv:hep-ex/0304006]

189. **"Measurements of CP-violating asymmetries and branching fractions in B meson decays to $\eta' K$"**
B. Aubert *et al.* [BABAR Collaboration]
Phys. Rev. Lett. **91**, 161801 (2003) [arXiv:hep-ex/0303046]

190. **"Evidence for $B^+ \to J/\psi p\overline{\Lambda}$ and search for $B^0 \to J/\psi p\bar{p}$"**
B. Aubert *et al.* [BABAR Collaboration]
Phys. Rev. Lett. **90**, 231801 (2003) [arXiv:hep-ex/0303036]

191. **"Observation of the decay $B^\pm \to \pi^\pm\pi^0$, study of $B^\pm \to K^\pm\pi^0$, and search for $B^0 \to \pi^0\pi^0$"**
B. Aubert *et al.* [BABAR Collaboration]
Phys. Rev. Lett. **91**, 021801 (2003) [arXiv:hep-ex/0303028]

192. **"Study of time-dependent CP asymmetry in neutral B decays to $J/\psi\pi^0$"**
B. Aubert *et al.* [BABAR Collaboration]
Phys. Rev. Lett. **91**, 061802 (2003) [arXiv:hep-ex/0303018]

193. **"Measurement of the branching fraction and CP-violating asymmetries in neutral B decays to $D^{*\pm}D^{\mp}$"**
B. Aubert *et al.* [BABAR Collaboration]
Phys. Rev. Lett. **90**, 221801 (2003) [arXiv:hep-ex/0303004]

194. **"Measurement of $B^0 \to D_s^{(*)+}D^{*-}$ branching fractions and $B^0 \to D_s^{(*)+}D^{*-}$ polarization with a partial reconstruction technique"**
B. Aubert *et al.* [BABAR Collaboration]
Phys. Rev. D **67**, 092003 (2003) [arXiv:hep-ex/0302015]

195. **"The control system for the CMS tracker front end"**
F. Drouhin *et al.*
IEEE Trans. Nucl. Sci. **49**, 846 (2002)

196. **"Simultaneous measurement of the B^0 meson lifetime and mixing frequency with $B^0 \to D^{*-}\ell^+\nu_\ell$ decays"**
B. Aubert *et al.* [BABAR Collaboration]
Phys. Rev. D **67**, 072002 (2003) [arXiv:hep-ex/0212017]

197. **"Measurement of the B^0 meson lifetime with partial reconstruction of $B^0 \to D^{*-}\pi^+$ and $B^0 \to D^{*-}\rho^+$ decays"**
B. Aubert *et al.* [BABAR Collaboration]
Phys. Rev. D **67**, 091101 (2003) [arXiv:hep-ex/0212012]

198. **"Experimental and simulation study of the behaviour and operation modes of MSGC + GEM detectors"**
M. Ageron *et al.*
Nucl. Instrum. Meth. A **489**, 121 (2002)

199. **"A study of the rare decays $B^0 \to D_s^{(*)+}\pi^-$ and $B^0 \to D_s^{(*)-}K+$"**
B. Aubert *et al.* [BABAR Collaboration]
Phys. Rev. Lett. **90**, 181803 (2003) [arXiv:hep-ex/0211053]

200. **"A measurement of the $B^0 \to J/\psi\pi^+\pi^-$ branching fraction"**
B. Aubert *et al.* [BABAR Collaboration]
Phys. Rev. Lett. **90**, 091801 (2003) [arXiv:hep-ex/0209013]

201. **"Study of inclusive production of charmonium mesons in B decay"**
B. Aubert *et al.* [BABAR Collaboration]
Phys. Rev. D **67**, 032002 (2003) [arXiv:hep-ex/0207097]

202. **"Measurement of the branching fraction for inclusive semileptonic B meson decays"**
B. Aubert *et al.* [BABAR Collaboration]
Phys. Rev. D **67**, 031101 (2003) [arXiv:hep-ex/0208018]

203. **"Measurements of branching fractions and CP-violating asymmetries in $B^0 \to \pi^+\pi^-$, $K^+\pi^-$, K^+K^- decays"**
B. Aubert *et al.* [BABAR Collaboration]
Phys. Rev. Lett. **89**, 281802 (2002) [arXiv:hep-ex/0207055]

204. **"Measurement of the CP-violating asymmetry amplitude $\sin 2\beta$"**
B. Aubert *et al.* [BABAR Collaboration]
Phys. Rev. Lett. **89**, 201802 (2002) [arXiv:hep-ex/0207042]

205. **"Measurement of the branching fraction and CP content for the decay $B^0 \to D^{*+}D^{*-}$"**
B. Aubert *et al.* [BaBar Collaboration]
Phys. Rev. Lett. **89**, 061801 (2002) [arXiv:hep-ex/0203008]

206. **"Search for T and CP violation in $B^0 - \overline{B}^0$ mixing with inclusive dilepton events"**
B. Aubert *et al.* [BABAR Collaboration]
Phys. Rev. Lett. **88**, 231801 (2002) [arXiv:hep-ex/0202041]

207. **"Measurement of the B^0 lifetime with partially reconstructed $B^0 \to D^{*-}\ell + \nu_\ell$ decays"**
B. Aubert *et al.* [BABAR Collaboration]
Phys. Rev. Lett. **89**, 011802 (2002) [Erratum-ibid. **89**, 169903 (2002)] [arXiv:hep-ex/0202005]

208. **"Robustness test of a system of MSGC+GEM detectors at the cyclotron facility of the Paul Scherrer institute"**
M. Ageron *et al.*
Nucl. Instrum. Meth. A **471**, 380 (2001)

209. **"Test of the CMS Microstrip Silicon tracker readout and control system"**
A. Zghiche [CMS Tracker Collaboration]
Nucl. Instrum. Meth. A **461**, 470 (2001)

210. **"Corrections to the one-photon approximation in the 0+ —¿ 2+ transition of 12C"**
P. Gueye *et al.*
Phys. Rev. C **63**, 051303 (2001)

211. **"First results of Micromegas detector with fast integrated electronics"**
F. Jeanneau *et al.*
Nucl. Instrum. Meth. A **450**, 313 (2000)

212. **"Beam test results of a wedge-shaped MSGC + GEM detector at CERN"**
Y. Benhammou *et al.*
Nucl. Instrum. Meth. A **441**, 452 (2000)

213. **"Large scale test of wedge shaped micro strip gas counters"**
M. Ackermann *et al.*
Nucl. Instrum. Meth. A **436**, 313 (1999)

214. **"Λ and $\overline{\Lambda}$ polarization from deep inelastic muon scattering"**
M. R. Adams *et al.* [E665 Collaboration]
Eur. Phys. J. C **17**, 263 (2000) [arXiv:hep-ex/9911004]

215. **"Coulomb distortion measurements by comparing electron and positron quasielastic scattering off C-12 and Pb-208"**
P. Gueye *et al.*
Phys. Rev. C **60**, 044308 (1999)

216. **"Background light in potential sites for the ANTARES undersea neutrino telescope"**
P. Amram *et al.* [ANTARES Collaboration]
Astropart. Phys. **13**, 127 (2000) [arXiv:astro-ph/9910170]

217. **"A study of various coatings for MSGCs"**
V. Mack, J. C. Fontaine, D. Huss, J. M. Brom, A. Zghiche and J. Schunck
Nucl. Instrum. Meth. A **423**, 369 (1999)

218. **"Subthreshold K+ production in proton nucleus collisions"**
M. Debowski *et al.*
Z. Phys. A **356**, 313 (1996)

219. **"Study of the ABC enhancement in the d(pol.) d −¿ alpha X0 reaction"**
R. Wurzinger *et al.*
Phys. Lett. B **445**, 423 (1999) [arXiv:nucl-ex/9810010]

220. **"Subthreshold K+ production in proton nucleus collisions and the nuclear spectral function"**
M. Debowski *et al.*
Acta Phys. Polon. B **27**, 3015 (1996)

221. **"Test of a CMS MSGC tracker prototype in a high-intensity hadron beam"**
D. Abbaneo *et al.*
Nucl. Instrum. Meth. A **409**, 37 (1998)

222. **"Comparative studies of MSGC and MSGC-GEM detectors"**
Y. Benhammou *et al.*
Nucl. Instrum. Meth. A **419**, 400 (1998)

223. **"Inclusive single-particle distributions and transverse momenta of forward produced charged hadrons in μ p scattering at 470-GeV"**
M. R. Adams *et al.* [E665 Collaboration]
Z. Phys. C **76**, 441 (1997)

224. **"Diffractive production of $\rho^0(770)$ mesons in muon proton interactions at 470-GeV"**
M. R. Adams *et al.* [E665 Collaboration]
Z. Phys. C **74**, 237 (1997)

225. **"eta-helium quasi-bound states"**
N. Willis *et al.*
Phys. Lett. B **406**, 14 (1997) [arXiv:nucl-ex/9703002]

226. **"Anomaly in the transverse longitudinal ratio for He-3 (e, e-prime p) X reaction at 260-MeV/c recoil momentum"**
J. M. Le Goff *et al.*
Phys. Rev. C **55**, 1600 (1997)

227. **"Measurement of polarization transfer kappa(0) and tensor analyzing power T(20) in the backward elastic d p scattering"**
V. Punjabi *et al.*
Phys. Lett. B **350**, 178 (1995)

228. **"Proton and deuteron structure functions in muon scattering at 470-GeV"**
M. R. Adams *et al.* [E665 Collaboration]
Phys. Rev. D **54**, 3006 (1996)

229. **"Nuclear decay following deep inelastic scattering of 470-GeV muons"**
M. R. Adams *et al.* [E665 Collaboration]
Phys. Rev. Lett. **74**, 5198 (1995) [Erratum-ibid. **80**, 2020 (1998)]

230. **"Shadowing in inelastic scattering of muons on carbon, calcium and lead at low $x_{\rm Bj}$"**
M. R. Adams *et al.* [E665 Collaboration]
Z. Phys. C **67**, 403 (1995) [arXiv:hep-ex/9505006]

231. **"An Active storage cell for a polarized gas internal target"**
K. P. Coulter *et al.*
Nucl. Instrum. Meth. A **350**, 423 (1994)

232. **"Extraction of the ratio $F2_n/F2_p$ from muon - deuteron and muon - proton scattering at small x and Q**2"**
M. R. Adams *et al.* [E665 Collaboration]
Phys. Rev. Lett. **75**, 1466 (1995)

233. **"Measurement of nuclear transparencies from exclusive ρ^0 meson production in muon - nucleus scattering at 470-GeV"**
M. R. Adams *et al.* [E665 Collaboration]
Phys. Rev. Lett. **74**, 1525 (1995)

234. **"Short range interaction of nucleons inside the nucleus via He-4 (e, e-prime p) R reaction"**
J. M. Le Goff *et al.*
Phys. Rev. C **50**, 2278 (1994)

235. **"The Longitudinal And Transverse Structure Functions Of The He-4 (E, E' P) H-3 Reaction"**
J. E. Ducret *et al.*
Nucl. Phys. A **556**, 373 (1993)

236. **"Longitudinal and transverse responses in quasielastic electron scattering from Pb-208 and He-4"**
A. Zghiche *et al.*
Nucl. Phys. A **572**, 513 (1994) [Erratum-ibid. A **584**, 757 (1995)]

237. **"Test of bound nucleon form-factors through (e, e-prime p) cross-section measurements on H-2, He-3 and He-4 up to 0.9-GeV/c momentum transfer with L/T/TL separation"**
J. E. Ducret *et al.*
Nucl. Phys. A **553**, 697C (1993)

238. **"Two-Body Correlations In The Li-6 Nucleus Through The (E, E-Prime D) Reaction"**
M. Jodice *et al.*
Phys. Lett. B **282**, 31 (1992)

239. **"A Waterfall target for electron scattering experiments"**
F. Garibaldi *et al.*
Nucl. Instrum. Meth. A **314**, 1 (1992)

240. **"DEEP INELASTIC ELECTRON SCATTERING IN THE DISTORTED WAVE BORN APPROXIMATION: AN ANALYTIC APPROACH"**
M. Traini, S. Turck-Chieze and A. Zghiche
Phys. Rev. C **38**, 2799 (1988)

241. **"A Study Of The Electrodisintegration Reaction He-4 (E, E-Prime P) H-3 With Transverse Longitudinal Separation"**
A. Magnon *et al.*
Phys. Lett. B **222**, 352 (1989)